Technologist Presentations

A Note on 2018 Technologist Abstracts

For the Technologist Abstract track, **35 scientific papers** have been accepted for presentation at the 65th SNMMI Annual Meeting at the Philadelphia Convention Center, Philadelphia, PA. The Program Committee for the SNMMI Technologist Section (SNMMI-TS) will be hosting 5 oral sessions to present these scientific papers, to be held on Sunday, June 24, and Monday, June 25; refer to the 2018 Annual Meeting Program Book for specific times and locations. Each oral session is 90 minutes in duration and includes up to seven 12-minute presentations per session.

For the Technologist Abstract track, **70 scientific posters** have been accepted for presentation. The SNMMI-TS Program Committee will be hosting a Technologist "Meet the Author" poster session, scheduled for Monday, June 25, from 3:00PM-4:30PM. The posters will be on display and available for viewing by attendees in the Poster Hall (Exhibit Hall C).

SNMMI Abstracts Online: Accepted abstracts for the 65th SNMMI Annual Meeting are citable and searchable by visiting the JNM website at: http://jnm.snmjournals.org/

SUNDAY SESSIONS

Tech Papers I: Clinical PET

Moderator: Mary Beth Farrell, MS, CNMT, NCT, FSNMMITS
Co-Moderator: April Mann

2101

Ga^{68}PSMA PET/MRI a revolution to detect primary prostate cancer. Sylvia Schachoff[1], Tobias Maurer[2], Stephan G. Nekolla[1], Markus Schwaiger, MD[1], Wolfgang A. Weber, MD[1], Matthias Eiber, MD[1]; [1]Nuclear Medicine, TU Munich, Munich, Germany, [2]Department of Urology, Munich, Germany. (2095)

Aim: Define a PET/MR study protocol using Ga68-PSMA for patients with elevated PSA value and negative prostate biopsies but high suspicion of tumor.
Methods: For patients with suspected primary prostate cancer, Ga68-PSMA-PET MRI is a novel and promising imaging technique. Ga68-PSMA is a new PET tracer that targets the active center of the extracellular domain of PSMA - a protein with high expression in prostate cancer but low anywhere else in the body. In our clinical routine 45 % of Ga68-PSMA PET/MR examinations are for primary prostate cancer with half of them in patient with increased PSA and prior negative prostate biopsies. Our PET/MRI protocol combines the advantages of molecular information from PET with a state of the art multi-parametric MRI of the prostate (T2w 3D, diffusion, dynamic contrast-enhanced sequence). The examination takes about 35 minutes and requires an optimal preparation of the patients (e.g. MRI contraindications, laboratory values such as PSA and creatinine).
Results: Ga68-PSMA PET imaging allows direct visualization of PSMA-avid tumor lesions independent of metabolism - thus regenerative and inflammatory change have hardly any influence). The soft-tissue contrast of MRI-sequences and their anatomical resolution in combination with the PET-signal, clearly help to diagnose prostate cancers, especially in the transition zone which is difficult for MRI alone. The information of our Ga68-PSMA PET/MR dataset is used in by local urologists to perform PET-MRI-Ultrasound-Fusion guided biopsies. This helps to increase cancer detection rate in a difficult patient population.
Summary: Ga68-PSMA PET/MR is a novel method to detect prostate cancer in men with prior negative biopsies but persistently elevated PSA-values. Combining PET with MRI using PET/MRI rather than PET/CT allows integral assessment of functional and molecular information and provide soft-tissue contrast to enable imaging guided biopsy. Based on our experience additional investigations are necessary to define the exact value of this promising approach. Interesting innovation arise from the application of fluorinated PSMA-ligands yielding F18-specific advantages compared to Ga68 (e.g. longer Half-life, lower positron range, higher production of activity).

Authors listed for this abstract reported no relevant financial disclosures.

2102

The evaluation of the spatial resolution of ^{11}C-, ^{18}F- and ^{64}Cu-PET images on a clinical PET/CT scanner using Monte Carlo Simulation and phantom examination. Saki Kimoto[1], Naoki Hashimoto[1], Ayano Shoji[1], Yuji Tsutsui[1,2], Kazuhiko Himuro[2], Shingo Baba, MD, PhD[2], Akihiko Takahashi[1], Masayuki Sasaki, MD, PhD[3]; [1]Kyushu University, Fukuoka, Japan, [2]Kyushu University Hospital, Fukuoka, Japan, [3]Dept Rad Sci Sch of Health Sci Kyushu Univ, Fukuoka, Japan. (1762)

Purpose: The goal of this study was to evaluate the spatial resolution of PET images on PET/CT scanner using ^{11}C (0.960 MeV), ^{18}F (0.633 MeV) and ^{64}Cu (0.650 MeV) by Monte Carlo Simulation (MCS) and phantom examination.
Materials and Methods: In MCS, spherical sources (diameter: 0.7 mm) of ^{11}C, ^{18}F and ^{64}Cu were generated and 10, 000 annihilation positions of positrons were recorded. The full width at half maximum (FWHM) and the full width at tenth maximum (FWTM) were measured from the distribution function of the positron annihilation positions, and the FWHM to FWTM ratio (FWHM/FWTM) was then calculated. In the phantom examination, the PET data were acquired using a Biograph mCT scanner. The point sources (inner diameter: 0.7 mm) with ^{11}C, ^{18}F and ^{64}Cu were placed at transaxial positions (0, 1) cm. The radioactivity concentration was 21.2 MBq/mL. The data were acquired in the three-dimensional list mode and then were reconstructed using filtered back projection. A Gaussian filter was not used. The image matrix was 400×400 and the slice thickness was 5 mm. The FWHM, the FWTM and the FWHM/FWTM were calculated from the PET images.
Results: On MCS, the FWHM/FWTM of ^{11}C, ^{18}F and ^{64}Cu were 0.284, 0.396 and 0.396, respectively. ^{11}C, which has the highest positron energy, showed the smallest FWHM/FWTM. On the phantom examination, the FWHM/FWTM of ^{11}C, ^{18}F and ^{64}Cu were 0.439±0.03, 0.423±0.03 and 0.444±0.04, respectively. There were no significant differences among the FWHM/FWTM of ^{11}C, ^{18}F and ^{64}Cu.
Conclusions: In conclusion, the positron energy was considered to influence the theoretical spatial resolution of positron imaging in MCS, but no such influence was observed on the clinical PET images. Therefore, the spatial resolution of clinical PET images seems to be too low to measure differences in positron energy among ^{11}C, ^{18}F and ^{64}Cu.

Authors listed for this abstract reported no relevant financial disclosures.

2103

Evaluation of metabolic tumor volume using different image reconstruction algorithm on 18F-FDG PET image. Seok Hwan Yoon[1], Hong Jae Lee[1], Gyeong Woon Noh[1], Jae Sung Lee, PhD[2], Jin Chul Paeng, MD, PhD[1], Keon Wook Kang, MD, PhD[1], Dong Soo Lee, MD, PhD[1], June-Key Chung, MD, PhD[1]; [1]Seoul National University Hospital, Seoul, Korea, Republic of, [2]Seoul National University, Seoul, Korea, Republic of. (1562)

Purpose: Recently, MTV(Metabolic tumor volume) has been used as indices of the whole tumor FDG uptake on FDG PET image. but it is influenced by image reconstruction. The purpose of this study was to evaluate the correlation of MTV applied different SUVmax threshold for different reconstruction algorithm on phantom and patient study.
Methods: In phantom study, Measurement were performed on a Siemens Biograph mCT40 PET/CT using a NEMA IEC body phantom containing different size six spheres filled with F18-FDG by applying four signal to background ratios (4:1, 8:1, 10:1, 20:1). MTV of images reconstructed four algorithms (OSEM3D, OSEM3D+PSF, OSEM3D+TOF, OSEM3D+PSF+TOF) were measured with different SUVmax threshold. (30%, 35%, 40%, 45%, 50%, 55%, 60%). In patient study, we compared MTV of tumor by applying different threshold of SUVmax in FDG PET images of 52 patients with lung cancer. To evaluate statistical analysis, Wilcoxon test, Concordance correlation coefficient and Kruskal-Wallis test were performed.
Results: In phantom, Overall, the use of increasing SUVmax threshold result in decreasing MTV. and increasing the SBR decreased MTV of all spheres on same SUVmax threshold. and the 40% threshold of SUVmax gave the best concordance between measured and actual volume in OSEM3D+PSF(P=0.3758, Pc=0.9982, C_b=0.9999) and OSEM3D+PSF+TOF(P=0.8864, Pc=0.9985, C_b=0.9999) reconstruction image. and the 45% threshold had the best correlation between the volume measured and actual volume in OSEM3D(P=0.0946, Pc=0.9985, C_b=0.9995) and OSEM3D+TOF(P=0.9431 Pc=0.9989, C_b=1.0000) reconstruction image. In patients, there were no statistical significance of the difference between MTV of OSEM3D+PSF, OSEM3D+PSF+TOF images by applying 40% SUVmax threshold and MTV of OSEM3D, OSEM3D+TOF images by applying 45% SUVmax threshold (P=0.9765)
Conclusions: In this study, The MTV of 40% threshold in OSEM3D+PSF and OSEM3D+PSF+TOF reconstruction image was high correlation with the MTV of 45% threshold in OSEM3D and OSEM3D+TOF reconstruction image.
Key Words: FDG PET, MTV, OSEM3D, OSEM3D+PSF, OSEM3D+TOF, OSEM3D+PSF+TOF

Authors listed for this abstract reported no relevant financial disclosures.

2104

Quantitative Relation and activity diagnostic efficacy of plasma PTX3 under the guidance of 18F-FDG PET/CT in patients with Takayasu's arteritis. Xiang Zhou[1], Jing Wang, PhD[2], Shengjun Wang[3], Fei Kang, MD[4]; [1]Department of Nuclear Medicine, Xijing Hospital, Xian, China, [2]Xijing Hospital, Xian, China, [3]Nuclear Medicine, Xi'an, China, [4]Xi'An, China. (1613)

Objectives: Pentraxin-3(PTX-3), a new type of inflammatory markers, is mainly induced by inflammatory stimuli, it rapidly producted at the systemic level or within tissues which has been shown to correlate with the severity of some clinical conditions. The aim of this study is to investigate the quantitative correlation between plasma PTX-3 and lesion activity evaluated by ^{18}F-FDG PET/CT in patients with Takayasu's arteritis (TKA), and compare the diagnosis efficiency of ptx3 with that of traditional serum markers (ESR and CRP) under the guidance of ^{18}F-FDG PET/CT.
Methods: 65 patients with clinical diagnosis of TKA from 2016.01-2017.10 were retrospectively studied. All patients underwent ^{18}F-FDG PET/CT scans, the SUV data and volum of main artery lesions were measured. Their blood was drawn before the injection of ^{18}F-FDG for measuring the levels of CRP and ESR. Plasma PTX3 levels were also measured by enzyme-linked immunosorbent assay (ELISA) in all of the above patients. We have introduced a new indicator named Ratio.V(Ratio.V = artery/liver * volum of the lesion) as a quantitative indicator which considering the volum of lesion measured in ture D mode. The Ratio(artery/liver) >1.0 was set as the gold standard to determine the activity of arteritis, according to the previous clinical studies.
Results: 34 patients in TKA group were determined to be active by ^{18}F-FDG PET/CT. The level of plasma PTX-3 in active TKA patients was significantly higher than that in non-active TKA patients (3.56±0.54 v.s. 1.15±0.09, $p<0.05$). PTX3 level was positively correlated with the Ratio.V (Spearman r=0.59,p<0.001). No significant correlation were found between the Ratio.V and the level of CRP or ESR (Spearman r=0.37 and 0.23, p =0.04 and 0.21). Under the guidance of ^{18}F-FDG PET/CT, the specificity of PTX-3 diagnosis was 79.41% and the sensitivity was 87.10%, and the area under the receiver operating characteristic curve (AUC) was 0.88. This result is significantly better than the results of CRP (76.47%,67.74%,0.72) or ESR(79.41%,58.06%,0.72).
Conclusion: The serum level of PTX3 was significantly correlated with the inflammatory activity of TKA detected by 18F-FDG PET/CT and its quantitative relevance was much better than CRP or ESR. The diagnostic efficacy especially sensitivity was also superior to that of CRP and ESR. PTX3 may better reflect the severity of TKA and may be a potential biological marker to monitor the disease status of TKA.

Authors listed for this abstract reported no relevant financial disclosures.

2105

The influence of time of flight (TOF) information on scatter fraction and the effect of scatter correction on ^{18}F-PET images. Saki Kimoto[1], Tomoya Hirose[1], Naoki Hashimoto[1], Ayano Shoji[1], Yuji Tsutsui[1,2], Kazuhiko Himuro[2], Shingo Baba, MD, PhD[2], Masayuki Sasaki, MD, PhD[3]; [1]Kyushu University, Fukuoka, Japan, [2]Kyushu University Hospital, Fukuoka, Japan, [3]Dept Rad Sci Sch of Health Sci Kyushu Univ, Fukuoka, Japan. (1770)

Purpose: The goal of this study was to examine the influence of time of flight (TOF) information on the scatter fraction and the effect of scatter correction (SC) on ^{18}F-PET images.
Materials and Methods: The examinations were performed using a NEMA IEC PET Scatter Phantom. The line source with ^{18}F solution was inserted into this phantom. The radioactivity concentration was 72.1 MBq/mL. The PET data were acquired 14 times using a Biograph mCT for 25 minutes each in the three-dimensional list mode. The scanner was equipped with a single scatter simulation algorithm for SC. The PET images were reconstructed using ordered subset expectation maximization (OSEM) and OSEM+TOF with and without scatter correction. A Gaussian filter was not used. The image matrix was 400×400, and the slice thickness was 5mm. Three regions of interest (ROIs) were established on PET images: ROI1 surrounding the line source for both true and scatter counts, ROI2 for the background around the line source and ROI3 for the entire phantom. The estimated percentage of scatter (%S) was calculated based on the ratios of scatter counts to the total counts of all 56 slices.
Results: On the OSEM, the %S was 25.8±0.5% for SC(-) and 6.6±1.1% for SC(+). On the OSEM+TOF, the %S was 27.2±1.5% for SC(-) and 6.0±0.7% for SC(+). The %S was not markedly different between OSEM images and OSEM+TOF images irrespective of SC.
Conclusions: In conclusion, the estimated percentage of scatter on ^{18}F-PET images were not influenced by TOF information. The effect of scatter correction was not markedly different regardless of the utilization of TOF information.

Authors listed for this abstract reported no relevant financial disclosures.

2106

A new powerful compact cyclotron. Samy Bertrand[1], Ilse Vaneycken[2], Tony Lahoutte[2], Peter Covens[3], Vicky Caveliers[3], Eric Kral[1], Jean-Michel Geets[4], Benoit Nactergal[1], Michel Ghyoot[1], Fabienne Devillet[5]; [1]IBA, Louvain La Neuve, Belgium, [2]Universitair Ziekenhuis Brussel, Brussels, Belgium, [3]Universitair Ziekenhuis Brussel, Louvain La Neuve, Belgium, [4]Couthuin, Belgium, [5]IBA, Louvain-la-Neuve, Belgium. (2932)

Objectives: 18F is one of the most used radionuclides (> 90%) in PET procedures and its demand will continue to raise. With the increasing number of fluorine-18 (18F) procedures (annual growth of more than 10% foreseen [5]), there is an urgent need for a more cost-effective and simple solutions allowing the production of much larger quantities of [18F]F-.
In order to respond to this the increasing market for 18F radionuclide IBA proposes a new mid-energy cyclotron, a state-of-the-art industrial cyclotron with maximal reliability, minimal maintenance requirements, energy-efficient, cost-efficient, fully automated and yet flexible. This cyclotron is capable of producing up to 300 µA of proton beam at 18 MeV; i.e. 30 Ci of 18F in 2 hours. A stable and circular beam optics is provided on the eight exit ports fixed around the horizontal median plane. High current proton beam can also be extracted to high power solid targets for 89Zr, 99mTc & other solid isotopes.
Methods: A proton only optimized cyclotron (18 MeV energy) has been designed using the well-known internal ion source, negative ions H- acceleration and stripping extraction. The technology is derived from the Deep Valley patented design [6], which significantly reduces total power requirement. The major innovations [1] to reach the required target current with such conditions were: - Construction process: smaller vacuum chamber volume and higher pumping capacity to allow better base vacuum. - Cyclotron core redesign: pole inserts to allow improved magnetic field symmetry over the accelerating path and gradient correctors on extraction path to obtain a near circular beam spot on the targets [2]. - New dual-stripper system for high beam current (2x 150 µA). The overall maintainability and beam performance stability were further improved thanks to an auto-positioning ion source system. The ion source is radially mounted on a bi-axial table, which movement regulation throughout bombardment can compensate thermal and mechanical effects. This further reduces the need for lengthy maintenance inside the cyclotron. The cyclotron is offered with the dual[4] proton source system for higher reliability and extended operating period. This hence can guarantee 300 µA on target over a lifetime exceeding 800 h without human intervention in the machine.
Results: Some technical challenges were faced to be able to maintain 300 µA steadily over time while using an internal ion source. Indeed, raising the ion source output inherently increases the amount of polluting gas that could deteriorate the cyclotron transmission. The combination of the different technologies described above demonstrated a sustainable target current over 300 µA with large security margin and excellent stability over time. Using IBA Conical [3] Fluorine target and dual bombardment, a production capacity of 30 Ci of 18F was successfully demonstrated, which meets the original requirements. The cyclotron design is at least twice more energy-efficient than a standard mid-energy PET cyclotron.
Conclusions: The cyclotron design is completed and the first units are already running in daily production. The complete design and first prototype validation were delivered in less than two years [1]. The UZ Brussel (Belgium) became today one of the State of the Art PET radioisotope production centres, achieving large batches of 18F with a cost-efficient industrial cyclotron solution.

Authors listed for this abstract reported no relevant financial disclosures.

2107

Management Impact of Prostate Cancer Imaging with Axumin. Patrick F. Wojtylak, NMTCB, PET, RT(R)[1], Elisha Fredman, M.D.[2], Bryan Traughber, M.D.[2,3], Rodney Ellis, M.D.[2], James O'Donnell, M.D.[4]; [1]Radiology, Nuclear Medicine, University Hospitals of Cleveland, Cleveland Medical Center, Cleveland, OH, USA, [2]Radiation Oncology, University Hospitals of Cleveland, Cleveland Medical Center, Cleveland, OH, USA, [3]Radiation Oncology, Louis Stokes Cleveland VA Medical Center, Cleveland, OH, USA, [4]Radiology, Nuclear Medicine, University Hospitals of Cleveland, Cleveland Medical Center, Cleveland, OH, USA. (1345)

Aim: Management impact of PET/CT Prostate Cancer Imaging with Axumin (18F-fluciclovine).
Objectives: To evaluate the impact of PET/CT imaging with Axumin (18F-fluciclovine) on clinical management choices for men with biochemical recurrence (BCR) of prostate cancer.
Methods: 81 patients underwent PET/CT imaging with suspected prostate cancer recurrence based on elevated prostate specific antigen (PSA) levels following prior treatment. All patients received 10 mCi Axumin (18F-fluciclovine) intravenous and were immediately imaged post injection from pelvis to top of the skull. Images sets were then reviewed for diagnostic quality by physicians experienced in clinical PET/CT with correlating of standard-of-care imaging which could include; CT and/or MRI of pelvis and bone scan imaging.
Results: 67 of the 81 patients had positive Axumin (18F-fluciclovine) scans. Of the 67 patients 18 then had osseous bone lesions and 21 lymph node involvement. 40 patients had standard of care imaging; 15 had MRI of prostate, 2 CT of pelvis and 23 had bone scan imaging. 41 had no other imaging studies. Patients had their clinical management changed when results of Axumin (18F-fluciclovine) PET/CT imaging were added to the standard-of-care diagnostic work-up.
Conclusions: PET/CT scanning with Axumin was seen as beneficial for the localization of recurrent prostate disease and changing their clinical management for men with biochemical recurrence (BCR) of prostate cancer.

60 male with adenocarcinoma of the prostate, s/p radical prostatectomy and LN dissection with rising PSA of 0.53.

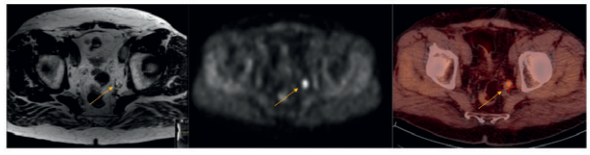

10 mm lesion within the left hemi-pelvis within the obturator space read on MRI as cystic changes. Axumin PET/CT shows radiotracer uptake is seen within the left deep pelvis lymph node which is suspicious for metastatic disease. Positive node findings on Axumin PET/CT changed patient radiation therapy management from microscopic dose (45 Gy) to full dose (72 Gy)

Authors listed for this abstract reported no relevant financial disclosures.

Tech Papers II: Cardiovascular Sciences and Pre-clinical Studies

Moderator: April Mann, MBA, CNMT, NCT, RT(N)
Co-Moderator: Thomas Morneau, CNMT

2108

Effect of different acquisition arcs on the appearance of each left ventricular wall in myocardial perfusion SPECT. Huang Kemin; the First Peoples Hospital of Foshan, Foshan, China. (46)

Aim: Effect of different acquisition arcs on the appearance of each left ventricular wall in myocardial perfusion SPECT
Background: Conventional Single-photon emission computed tomography (SPECT) myocardial perfusion imaging (MPI) is performed in the supine

position range RAO45°−LPO45°, but the effect of other acquisition arcs on imaging quality are not well described. In this study, we compared radioactivity activity over left ventricle walls as measured by different acquisition arcs to identify optima for specific applications.
Methods: In total,125 low-risk coronary heart disease patients underwent 99mTc-MIBI stress MPI, of which 52 received 360° acquisition with reconstruction using different 180° projections and the remaining 73 received conventional 180° (LPO45°−RAO45°) and left-side 180°(POST180°−ANT0°) acquisition consecutively. Statistically compare the radioactive activity and defect score of each left ventricular wall from different acquisition arcs. Voluntary informed consent was obtained from all study population, and I declare that the work described in this abstract has appropriate approval under local ethical rules.
Results: Myocardial slices reconstructed from POST180°−ANT0° yielded highest radioactivity uptake from inferior, lateral, and septal walls, LPO45°−RAO45° from the anterior wall, and LPO35°−RAO55° from the apical region. Compared to conventional 180° acquisition, the segments with decreased defect scores were observed in 27.67% (101/365) using left-side 180° acquisition. The proportion was significantly higher for males (P=0.035) and patients with high BMI (P=0.036). Segments with decreased defect score were mainly in inferior, septal, and lateral walls, and a greater proportion of males than females exhibited in inferior wall (P=0.004).
Conclusions: The different arc of data acquisition could significantly affect the appearance of each wall of the left ventricle, POST180°−ANT0° acquisition arc represents a useful and significantly enhanced imaging quality of inferior walls especially in males.
1

Authors listed for this abstract reported no relevant financial disclosures.

2109

Comparison of electrocardiogram synchronization and asynchronization in myocardial blood flow measurement with 15O-H2O PET. Shinya Kato, BSc[1], Tadao Aikawa[2], Masanao Naya, MD[3], Keiichi Magota, PhD[2], Osamu Manabe[4], Keisuke Kawauchi[5], Chietsugu Katoh, MD[6]; [1]Hokkaido University Graduate School of Biomedical, Sapporo, Japan, [2]Hokkaido University Graduate School of Medicine, Sapporo, Japan, [3]Hokkaido University, Hokkaido, Japan, [4]Hokkaido University, Sapporo, Japan, [5]Faculty of Health Siences,School of Medicine,Hokka, Sapporo, Japan, [6]Hokkaido University School of Medicine, Sapporo, Japan. (1666)

Purpose: Recently, many attempts to quantify myocardial blood flow from 15O-H2O myocardial dynamic PET have been reported. In this study, we developed a new method to estimate stable and accurate myocardial blood flow (MBF) in the ischemic myocardial lesion. It is hard to avoid the left ventricular (LV) wall motion artifacts in the conventional myocardial dynamic PET images. Therefore, in order to estimate accurate MBF, 15O-H2O Myocardial dynamic PET data and electro-cardiogram (ECG) are acquired at the same time, and we developed the software that extracts the end-diastolic myocardial data. Then, we analyzed the ECG-gated end-diastolic dynamic data and estimated rest and stress MBF, coronary flow reserve (CFR = stress MBF/ rest MBF) in the ischemic myocardial lesion. ECG gated myocardial dynamic PET would reduce heart beat motion artifact. Estimated CFR from the new method were compared with those from the conventional non-gated dynamic PET.
Methods: Twenty-seven patients with ischemic heart disease (67±11 years old, male 17, female 10) underwent dynamic 15O-H2O PET during rest and pharmacological (ATP) stress. We used Philips Gemini TF64. For each scan, 500MBq of 15O-H2O was infused slowly for 2min, dynamic data were scanned for 6min. Using list mode PET data and ECG signals, both non-gated dynamic data and ECG-gated end-diastolic data were reconstructed. Coronary arteriograms were also carried out for each patient, totally 50 ischemic segments with over 90% stenosis and 128 normal segments were evaluated in these patients. Single compartment model was used to estimate MBF and the perfusable tissue fraction (PTF). In addition, software for extracting end diastole images from ECG-gated PET data was developed using programming language C #, C++. Then we used visual studio 2017. Analyze and compare end-diastolic ECG-gated data and non-gated data.
Results: In the ischemic lesion, parameters (PTF, CFR and MBF) from ECG-gated dynamic PET and from non-gated PET were compared as follows. In the resting, PTF values from ECG-gated presented significantly lower (0.63 ± 0.09 (ml/ml)) than those from non-gated (0.72±0.09 (ml/ml)) ($p<0.001$). In the stress state, PTF values from ECG-gated yielded significantly lower (0.57 ± 0.10 (ml/ml)) than those from non-gated (0.65 ± 0.11 (ml/ml)) ($p<0.001$). CFR in the ischemic lesion, the former showed 1.23 ± 0.29, and the latter yielded 1.69 ± 0.71 ($p<0.001$). Beside in the normal site, the former presented 2.15 ± 0.76, the latter yielded 2.24 ± 0.79 (N.S), no significant difference was shown. MBF in the stress state, ECG-gated presented 1.00 ± 0.26 (ml/min/g), and non-gated yielded1.24 ± 0.44 (ml/min/g) ($p<0.001$), significant difference was shown.
Conclusions: In the ischemic lesion, ECG-gated PET estimated lower perfusable tissue fraction (PTF) than non-gated PET. This is shown that ECG-gated imaging decreased the LV wall motion artifact, and presented less blood fraction in the ischemic myocardial tissue ROI than the conventional imaging. More accurate estimation of PTF will lead to calculate more accurate MBF, and ECG-gated imaging dedicated lower MBF in the stress state than non-gated imaging.
In the normal site, no significantly different CFR were estimated between ECG-gated and non-gated imaging. However, in the ischemic lesion, significantly lower CFR were yielded with ECG-gated than with non-gated imaging. These results show that ECG-gated dynamic PET improves detecting ischemic myocardial lesions.

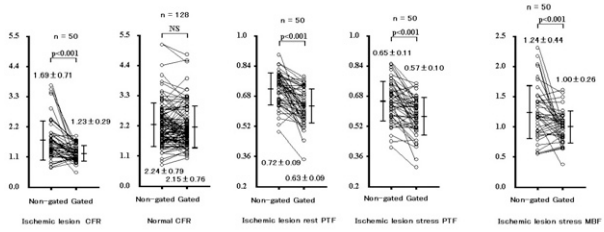

Authors listed for this abstract reported no relevant financial disclosures.

2110

The impact of myocardial counts and cardiac frames on phase analysis of gated myocardial perfusion SPECT. Ringo Tatami[1], Masahisa Onoguchi, PhD[1], Takayuki Shibutani[1], Hiroto Yoneyama, PhD[2], Koichi Okuda, PhD[3], Kenichi Nakajima, MD[4]; [1]Kanazawa University, Kanazawa, Japan, [2]Department of Radiological Technology, Kanazawa University Hospital, Kanazawa, Japan, [3]Kanazawa Medical University, Ishikawa, Japan, [4]Department of Nuclear Medicine, Kanazawa University Hospital, Kanazawa, Japan. (2636)

Purpose: The influence of acquisition protocols on phase analysis of gated myocardial perfusion SPECT (GMPS) has been investigated in previous studies. However, the dependence of phase parameters of GMPS on myocardial counts and the number of frames per cardiac cycle (cardiac frames) is unclear. The aim of this study was to assess the impact of myocardial counts and cardiac frames on phase parameters of GMPS.
Methods: A total of eighty-three patients (56 males, 27 females, 72.6±14.8 years) who underwent Tc-99m sestamibi or tetrofosmin GMPS were diagnosed as normal perfusion. Region of interest (ROI) was drawn on the myocardial part of the 45° left anterior oblique position for obtaining myocardial counts. The GMPS data was acquired using 16 cardiac frames. On the other hand, the GMPS data with 8 cardiac frames were converted from short axis images or projection data with 16 cardiac frames. Thus two types of the short axis images were created using 8 and 16 cardiac frames for phase analysis. The short axis images were reconstructed using filtered back projection (FBP) with Butter worth filter. Phase parameters of phase histogram SD (PSD), histogram bandwidth (BW), and entropy were evaluated by the correlations with myocardial counts and the differences between 16 and 8 cardiac frames using four software tools: Emory cardiac toolbox (ECTb; Syntermed, Atlanta, GA, USA), quantitative gated SPECT (QGS; Cedars-Sinai Medical Center, Los Angeles, CA, USA), cardioREPO (cREPO; FUJIFILM RI Pharma, Tokyo, Japan), and heart risk view-function (HRV-F; Nihon Meji-physics, Tokyo, Japan).
Results: Negative correlations between phase parameters using 16 cardiac frames and myocardial counts were found in all software tools. Moreover,

cREPO and HRV-F showed significant correlations. Following values were the mean phase parameters with standard error using 16 and 8 cardiac frames. PSDs (degree) were 13.2±0.7 and 17.4±1.0 for ECTb, 5.9±0.4 and 7.8±0.9 for QGS, 11.8±0.3 and 14.5±0.4 for cREPO, and 7.1±0.3 and 6.5±0.4 for HRV-F. BWs (degree) were 35.8±1.2 and 44.9±2.0 for ECTb, 24.0±1.2 and 25.0±3.0 for QGS, 46.0±1.3 and 59.3±1.5 for cREPO, and 25.3±1.1 and 23.3±1.0 for HRV-F. Entropys (%) were 26.6±1.0 and 28.6±1.0 for QGS, and 46.0±0.7 and 50.0±0.6 for cREPO. Phase parameters with 8 cardiac frames calculated by ECTb, QGS, and cREPO were significantly higher than those with 16 cardiac frames. However, HRV-F showed no significant difference between phase parameters with 16 and 8 cardiac frames. In addition, negative correlations between phase parameters using 8 cardiac frames and myocardial counts were also observed in all software tools, and HRV-F showed significant correlation.
Conclusion: This study indicated that myocardial counts and cardiac frames have an influence on phase analysis using GMPS.

Authors listed for this abstract reported no relevant financial disclosures.

2111

Direct Comparison of Supine and Prone SPECT Studies in Female Veterans Administration Patients Undergoing Myocardial Perfusion Imaging. Ejda Bajric, MHA, CNMT, NMTCB(CT), NCT, PET, NMTCB(RS)[1], Abbey Sundermeyer, BS, CNMT[1], Medhat M. Osman, MD, PhD, MS[2], Barbara Sterkel, MD[1]; [1]John Cochran VA Medical Center, Saint Louis, MO, USA, [2]St. Louis University, St Louis, MO, USA. (3016)

Objectives: cardial perfusion imaging (MPI) with SPECT is a well-established NM study that is usually used as the gatekeeper for invasive coronary angiography and evaluation of therapy effectiveness. Attenuation correction (AC) represents an important consideration to improve the specificity and normalcy rates of SPECT MPI. In hybrid SPECT/CT cameras, CT AC reduces inferior wall artifacts; however, registration errors between CT and SPECT images may result in anterior wall and apical artifacts. Given the high likelihood of attenuation from breast tissue, such artifacts are potentially more problematic in the female population. Furthermore, the additional radiation dose from the CT portion is concerning in women due to the high sensitivity of breast tissue to the potential carcinogenic effects of radiation. Prone imaging has been advocated as an alternative to CT AC, however its value in females is not well studied. For the purpose of increasing diagnostic clarity, we evaluated the addition of prone imaging for female Veteran Administration (VA) patients undergoing MPI.
Methods: Supine and prone stress images from 21 female patients undergoing MPI were retrospectively reviewed. All patients were imaged using a Siemens EVO gamma camera. Stress was achieved by either pharmacologic or exercise testing. Reconstructed perfusion images were reviewed in Cedars Sinai QPS by an American Board of Nuclear Medicine certified physician, unaware of the clinical information. The reader assigned a diagnostic code to each of the MPI studies after reviewing the rest and supine stress images. Diagnostic codes assigned were as follows: 1= Normal, 2= Probably Normal, 3= Indeterminant, 4= Probably Abnormal, and 5= Abnormal. The reader then reviewed each of the MPI studies with prone imaging, and a separate set of diagnostic codes were assigned. The two sets of diagnostic codes were compared.
Results: There was no change in 10 of 21 cases (48%); whereas the diagnostic code changed in the remaining 11 of 21 patients (52%). For 3 of the 21 patients (14%), the diagnostic code was changed from a 1 to a 5 or a 5 to a 1. A diagnostic code of 2, 3, or 4 was changed to a 1 or 5 in 7 of 21 patients (33%). Only the diagnostic code of one study (5%) was changed from a 1 or 5 to a 2, 3, or 4.
Conclusions: We continue to accrue data; however, our initial results show that adding prone SPECT stress imaging to supine SPECT stress imaging increases the diagnostic certainty for women undergoing MPI. Prone imaging may also eliminate the need for CT AC and minimize radiation exposure to the radiosensitive breast tissue of female patients.

Authors listed for this abstract reported no relevant financial disclosures.

2112

Thallium-201 washout rate analysis for myocardial perfusion SPECT using a CZT cardiac camera. Masaru Ishihara, MS[1,2], Masahisa Onoguchi, PhD[2], Takayuki Shibutani[3], Yasuyo Taniguchi, MD[4]; [1]Department of Radiology, Hyogo Cancer Center, Akashi, Japan, [2]Department of Quantum, Graduate School of Medical, Kanazawa, Japan, [3]Kanazawa University, Kanazawa, Japan, [4]Department of Cardiology, Hyogo Brain and Heart Center at Himeji, Himeji, Japan. (1181)

Objectives: For a diagnosis of coronary artery disease, the thallium-201-chloride (^{201}Tl) washout rate (WOR) is a valuable tool for assisting myocardial perfusion single-photon emission computed tomography (SPECT). Most of ^{201}Tl WOR analysis using a cadmium-zinc-telluride (CZT) cardiac camera is not investigated, and no differences in WOR values between CZT SPECT and conventional Anger-type SPECT have been reported. The present study aimed to verify the accuracy of the ^{201}Tl WOR analysis for myocardial perfusion SPECT using a CZT SPECT in the phantom study, and to compare it with conventional SPECT in clinical cases.
Methods: For CZT SPECT, a D-SPECT cardiac imaging system (Spectrum Dynamics Medical, Caesarea, Israel) was used. For the phantom study, myocardial phantom (model RH-2, Kyoto-Kagaku, Kyoto, Japan) was injected into the myocardium area with ^{201}Tl (52.6 kBq/mL), and 10-minute acquisitions were performed after 0, 24, 46 and 62 hours to reflect natural decay rates. The global WOR values were analyzed for 0 and 24 hours (infarction model), 0 and 46 hours (ischemia model), and 0 and 62 hours (normal model), respectively. Each value between the theoretical WOR as reference standard and the phantom WOR as measured were compared. For the patient study, 52 consecutive patients (mean age 73.1 ± 8.5 years, 36 [69.2%] men) were examined with ^{201}Tl stress/redistribution imaging (111 MBq for stress imaging) for ergometer (13 patients) or adenosine (39 patients). In all cases, CZT SPECT and conventional SPECT (BrightView; Philips Medical Systems, Cleveland, OH, USA) were performed as consecutive acquisition. CZT SPECT was performed with a 5-minute acquisition and conventional SPECT with a 10- to 12.5-minutes acquisition. Stress imaging was performed 5-10 minutes after the ^{201}Tl injection, and redistribution imaging was performed 3-4 hours later. The global WOR values were compared. Additionally, we compared the normal and multi-vessel disease myocardial perfusion patients in each of the two SPECT devices. Patient study results were calculated as the percent per hour. All differences between CZT SPECT and conventional SPECT were assessed using the Mann-Whitney U test.
Results: For the phantom study, the theoretical WOR values versus the phantom WOR values were 20.40% vs. 20.79% at 0 and 24 hours, 35.42% vs. 35.63% at 0 and 46 hours, and 44.53% vs. 45.13% at 0 and 62 hours, respectively. For the patient study, CZT SPECT versus conventional SPECT WOR values for 52 patients were 12.59 ± 2.26%/hour vs. 12.57 ± 2.27%/hour ($p = 0.984$); the stress-redistribution imaging time intervals were 3.47 ± 0.23 hours vs. 3.46 ± 0.22 hours. The CZT SPECT versus conventional SPECT WOR values for seven normal myocardial perfusion patients were 13.42 ± 1.53%/hour vs. 13.93 ± 1.24%/hour ($p = 0.338$), and for seven multi-vessel disease myocardial perfusion patients were 10.64 ± 2.20%/hour vs. 10.84 ± 2.26%/hour ($p = 0.848$).
Conclusions: ^{201}Tl WOR analysis using CZT SPECT demonstrated excellent accuracy in the phantom study. Clinically, ^{201}Tl WOR values obtained with CZT SPECT that enabled significantly reduced acquisition time were similar to those with conventional SPECT.

Authors listed for this abstract reported no relevant financial disclosures.

2113

Effects of fasting duration on mouse intestinal imaging of ^{18}F-FDG. Wenchang Xiao, PhD[1], Huanhuan Yan[1], Lu Wan[2]; [1]Huazhong University of Science and Technology, Wuhan, China, [2]Wuhan Raydata Technology Co., Ltd, Wuhan, China. (2491)

Purpose: 18F-Fludeoxyglucose (^{18}F-FDG) is a powerful radiotracer for Positron Emission Tomography (PET) scanning that has been wildly used in numerous researches and diagnostic applications, such as oncology, neurology, cardiology, and so on. Although ^{18}F-FDG has been proved

to be an ideal indicator of glucose metabolic status, the most appropriate procedures for intestinal imaging of ^{18}F-FDG still reminds unclear. Since ^{18}F-FDG uptake is highly affected by the fasting duration, we have focused on how the fasting duration affects the intestinal imaging of ^{18}F-FDG.
Materials and Methods: Mouse model: 6 adult male wild type C57BL/6J mice were equally divided into two groups: group A and group B. Mice of each group were fed in one cage together for 3 months. Reagents: 2-Deoxy-2-(^{18}F)fluoro-D-glucose (^{18}F-FDG) Equipments: Trans-PET ® BioCaliburn ® 700 (Raycan Technology Co., Ltd, Suzhou, China) Methods: Group A and group B mice were fasted before ^{18}F-FDG administration and PET scanning. In the first week, group A mice were fasted for 15 hours (hr) from 18:00 pm to 9:00 am in the next day, and group B mice were fasted for 6 hours from 8:00 am to 14:00 pm. Then Mice were injected with ^{18}F-FDG via tail vein 60 minutes (min) before they were placed on the PET bed for 14min PET static scanning (7min/bed, 2 beds, inhaled anesthesia with 2% isoflurane). In the second week, group B mice were fasted for 15hr from 18:00 pm to 9:00 am in the next day, and group A mice were fasted for 6hr from 8:00 am to 14:00 pm. Then the following operations were administered as above. In the following 4 weeks, mice of group A and group B received 15hr and 6hr fasting as above in turns until both group were processed 3 times for both fasting duration. Last, images were analyzed together.
Results: ^{18}F-FDG PET scanning images of each group in the same experiment showed that intestinal images of the same group were similar. As mice fed in same cage were usually with the parallel gut microbiota, the similarity above was reasonable. We also found that imaging quality and SUV(Standard Uptake Value) of 3 times experiences of each group with same fasting duration were stable. Interestingly, ^{18}F-FDG PET images of fasting duration for 15hr were more distinct t than that of 6hr of the same group.
Conclusion: Intestinal ^{18}F-FDG PET scanning images are similar in mice fed in the same cage, and stable for multiple testing during a short period, such as in one month. More importantly, 15hr fasting duration overnight is better than 6hr for intestinal ^{18}F-FDG PET imaging.

Authors listed for this abstract reported no relevant financial disclosures.

2114

The assessment of myocardial images in simultaneous acquisition by SPECT and PET tracer with a novel small animal phantom.
Takayuki Kanno[1], Masahisa Onoguchi, PhD[1,2], Takayuki Shibutani[1,2], Shun Ogihara[2], Akiho Tanaka[2], Takafumi Mochizuki[3], Kazuhiro Shiba, PhD[4]; [1]Department of Quantum Medical Technology, Graduate School of Medical Sciences, Kanazawa University, Kanazawa, Japan, [2]Department of Radiological Technology, School of Health Sciences, Kanazawa University, Kanazawa, Japan, [3]Knazawa Advanced Medical Center, Kanazawa, Japan, [4]Division of Tracer Kinetics, Advanced Science Research Center, Kanazawa university, Kanazawa, Japan. (1925)

Aim: A small-animal SPECT-PET/CT system enables simultaneous submillimeter imaging of single-photon and positron-emitting radio labeled tracers. The combination of ^{18}F-FDG and ^{99m}Tc labeled flow tracer has an important role in the assessment of myocardial viability, although it is possible that the down scatter from ^{18}F tracer would influence ^{99m}Tc images. The purpose of this study was to create a novel small animal phantom and evaluate myocardial ^{99m}Tc and ^{18}F images obtained by only ^{99m}Tc acquisition or dual-isotope simultaneous acquisition (DISA) with the phantom.
Methods: Data acquisition was performed using a small animal SPECT-PET/CT system equipped with a clustered multi-pinhole collimator. We created a small animal phantom simulated myocardium, liver, lungs and spine. In particular, a myocardial phantom could imitate defective area attaching an insert on inferior wall. The phantoms except for spine were filled with solution containing either only ^{99m}Tc or both ^{99m}Tc and ^{18}F. Projection data was reconstructed by a pixel-based ordered-subsets expectation maximization algorithm with the Gaussian filter. For assessment, the percentage of uptake (%uptake) was calculated using a polar map for normal and defective myocardial images obtained by only ^{99m}Tc acquisition or DISA. In addition, the circumferential profiles were generated by reconstructed short-axis slices of the defective myocardial phantom.
Results: In the normal myocardium, %uptake of only ^{99m}Tc image was from 81% to 94% and %uptake of ^{99m}Tc and ^{18}F image in DISA was from 80% to 90% and 73% to 95%, respectively. In addition, the average %uptake in defective segments was 72.5% for only ^{99m}Tc image and 71.5% and 81.5% for ^{99m}Tc and ^{18}F image in DISA, respectively. In the circumferential profiles at slices which had defective area, the minimum value for ^{99m}Tc and ^{18}F image in DISA was respectively 8.9% and 32.4% higher than only ^{99m}Tc image.
Conclusions: It was suggested that we might sufficiently assess the myocardial images acquired by simultaneous ^{99m}Tc and ^{18}F as well as only ^{99m}Tc under the condition of this study with a small-animal SPECT-PET/CT system.

Authors listed for this abstract reported no relevant financial disclosures.

MONDAY SESSIONS

Tech Papers III: Diagnostic & Therapeutic Nuclear Medicine

Moderator: Thomas M. Morneau, CNMT
Co-Moderator: Mary Beth Farrell, MS, CNMT, NCT, FSNMMITS

2115

Efficient Clinical Workflow for a Superfast Breast Lymphoscintigraphy Imaging Technique. Martha Mar[1], Scottie Jones[1], Homer A. Macapinlac, MD[2], Yang Lu[1]; [1]MD Anderson Cancer Center, Houston, TX, USA, [2]UT M.D. Anderson Cancer Center, Houston, TX, USA. (3011)

Background: Breast lymphscintigraphy to guide a sentinel lymph node biopsy (SLNB) is the standard of care for axillary nodal staging in patients with invasive breast cancer and clinically negative nodes. The injection procedure is painful, and variation in proficiency exists among operators. The optimal injection technique has been the subject of lively debate. And most lymphoscintigraphy methods require multi-time point scanning to ensure visualization of SLN. To improve patient experience and clinical workflow efficiency in our busy clinical service, we designed a "superfast" and efficient breast lymphscintigraphy workflow, with total 2 minutes of image acquisition time (1min/view x 2) versus traditional 30minutes image acquisition time. We set to evaluate the clinical workflow efficacy for this "superfast" breast lymphoscintgraphy imaging technique.
Methods: Based on our physicians' experience and group discussion, a "superfast" breast lymphscintigraphy technique was developed. The method utilized periareolar/peritumor intradermal injection technique, with images obtained immediately post injection. For every breast lymphoscintigraphy, only one-minute transmission anterior and one-minute transmission lateral images would be obtained. If no draining lymph node visualized on these 2-min images, further delayed images would be obtained. For the first 20 cases, immediate 1-min transmission only images were compared with standard image set consists of ten-minute emission and three-minute transmission anterior, posterior and lateral images. Imaging quality and scanner acquisition time were evaluated at department meeting with consensus among physicians and technologists. Pathology results of the SLNs and correlative clinical information were reviewed at time of data analyses.
Results: Among the 20 patients underwent the "superfast" breast lymphoscintigraphy, 19/20 showed immediate lymphatic drainage, 1/20 showed delayed lymphatic drainage at 1hr post injection, which become more obvious at 3hr post injection. The delayed visualization of SLN in the one patient is probably due to the patient's history of breast reduction surgery, which destroyed local lymphatic vessel. Nonetheless, all the "superfast" images (1min/view) are satisfying to our group physicians, and demonstrated no inferior image quality comparing with the prior standard images acquired with longer scanner time. Follow up pathology results of the biopsied SLNs with satisfying clinical results, and no false negative SLN results within 4 months follow up. Feedback from nuclear medicine technologists are in favor of the "superfast" imaging technique, as the 2 minute scanner time minimized patient waiting time and streamline the clinical workflow thereafter. Furthermore, with the improvement of injection technique, delayed images were rarely needed. There has been a decrease related to technologist overtime tied to this procedure as the change in the scanning protocol has resulted in fewer patients needing to have a delayed or second procedure.
Conclusion: Acquiring immediate one-minute transmission anterior and lateral breast lymphoscintigraphy images improved the clinical workflow by allowing the flexibility of broader scan times dependent on clinical volumes. Decreasing the imaging time from 30min to 2min acquisition time decreased the amount of patient imaging time on the scanner, shortened the patient's length of stay in our department and opened up the scanner for higher patient volumes.

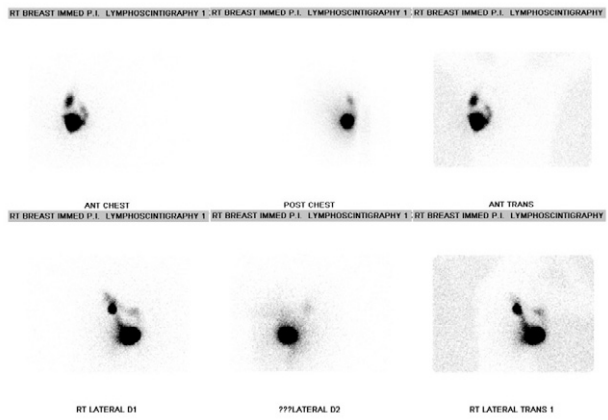

Authors listed for this abstract reported no relevant financial disclosures.

2116

Molecular Breast Imaging: Reasons for Modification of Views Acquired. Lacey R. Ellingson, CNMT[1], Tiffinee Swanson[1], Thuy T. Tran[1], Courtney M. Solberg, CNMT[1], Ashlee L. Stanke[1], Amy L. Conners, MD[1], Katie N. Hunt, MD[1], Deborah J. Rhodes, M.D.[1], Michael K. O'Connor, PhD[2], Carrie B. Hruska, PhD[1]; [1]Mayo Clinic, Rochester, MN, USA, [2]Radiology, Mayo Clinic, Rochester, MN, USA. (1522)

Objectives: Molecular breast imaging (MBI) is a functional imaging technique of the breast that uses Tc-99m sestamibi and a dedicated gamma camera and has shown utility in detecting mammographically-occult cancers in women with dense breast tissue. The typical patient imaging protocol for MBI in use at our institution comprises bilateral craniocaudal (CC) and mediolateral oblique (MLO) views acquired for 10 min per view. Occasionally, this protocol may be modified for special clinical situations such as large breasts or difficulty visualizing a lesion. Our objective was to examine the frequency of using a modified protocol in our practice and the reasons why it is used.
Methods: We performed a retrospective review of all patients undergoing MBI at our institution from January to October 2017. MBI examinations and records were reviewed to assess the number of patients with a modified protocol and the reason for the modification.
Results: In a total of 981 patients who underwent MBI, a modified protocol with views differing from the typical CC/MLO protocol was used in 22 (2.2%) patients. Three types of modifications were noted: tiled MLO views (N=11), tiled MLO views with an additional CC view (N=5), or the typical CC/MLO protocol with additional views (N=6). A tiled MLO protocol was used in 11 (1.1%) patients. Tiled MLO refers to acquisition of 2 MLO views - one of the superior and one of the inferior breast - instead of the typical CC/MLO protocol (Figure 1). This tiled MLO protocol was used at the technologists' discretion for patients with larger breasts exceeding the detector field of view (20" x 16"; LumaGem, Salem, NH). Tiled MLO views allow visualization of all or most of breast tissue while not extending the total exam time. In 5 (0.5%) patients, the tiled MLO protocol was performed with an additional view in the CC projection due to presence of a lesion seen on one of the MLO views (N=3) or to obtain a nipple in profile view as the nipple appeared rolled in the initial views (N=2). This additional CC view allows the radiologist to better determine lesion location. In 6 (0.6%) patients, additional views beyond the typical CC/MLO protocol such as exaggerated cranial caudal (XCC) view, medial lateral (ML) view, or an axillary tail (AT) view were acquired. Additional views were acquired in cases where a lesion was seen on the edge of the FOV (N=5). In a single patient (N=1), additional views with the nipple in profile were performed as the nipple appeared rolled on the original acquisition.
Conclusions: Although use of a modified protocol was rarely performed, special situations such as large breasts and lesions at the edge of the detector FOV may benefit from tiled views or additional views on MBI.
Figure 1: Images of a tiled MLO protocol:

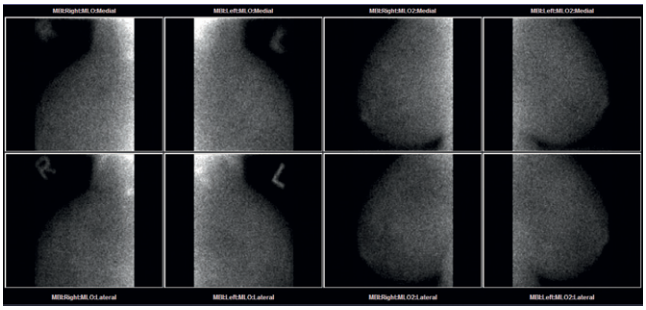

Authors listed for this abstract reported no relevant financial disclosures.

2117

PET/MR Technologist. Peter V. Kamvosoulis, BS, PET, RT[N, CT, MR]; Magnetic Resonance, Memorial Sloan Kettering Cancer Center, New York, NY, USA. (1264)

Objectives: The objective of our investigation was to determine the effect of an MR field on the PET imaging of a prompt gamma emitter, specifically Yttrium-86. We conducted phantom simulations to test the hypothesis that results of the Y-86 phantom acquisitions in a PET/CT scanner and PET/MR scanner would correlate.
Methods: Data were analyzed retrospectively for 5 patients to establish realistic Y-90 SIRT therapeutic doses from which to determine a Y-86 dosimetry dose in a phantom test area. The determination was made that a 40:1 ratio of Y90:Y86 is necessary for a successful Y86 dosimetry/imaging session followed by a successful Y-90 SIRT post therapeutic imaging session, both imaged with either or both PET/CT and PET/MR. One subsequent phantom experiment was run using a Jaszczak phantom with Y-86 (14 hour half-life) on a GE Signa PET/MR followed by the same phantom on a GE 710 PET/CT. Six cylindrical regions of the phantom were filled with similar activities at a concentration of 10uCi/cc, approximately 600uCi in total. The phantom was imaged in the PET/MR field at one bed position (25cm) for 10min and imaged in the PET/CT field at two bed positions (15cm/bed) for 3min/bed. CTAC and MRAC were performed prior to each scan, CTAC actual and MRAC derived from database. Using a third party processing software one manually drawn ROI was simultaneously placed over each ROI in each phantom, thus ROI 1 in the MR field coincides directly with the same ROI in the CT field to produce the following correlative graph.
Results: Maximum initial background and decay-corrected region of interest (ROI) counts per pixel were higher for the PET/MR scanner versus the PET/CT scanner (MR_{mean} 238,576 versus CT_{mean} 184,879, a 129% difference). The MR field ROI data ranged from 200,935 to 282,504 and the CT field ROI data ranged from 140,155 to 194,523. The MR and CT data correlate strongly (r^2=0.95, p<0.0001).
Conclusions: The higher photon counts in the MR field reveal that the PETMR system is slightly more sensitive to obtaining photon data, and that the MR field has no impact on the prompt gamma emitter, Y-86. Further research is necessary to validate this conclusion.

Authors listed for this abstract reported no relevant financial disclosures.

2118

The synthesis and study of 3PRGD$_2$-Pyro for targeted photosensitizer. Shi Gao[1], Xiaoguang Ge[2]; [1]China-japan Union hospital of Jilin University, Changchun, China, [2]China-japan Union hospital of Jilin University, Changchun, Jilin, China. (1361)

Objectives: Photodynamic therapy (PDT) is a promising treatment for cancer. Photosensitizer (PS) plays an important role in photodynamic therapy. A hydrosoluble and targeted PS was synthesized by modifying pheophorbide a (Pyro) with E[PEG4-c(RGDfK)]2(3PRGD2), In addition, its application value was further investigated in this study.
Methods: High Performance Liquid Chromatography (HPLC) and Mass Spectrum (MS) were used to analysis the purity and molecular weight of PS (3PRGD$_2$ -Pyro). A549 cells was treated with Pyro, Pyro +PDT, 3PRGD$_2$-Pyro and 3PRGD$_2$-Pyro +PDT, respectively. Then the cell viability and 50% inhibition concentration were calculated by MTT assay. The confocal laser scanning microscopy was used to research the targeting in vitro of 3PRGD$_2$-Pyro. The distribution of 3PRGD$_2$-Pyro in vivo was evaluated by in vivo imaging system with subcutaneous A549 xenograft mice injected Pyro and 3PRGD$_2$-Pyro. In vivo, we administered PBS, Pyro +PDT, 3PRGD$_2$-Pyro +PDT through vena caudalis to each group of athymic nude mice with A549 tumors. And the volume of tumors were examined to detect the therapeutic effect of PDT.
Result: The purity of 3PRGD$_2$-Pyro was greater than 98%. In addition, the water solubility of 3PRGD$_2$-Pyro was much better than Pyro. In MTT assay, 3PRGD$_2$ -Pyro exhibited significant photocytotoxicity in A549 cells and lower darktoxicity. Pyro modified with 3PRGD$_2$ reduced the survival rate of cells, and the 50%inhibition concentration for 3PRGD$_2$-Pyro is 0.1μM,which is much lower than the 50%inhibition concentration for Pyro (0.3μM). The confocal laser scanning microscopy revealed that 3PRGD$_2$-Pyro is well targeted to the cytomembrane of A549 cells. Through in vivo imaging system, it can be observed obviously that 3PRGD$_2$-Pyro was abundant in tumor, while the uptake of Pyro in tumor was lower than that of 3PRGD$_2$-Pyro. For the therapeutic effect of PDT, 3PRGD$_2$-Pyro +PDT group can obviously reduced the tumor size, and the tumor disappeared after a week's treatment. In addition, the decrease of tumor size was slower in Pyro +PDT group when compared to 3PRGD$_2$-Pyro +PDT group, suggesting Pyro laser radiation constrain the tumor growth.
Conclusions: In summary, targeted and hydrosoluble 3PRGD$_2$-Pyro with lower darktoxicty exhibited satisfactory effect in photodynamic therapy, which should be of great potential in photosensitizer.

Authors listed for this abstract reported no relevant financial disclosures.

2119

Comparison of liver-spleen ratios in radiocolloid SPECT/CT scintigraphy with attenuation correction and without attenuation correction. Shashi P. Khandekar, CNMT[1], Donald R. Neumann, MD, PhD[2], Nancy A. Obuchowski, PhD[2], Sagar Patel[2]; [1]Nuclear Medicine, Cleveland Clinic Foundation JB-3, Cleveland, OH, USA, [2]Cleveland Clinic, Cleveland, OH, USA. (1222)

Objectives: SPECT/CT imaging is fast becoming the preferred modality for uptake ratios for the scintigraphic diagnosis of cirrhosis or hypersplenism. The primary objective of the study was to compare the liver-spleen ratio on SPECT/CT with attenuation correction (AC) to that of SPECT/CT without attenuation correction (no AC).
Methods: This is a retrospective study of 78 consecutive subjects referred for radiocolloid scintigraphy. All subjects underwent both planar and SPECT/CT imaging after I.V. administration of Tc99m sulfur-colloid (range 5.0-5.5mCi). ROIs were drawn on transverse SPECT tomograms with AC. Similar ROIs were drawn on corresponding SPECT tomograms without AC. Liver-spleen ratios were calculated.
Results: The SPECT with AC liver-spleen ratios ranged from 0.10 to 40.4 with a median of 1.31 (SD=4.46) and SPECT without AC liver-spleen ratios ranged from 0.36 to 19.5 with a median of 1.26 (SD=2.11). The SPECT liver-spleen ratios with AC and without AC were highly correlated (r=0.99, P value < 0.001). The mean SPECT liver-spleen ratio with AC was significantly higher than the mean SPECT liver - spleen ratio without AC, with an estimated difference of 0.32 (p=0.008). The best fitting relationship is linear with intercept of 0.004 and linear slope of 1.04 (with 95% < 1 of [0.93, 1.15]). See table 1

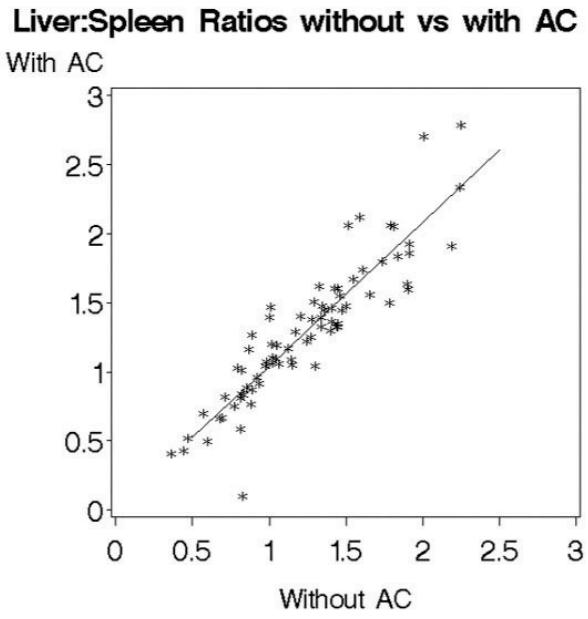

Conclusions: Liver-spleen ratios on SPECT with attenuation correction are not significantly different from the liver-spleen ratios on SPECT without attenuation correction.

Authors listed for this abstract reported no relevant financial disclosures.

2120

Hotair could be used as biomarker for assessing the therapeutic effect in thyroid cancer patients. Peng Fu, PHD; Nuclear Medicine, The First Affiliated Hospital of Harbin Medical Un, Haerbin, China. (1877)

Objectives: This research aimed to the relation of long chain non-code RNA HOTAIR expression in serum with the efficiency of thyroid cancer treatment in radionuclide ^{131}I.
Method: Total thyroidectomy was amid to 62 patients with thyroid papillary carcinoma before ^{131}I radionuclide therapy.The serum of patients after total thyroidectomy were collected.The free RNA of serum was extracted by Trizol LS. Fluorescent Quantitation Polymerase Chain Reaction was applied to evaluate the expression of long chain non-code RNA HOTAIR.The therapeutic effector was evaluated through comparing HOTAIR expression before and after treatment in Paired t test.
Result: The result showed that there was a significant difference in the expression of HOTAIR before and after treatment.The HOTAIR relative expression was 1±0.71 and 0.29±0.09 before and after treatment, respectively(p=0.026).It meant statistical significance in HOTAIR between before and after treatment.
Conclusion: Paired t test indicated that HOTAIR relative expression was lower significantly after treatment than before treatment in thyroid papillary cancer patients.Taken together,these data meant that HOTAIR relative expression could have associated with therapeutic efficacy of patients with thyroid papillary carcinoma,which could be used as serum biomarker for assessing the therapeutic effect of thyroid papillary carcinoma.
Key words: Radionuclide; ^{131}I; HOTAIR; thyroid papillary carcinoma

Authors listed for this abstract reported no relevant financial disclosures.

2121

Preferred Criterion for Deciding Laparoscopic Cholecystectomy for Patients with Chronic Cholecystitis Using Radionuclide Tc99m Hepatobiliary Scans. Duy Tran, R.T (N), CNMT, NMTCB (CT)[1], Cheryl L. Rickley, CNMT[2], Charles M. Intenzo, MD[2], Sung M. Kim, MD[3]; [1]Nuclear Medicine, Thomas Jefferson University Hospital, Philadelphia, PA, USA, [2]Thomas Jefferson University Hospital, Philadelphia, PA, USA, [3]Thomas Jefferson Univ. Hosp., Philadelphia, PA, USA. (1874)

Objectives: To determine what gastroenterologist prefer for laparoscopic cholecystectomy when using Tc99m hepatobiliary scans.
Methods: 33 patients who were diagnosed with chronic cholecystitis were evaluated in whether or not would have laparoscopic cholecystectomy. The 33 patients fell within 3 categories:
1: Gallbladder ejection fraction (GBEF) <35%
2: No Gallbladder (GB) visualized after 1.5 Hr but bowel visualized
3: Delayed Gallbladder visualization after 1 Hr with bowel activity
Technique: Patient are to be NPO for at least 4 hrs. A hepatobiliary scan was obtained following IV administration of 7 mCi Tc99m Choletech, dynamic imaging for 1 hr was obtained. If necessary, additional static images were also obtained at 90 mins. Additionally, ordering physicians may want to determine GBEF so fatty meal or CCK was given.
Results: 24 out of 33 patients with chronic cholecystitis ended up with laparoscopic cholecystectomy. 8 out of 19 patients with GBEF <35% ended up with laparoscopic cholecystectomy. 9 out of 11 patients with NO GB after 1.5 Hr but bowel visualization ended up with laparoscopic cholecystectomy. And 2 out of 2 patients with delayed GB visualization with bowel had laparoscopic cholecystectomy. 7 of out the 33 patients had no data or follow up on whether they had surgery.
Conclusions: Use of Tc99m hepatobiliary scans is pertinent on whether or not patients undergo laparoscopic cholecystectomy. Of the 3 categories, No GB after 1.5 Hr but bowel visualization seems to be the highest choice for gastroenterologist.

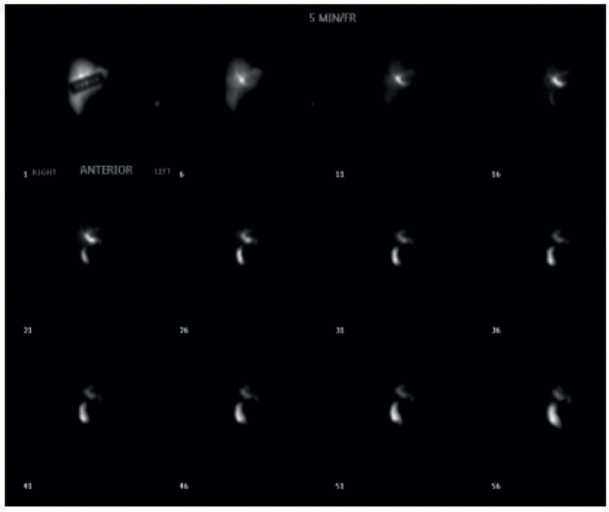

Dynamic 5 min/frame

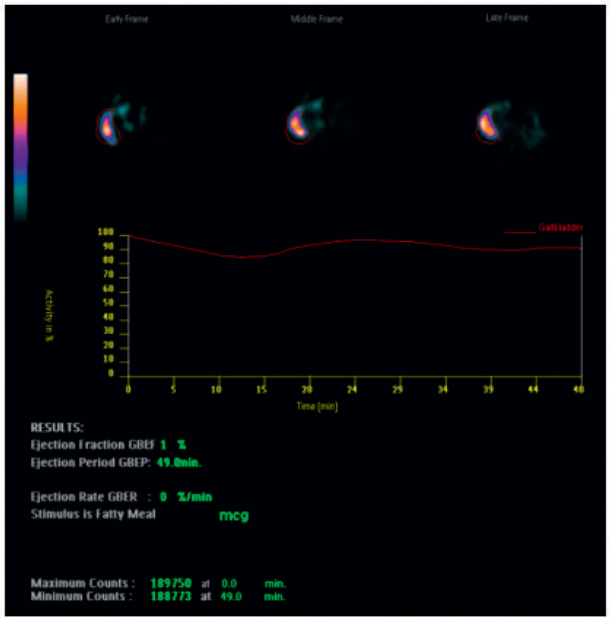

Authors listed for this abstract reported no relevant financial disclosures.

Tech Papers IV: Instrumentation & Data Analysis

Moderator: Mary Beth Farrell, MS, CNMT, NCT, FSNMMITS
Co-Moderator: Thomas M. Morneau, CNMT

2132

Comparison between Poisson Resampling and List Mode Bone Scan Using a CZT Whole-Body Gamma Camera. Atsushi Kondo[1,2], Yuuki Miyazaki[1], Masafumi Takahashi[1], Toshihiko Ehara[1], Kenji Koga[1], Tomohiko Yamane, MD, PhD, FANMB[3], Ichiro Matsunari, MD[4]; [1]Saitama Medical University Hospital, Iruma-gun, Japan, [2]Graduate School of Human Health Sciences, Tokyo Metropolitan University, Tokyo, Japan, [3]Department of Nuclear Medicine, Saitama Med. Univ. International Med. Center, Hidaka, Japan, [4]Division of Nuclear Medicine, Department of Radiol, Saitama Medical University Hospital, Iruma-gun, Japan. (2712)

Objectives: Poisson resampling has been introduced as a tool to simulate short time acquisition/low dose images. However, its validation is a challenge in clinical settings because of necessity for repeated acquisitions. The recently introduced novel whole-body gamma camera with cadmium-zinc-telluride (CZT) detectors (Discovery NM/CT 670 CZT) is capable of generating true short time acquisition images without additional scans using list mode. The aim of this study was to compare Poisson resampling simulation with list mode bone scan images using the CZT-based whole-body camera.
Methods: We enrolled a total of 29 consecutive patients (55-88 y, median 77 y, Female 9, Male 20) who underwent bone scan for the detection of bone metastasis from prostate cancer (n = 16), lung cancer (n = 8), breast cancer (n = 3), and hepatocellular carcinoma (n = 2). Bone scan images were acquired in the list mode for 15 minutes. Then, the 10 min, 5 min, 3 min, and 1 min images were generated using the lister tool. Similarly, simulated images were generated using Poisson resampling. On each generated image, bone scan index (BSI) was calculated as a quantitative index of abnormality using an automated analysis software (BONENAVI). The relationship between Poisson resampling and list mode images was assessed by intra-class correlation coefficient (ICC).
Results: Injected Tc-99m labeled radiotracer dose was 789.7 ± 69.5 MBq (average ± standard deviation). Average count of anterior and posterior whole-body image was 2,333,966 ± 464,433 on the 15 min image. The ICCs of BSI between the Poisson resampling vs list mode for the 10 min, 5 min, 3 min, and 1 min images were 0.997 (0.994-0.999), 0.995 (0.990-0.998), 0.978 (0.962-0.989), 0.938 (0.868-0.971), respectively.
Conclusions: Our data show that the short time acquisition bone scan images simulated by Poisson resampling were closely correlated with those by list mode when BSI was used as a quantitative index of abnormality. Thus, Poisson resampling provides a reliable alternative to true short time acquisition images.

Authors listed for this abstract reported no relevant financial disclosures.

2133

Evaluation of the consistent between cerebral perfusion and glucose metabolism to reflect brain function by simultaneous PET/MRI, a preliminary study. Weiwei Ruan, PhD[1], Fang Liu, MD[2], Xiaoli Lan, MD, PhD[3]; [1]Wuhan Union Hospitol, Wuhan, China, [2]Union Hospital, Wuhan, China, [3]Dept Nuclear Medicine, Wuhan Union Hospital, Wuhan. (2746)

Objectives: Cerebral glucose metabolism and cerebral perfusion are usually in principle coupled. The cerebral glucose metabolism is well established to reflect the change of brain function. Cerebral perfusion is also highly related with neural activity, which is also one of important surrogate markers of brain function. Some studies suggest that measured cerebral glucose metabolism and cerebral perfusion have reasonable correlations[1]. However, the consistent between cerebral perfusion and glucose metabolism to reflect the change of brain function in cognitive impairment by simultaneous PET/

MR has not been reported before. In this study, the glucose metabolism data, standard uptake value (SUV), from fluorine-18 fluoro-deoxyglucose (F-FDG) positron emission tomography (PET) and the cerebral blood flow (CBF) from arterial spin labeling (ASL) MRI were acquired from three patients who had mild cognitive impairment by simultaneous PET/MRI, which were used to evaluate the consistent between perfusion and glucose metabolism to reflect the brain function.

Methods: Three patients who had mild cognitive impairment were scanned by GE SIGNA PET/MRI (3.0 T). The brain PET, ASL MRI and three-dimensional (3D) T_1 weight images were obtained at the same position and the beginning time for PET and MRI scanning was also consistent, 40 min after injecting ^{18}F-FDG (0.1 mCi/kg). The total scanning time for PET was 15 min. The scanning parameters of MRI were as follows: ASL (postlabel delays=2000 ms, TE/TI/TR=10.7/2015/4852 ms, slices=36 and matrix=128×128) and 3D T_1 weight imaging (flip angle=12°, TE/TI/TR=2.6/450/7.0 ms and matrix=256×256). The ^{18}F-FDG data were attenuation corrected by a zero TE sequence (ZTE). The DICOM data including standard uptake value (SUV) maps, CBF maps and T_1 images of brains were exported and processed by SPM12 (http://www.fil.ion.ucl.ac.uk/spm/download/) and MATLAB 2016a (Mathworks, Natick, MA, USA). The 3D T_1 structural images were smoothed and segmented to obtain the gray matter mask and white mask. The SUV maps and CBF maps were all co-registered with the corresponding structural images. With the gray and white mask, the SUV and CBF distribution in the gray and white matter could be obtained, respectively. The CBV and SUV were then all normalized for better comparison. A linear regression analysis was conducted on pixel-by-pixel to evaluate the correlation between CBV and SUV in the gray matter and white matter, respectively.

Results: Fig.1 displayed the distribution of the normalized SUVs (left) and CBF values (right) through the box-plots in the gray matter and white matter, respectively for the three patients. The box-plots suggested that the distributions between the SUV and CBF were almost consistent for the three patients. Fig.2 displayed the scatter plots between the SUVs (vertical axis) versus CBF values (horizontal axis) from all pixels in the gray matter and white matter, respectively. The corresponding linear fitting curves and regression coefficient r were also displayed. The SUV was relatively correlated with the CBF in the gray matter and white matter. And the correlation was seemingly higher in the white matter ($r>0.5$, $p<0.00$) compared to that in the gray matter.

Conclusions: The simultaneous PET/MRI make the T_1 structural images and functional images, including ASL and FDG PET obtained at the same position and nearly same time, which was very good for the co-registration and analysis of consistent between the CBF and SUV. ASL is a MRI technique used to assess cerebral blood flow, which become increasingly popular due to the noninvasive nature. The CBF obtained by ASL might provide FDG like brain data, an opportunity for combined specific tracer PET/ASL MRI applications.

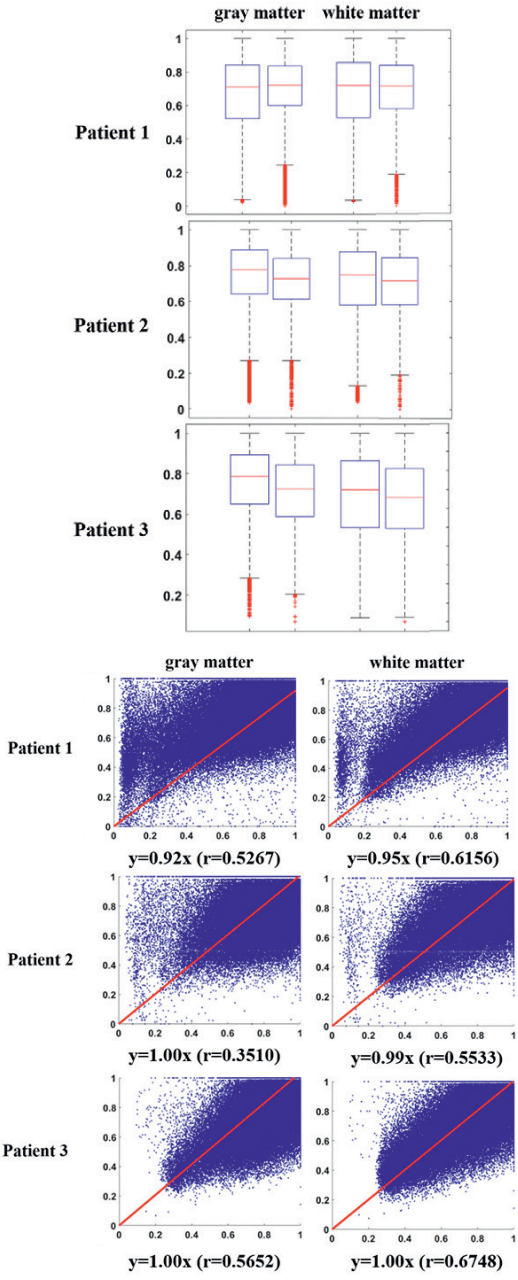

Authors listed for this abstract reported no relevant financial disclosures.

2134

Technical aspects of PET/CT phantom data collection and submission utilizing a newly developed Joint-Commission (JC) compliant phantom program. Lisa Dunnwald, MPH, PET, CNMT, John J. Sunderland, PhD; University of Iowa, Iowa City, IA, USA. (3071)

Objectives: The Joint Commission (JC) released annual performance evaluation requirements for PET imaging systems in 2015 with limited guidance on best practices to achieve compliance in meeting the newly defined standards. Recognizing that over 80% of hospitals are JC accredited, and the potential demand for assistance in meeting JC requirements, we tested a prototype JC compliant phantom program that provides detailed technical instructions for phantom filling and data upload. In return, the end-user receives a comprehensive evaluation of scanner performance designed to meet JC requirements, including correctable actions, if warranted.

Methods: The JC compliant phantom program requires acquisition of: (1) an off-axis uniform cylinder phantom, and, (2) either a NEMA

Image Quality (IQ) phantom (at 4:1 contrast) or SNMMI Clinical Trials Network (CTN) oncology phantom (at 4:1 contrast). All 3 phantoms were prepared and scanned for purposes of evaluating the phantom program. Uniform and NEMA phantom preparation required a precision scale for measuring weight of phantom and water. Phantom fills were performed using [^{18}F]-FDG dilutions and scan start times were approximately one hour post the initial [^{18}F]-FDG assay. Scan acquisition and reconstruction parameters were per our institutional standard FDG oncology protocol as per program instructions. Image data and phantom fill data documentation were uploaded using a password-protected log in to access the cloud-based server.
Results: Automated phantom analysis software downloaded and analyzed data, generating a full JC compliant scanner performance report in PDF format. System reconstructed resolution, system uniformity, absolute calibration, noise assessment, a recovery coefficient curve, lesion detectability, and artifact assessment were included in the report. A medical physicist reviewed images and the report for final approval.
Conclusion: The JC compliant phantom program provides detailed technical instructions for phantom filling, acquisition, and data upload for any skilled technologist to follow. Generated reports easily delineate scanner performance metrics and JC compliance.

Authors listed for this abstract reported no relevant financial disclosures.

2135

Clinical practicality of quantitative 99m-MDP SPECT/CT in patients with breast and prostate osseous metastatic disease. Valerie Frederick, CNMT, R.T. (R), James R. Galt, PhD, James J. Fitz, ARRT(R)(N), Ephriam E. Parent, MD, PhD; Nuclear Medicine and Molecular Imaging, Emory University Hospital, Atlanta, GA, USA. (1188)

Objectives: Bone scans are the standard of care in both breast and prostate cancer patients to evaluate for osseous metastatic disease. However, traditional bone scintigraphy (whole body imaging and SPECT or SPECT/CT) is unable to quantitate disease progression, therefore oncologists use NaF PET/CT for this.
Purpose: Quantitative reconstruction has recently become available for SPECT/CT but adds complexity (additional quality control and patient setup) and radiation dose from the CT. The purpose of this work is to 1) evaluate the practicality of quantitative SPECT/CT in patients with osseous metastatic disease for initial diagnoses and subsequent tracking, 2) establish an imaging protocol for future quantitative Tc-99m MDP SPECT/CT imaging studies, and 3) evaluate the feasibility of performing quantitative Tc-99m MDP SPECT/CT as a standard of care in patients with known osseous metastatic disease.
Methods: Quantitative SPECT/CT (Siemens xSPECT Quant) was implemented on a clinical SPECT/CT system (Siemens Intevo T16). Quality control for quantitation includes routine calibration with a known source, preferably a NIST calibration source, and checked with a NEMA IEC Body Phantom (Data Spectrum Corporation) which consists of a body phantom, lung insert, and spheres ranging from 10 mm to 37 mm. The phantom sphere/background activity ratio was 4/1 and imaged with the clinical protocol. Patient set-up procedures include recording and input of patient demographics, assayed radiopharmaceutical dose/residual dose, and assay/injection times. Patients are injected intravenously with 25mCi (925 mBq) +/- 10% of Tc99m-MDP with imaging 2.5-3 hours following injection for their whole body scan and lateral images of the skull. If the clinician desires, this is followed by SPECT/CT using the quantitative protocol. A clinical protocol designed for tracking includes the whole torso, a 2-bed position SPECT/CT from the clavicles through the pelvis. Both phantom and patient SPECT reconstruction used xSPECT Quant (based on the OSCG algorithm) which includes attenuation correction, scatter compensation and collimator resolution modeling. SPECT images from this algorithm are calibrated for SUV analysis and analyzed on MIM software workstations.
Results: Phantom images gave background SUV average of 1 as expected. Maximum SUVs from the spheres varied with size due to partial volume effects. Sphere SUV max was 5.5, 5.4, 4.0, 2.7 for the 37 mm, 28 mm, 22 mm, and 17 mm spheres (activity ratio of 4.1). Patient images provided a different texture with quantitative reconstruction verses OSEM reconstruction. Lesions with both reconstructions were identified and SUVs recorded. At this time, quantitative measurements were not included in the clinical report. Implementation of quantitative disease tracking would require SPECT/CT at each patient visit.
Conclusions: Phantom measurements showed that the quantitative reconstruction was accurate. Patient imaging demonstrated that the technique is feasible for the clinical setting. While there is some increased cost, time and effort in quantitative SPECT/CT, the ability to assess tumor response and regression using bone scans with SPECT/CT may eventually allow for the standard of care with its lower cost and availability than NaF PET/CT.

Authors listed for this abstract reported no relevant financial disclosures.

2136

Evaluation of the use of a modular detector system to collect data in real-time data to detect and assess infiltration. Shelley Nicole Acuff, CNMT, RT(R) (CT)[1], Erica Baxter[2], Chris Carr[2], Dustin Osborne, PhD[3]; [1]University of Tennessee Graduate School of Medicine, Knoxville, TN, USA, [2]Radiology, University of Tennessee Medical Center, Knoxville, TN, USA, [3]University of Tennessee Graduate School of Medicine, Knoxville, TN, USA. (2985)

Intro: A modular radiation detector system has been developed by Lucerno Dynamics, LLC. The detector device was developed, and is FDA approved for use in detecting infiltrations of radioactive tracers injected for molecular studies. The current version of this device collects all data during the uptake time and then is uploaded to a server where the data can be visualized and assessed for signs of infiltration. If a severe infiltration were present, the patient would be rescheduled. The objective of this study is to test the feasibility of using this device for real time assessment of the injected dose rather than the current mechanism that allows retrospective analysis of the acquired data.
Materials and Methods: For this feasibility assessment, seven PET/CT patients were connected to the detector device prior to their FDG injections. Two small detectors were placed on the patients with one on the injection arm distal to the injection site, and the other placed on the opposite arm in the same area to serve as a control. During the delivery of the tracer, counts from seven time points were manually captured from the detector device: 5sec, 10sec, 20sec, 30sec, 40sec, 50sec, and 60sec post-injection. Using this data, predictions were made on whether an infiltration had occurred or not based on how rapidly the counts decreased to typical baseline values of 200-400 counts. The standard automated data collection using the device continued from the time of injection until the completion of the patient uptake time (approximately 60 minutes). The data were then uploaded to the device server to obtain the complete time activity curves. This automated system also calculates a score for each injection which provides a quantitative metric of the degree of infiltration. Manually collected data points were compared to the device-collected curves to assess if the data converged, and if so, how rapidly. Convergence rates were compared to the scoring system to determine if manual predictions were accurate, and at what minimum times could real-time assessments provide a reasonable determination of an infiltration.
Results: Based on manual, real-time data collection, baseline threshold values were reached within 30 seconds. From manually collected data, we predicted no infiltrations for all seven patients. When compared to the automated device assessment and scoring system, it confirmed that none of the seven patients experienced an infiltration.

Patient	5sec	10 sec	20 sec	30 sec	40 sec	50 sec	60 sec
Patient 1		780	427	345	395	327	303
Patient 2	1315	452	366	358	327	340	327
Patient 3	Read Error	440	228	226	214	198	218
Patient 4	5943	709	402	359	318	353	305
Patient 5	3511	333	225	237	202	190	170
Patient 6	12730	1546	666	492	367	327	271
Patient 7	2258	271	180	165	174	138	165

Conclusions: An external detector device may be used to ascertain that an injection is sufficient within only a 30-45 second acquisition. Although less accurate than being able to analyze a longer and more complete set of

time activity curves, severe infiltrations would take much longer to reach baseline compared to non-infiltrated injections. The standard method for using this device is to inject the entire patient dose and then assess the injection quality following the full uptake time. If severely infiltrated, the patient must be rescheduled but they still will have received the full radiation burden of the injected PET tracer. This initial analysis suggests that use of a real-time measurement technique can potentially reduce patient dose by enabling an injection of only a small amount of the patient dose to test the IV placement. If the injection site is infiltrated a new IV will be started or the patient rescheduled without having to inject the full patient dose.

Image:

Averaged real-time TACs vs. averaged detector device acquired TACs: Shows convergence of curves at approximately 30-45 seconds.

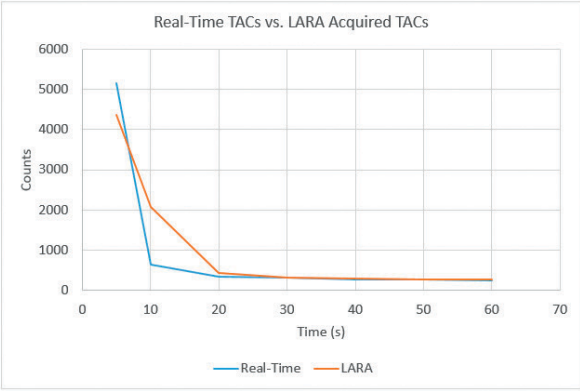

Authors listed for this abstract reported no relevant financial disclosures.

2137

On the Quantitative Accuracy of xSPECT Quant Based Renal Uptake Determination for Internal Dosimetry in ^{177}Lu-PSMA Radioligand Therapy. Johannes Tran-Gia, PhD, Hashan Neumayer, Michael Lassmann, PhD; University of Wuerzburg, Wuerzburg, Germany. (1616)

Aim: Quantitative assessment of radioactivity distributions is critical for internal dosimetry of molecular radiotherapies. The aim of this work was to evaluate the accuracy of the recently presented xSPECT Quant reconstruction method for quantitative SPECT/CT imaging in a small patient cohort undergoing ^{177}Lu-PSMA radioligand therapy.

Materials and Methods: 5 patients suffering from metastatic castration-resistant prostate cancer, which had undergone ^{177}Lu-PSMA radiotherapy at our institution, were selected. All patients gave written informed consent to the procedure. Imaging was performed ~24h p.i. on a Siemens Intevo Bold SPECT/CT system (MELP, TEW, 60x15s, 2 bed positions, standard low-dose CT). Reconstructions were performed using the 3 reconstruction modes provided by the manufacturer (*Fast*, *Normal*, *Best*) where iterations, subsets, and 3D Gaussian post-filtering are automatically selected based on the total number of counts. Additionally, a user-defined parameter set was applied (*In-House*). After reading out the reconstruction parameters for each patient, resolution estimates for all applied reconstructions were determined as described in [1] by applying a matched-filter approach to a ^{177}Lu NEMA sphere phantom dataset.

Table 1: Reconstruction Parameters.

	Preset 1			Preset 2			In-House
Recon-struction Mode	**Fast**	**Standard**	**Best**	**Fast**	**Standard**	**Best**	/
# Iterations	12	16	24	24	36	48	48
# Subsets	1	1	1	2	1	1	1
Post-Filter (mm)	20.8	20.8	20.8	16.0	16.0	16.0	0
Resolution Estimate (mm)	25.3	24.8	23.0	18.4	18.4	18.4	12.0
Patient #	4			1 / 2 / 3 / 5			all

The kidneys were segmented based on the CT (1mm isotropic voxel size) using 3D Slicer [2]. 2 of 10 kidneys had to be excluded due to adjacent tumors. Geometry-specific recovery coefficients (RC) were calculated by combining the segmentations with the resolution estimates as described in [1]. Finally, the activity was determined in each kidney by 1) determining the mean activity concentration c_{mean} in a VOI of exactly the segmented volume (an intensity-based threshold was adjusted to match the volume), 2) multiplying c_{mean} with the segmented volume, and 3) dividing the resulting activity by RC.

Results and Discussion: Figure 1: While the left kidney can be separated from the neighboring intestine (red arrow) for the *In-House* reconstruction (B), this is almost impossible for the *Fast* reconstruction setup (A).

Figure 1: Coronal sections of P4 for 2 exemplary reconstructions.

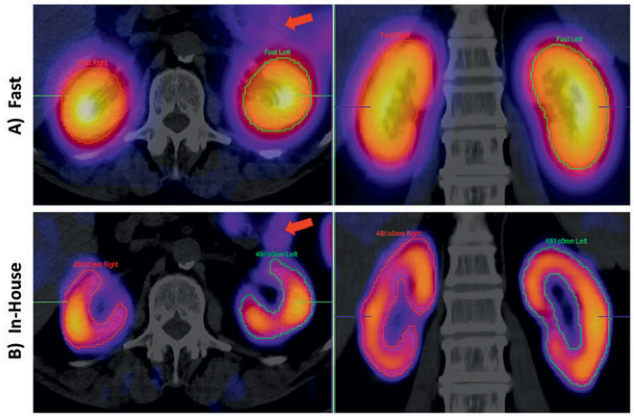

Table 2: For preset 1 (P1, P2, P3, P5), both c_{mean} and c_{max} lie in the same range for each kidney. This is caused by the same post-filter being applied for all reconstruction modes. The larger variations occurring for preset 2 (P4) are caused by the lower update numbers (12, 16, 24), for which the resolution is still considerably improved. A considerable difference between all presets and the *In-House* reconstruction indicates that the post-filter (16-21mm versus 0mm) has a much stronger influence on both parameters than the number of updates (16-48 versus 48).

Table 2: Average (c_mean) and maximum (c_max) activity concentration.									
	Mode	P1 Right	P1 Left	P2 Left	P3 Left	P4 Right	P4 Left	P5 Right	P5 Left
c_{mean} (MBq/mL)	Fast	0.36	0.29	0.39	0.31	0.29	0.29	0.60	0.70
	Normal	0.37	0.30	0.40	0.33	0.37	0.36	0.60	0.70
	Best	0.37	0.31	0.40	0.34	0.35	0.34	0.60	0.71
	In-House	0.47	0.40	0.50	0.44	0.46	0.46	0.72	0.85
c_{max} (MBq/mL)	Fast	0.57	0.53	0.55	0.46	0.45	0.43	1.03	1.12
	Normal	0.59	0.54	0.56	0.52	0.58	0.55	1.03	1.12
	Best	0.59	0.56	0.60	0.58	0.55	0.51	1.05	1.14
	In-House	1.08	0.91	0.80	0.81	0.94	0.87	1.37	1.62

Table 3: While the RCs are in a similar range for the *In-House* reconstruction (RC = 0.78 ± 0.20), smaller RC values with larger variations occur for all 3 presets (RC = 0.66 ± 0.05). Although smaller RC values imply more pronounced partial volume effects, the applied partial volume correction leads to an acceptable variation in the calculated activities (average rel. error: 6.3%).

Table 3: Volumes, geometry-specific recovery coefficients (RC) and calculated activities (A).									
		P1 Right	P1 Left	P2 Left	P3 Left	P4 Right	P4 Left	P5 Right	P5 Left
Volume (mL)		173.4	231.6	151.4	166.1	169.6	187.5	169.4	160.9
RC	Fast	0.69	0.74	0.65	0.68	0.57	0.57	0.68	0.67
	Normal	0.69	0.74	0.65	0.68	0.58	0.58	0.68	0.67
	Best	0.69	0.74	0.65	0.68	0.60	0.60	0.68	0.67
	In-House	0.79	0.82	0.75	0.78	0.77	0.77	0.78	0.77
A (MBq)	Fast	93.2	95.5	94.3	78.6	89.7	99.8	152.8	173.1
	Normal	94.4	98.2	95.6	82.7	111.0	120.6	152.8	173.2
	Best	95.5	98.8	96.6	85.9	101.5	110.9	154.4	175.1
	In-House	106.5	114.7	102.3	96.2	105.0	116.9	161.6	184.7

Conclusions: Although xSPECT Quant holds the potential for a standardization of quantitative ^{177}Lu SPECT imaging, the use of the manufacturer-defined reconstruction modes introduces a certain variability. For the acquisitions in this study, a varying number of 12-48 updates combined with strong post-filtering between 16-21mm were automatically chosen. This led to a loss in standardization especially with respect to the resolution (18-25mm), in turn leading to a varying influence of partial volume effects. Moreover, the separation of neighboring "hot" objects is impeded by the strong post-filtering, which is included in all presets. Therefore, a user-defined reconstruction preset with a sufficient number of updates and very cautious post-filtering is highly recommended to achieve a reliable activity determination.

LITERATURE:

[1] Tran-Gia et al., JNM (2017);doi:10.2967/jnumed.117.200170.
[2] Fedorov et al., MRI (2012);30(9):1323-41.

Authors listed for this abstract reported no relevant financial disclosures.

2138

A Gaussian filter influenced the texture features on PET images.

Ayano Shoji[1], Keishin Morita[2], Toshiki Takeshita[3], Naoki Hashimoto[1], Saki Kimoto[1], Yuji Tsutsui[1,4], Kazuhiko Himuro[4], Shingo Baba, MD, PhD[4], Masayuki Sasaki, MD, PhD[5]; [1]Kyushu University, Fukuoka, Japan, [2]Kyoto University Hospital, Kyoto, Japan, [3]Teikyo University Hospital, Mizonokuchi, Kanagawa, Japan, [4]Kyushu University Hospital, Fukuoka, Japan, [5]Dept Rad Sci Sch of Health Sci Kyushu Univ, Fukuoka, Japan. (1760)

Purpose: Generally, the standardized uptake value is primarily used for the analyses in FDG PET. Recently, an increasing number of publications have described the application of textural features in PET image analyses. However, the influence of reconstruction parameters on the evaluation of the heterogeneous uptake has not yet been sufficiently elucidated. The purpose of this study was to examine the impact of a Gaussian filter on evaluating the heterogeneous uptake in PET images as assessed by texture analysis using numeric phantoms.

Materials and Methods: The numeric phantoms represented a high activity homogeneous model, three heterogeneous models with high, medium and low activity and four heterogeneous models with high and medium activity. The images of the numeric phantoms were 15×15 pixels and filtered by the Gaussian filter using the Prominence Processor (Version 3.1). The full width at half maximum of the Gaussian filter (GF-FWHM) was 6 mm. The heterogeneity was evaluated based on 13 texture features on a co-occurrence matrix and 11 texture features on a size zone matrix.

Results: In images without a Gaussian filter, all features on the co-occurrence matrix and six features on the size zone matrix differed between the homogeneous and heterogeneous models. In images with a GF-FWHM of 6 mm, 10 features on the co-occurrence matrix and 5 features on the size zone matrix differed between the homogeneous and heterogeneous models. Three features that reflected the small zones on the size zone matrix were influenced by the Gaussian filter. The influence of the Gaussian filter on the co-occurrence matrix was small. Thus, a Gaussian filter is considered to affect the evaluation of the heterogeneity by the texture analysis. Furthermore, the Gaussian filter had greater effects on the size zone matrix than on the co-occurrence matrix.

Conclusions: The results of this study suggested that the evaluation of heterogeneity as assessed by texture analysis was affected by the Gaussian filter, which had a greater influence on the size zone matrix than on the co-occurrence matrix.

Authors listed for this abstract reported no relevant financial disclosures.

Tech Papers V: Professional Practices & Educational Exhibits and Radiopharmaceutical Science, Biology & Dosimetry

Moderator: Mary Beth Farrell, MS, CNMT, NCT, FSNMMITS
Co-Moderator: Thomas M. Morneau, CNMT

2150

Reduce wait time for add-on OR patients in Clinical Nuclear Medicine.

Alfredo J. Gonzalez, RT(N), PET, CT[1], Dao Le, Pharm D[1], Scottie Jones[1], Homer A. Macapinlac, MD[2]; [1]M.D. Anderson Cancer Center, Houston, TX, USA, [2]UT M.D. Anderson Cancer Center, Houston, TX, USA. (3036)

Objectives: To evaluate a change of practice from using unit doses of ^{99m}TC-Filtered Sulfur Colloid (^{99m}Tc-FSC) to bulk vial dispensing of ^{99m}Tc-FSC for routine and add-on procedures in the operating room.

Methods: Prior to being able to draw unit doses from a ^{99m}Tc-FSC bulk vial(s), the United States Pharmacopeia (USP) Sterile Compounding Chapter (797) guidelines were taken into account. Some of the tasks needed to be completed include air quality certification and environmental monitoring of the biological safety cabinets and hot lab area. Further, Nuclear Medicine

Technologists (NMT) were required to document various handling training such as aseptic technique and media fill testing. Once the hot lab, laminar flow hoods and NMTs satisfied all required parameters for low risk sterile compounding, an initial trial period of dispensing ^{99m}Tc-FSC unit doses from a bulk vial began. To assess feasibility, data was collected for the three listed endpoints: (1) To evaluate operational efficiency, a survey was conducted amongst team members to determine if bulk vial use improved the ^{99mTc}-FSC ordering/dispensing process and overall ^{99m}Tc-FSC turnaround time. (2)To evaluate the improvement of ^{99m}Tc-FSC delivery time once an add-on STAT order is placed. (3)To measure cost savings, we documented, in a three month period, the number of individual doses dispensed from a bulk vial and compared it to the hypothetical cost of ordering individual unit doses from the radiopharmacy.
Results: Survey results from NMT and stakeholders demonstrated that ^{99m}Tc-FSC bulk use was highly favored. NMTs could readily draw unit doses from the bulk vials when needed for scheduled patients and any add-on/STAT requests. The turn-around time for our stakeholders was significantly reduced from an estimated two hours to less than 15 minutes wait time. Additionally, the project proved to be highly cost effective. A cost comparison was done for the month of April 2017, with a total estimated savings of $9,410.00 in one month.
Conclusions: The overall consensus favored utilizing bulk ^{99m}Tc-FSC over purchasing unit doses from the radiopharmacy. The use of bulk ^{99m}Tc-FSC has effectively streamlined our operation, proven to be financially favorable and improved turnaround time for add-on procedures by making the drug easily accessible and reducing the wait time for ^{99m}Tc-FSC.

Authors listed for this abstract reported no relevant financial disclosures.

2151

Challenges and practicalities in the clinical implementation of Lutetium 177 for therapeutic nuclear medicine: a technologist's perspective. Ryan Warhoover, CNMT[1], Sarah Frye, MBA, CNMT, PET, NCT[2], Ross J. Frye, MBA, CNMT[3], Medhat M. Osman, MD, PhD, MS[4], Barbara B. Sterkel, MD[5]; [1]VA St. Louis Healthcare System John Cochran Division, St. Louis, MO, USA, [2]Department of Medical Imaging and Radiation Therap, St. Louis University, Saint Louis, MO, USA, [3]VA St. Louis Healthcare System John Cochran Divisi, St. Louis, MO, USA, [4]St. Louis University, St Louis, MO, USA, [5]VA St. Louis Healthcare System, Saint Louis, MO, USA. (1428)

Objectives: FDA approval of Lutetium177 (Lu177) treatment of neuroendocrine tumor is pending. Lu177 therapy is logistically different than any other currently used radionuclide therapeutic agent. We aim to present a technologist's perspective on potential challenges related to the implementation of Lu177 therapy including developing an institution's policy, identifying needed location/space, supplies, and staff requirements.
Methods: A Lu177 treatment regimen consists of 4 intravenous infusions of 200 mCi at 8 week intervals. Each therapeutic infusion is 4-6 hours, consists of the Lu177 infusion along with an infusion of amino acids and requires nursing supervision. During this process, to reduce radiation exposure, the patient must walk to the restroom every thirty minutes with an IV pole to void. The technologists met with the Authorized Users (AU), the Radiation Safety Officer (RSO), and the other staff involved to review the requirements of radiation safety, workflow, and protocol of this therapy.
Results: The radioactive materials license is to be amended. It was determined that Lu177 administration would ideally occur in our PET division due to department layout and patient flow. While the general nuclear medicine department has an injection room suited for therapeutic use, the restroom is not in close proximity, which is a radiation safety concern. In our PET center, there are 2 comfortable injection rooms used for long uptake periods located next to a restroom dedicated for radioactive patients. Due to the stated length of the Lu177 therapy session, the PET diagnostic schedule will be reduced on Lu177 therapy days. Lu177 therapies will be scheduled in coordination with other departments including oncology; pharmacy for obtaining amino acids; and nursing for the administration of IV fluids and vital sign monitoring. After the infusion is completed and the injection room is cleaned, radioactive waste will be moved to long term storage.
Conclusion: Lu177 therapy is an exciting new development in the field of radionuclide therapy: however, its implementation brings new challenges to meet both radiation safety and protocol requirements. Space, workflow, and staffing must all be considered. Lu177 therapies will involve the coordination of AUs, the RSO, technologists, nursing staff, pharmacist, and logistics personnel. Having a successful Lu177 therapy program requires team work to develop site-specific and tailored solutions.

Authors listed for this abstract reported no relevant financial disclosures.

2152

Intersocietal Accreditation Commission (IAC) QI Self-Assessment Tool Utilization and Improved Accreditation Outcome. Maria Costello, BS, CNMT[1], Mary Beth Farrell, MS, CNMT, NCT, FSNMMITS[2]; [1]Nuclear/PET, Intersocietal Accreditation Commission, Columbia, MD, USA, [2]IAC, Langhorne, PA, USA. (1346)

Introduction: Accreditation is often viewed as a benchmark of quality. The Intersocietal Accreditation Commission (IAC) has been evaluating and accrediting nuclear medicine and PET labs since 1997. As part of the accreditation process, the quality of staff credentials, equipment, protocols, study appropriateness, imaging, interpretation, reporting, and the quality improvement (QI) program are evaluated. Historically, deficiencies have been identified for approximately 70% of labs applying for IAC nuclear/PET accreditation. In 2016, to assist labs in self-evaluating and improving the quality of their diagnostic imaging studies, the IAC created a QI Self-Assessment Tool. The QI Self-Assessment Tool concentrates on four quality areas: test appropriateness, image quality/safety, interpretive quality, and report timeliness/completeness. The results of the self-assessment can be used to fulfill the annual QI accreditation requirements. The ability of IAC QI Tool to improve diagnostic imaging study quality is known. Using the IAC accreditation decision with its inherent identification of quality issues as an outcome variable, the aim of this study is to evaluate the effect of IAC QI Self-Assessment Tool utilization on subsequent accreditation decision by labs applying for IAC nuclear/PET accreditation.
Methods: All facilities applying for IAC nuclear/PET accreditation from October 2016 through November 2017 were evaluated. Variables measured included: application date, accreditation area (myocardial perfusion imaging (MPI), equilibrium radionuclide angiography (ERNA), general nuclear medicine (GNM), and PET), accreditation decision (delay = issues identified, grant = no significant issues identified), date of first QI self-assessment, self-assessment completed before submission of application (yes/no), number of assessments per lab, cases per assessment, and reviewers per assessment. The number and percentage was reported for categorical variables, and the median and interquartile range was reported for continuous variables. Comparisons were made using Chi-square tests (X^2) and logistic regression analysis with a p-value of <.05 significant.
Results: Between October 2016 and November 2017, 784 labs applied for IAC nuclear/PET accreditation. Of those labs, 161 (20.5%) completed a QI self-assessment and 55 (7.0%) completed a self-assessment prior to submitting an accreditation application. The median number of assessments per lab was 2 (Q1=1, Q3=4). The median cases per assessment was 6.7 (Q1=2.6, Q3=13.1), and the median reviewers per assessment was 1.0 (Q1=1, Q3=2). Overall, quality issues (delayed accreditation), that must be corrected before accreditation is granted, were identified at 559 (71.3%) applicant labs. A smaller number of labs that utilized the QI Self-Assessment Tool had quality issues identified at the time of accreditation than those that did not use the tool (49.1% vs. 73.0, p<.0001). Controlling for the number of assessments, average cases per assessment, average reviewers per assessment, volume of studies, and type of lab, nuclear/PET labs that utilize the IAC QI Self-Assessment Tool are 3.46 times more likely to be granted accreditation.
Conclusion: The IAC QI Self-Assessment Tool demonstrates a positive effect in identifying and correcting quality issues leading to positive accreditation outcomes.

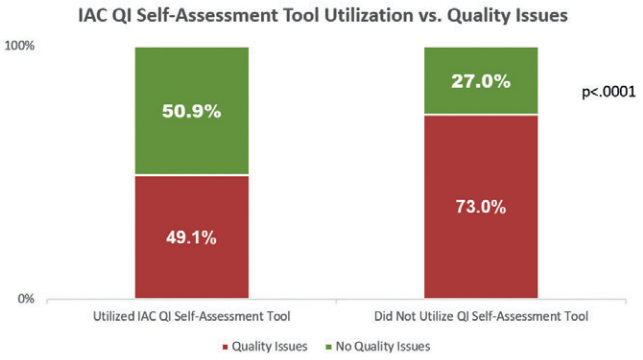

Authors listed for this abstract reported no relevant financial disclosures.

2153

Improving patient care and efficiencies through multi-departmental collaborations. Eleanor S. Mantel, CNMT, RT(N), FSNMMI-TS; Hospital of the University of Pennsylvania, Philadelphia, PA, USA. (1851)

Introduction: Demands and the utilization of services of emergency departments (ED) and short stay observation units (EDOU) continue to increase by individuals without primary care physicians or health insurance coverage. Healthcare institutions need to develop ways to triage, treat and manage these patients in an effort to alleviate and avoid finding themselves in a gridlock with patients waiting for care in the ED.
Material and Methods: A need was identified to manage these patients that presented to the emergency department (ED) with chest pain/discomfort. Providing care to this patient population would need to be a collaborative effort between numerous departments and medical specialties. Once stakeholders were identified, the challenge of coordinating meetings would begin. As expected, everyone had their own idea of how to manage it. Option 1: Schedule staff to work half-day Saturdays to perform nuclear stress tests. This option was met with resistance from the physicians and the cardiac nursing team as they did not want to work on weekends. This caused the need for the development of an alternative plan. Option 2: Discharge these patients and schedule them to return for a nuclear stress test. It was determined that option 2 was potentially a viable solution and work began to develop a process. All patients presenting to the emergency department with chest pain would have a cardiac work-up. They would have an electrocardiogram and a series of cardiac enzymes performed. If all testing was negative, the patient would be scheduled to return the following Tuesday to undergo a myocardial perfusion scan nuclear stress test with either 99mTc sestamibi or a rubidium PET stress test. The patient's BMI was the determining factor whether they would be scheduled for a SPECT versus PET stress test. Patients with BMIs greater than or equal to 40 would undergo a rubidium PET myocardial perfusion scan. Prior to discharge from the emergency department, the patients were provided with the description of the study, preparation for the study as well as an appointment. They were given ample time to have their questions answered. The insurance pre-certification team would then begin the process of trying to obtain authorizations. These studies were given priority status with the team in an effort to obtain authorizations prior to the patients returning as outpatients.
Results: For the first year of this program, there were 187 after-hour stress tests ordered. Of those, there were 60 refusals/cancellations/no-shows, just over 30%. Of the remaining 127 patients, approximately 8% had positive stress tests. These results are what we had anticipated seeing.
Discussion: Prior to implementing this procedure, patients were having to stay in the ED and EDOU until at least Monday so the cardiac testing could be performed. Not only was this an inconvenience for the patients, it also reduced the availability of beds for other individuals needing treatment in the ED/EDOU, especially since a vast majority of the testing were negative.
Clinical Relevance/Application: This process shows the value and importance of multi-departmental collaboration in streamlining patient care. Putting patient care first has provided patients with a better overall experience by decreasing their wait times and providing quicker discharges without compromising the quality of care received. An additional benefit to our facility has been to free up resources to allow us to provide services to additional patients without incurring additional staffing expenses. We will continue to work this process as a way to provide our patients with optimal care while decanting the ED and EDOU.

Authors listed for this abstract reported no relevant financial disclosures.

2154

Reduction of Y90 radiation exposure using modified leaded glasses. Shelley Nicole Acuff, CNMT, RT(R) (CT)[1], Dustin Osborne, PhD[2]; [1]University of Tennessee Graduate School of Medicine, Knoxville, TN, USA, [2]University of Tennessee Graduate School of Medicine, Knoxville, TN, USA. (3043)

Objectives: The use of Yittrium-90 (Y90) for selective internal radiation therapy for liver cancer is growing. In the US, most institution's Interventional Radiologist have the task of administering these Y90 spheres. Devices such as lead aprons and lead eyeglasses are used to lower the radiation exposure on a daily bases for these doctors. However, when handling beta emitters like Y90 acrylic is the most effective to lower radiation exposure. The objective of this study is to evaluate how effective eyewear using a combination of lead and acrylic is compared to the standard lead eyeglasses when using Y90.
Materials: A vial of 56mCi of Y90 was placed at a set distance of 16 cm from a Geiger counter. A standard pair of lead glassed eyewear was placed directly in front of the vial. A piece of (add thickness) acrylic was added to the lead glasses. Six measurements were taken and recorded with lead glasses only and lead glasses + acrylic.
Results: Data show a clear reduction in exposure rates with average exposure rates reduced from 1.2 mR/hr with lead only glasses to an average of 0.167 ± 0.03 mR/hr with the addition of acrylic to the lead glass surface. The differences between values were statistically significant with $p << 0.05$.

Lead Glasses	Lead + Acrylic
1.2mr/hr	.15mr/hr
1.2	.15
1.2	.15
1.2	.15
1.2mr/hr	.2mr/hr
1.2	.2

Conclusions: The addition of a layer of acrylic to leaded glasses may help in reducing radiation dose to the eyes in the instances during radioembolization therapy. This is most useful when the physicians experience enhanced exposure during infusion and in the instance where stasis is reached and Y90 beads are trapped in the catheter tubing with minimal shielding and distance from the physicians and staff.

Authors listed for this abstract reported no relevant financial disclosures.

2155

Feasible method to remove the residual impurity after [^{11}C] methionine production. Hyunsik Park, Byung Seok Moon, PhD, Hyun Ho An, Hong Jin Lee, Byung Chul Lee, PhD, Won-Woo Lee, MD, PhD, Sang Eun Kim, MD, PhD; Department of Nuclear Medicine, Seoul National University Bundang Hospital, Seongnam, Korea, Republic of. (2703)

Objectives: [^{11}C]Methionine is widely used for tumor imaging as a radiopharmaceutical, i.e., gliomas in neurooncology as well as a supplementary in adenocarcinoma by positron emission tomography (PET) and simple synthetic methods are well established with more efficient, reliable and simple setups. Among them, a solid-phase extraction (SPE) cartridge method is nowadays the most common procedure for highly convenient and efficient production of [^{11}C]methionine. However, it was often contaminated by an additional impurity such as sodium iodide not mentioned in the Eu. Ph. Monograph. and consequently contained in the final injectable solution. We herein describe the further purification method that can be easily removed an impurities in the process of production for [^{11}C]methionine or before.

Methods: Three methods were tried to remove an additional impurity which is generated during [^{11}C]methionine production: i) Cleaning method for the [^{11}C]methyl iodide synthetic loop part in the automatic synthesizer with helium flow and heating (750 ºC) for 2 hrs, ii) Introduction of an additional NaOH cartridge in the next part of Porapak Q which was trapped [^{11}C]methyl iodide source and iii) Additional installation of anion-exchange resin cartridge before sterile filtration. In order to analyze the change of concentration for sodium iodide according to the three methods, it was evaluated by radio-HPLC under the following conditions: YMC triart-C18 column (3.9 x 250 mm), 10 µL of injection volume taken from each final solution, flow rate of 0.9 mL/min, elution solvent of 0.01 M NaH_2PO_4, UV-220 nm and gamma-ray detector.
Results: The concentration analyzed by HPLC after cleaning of synthetic loop for [^{11}C]methyl iodide synthesis with helium flow and heating was decreased around 37% compared with that of maximum impurity but increased again after re-production. The method for additional introduction of NaOH cartridge showed around 28% of reduction. However, introduction of conventional QMA cartridges (anion-exchange resin) was able to remove up to 95% by controlling the pH of collected solution before sterilization. The produced [^{11}C]methionine after further introduction of anion- exchange resin was suitable to the European Pharmacopoeia standards for quality controls with no change of radiochemical yield.
Conclusions: We can be successively removed the impurity (iodide) generated in the [^{11}C]methionine production process using SPE cartridges as introduction an additional anion-exchange resin cartridge. The developed method expected that it can be well adapted to other [^{11}C] radiopharmaceuticals produced by SPE method.

Authors listed for this abstract reported no relevant financial disclosures.

2156

In-house automated synthesis of L-[^{11}C]Glutamine with the use of a Siemens H^{11}CN Box. Simon Joseph, Anirudh Sattiraju, Shunichi Oya, PhD, Agata Jurewicz, John W. Castrillon, Mark Soffing, Akiva Mintz, Patrick Carberry, PhD; Radiology, Columbia University Medical Center, New York, NY, USA. (2927)

Objectives: Glutamine is a readily available nutrient used for energy in both normal and tumor cells [1]. L-[^{11}C]glutamine takes advantage of various tumor metabolic pathways for when [^{18}F]FDG is limited. There is therefore a need in the PET community for an automated synthesis of L-[^{11}C]glutamine. We have developed a method for the routine automated production of L-[^{11}C]glutamine.
Methods: L-[^{11}C]glutamine was prepared with the use of an in-house Glutamine Module attached to a Siemens H^{11}CN(Cyanide)Box. [^{11}C]CO_2, produced from a Siemens Eclipse HP Cyclotron, is converted into H^{11}CN with the use of nickel/platinum catalysts. Radioactive cyanide gas is trapped in reaction vessel 1 with the use of 18-crown-6/cesium hydrogen carbonate base in *N,N*-dimethylformamide. The glutamine precursor, (s)-*tert*-butyl 2-((*tert*-butoxycarbonyl)amine)-4- iodobutanoat, is then added and heated to 90 ºC for 8 min. Trapping on a pre-conditioned *t*-C_{18} plus cartridge is achieved with the use of HPLC grade water. The radiolabeled intermediate is then released into reaction vessel 2 by way of acetonitrile. This is then dried at 120 ºC over a stream of argon. This process is repeated with the use of acetonitrile. The dried intermediate is then deprotected with the use of (4:1) trifluoroacetic acid:sulfuric acid and heated to 90 ºC for 5 min. Quenching with sterile water for injection and slowly passing through 5.0 g of Ag11 A-8 resin provided L-[^{11}C]glutamine. Chemical identity, purity and L:D isomeric ratio of the labeled radioligand was determined by reversed-phase HPLC. Quality control (QC) conditions were tested and passed for each production of L-[11C]glutamine; these tests include radionuclidic purity, pH, chemical identity, ratio of L/D-glutamine isomer, excipients, half-life and sterility. An *in vitro* cell uptake assay was performed using a glioblastoma (GBM) cell line to evaluate the reactivity and specificity of L-[^{11}C]glutamine. Excess L-glutamine was used to block control samples. SOPs and Batch Record were created prior to validation runs.
Results: L-[^{11}C]glutamine was successfully produced operating our automated in-house module connected to a Siemens H^{11}CN Box. Routine production provided 17.5 - 32.5 mCi (n = 6) at end-of-synthesis (EOS), starting with approximately 1,400 mCi of [^{11}C]CO_2. The average radiochemical purity = 95 ± 1.6% with an average enantiomeric excess (e.e.) = 96 ± 1.8 % and a pH value ranging from 7.5 to 8.0. Total synthesis time ranges from 74 to 82 min. In *in vitro* assay, L-[^{11}C]glutamine was taken up by GBM cells and was inhibited by ~65% when blocked with excess cold L-glutamine, indicating binding specificity.
Conclusions: A method for the automated production of L-[^{11}C]glutamine was achieved with the use of an in-house module attached to a Siemens H^{11}CN module. Specificity and reactivity of the produced L-[^{11}C]glutamine was validated *in vitro* using a glioblastoma cell line. This provides a platform for consistent-routine production of L-[^{11}C]glutamine which can be used as a potential PET imaging agent.
References: [1] L. Zhu, et. al. *J. Nucl. Med.* **2017**, *58*, 533-537.

Authors listed for this abstract reported no relevant financial disclosures.

2156a

Using a formula based on BMI and BSL for administration of Actrapid for FDG-PET scans where the patient's BSL is elevated on arrival. L. MacFarlane, D. Pattison; Peter MacCallum Cancer Centre, Melbourne, Australia

Background: FDG-PET scans are the most common type of PET scan performed worldwide. Our pre-scan preparation is reasonably standard; in addition, diabetic patients are given a morning appointment with cessation of morning insulin (+/- cessation of metformin for 48 hours). The impact of cessation of insulin +/- metformin can be significant. At our centre, ~10% of patients who attend are diabetic, and of these diabetic patients, ~20% arrive with a BSL greater than our protocol dictates. Management of these patients was empirical based on our existing protocol.
Aims: To analyse whether a formula based on BMI and BSL could be a useful tool in prescribing short-acting insulin (Actrapid) in our PET department.
Methods: A prospective review of patients from April 2015 to March 2016 (cohort2) was undertaken whereby if a patient's BSL was elevated on arrival for FDG-PET, the formula would be applied and the amount of Actrapid suggested would be given.
A retrospective review of patients prior to the introduction of the formula from April 2014 to March 2015 (cohort1) was undertaken, with the same parameters recorded, and the results compared.
Results: Mean time from Actrapid administration to FDG administration reduced from 132mins (range 68-287) in cohort1 to 108mins (range 70-237mins) in cohort2 (p=0.0004).
The average time to FDG injection when only a single Actrapid administration was required also reduced from 123mins (range 68-259) for cohort1 to 108mins (range 70-215) for cohort2 (p=0.0013).
Conclusion: The formula is a useful tool in our department for managing patients who arrive with an elevated BSL and who require Actrapid administration. The introduction of an objective method to calculate insulin dosage significantly decreased both the time to FDG injection and the proportion of patients requiring multiple administrations. Future developments include making this a mobile app for use in the wider PET community.

Technologist Poster Session

1789

To evaluate the expression level of HDACs in Tg2576 transgenic mouse model of Alzheimer's disease. Ming-Hsin Li[1], Chen-Hsien Liang[2], Yuan-Ruei Huang[2], Chun-Fang Feng[3], Shih-Wei Lo[4]; [1]Institute of Nuclear Energy Research, Tauyuan City, Taiwan, [2]Institute of Nuclear Energy Research, Taoyuan City, Taiwan, [3]Institute of Nuclear Energy Research, Taoyuan, Taiwan, [4]Taichung, Taiwan. (2266)

Epigenetic modifications mediated by histone deacetylases (HDACs) play an important role in many diseases, including a wide range of brain disorders and many types of cancer. HDACs regulate the level of histone acetylation which is involved in gene expression. Abnormal acetylation of histone is involved in a wide range of brain disorders such as Alzheimer's disease (AD). Thus, HDAC proteins may be therapeutical targets for AD treatment. Histone deacetylase inhibitors (HDACIs) which have been

shown as anticancer drugs, are recently suggested to act as neuroprotectors in AD. However, HDAC proteins serve a very distinct function in the brain. Therefore, the use of HDAC inhibitors in the treatment of AD should be careful. To identify the differential protein expression level of HDACs between Tg2576 transgenic mouse model of Alzheimer's disease(AD) and normal mouse model may helpful in discovering the pathological mechanism of AD and in developing selective HDAC inhibitors. Here, we used HDACs antibody to detect the protein expression of HDACs in brain tissue of Tg2576 (five months age) transgenic mice and normal mice by using immunohistochemical staining. These data will help us to select HDACIs which were used in AD treatment.

1790

Verification of physical parameters of whole-body dynamic imaging with continuous bed motion positron emission tomography. Hideo Yamamoto, MPAS[1], Shota Takemoto, MPAS[2], Akira Maebatake, MPAS[1], Yuki Yamashiro, MD[3], Atsushi Nakanishi, MD,PhD[4], Koji Murakami, MD, PhD[4]; [1]Radiology, Juntendo University Hospital, Tokyo, Japan, [2]Juntendo University Hospital, Tokyo, Japan, [3]Juntendo University, Tokyo, Japan, [4]Juntendo University, Tokyo, Japan. (113)

Objectives: In recent years, whole-body dynamic imaging with positron emission tomography (PET) has been increasingly recognized for its quantitative utility in diagnosis and therapy monitoring. Conventionally, PET acquisition takes place in a series of bed positioning from one to the next called step and shoot (SS) with overlapping bed to account for differential sensitivity along the axial field of view (FOV). Continuous bed motion (CBM) acquisition had become clinically available for commercial PET systems since several years ago, whereby the entire axial FOV is acquired in one series with a continuous movement of the patient bed without overlapping bed positions seen in SS technique. In the whole-body dynamic PET using CBM (WBDCBM-PET), one must consider pass numbers in addition to bed velocity. Evaluation of physical parameters is exceedingly crucial to ensure the quantitative accuracy and image quality of WBDCBM-PET. This study seeks to verify physical parameters in WBDCBM-PET and investigate the effects of the pass numbers and bed velocity on quantitative accuracy and image quality.

Methods: Seven bed velocity (2 to 7 mm/sec) settings for WBDCBM-PET in combination with the pass numbers up to 21 were performed on NEMA body phantom. We defined a dynamic index (DI) as a parameter of acquisition time in WBDCBM-PET, and it was obtained by following formula: [P/S], where P is the pass number and S is the bed velocity (mm/sec). The physical parameters were evaluated as follows: the noise equivalent count rate ($NECR_{phantom}$), the percent background variability at twelve circular regions of interests (ROI) of 10 mm in diameter drawn in the background area (N_{10mm}), the percent contrast of the 10 mm hot sphere ($Q_{H,10mm}$), the $Q_{H,10mm}/N_{10mm}$ ratio, and the maximum standardized uptake values (SUV_{max}). Furthermore, visual evaluation was performed using a five-point scale for the optimal slice in which all spheres were detected most clearly.

Results: The $NECR_{phantom}$ were constant, and it did not depend on any bed velocity in the same DI. The increase in DI led to the N_{10mm} decrease, and significant differences ($p < 0.001$) were noted among bed velocities. The N_{10mm} of WBDCBM-PET in all bed velocity was approximately equivalent non-dynamic CBM. Moreover, there was no significant difference ($p = 0.816$) between $Q_{H,10mm}$ and DI and no correlation was found between $Q_{H,10mm}$ and bed velocity. On the other hand, the strong correlation between $Q_{H,10mm}/N_{10mm}$ ratio and DI was found in all velocities ($p < 0.001$), however, there was no correlation between $Q_{H,10mm}/N_{10mm}$ ratio and bed velocity. The SUV_{max} of the spheres had no impact on DI. The coefficient of variations (CV) due to bed velocity ranged from 3.32 to 11.23% and decreased with larger sphere size. There was no significant difference among any bed velocities in visual evaluation.

Conclusions: WBDCBM-PET provides equivalent quantitative accuracy and image quality with non-dynamic CBM regardless of bed velocity and pass numbers during acquisition.

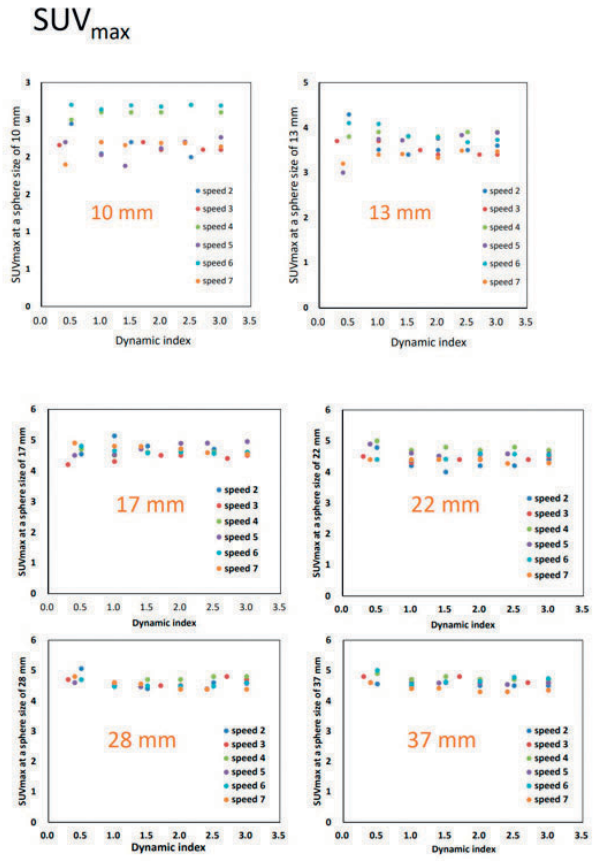

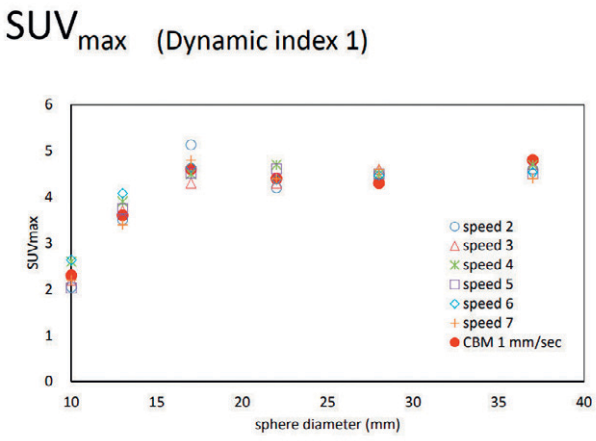

Authors listed for this abstract reported no relevant financial disclosures.

1791

A review on the role of Renal Functional Reserve as an assessment tool of renal insufficiency in the early stages of Diabetes. Michael Tong; National University Hospital, Singapore, Singapore. (2785)

Objectives: Early detection before renal impairment takes place is an understated important goal. This goal is made more challenging when most renal structural injuries tend to take place in absolute clinical silence. The measurement of renal functional reserve (RFR) in diabetic patients is challenging since the presence of high glucose levels stimulate hyperfiltration and it is necessary to dissociate both effects. In the early stages of diabetes, RFR with maintained filtration capacity has been found to be diminished. Various studies have since shown that insulin-dependent diabetic mellitus (IDDM) is associated with hyperfiltration in

the early stages of the disease. The response to an acute protein load in hyperfiltrating diabetic patients is that of a fall in GFR while renal blood flow remains constant. The association of early hyperfiltration and late diabetic nephropathy (DN) has also been observed. Although it has been widely accepted that hyperfiltration is associated with RFR loss, the value of RFR in diabetes has not been constantly assessed.
Methods: A review on study designs such as diagnostic cross sectional studies and cohort studies on diabetes and renal diseases were carried out. Randomised studies of RFR measurement with glomerular filtration rate (GFR) were also reviewed.
Results: RFR of diabetic patients were compared with normal healthy subjects in 6 studies. Type 1 diabetes patients were studied in 4 RFR investigations[1,2,3,4]. 3 studies looked into RFR of Type 2 diabetes mellitus patients[4,5,6]. 2 studies specifically looked into RFR of IDDM patients[2, 7]. RFR values were calculated as the difference between stimulated and baseline GFR values. There were certain evidences of absent or diminished response of renal reserve among the 6 studies. Control group subjects and patients without microalbuminuria showed retained RFR functions while patients with micoralbuminuria demonstrated the loss of the function.
Conclusions: At current, the presence of microalbuminuria is the strongest available and non-invasive risk predictor of developing DN. However, various studies have indicated that the risks of developing DN exist even when urinary albumin excretion (UAE) values are normal[8]. In some type 1 and type 2 diabetic patients, decreased GFR values were found even when UAE appears within normoalbunimuria[9], demonstrating that normoalbuminuria does not necessarily equate to normal GFR in both type 1 and type 2 diabetic patients. At the same time, some patients with microalbuminuria may revert to normoalbuminuria. Even so, a significant proportion of normoalbuminuric diabetic patients have been found with well established DN lesions. In fact, there is now accumulating evidence pointing out that the risk of DN progression starts when UAE are still within normoalbuminuria[7, 9]. Microalbuminuria is uncommon within the first 10 years of type 1 diabetes and first screening has been recommended at 5 years after diagnosis[10]. Keeping in mind that normoalbuminuria does not necessarily rule out DN, earlier than 5 years screening for microalbuminuria may then not be the answer to early detection of DN, and the role of microalbuminuria may be more of a marker than an early predictor of DN. New innovative tests need to be investigated and validated for their efficacies in providing better predictions of the risk of DN before renal implications are established, and one of the possibilities could be the evaluation of RFR through a stress GFR test. From the literatures reviewed, RFR has performed well in its indicative role in detecting glomerular changes in established diabetic patients. However, with the wide spectrum of conditions in diabetes, current evidence is not yet conclusive regarding RFR's potential predictive role in the early stages of diabetes, especially in pre-diabetes (of both type 1 and 2 diabetes mellitus).

Authors listed for this abstract reported no relevant financial disclosures.

1792

Phantom and clinical evaluation of bone SPECT/CT image reconstruction using novel conjugate gradient method. Noriaki Miyaji[1], Kenta Miwa, PhD[2], Reo Nemoto[3], Kei Wagatsuma[4], Mitsuru Koizumi, MD, PhD[1]; [1]The Cancer Institute Hospital, Japanese Foundation For Cancer Research, Tokyo, Japan, [2]Department of Radiological Sciences, International University of Health and Welfare, Ohtawara, Japan, [3]International University of Health and Welfare Hospital, Ohtawara, Japan, [4]Research Team for Neuroimaging, Tokyo Metropolitan Institute of Gerontology, Tokyo, Japan. (2696)

Objectives: Two new proposed methods of image reconstruction comprise xSPECT Quant (xQ) and xSPECT Bone (xB) using an ordered subset conjugate gradient minimizer (OSCGM) for bone SPECT/CT. The present study compares performance characteristics among xQ, xB and Flash3D (conventional) reconstruction using images derived from phantoms and patients.
Methods: A custom-designed body phantom for bone SPECT was scanned using a Symbia Intevo xSPECT system (Siemens). The phantom with four spheres (diameters 13 -28 mm) containing background ^{99m}Tc, had sphere-to-background ratios (SBR) of 6, 12, 24 and 60. The FWHM of a simulated spinous process (10 mm), coefficient of variance (CV) and recovery coefficient (RC) of a simulated spine on SPECT images were measured. Images were acquired from 20 patients with suspected bone metastases (male, n = 13) using ^{99m}Tc-MDP SPECT/CT, then the CV and standardized uptake value (SUV) at the 4th lumbar vertebra (L4) were measured. All data from the phantoms and patients were reconstructed with Flash3D, xQ, xB and compared.
Results: Spatial resolution was better for xB than xQ and Flash 3D regardless of the number of subsets and iterations during reconstruction. The CV and RC were better for xQ and xB than Flash3D. The RC significantly differed between xQ and xB, although those of xQ and xB became almost saturated at higher subsets and iterations. In contrast, the CV and SUV of the patients did not significant differ between xQ and xB.
Conclusion: The performance of both xQ and xB reconstructions was better than conventional reconstruction using Flash3D. The image quality and quantitation of SPECT images using xQ and xB were equivalent, except for spatial resolution.

Authors listed for this abstract reported no relevant financial disclosures.

1793

^{11}C-ethoxy-OTSSP167 inhibits maternal embryo leucine zipper kinase for PET / CT imaging of triple-negative breast cancer. Jia Hu, PhD, Fan Hu, Xiaoli Lan, Yongxue Zhang; WuHan Union Hospital, WuHan, China. (2362)

Objectives: Breast cancer seriously endangers the health of middle-aged and elderly women. At present, the diagnosis and treatment of Non-triple-negative breast cancer patients are maturing, but there is no effective diagnosis and treatment for patients with triple negative breast cancer (TNBC). A large number of literatures confirm that MELK (maternal embryo leucine zipper kinase) is highly expressed in TNBC. Based on this, OTSSP167 (a small molecule compound MELK) was significantly inhibited, and a new diagnostic TNBC targeted imaging 11C-ethoxy-OTSSP167, which is a small molecule, is easy to prepare and can be used to dynamically monitor the changes of TNBC patients in real time.
Methods: Breast cancer cell line, MDA-MB-231-UR and MCF-7, were sued as MELK overexpression and underexpression models, respectively. OTSSP167 was labeled with ^{11}C using Ethylene glycol bis-p-toluenesulfonate and N, N-diisopropylethylamine (ethoxy). MicroPET/CT imaging, biodistribution, and autoradiography studies were performed at the time of 30min, 60min, 90min and 120min in mice bearing MDA-MB-231-UR tumors after injection of ^{11}C-ethoxy-OTSSP167 to verify the targeting ability of the tracer.
Results: ^{11}C-ethoxy-OTSSP167 was successfully synthesized with labeling efficiency. MicroPET/CT images, biodistribution, and autoradiography studies showed high uptake of the tracer in MDA-MB-231-UR tumors. OTSSP167 caused dose- and time-dependent growth inhibition and apoptosis in melanoma cells in vitro, and suppressed MDA-MB-231-UR tumor growth in vivo.
Conclusions: OTSSP167, an MELK inhibitor, inhibits tumor growth and MELK expression. ^{11}C-ethoxy-OTSSP167, an easily-prepared probe, can be used to visualize MELK positive tumors and to monitor the effect of OTSSP167 therapy, suggesting its prospective clinical application.

Authors listed for this abstract reported no relevant financial disclosures.

1794

The imaging research of chemokine receptor 4. Peng Xu, master; nuclear medicine, The first affiliated hospital of Haerbin medical university, Harbin, China. (1820)

Objectives: To investigate the possibility of using CXCR4 siRNA labeled with ^{99m}Tc for the breast cancer CXCR4 gene imaging in nude mice.
Methods: (1)The siRNAs targeting CXCR4 mRNA and control siRNA were designed using BLAST software. The best siRNA sequences was screened by qRT-PCR or westetrn blotting. The synthesis of radionuclide probe with HYNIC as chelating agent and SnCl2 as reducing agent. (2)30 nude mice were divided into 6 groups(5/group). Three groups of mice were implanted with control cell line T-47D, the other were implanted with T-47D-CXCR4. The nude mice impalnted diffrent cell lines were

injected with ^{99m}TcO4-, ^{99m}Tc-HYNIC-control-siRNA and ^{99m}Tc-HYNIC-siRNA1026, respectively. After injection of the probe, the above six groups of nude mice were visualized at 1h, 4h and 10h respectively. Then we calculated the radioactivity count ratio between tumor and contralateral limb (T/M ratio). The measured data were analyzed by one-way ANOVA.
Results: The labeling rate and the radiochemical purity of molecular probe was (62.71±3.26)% and more than 95%, respectively. The ^{99m}Tc-HYNIC-siRNA had stable chemical properties and bond to the target gene sequence. The probe gathered in tumor for a long time. At 10 hours after the injection of the probe, the concentration of radionuclides is obvious in the tumor tissue.
Conclusions: With the bifunctional chelator HYNIC and $SnCl_2$, the CXCR4 siRNA molecules probe that labeled with ^{99m}Tc was constructed successfully. The molecular probe has the better labeling efficiency, stability and interference activity. The ^{99m}Tc-HYNIC-siRNA1026 could specificity accumulated in the tissue with CXCR4 overexpression.
Key words: CXCR4; siRNA; T-47D cells; ^{99m}Tc

Authors listed for this abstract reported no relevant financial disclosures.

1795

Comparative study of GFR measured by SPECT/CT with low energy high resolution collimator and low energy general resolution collimator. Chi Qi, MD[1], Yue Chen, MD[2]; [1]Department of Nuclear Medicine, The Affiliated Hospital.Southwest Medical University, Luzhou,Sichuan, China, [2]Department of Nuclear Medicine, The Affiliated Hospital, Southwest Medical University, Luzhou, Sichuan, China. (1319)

Objectives: To evaluate the differences in measuring glomerular filtration rate(GFR) by renal dynamic imaging of SPECT/CT with low energy high resolution collimator and low energy general resolution collimator.
Methods: The group A which used low energy high resolution (LEHR) collimator to measure gGFR (n_A=605), and the group B which used low energy general resolution (LEGR) collimator to measure gGFR (n_B=228) were included. The dGFR of All cases were measured by double-phase plasma method. Both of the two groups were respectively divided into 4 sub-groups according to the results of double-phase plasma method: 1. the severely reduced group (0-29.9) 2. the medium reduced group (30-59.9), 3. the mild reduced group 60-89.9 4. the normal group>90 (mL·min1·1.73 m^2) 1. The results of double-phase plasma method (dGFR) were used as gold standard. To test the normal distribution of the data with the Kolmogorov Smilov (K-S)
Methods: Paired T test was used to compare the diagnostic efficacy difference between the gold standard and each groups.
Results: The standard deviations of group A and B were 21.92 and 22.73 with no statistical significance (P=0.083). And there were no statistical significance between 1,3,4 groups of A and B with P values of 0.1, 0.899, 0.864. But the difference of group3 between group A and B was statistically significant (P<0.001).
Conclusions: GFR messured by spect with LEHR and LEGP have the same efficiency in measuring GFR for group 1,3,4. The spect with LEGR collimator has the better efficiency in measuring the one with mild renal function loss. So, it is better to perform Renal dynamic imaging measuring GFR with LEGP collimator.

Authors listed for this abstract reported no relevant financial disclosures.

1796

Radiation level in the surroundings of patients undergoing ^{99m}Tc-MDP SPECT bone imaging and influence factors. Zuowei Zou; Cancer Hospital, Beijing, China. (1949)

Objectives: To study the radiation level of 99mTc-MDP SPECT bone scan patients and its influencing factors and provide experimental data for the radiation safety of personnel around the patients.
Methods: 367 patients of whole-body bone scan were investigated to measure the dose rate around the patients at different time and different distance from the patients, analyze the dose rate variation with time and distance, estimate the dose level at different distances around the patient, and evaluate the radiation dose of personnel around the patient.
Results: The dose rate around the patient decayed exponentially with time, and the effective half-life increased with time; the dose rate varied by power function with distance within 4 meters from the patient. The power value was -1.453; the radiation levels were 238.3μSv at 0.5 m, 99.7μSv at 1 m, and 61.8μSv at 1.5m off the patient from ^{99m}Tc injection to vanishing in patients body; at different time points, the radiation dose at 0.5 m off the patient for 10 min was 0h: 9.9μSv, 3h: 3.0μSv, 6h: 1.9μSv.
Conclusions: The dose rate around the patients undergoing ^{99m}Tc-MDP SPECT bone imaging decrease rapidly with time and distance. The patients can cause a certain number of radiation dose on the surrounding personnel, but the dose level is far lower than the national standard. The patients should be suggested not to conduct other diagnosis and treatment that needed long-term close-contact of medical staff on the day of bone scan.

Authors listed for this abstract reported no relevant financial disclosures.

1797

Influences of different processing methods of SPECT on functional indicators of myocardial perfusion imaging. Fan Hu, Xiaoli Lan; Department of Nuclear Medicine, WuHan, China. (2685)

Objectives: To access whether there are differences between the results obtained by FBP and OSEM (with different iterations and subset numbers) methods in myocardial perfusion imaging (MPI) post-processing. And to recommend better reconstruction parameters for clinical use by comparing the above results with that of coronary artery CTA and ultrasonic cardiogram (UCG).
Methods: The data of MPI from 99 patients were collected from January 2012 to December 2014. All patients conducted coronary artery CTA in two days, in which 66 patients performed ultrasonic cardiogram. simultaneously. Gated MPI data was acquired by Siemens Symbia T6, and reconstructed on the workstation of e-soft by FBP and OSEM (subset number of 4, 8, 12, 16, 12 and corresponding number of iterations of 2, 2, 2, 2, 4 were selected) method, respectively. After reconstruction, polar bull' eye which was obtained by QPS was divided into three districts according to the coronary artery distribution, and ischemia rate in each area was measured, cardiac functional parameters (LVEF, EDV and ESV) were also calculated by QGS. The differences of myocardial ischemia rate and functional parameters obtained by 6 kinds of reconstruction methods were first analyzed. In order to determine a better method for clinical use, the correlation between myocardial ischemia rate and the stenosis rates of LAD, LCX and RCD that obtained from coronary artery CTA was analyzed. For those patients who performed UCG, the correlation of cardiac functional parameters from QGS and UCG was analyzed. Data was analyzed by SPSS 17.0 statistical software. Single factor analysis of variance (ANOVA) was adopted for analyzing the differences among groups; LDS-t was used to analyze multiple comparisons among multiple samples; T test was used for analyzing the differences of average values before and after the processing method, and χ^2 test was used for comparing two constituent ratios or pairwise among several constituent ratios. P<0.05 was considered statistically significant.
Result: The myocardial ischemia rate (LAD:χ^2=74.911, P=0.000;LCX:χ^2=91.972, P=0.000;RCD:χ^2=12.919, P=0.044) and functional parameters (LVEF:F=8.932, P=0.000, EDV:F=2.705, P=0.020, ESV:F=2.14, P=0.060) of the 99 cases obtained from the 6 reconstruction methods were statistically different. Through analyzing myocardial ischemia rate with the stenosis rates by χ^2 test, the OSEM method of 2 iterations and more than 12 subsets was better for clinical use.The 6 reconstruction methods were taken into pairs with t-test to analyzed functional parameters, there was no statistical difference between the OSEM method with 2 iterations, 12 subsets and more than 12 subsets; Then compared LVEF obtained from MPI of the 66 patients with UCG, the OSEM method with 2 iterations and more than 12 subsets was more appropriate. According to the principle of OSEM reconstruction, with the growing numbers of iteration and subset, the image quality will be improved. However, too many iterations would lead to redundancy, which will increase the waiting time and the working load of workstation. Therefore, we recommended the OSEM method (2 iterations, 12 subsets).
Conclusions: The myocardial ischemia rate and functional parameters obtained by 6 kinds of MPI reconstruction methods were different, among

them, the OSEM (2 iterations, 12 subsets) method was better for clinical use.

Authors listed for this abstract reported no relevant financial disclosures.

1798

Establishment of the Standard Uptake Values in SPECT-CT Quantification of Normal Systemic Thoracic and Lumbar Vertebrae.
Meng Qingyuan[1], Shou Yi, MD[2], Zhiwen You[1], Jianjun Jiang[1], Jieping Song, MS[1], Zhao Jun, MD[1]; [1]Shanghai East Hospital, Shanghai, China, [2]East Hospital Affiliated to Tongji University, Shanghai, China. (2773)

Objectives: Our study performed systemic thoracic and lumbar vertebral tomography with technetium-99m methylene diphosphate (Tc-99m MDP) single photon emission computed tomography (SPECT/CT) to measure the maximum standard uptake value (SUVmax) and establish the maximum standard uptake value(SUVmax) ranges of Tc-99m MDP for different normal thoracic and lumbar vertebrae.
Methods: Analyzed the data of patients undergoing quantitative tomography in our hospital retrospectively, all the patients with normal thoracic and lumbar vertebrae were diagnosed by two senior nuclear medicine physicians, divided the obtained data into four groups according to subjects' sex and examined parts, including thoracic vertebrae of 25 males and 21 females; lumbar vertebrae of 28 males and 37 females. Imaging agent was Tc-99m MDP, injection dose of subjects was 25mCi, performed planar imaging of the whole body 4-5 hours after the injection, and quantitative imaging of the thoracic and lumbar vertebrae. The instrument was Symbia Intevo SPECT/CT of Siemens, whose collected parameters were as following: 20 seconds per frame for a total of 30 frames, rotation of the single probe was 180°, of the single time was 6°; after reconstructing images of the acquired data with ordered subset conjugate gradient (OSCG) algorithm, measured the maximum standard uptake value (SUVmax) of each thoracic and lumbar vertebra with ROI mapping technique. Analyzed differences among each vertebral centrum with SPSS20 statistics;
Results: After statistical analysis, there was no statistically significant difference of each thoracic and lumbar vertebral SUVmax among subjects with the same sex, while there was a statistical difference of thoracic and lumbar vertebral SUVmax among subjects with different sexes. Male thoracic vertebrae were 8.1978±1.67770; lumbar vertebrae were 8.3825±1.83047; female thoracic vertebrae were 7.7169±1.75655; lumbar vertebrae were 7.8104±1.78647.
Conclusion: This article initially established the normal range of normal thoracic and lumbar vertebral SUVmax in different sexes, to provide a reference for clinical diagnosis and the evaluation of curative effect.

Authors listed for this abstract reported no relevant financial disclosures.

1799

Unusual Delayed Clearance of I-131 MIBG in a Neuroblastoma Patient.
Miguel de la Guardia, BS, RT(N)[1], Susan Corey, CNMT[1], Jaime Barnes, RRPT[1], Meaghan Granger, MD[2]; [1]Radiology, Cook Children's Medical Center, Fort Worth, TX, USA, [2]Hematology / Oncology, Cook Children's Medical Center, Fort Worth, TX, USA. (3115)

Objectives: Neuroblastoma is by far the most common cancer in infants accounting for about 6% of all cancers in children. There are about 700 new cases of neuroblastoma each year in the United States. (1) Meta-iodobenzylguanidine labeled with the theranostic agent iodine-131 (^{131}I-MIBG) has shown activity against neuroblastoma, with response rates for relapsed disease as high as 50%. (2) After intravenous injection of ^{131}I-MIBG, approximately 50% of the administered radioactivity is excreted in the urine during the first 24 hours, and 90% within 96 hr (3). Here we report on a case with Curie score of 21 where due to the tumor burden in bone, the elimination half-life of the I-131 mIBG after 24 hours, was 3 days long (Figure 1). Imaging with I-123 mIBG is required before a second treatment is administered to determine there is stable disease or response after the most recent infusion and determine if the patient has is eligible for an additional treatment (4). The patient was administered 483 mCi of I-131 mIBG prior to the planned injection of the I-123 mIBG for the diagnostic scan. Due to the slow rate of excretion we were not sure if additional activity of I-123 mIBG would be required to perform an optimal scan 7 weeks after the therapy in order to overcome the scatter from any remaining I-131 mIBG. To our knowledge there is no record of patient dose rate or imaging performed after such a prolonged time after therapy. Upon arrival to Nuclear Medicine 6 weeks after treatment, the patient was surveyed with a Ludlum 9DP1 ion chamber survey meter. Initial radiation exposure readings were 0.03 mR/hr at 1 meter, and 0.1 mR/hr on contact from the umbilicus. A survey was performed over the areas of the spine that had increased uptake in the I-131 mIBG post therapy scan. The recorder readings varied from 0.03 mR/hr and 0.04 mR/hr on contact. A planar scan over the area with the highest reading was performed with a scan on the iodine-131 setting demonstrated background activity, but not focal uptake. Therefore, the decision was made to proceed with the planned injection of I-123 mIBG for the diagnostic scan the next day. While there is much delayed excretion, the remaining activity cleared from tumors fast enough so there was no interference with the I-123 mIBG diagnostic scan. However, several questions arise that require additional data to determine if:
1) Does Curie score affect retention time of the I-131 in all patients or is this an anomaly?
2) The time required to release patients from radiation isolation predictable on the basis of activity administered and the Curie score?
3) Patients with prolonged excretion rate require longer at-home precautions upon released from hospitalized radiation isolation?
References:
1) American Cancer Society. Cancer Facts & Figures 2016. Atlanta, Ga: American Cancer Society; 2016.
2) Katherine K. Matthay, Gregory Yanik, Julia Messina, et. al., Phase II Study on the Effect of Disease Sites, Age, and Prior Therapy on Response to Iodine-131-Metaiodobenzylguanidine therapy in Refractory Neuroblastoma. J Clin Oncol 2007; 25: 1054-1060.
3) Vallabhajosula S, Nikolopoulou A. Radioiodinated metaiodobenzylguanidine (MIBG): radiochemistry, biology, and pharmacology. Semin Nucl Med 2011; 41(5): 324-333.
4) Neeta Pandit-Taskar and Shakeel Modak, Norepinephrine Transporter as a Target for Imaging and Therapy. J Nucl Med. September 1, 2017; 58: Supplement 2: 39S-53S

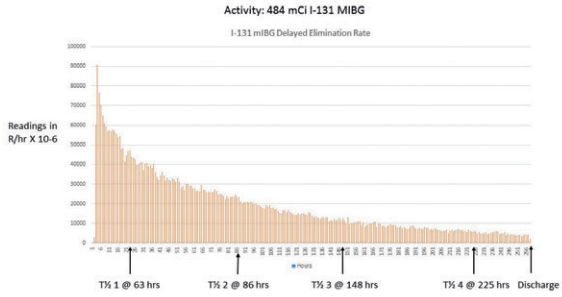

Authors listed for this abstract reported no relevant financial disclosures.

1800

Impact of different reconstruction algorithms and OSEM reconstruction parameters on quantitative results in SPECT/CT.
Huang Kemin; the First Peoples Hospital of Foshan, Foshan, China. (48)

Purpose: Impact of different reconstruction algorithms and OSEM reconstruction parameters on quantitative results in SPECT/CT
[Abstract]
Objectives: To evaluate the effects of 3-dimensional ordered subset expectation maximization(3D-OSEM), 2-dimensional ordered subset expectation maximization(2D-OSEM), filtered-back projection (FBP),and the number of OSEM iterations and subsets on quantitative results in SPECT/CT.
Methods: A Jaszczak cylindrical phantom and IEC body phantom were performed with routine SPECT/CT imaging using CT attenuation correction, scatter correction and 3D-OSEM reconstruct image. The system volume sensitivity(cpm/kBq) were acquired from the reconstructed image

of Jaszczak phantom study, we calculated the absolute activity concentration (kBq /ml)of the hot sphere from IEC phantom study, then checking computations the quantitative accuracy of all. Change the reconstruction algorithm (2D-OSEM, FBP) and OSEM reconstruction parameters (number of iterations and subsets) to reconstruct the IEC phantom, Compared the difference of quantitative results from different reconstruction algorithms and OSEM iterations and subsets.

Results: When reconstructing images with 3D-OSEM, 2D-OSEM and FBP, the average quantitative error of each sphere increases with the decrease of the spherical volume(r=0.831,0.831,0.826, *p* all<0.05). The average difference between the quantitative values and the true values of the different volume spheres among the three reconstruction algorithms was statistically significant (F = 8.850, p <0.05), among them that 3D -OSEM was less than 2D-OSEM (352 ± 198 and 423 ± 164 kBq / ml, p <0.05), 2D-OSEM was less than FBP (423 ± 164 and 695 ± 36 kBq / ml, p <0.05).The quantitative error of the seven different volume spheres (26.25 ~0.52ml) decreased with the increase of the number of iterations (r = 0.721, 0.681, 0.691, 0.711,0.845,0.893, *p* all<0.05), and decreased with the increase of the number of subsets (r = 0.670, 0.694, 0.717, 0.852, 0.956, 0.998, *p* all<0.05), But there was a significant difference in the variation between different volumetric spheres, the variation of the quantitative error tends to be stable when the number of iterations is greater than 8 and the number of subsets is greater than 6 in the larger sphere (26.25 ~ 5.57ml), and it was stable when the number of iterations is greater than 16,but it was continue to decreasd as the number of subsets increases in the smaller sphere (2.57 ~0.52ml).

Conclusions: The quantitative accuracy of 3D-OSEM reconstruction based on CT attenuation correction and scattering correction is significantly better than 2D-OSEM and FBP. Choosing the appropriate OSEM reconstruction parameters is helpful to improve the quantification accuracy in SPECT/CT.

Authors listed for this abstract reported no relevant financial disclosures.

1801

Clinical Characteristics of Precocious Puberty Girls and Comparison Analysis of GnRH Test Results with Diagnosis Type. Kim Jungin, WonHyun Kwon, KiChoon Moon, In Won Lee; Department of Nuclear Medicine, Seoul National University Bundang Hospital, Seongnam, Korea, Republic of. (1795)

Purpose: Precocious Puberty is defined as the development of secondary sexual characteristics in girls younger than 8 years. In this study, we retrospectively analyzed the diagnostic difference of the GnRH (Gonadotropin-releasing Hormone) stimulation test results with medical records of Precocious puberty in girls.

Methods: 118 girls were enrolled from Seoul National University Bundang Hospital Pediatrics, Endocrinology Internal Medicine due to early onset of sexual development from February 2016 to December 2016. They were divided into 3 groups; True precocious puberty group (n=57), early puberty group (n=39), and premature thelarche (n=22) group. Tanner stage, chronological age, bone age, height, and body weight for each group were collected. GnRH test results including LH (basal, 30min, 45min, 60min), FSH (basal, 30min, 60min) were compared for each group. peak value distribution of LH and FSH, peak LH/basal LH ratio, peak LH/Peak FSH ratio were assessed for each group. P-value 0.05 was used as statistical threshold.

Result: For height and weight, there was no significant difference among three groups (P>0.05). However, there was significant differences among three groups in the chronologic age and bone age (P=0.0002, for chronologic age 7.1yrs±0.81 vs 8.05yrs±0.03 vs 7.02yrs±0.58, for bone age 9.9yrs±0.9 vs 10.0yrs±0.62 vs 8.04yrs±1.29 for each group). In precocious puberty group, peak LH level was shown at 30min (82.5%), 45min(12.3%) or 60min(5.3%), and peak FSH level was shown at 30min(8.8%), or 60min(91.2%). In early puberty group, peak LH level was shown at 30min(79.5%), 45min(17.9%), or 60min(2.6%), and peak FSH levels at 30min(7.7%), or 60min(92.32%). In premature thelarche group, peak LH level was shown at 30min(32%), 45min(59%), or 60min(9.0%) and peak FSH levels at 60min(100%).

Conclusion: In order to diagnose the true precocious puberty, LH peak after GnRH stimulation is increased by more than two to three times compared to baseline or a predetermined level or more than 5~10 IU/L increases. GnRH stimulation test could be the most accurate method in diagnosis of precocious puberty by evaluating the hypothalamus-pituitary gland-gonad axis.

Authors listed for this abstract reported no relevant financial disclosures.

1802

Thallium-201 washout rate analysis for myocardial perfusion SPECT using a CZT cardiac camera. Masaru Ishihara, MS[1,2], Masahisa Onoguchi, PhD[2], Takayuki Shibutani[3], Yasuyo Taniguchi, MD[4]; [1]Department of Radiology, Hyogo Cancer Center, Himeji, Japan, [2]Department of Quantum, Graduate School of Medical, Kanazawa, Japan, [3]Kanazawa University, Kanazawa, Japan, [4]Department of Cardiology, Hyogo Brain and Heart Center at Himeji, Himeji, Japan. (1161)

Objectives: For a diagnosis of coronary artery disease, the thallium-201-chloride (^{201}Tl) washout rate (WOR) is a valuable tool for assisting myocardial perfusion single-photon emission computed tomography (SPECT). Most of ^{201}Tl WOR analysis using a cadmium-zinc-telluride (CZT) cardiac camera is not investigated, and no differences in WOR values between CZT SPECT and conventional Anger-type SPECT have been reported. The present study aimed to verify the accuracy of the ^{201}Tl WOR analysis for myocardial perfusion SPECT using a CZT SPECT in the phantom study, and to compare it with conventional SPECT in clinical cases.

Methods: For CZT SPECT, a D-SPECT cardiac imaging system (Spectrum Dynamics Medical, Caesarea, Israel) was used. For the phantom study, myocardial phantom (model RH-2, Kyoto-Kagaku, Kyoto, Japan) was injected into the myocardium area with ^{201}Tl (52.6 kBq/mL), and 10-minute acquisitions were performed after 0, 24, 46 and 62 hours to reflect natural decay rates. The global WOR values were analyzed for 0 and 24 hours (infarction model), 0 and 46 hours (ischemia model), and 0 and 62 hours (normal model), respectively. Each value between the theoretical WOR as reference standard and the phantom WOR as measured were compared. For the patient study, 52 consecutive patients (mean age 73.1 ± 8.5 years, 36 [69.2%] men) were examined with ^{201}Tl stress/redistribution imaging (111 MBq for stress imaging) for ergometer (13 patients) or adenosine (39 patients). In all cases, CZT SPECT and conventional SPECT (BrightView; Philips Medical Systems, Cleveland, OH, USA) were performed as consecutive acquisition. CZT SPECT was performed with a 5-minute acquisition and conventional SPECT with a 10- to 12.5-minutes acquisition. Stress imaging was performed 5-10 minutes after the ^{201}Tl injection, and redistribution imaging was performed 3-4 hours later. The global WOR values were compared. Additionally, we compared the normal and multi-vessel disease myocardial perfusion patients in each of the two SPECT devices. Patient study results were calculated as the percent per hour. All differences between CZT SPECT and conventional SPECT were assessed using the Mann-Whitney U test.

Results: For the phantom study, the theoretical WOR values versus the phantom WOR values were 20.40% vs. 20.79% at 0 and 24 hours, 35.42% vs. 35.63% at 0 and 46 hours, and 44.53% vs. 45.13% at 0 and 62 hours, respectively. For the patient study, CZT SPECT versus conventional SPECT WOR values for 52 patients were 12.59 ± 2.26%/hour vs. 12.57 ± 2.27%/hour (p = 0.984); the stress-redistribution imaging time intervals were 3.47 ± 0.23 hours vs. 3.46 ± 0.22 hours. The CZT SPECT versus conventional SPECT WOR values for seven normal myocardial perfusion patients were 13.42 ± 1.53%/hour vs. 13.93 ± 1.24%/hour (p = 0.338), and for seven multi-vessel disease myocardial perfusion patients were 10.64 ± 2.20%/hour vs. 10.84 ± 2.26%/hour (p = 0.848).

Conclusions: ^{201}Tl WOR analysis using CZT SPECT demonstrated excellent accuracy in the phantom study. Clinically, ^{201}Tl WOR values obtained with CZT SPECT that enabled significantly reduced acquisition time were similar to those with conventional SPECT.

Authors listed for this abstract reported no relevant financial disclosures.

1803

Evaluation of normalization methods for the Standardized Uptake Value in Bone SPECT/CT. Shohei Fukai[1], Takuro Umeda[1], Hiromitsu Daisaki, PhD[2], Noriaki Miyaji[1], Shuto Nakazawa[1], Ken Shimizu[2], Takashi Terauchi, MD[1], Mitsuru Koizumi, MD, PhD[1]; [1]The Cancer Institute Hospital, Japanese Foundation For Cancer Research, Tokyo, Japan, [2]Gunma Prefectural College of Health Sciences, Gunma, Japan. (1387)

Objectives: Standardized uptake value (SUV) normalized by lean body mass is recommended by positron emission tomography response criteria in solid tumors (PERCIST) to reduce the dependency of body weight in ^{18}F-FDG PET/CT. In this study, the dependency of body weight in SUV values were evaluated for each of normalization methods in bone SPECT/CT.
Methods: ^{99m}Tc-(H)MDP bone SPECT/CT was conducted with the use of Symbia Intevo (Siemens Healthcare, Erlangen, Germany). Patients who were not identified as having any bone metastases were retrospectively reviewed on 237 cancer patients (117 men, 120 women). SUV-mean values of the first lumbar vertebrae (L1) were measured in spheroidal volume-of-interest (2.41cm^3), using a vender-neutral software GI-BONE (AZE, Tokyo, Japan). The SUV-mean values were calculated by normalization parameters using body weight (SUV-bw), lean body mass (SUV-lbm), Japanese lean body mass (SUV-Jlbm), body surface area (SUV-bsa), and bone mineral (SUV-bone). The Pearson's correlation coefficient between body weight and each of SUVs were analyzed.
Results: The correlation coefficients in each of SUVs(SUV-bw, SUV-lbm, SUV-Jlbm, SUV-bsa, SUV-bone) were (r=0.235(p<0.05),r=0.062(p=0.50),r=-0.004(p=0.97),r=-0.069(p=0.46),r=-0.006(p=0.95)) in men and, (r=0. 342(p<0.05),r=0.086(p=0.35),r=0.046(p=0.62), r=0.023(p=0.80),r=0.092 (p=0.32)) in women respectively.
Conclusions: Although SUV-bw showed significantly positive correlation with body weight, SUV-lbm, SUV-Jlbm, SUV-bsa and SUV-bone showed no significantly positive correlations. Normalization method of SUV may be important especially for response assessment or follow-up using bone SPECT/CT.

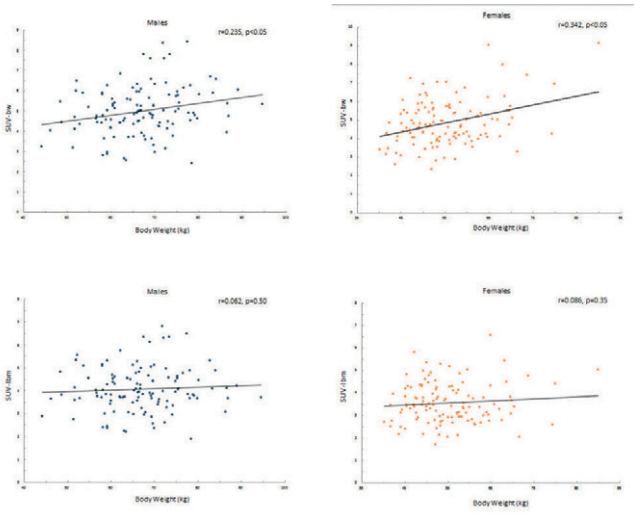

Authors listed for this abstract reported no relevant financial disclosures.

1804

Phase I IND-enabling studies for the amyloid-imaging peptide p5+14 (Api1832) - a novel agent for the detection of systemic amyloidosis. Alan Stuckey, CNMT[1], Angela D. Williams, MS[2], Tina A. Richey[3], Carmella Moody[4], Steve Kennel, PhD[1], Jonathan S. Wall[5]; [1]University of Tennessee Graduate School of Medicin, Knoxville, TN, USA, [2]University of Tennessee GSM, Knoxville, TN, USA, [3]University of Tennessee, Knoxville, TN, USA, [4]3RTI International, Research Triangle Park, NC, USA, [5]University of Tennessee, Graduate School of Medici, Knoxville, TN, USA. (1603)

Objectives: There are approximately 4,500 new cases each year of systemic amyloidosis in the US. Despite decades of active research that have increased our understanding of this devastating disease, systemic amyloidosis remains a poorly-diagnosed and, for this reason, a generally incurable disease. Due to the complexity of the disease and its low prevalence in the population, a correct diagnosis of amyloidosis can take many years. Consequently, the prognosis for patients is poor with a median survival of three years or less from diagnosis. Presently there are no FDA approved methods for imaging systemic amyloidosis in these patients although in major imaging centers Aβ amyloid imaging agents are being employed with variable efficacy. To address this we have developed a synthetic 45 all-L-amino acid peptide that, in preclinical studies binds many of the 30 diverse forms of systemic amyloidosis (Molecules. 2015; 20(5):7657-82). In preparation for an investigational new drug (IND) application to the US FDA for a single-site Phase I PET/CT imaging study of 124I-labeled peptide p5+14 we have characterized the peptide in preparation for developing appropriate release criteria for efficacy and safety. Peptide p5+14 drug substance, synthesized by Ambiopharm Inc, is ~95% pure based on HPLC profiling. The peptide was deemed safe In a single IV dose safety study in male and female rats using 50x and 100x the human equivalent dose. No adverse events were seen and the MTD and NOAEL were considered to be >17.6 mg/Kg. Peptide was radiolabeled using 2 mg of peptide and 5 mCi to yield a mono-iodonated preparation with a specific activity of <2.5 mCi/mg. Chromatographic evaluation of the drug intermediate, following sterile filtration, was used to determine the peptide concentration. The preparation was >90% pure and eluted as a single radioactive species with >90% radiopurity. Residual acetonitrile was <410 ppm by gas chromatography. The formulated peptide (in sterile PBS with 5% human serum albumin and 0.5 mg/mL ascorbic acid) was shown to be sterile (TSB and FTM media), particulate free, and with an endotoxin level of <175 EU/dose. Bioactivity of the formulated drug product was evidenced by >60% reactivity in a pull-down assay using synthetic human amyloid fibrils as the substrate and was deemed compatible with storage and delivery systems in a hold-up assay. The process we have developed for the production of 124I-p5+14 peptide drug product results in a sterile, endotoxin-free, mono-iodinated species with peptide carrier. The drug is bioactive with >90% radiopurity and peptide purity. We anticipate beginning the Phase I PET/CT exploratory study in patients with diverse forms of systemic amyloidosis in April 2018.

Authors listed for this abstract reported no relevant financial disclosures.

1805

Reduced acquisition time or activity dose for ^{123}I-FP-CIT SPECT with compressed sensing-based iterative reconstruction. Norikazu Matsutomo, PhD, Takeyuki Hashimoto, PhD. in Engineering, Tomoaki Yamamoto, PhD; Department of Medical Radiological Technology, Kyorin University, Mitaka, Japan. (1788)

Objectives: The compressed sensing is a signal processing technique that was initially proposed for spare signal recovery. And it is capable of reconstructing high quality images from a substantially smaller number of views than those needed in filtered back projection (FBP). This study aimed to evaluate CS-based iterative reconstruction (CS-IR) for ^{123}I-FP-CIT SPECT to reduce image acquisition time or activity dose.
Methods: We used the cylinder/sphere and the striatal digital phantom models. The total projection number was set at 120, 90, 60, and 30. In addition, acquired maximum number of photons in a projection was varied from 25 to 100. SPECT images were reconstructed using FBP, Maximum likelihood expectation maximization (MLEM), and CS-IR. The total-

variation transform with local image gradient in L1-norm was adopted in our compressed sensing algorithm. The effects of CS-IR were examined according to the resolution recovery factor, activity concentration linearity, percent coefficient of variation (%CV), and specific binding ratio (SBR).
Results: For the resolution recovery factor and activity concentration linearity, no differences were observed between each reconstruction when decreasing the projection number and counts. Decreasing the projection number and counts, %CV obtained by CS-IR was superior to that obtained by other reconstruction. %CV obtained by 60 projection CS-IR was equivalent to that obtained by 120 projection FBP and MLEM. The variation of SBR was the highest in FBP and SBR obtained by CS-IR was similar to that of MLEM.
Conclusions: We demonstrated that CS-IR with decreasing the projection number and acquisition count provided a good image quality compared to commonly SPECT reconstruction. Compressed sensing could help to reduce overall SPECT acquisition time or activity does in ^{123}I-FP-CIT SPECT.

Authors listed for this abstract reported no relevant financial disclosures.

1806

Radiation safety post liver Y90 therapy - Is the hospital ward safe? Michael Tong; National University Hospital, Singapore, Singapore. (3317)

Objectives: Liver radiomicrospheres treatments are carried out with Yttrium 90 (Y90) -resin incorporated in biocompatible microspheres. Y90 is a pure beta-particle-emitter with a physical half-life of 64.2 hours, 0.94 MeV decay energy, and an average penetrative depth of 2.4mm in human tissue. The patients in our institution are administered with a mean activity of 0.92 Gbq (+ 0.42). When patients are warded post-treatment to monitor their clinical conditions, these patients become a radiation source/concern mainly to the nurses and housekeepers during the hospital stays, and to visiting family members. The study strives to explore if the concerns are warranted.
Methods: The external radiation exposure rates of 30 patients were measured using a calibrated ionization survey meter. The measurements were taken at 1 meter, 2 meters, and 3 meters from the patients' supine body axis (liver to pelvis), immediately post therapy, and at 24 hours and 48 hours. Urinary excretions in 8 patients were also measured to estimate the potential risk from the discharge into the sewage system. Radiation levels of general/biohazard wastes, toilet bowl, and external radiation exposure rates were also measured.
Results: Dose rates of 16.6 ($\pm$1.3), 8.5 (+ 1.2), and 1.1 (+ 1.1) µSv/hr were measured at 1, 2, and 3 meters respectively immediately post therapy. All patients had exposure rates below 1 µSv/hr by 24 hours at 1 meter from the liver. The urinary bag had a maximum dose rate recorded at 1.2 µSv/hr at 6 hours post therapy. One unflushed toilet had a maximum reading at 0.9 µSv/hr, 6.2 hours post-therapy. Insignificant radiation dose readings were recorded from the waste bins and the room environment. The calculated assumption of a housekeeper at 1 meter from a patient at these dose rates for an average continuous 0.25 hours showed insignificant radiation exposure. The conservative assumption of a nursing staff or family member at an interaction distance of 1 meter from a patient at these dose rates for a continuous 6 hours based on the measurements is less than 0.1 mSv of radiation dose exposure, with decay taken into consideration. Mean TEDE dose was 0.04 mSv.
Conclusion: The beta dose delivery is mainly confined to the liver with minimal biologic elimination of Y90. There is minimal biologic elimination of Y90 from the patient's bodies, with only trace amounts detected. Routine housekeeping of the room during and post patients' stay/discharge is safe with unwarranted radiation concerns.

Authors listed for this abstract reported no relevant financial disclosures.

1807

PET department. Martin A. Schmitt, BS, CNMT, PET; Barnes-Jewish Hospital, Saint Louis, MO, USA. (1483)

Objectives: A review of our experience implementing a procedure for Positron Emission Tomography (PET) imaging for staging, restaging and monitoring neuroendocrine tumors (NETs). Using Netspot® ^{68}Ga Dotatate, we have been better able to serve the NETs patient population. The introduction of this new PET diagnostic agent and procedure has improved our physicians' ability to manage patients with NETs, as compared to traditional Nuclear Medicine imaging with Octreoscan® ^{111}In Pentetreotide. Bringing this agent to a busy PET department has however introduced new technical challenges that our department has not had much experience in dealing with. NETs are neoplasms arising from neural crest tissue within the adrenal medulla, pituitary, parathyroid, thyroid, and pancreas, respiratory and GI tracts. ^{18}F-FDG has a limited role in well-differentiated NETs, as they are slow growing with minimal FDG uptake. 111In-Octreoscan is a somatostatin analog that binds to somatostatin receptors on a variety of cells. This octapeptide concentrates in tumors containing a high density of somatostatin receptors. Netspot®, the PET diagnostic agent that was FDA approved in 2016, has been good for this disease because like Octreoscan® it has similar methods of pharmacological uptake. However, Netspot® is being reported as having higher sensitivity for lesion detection leading to accelerated adoption in the field. This rapid adoption can create technical challenges, as departments must be ready to use a different PET radionuclide. Use of ^{68}Ga requires a unique workflow, such as setting and calibrating the dose calibrator to this isotope and the addition of performing daily constancy checks on ^{68}Ga. Also, equally important to have imaging success is to create appropriate scanner protocols, establish patient prep and concomitant medication review. After 11 months of offering Netspot®, our institution had a significant volume increase due to demand for NETs imaging. This represents a population that ^{18}F-FDG PET in the past could not accurately serve. For referring physicians, this represents a diagnostic test with improved sensitivity and specificity over previous options. Additionally, scans are performed and reported on the same day, leading to decreased scan time compared to Octreoscan®. With the recent introduction of Netspot® ^{68}Ga Dotatate, Axium®, and amyloid imaging, our PET facility now serves a new group of patients that previously were not being imaged in PET. As a result, we are now offering referring physicians new diagnostic tool for patients with difficult diseases to manage, while also expanding the type of exams which we provide as a clinical PET service. The more PET expands from a single clinical exam to a true multi exam modality, the less vulnerable PET will be to external and uncontrolled market forces.

Authors listed for this abstract reported no relevant financial disclosures.

1808

Development of a novel 3D dynamic cardiac phantom simulated human anatomy. Yuta Maeda[1], Masahisa Onoguchi, PhD[1], Takayuki Shibutani[1], Narihiro Hara[2]; [1]Department of Quantum, Graduate School of Medical, Kanazawa University, Kanazawa, Japan, [2]Department of Radiology, Sumitomo Hospital, Osaka, Japan. (1322)

Objectives: We developed a dynamic cardiac phantom equipped with double pump can move both epi- and endocardium in previous study. However, that cardiac phantom was not simulated the form of the body contour such as oblique of the cardiac axis, and was not equipped with the liver and gallbladder simulated scatter and attenuation from human body as the structure of human anatomy. The aim of this study was to demonstrate the utility of development of the novel 3D dynamic cardiac phantom simulated the structure of human anatomy.
Methods: We improved previous phantom as follows: tilting approximately 30 degrees to body axis, changing the shape of body from circle to ellipse, attaching liver and gallbladder in phantom as other organs. In addition, the LV volume of cardiac created three-types which simulated small size as a small heart, size as normal heart and large size as a dilated cardiomyopathy. The cardiac true volumes of small, regular and large types were 20.8, 40.0 and 202.0 mL for ESV, 20.8-221.9, 40.0-241.1 and 202.0-403.1 mL for EDV, 0-90.6%, 0-83.4% and 0-49.9% for LVEF, respectively. The LV chamber and myocardial parts of the phantom filled with non-radioactive and ^{99m}Tc solution, respectively. A dual detector SPECT-CT (Symbia T6; Siemens) system with the low-energy high-resolution (LEHR) collimator used to acquire the phantom. Acquisition parameters were set on 16 flames per cardiac cycle, energy window 140 keV ±10%, 64×64 matrix, a rotation angle of 360, 60 projections. Acquisition time was determined from the average myocardial counts obtained by region of interest (ROI) on the lateral myocardial wall in left anterior oblique (LAO) 45 degree's view,

and the average myocardial counts set on approximately 140 counts per pixel. Image reconstruction was performed with filtered back projection (FBP) and ordered subset expectation maximization (OSEM) methods. The pre- and reconstruction filters for FBP method used the Butterworth with the cut-off frequency 0.39 cycles/cm and 16 and Ramp. Furthermore, the subset and iteration for OSEM method set 12 and 10, and Gaussian filter as post-filter was used with the full width at half maximum (FWHM) 13.2 mm. The full width at half maximum (FWHM) for Gaussian filter was set 13.2 mm. The attenuation, scatter and resolution corrections were not performed. The ESV, EDV and LVEF were analyzed using a quantitative gated SPECT (QGS).

Results: The correlation between true and measured value in each LV function such as the EDV, ESV and LVEF for the three types was very good.

Conclusion: We developed a novel dynamic cardiac phantom simulated human anatomy that is able to change the myocardial wall and LV volume. It was suggested that the phantom may be possible to the standardization.

Authors listed for this abstract reported no relevant financial disclosures.

1809

^{18}F-FDG PET/CT features of thoracolumbar tuberculosis. Tan Beibei, Bachelor of medicine; Southwest medical university affiliated hospital, Luzhou, Sichuan Province, China. (57)

Objectives: To investigate the ^{18}F-FDG PET/CT features of thoracolumbar tuberculosis.

Methods: 98 patients with vertebra bone destruction receiving ^{18}F-FDG PET/CT examination from January 2007 and May 2016 in our hospital were enrolled in the study and divided into tuberculosis group (n = 27) and non-tuberculosis group (n = 71) according to the result of pathology examination and follow-up. ^{18}F-FDG PET/CT signs were compared between the two groups, and binary classification logistic regression was used to screen out the statistically significant signs.

Results: 42, lesions and 114 lesions were detected in tuberculosis group (n = 27), non-tuberculosis group, respectively. Results of binary classification logistic regression analysis showed that continuous vertebral involvement, intervertebral disc involvement, vertebral body compression fractures, cold abscess, “radioactive cold area” were the independent factors to diagnose thoracolumbar tuberculosis ($P < 0.05$), and their sensitivity, specificity, positive predictive value, negative predictive value, Youden index were 73.8%, 69.3%, 47.0%, 87.8%, 43.1%, 71.4%, 74.6%, 50.8%, 87.6%, 46.0%, 54.8%, 79.8%, 50.0%, 82.7%, 34.6%, 21.4%, 99.1%, 90.0%, 77.4%, 20.6%, 61.9%, 81.6%, 55.3%, 85.3%,43.5%, respectivlyrespectively. The diagnosis efficiency of ”continuous vertebral involvement + intervertebral disc involvement” group was highest, and its sensitivity, specificity, positive predictive value, negative predictive value, Youden index were 71.4%, 81.6%, 58.8%, 88.6%, 53.0%, respectivlyrespectively.

Conclusions: For thoracolumbar tuberculosis, continuous vertebral involvement, intervertebral disc involvement, vertebral body compression fractures, cold abscess and “radioactive cold area” were the statistically significant ^{18}F-FDG PET/CT signs, and the combination of “”continuous vertebral involvement + intervertebral disc involvement”” group had the highest diagnosis efficiency.

Keywords: Positron-emission tomography; Thoracolumbar tuberculosis; Tomography; Differential diagnosis

Table 2 The results of multivariate logistic regression analysis

Variables	Regression coefficient	Standard error	OR value	95%CI	Waldχ2 value	P value
Continuous vertebral involvement	1.897	0.759	6.669	1.507~ 29.521	6.250	0.012
Inter-vertebral disc involvement	2.189	0.813	8.930	1.815~ 43.943	7.252	0.007
Vertebral body compression fractures	1.093	0.543	2.983	1.029~ 8.647	4.051	0.044
Cold abscess	2.585	0.916	13.266	2.203~ 79.883	7.965	0.005
“Radioactive cold area”	2.298	0.693	9.953	2.559~ 38.712	10.995	<0.001

Table 3 Comparison of diagnostic efficacy of various signs and their combinations

Variables	Sensitivity (%)	Specificity (%)	Positive predictive value	Negative predictive value (%)	Youden index
Continuous vertebral involvement	73.8	69.3	47.0	87.8	43.1
Intervertebral disc involvement	71.4	74.6	50.8	87.6	46.0
Vertebral body compression fractures	54.8	79.8	50.0	82.7	34.6
Cold abscess	21.4	99.1	90.0	77.4	20.6
"Radioactive cold area"	61.9	81.6	55.3	85.3	43.5
Continuous vertebral involvement+ Intervertebral disc involvement	71.4	81.6	58.8	88.6	53.0
Continuous vertebral involvement+ Vertebral body compression fractures	47.6	86.8	57.1	81.8	34.5
Continuous vertebral involvement+ Cold abscess	19.0	99.1	88.9	76.9	18.2
Continuous vertebral involvement+ "Radioactive cold area"	57.1	84.2	57.1	84.2	41.4
Intervertebral disc involvement+ Vertebral body compression fractures	50.0	82.5	51.2	81.7	32.5
Intervertebral disc involvement+ Cold abscess	16.7	99.1	87.5	76.4	15.8
Intervertebral disc involvement+ "Radioactive cold area"	54.8	83.3	54.8	83.3	38.1
Vertebral body compression fractures+ Cold abscess	14.3	100.0	100.0	76.0	14.3
Vertebral body compression fractures+ "Radioactive cold area"	45.2	84.2	51.4	80.7	29.4
Cold abscess+ "Radioactive cold area"	16.7	100.0	100.0	76.5	16.7

Authors listed for this abstract reported no relevant financial disclosures.

1810

Development of automated statistical Z-score calculation software using bone SPECT/CT. Kenta Miwa, PhD[1], Noriaki Miyaji[2], Kazunori Kawakami[3], Kei Wagatsuma[4], Yuto Kamitaka[1], Tensho Yamao[1]; [1]Department of Radiological Sciences, International University of Health and Welfare, Ohtawara, Japan, [2]Japanese Foundation For Cancer Research, Tokyo, Japan, [3]FUJIFILM Pharma, Co., Ltd, Tokyo, Japan, [4]Research Team for Neuroimaging, Tokyo Metropolitan Institute of Gerontology, Tokyo, Japan. (2747)

Objectives: Various strategies have been proposed to produce quantitative bone SPECT data. Bone metastasis has been diagnosed using a standardized uptake value (SUV), but various factors impact its quantitative accuracy and reproducibility. We previously reported that statistical Z-scores are highly accurate and reproducible quantitative indices for bone SPECT. The present study developed and used an automated software (eZIS-bone) to calculate Z-scores, and aimed to determine the accuracy and reproducibility of Z-scores compared with SUV as quantitative indices for bone SPECT.
Methods: We retrospectively analyzed ^{99m}Tc-MDP SPECT/CT data of the thoracic, lumbar and pelvic regions acquired from 50 patients with suspected bone metastasis of breast or prostate cancer. Bone metastasis was confirmed by CT, MRI or biopsy in 37 lesions. Our software enters the projection data and includes automated algorithms for image reconstruction, attenuation and scatter correction, and anatomical standardization processing. Normal CT and SPECT templates were constructed for anatomical standardization and Z-scores were calculated as indices of abnormal uptake. Amounts of displacement between the normal CT template and the CT datasets from each patient were represented as a vector field and applied to the deformation of concomitant SPECT images acquired using SPECT/CT. The Z-score based means and standard deviations derived from the normal SPECT template and the SUV_{max} were calculated from all data from the patients and the relationship between Z-scores and SUV_{max} was analyzed. The diagnostic performance was compared between Z-scores and SUV_{max} using ROC curves.
Results: The automated method calculated Z-scores independently of operators, reconstruction methods and corrections. Z-scores derived from bone SPECT/CT significantly correlated with SUV_{max} ($r=0.82$, $p<0.05$). Z-scores among patients without metastatic bone metastases ranged from a relatively stable 0.7 to 2.2 (average, 1.2), whereas SUV_{max} was the range of 2.7 - 8.9 (average, 5.3). The AUC of both indices in ROC curves were almost identical.
Conclusion: We developed automatic software to reduce the variability of Z-score calculations using bone SPECT/CT images. A completely automated method can serve as a consistent imaging biomarker with which to standardize quantitative changes in bone SPECT/CT data.

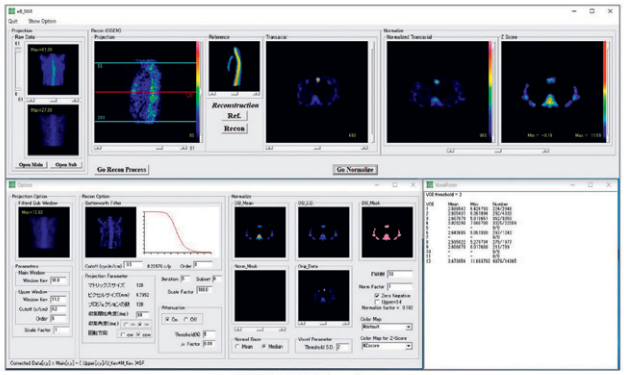

eZIS-BONE software

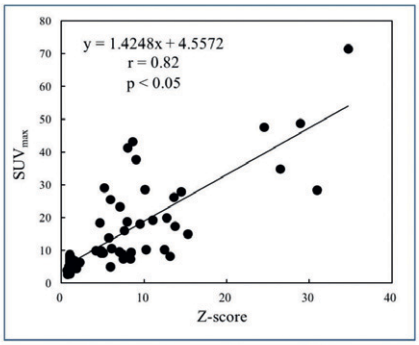

Relationship between Z-score and SUV_{max}

Authors listed for this abstract reported no relevant financial disclosures.

1811

Preparation & preliminary biological evaluation of ^{18}F-metal complex labeled glycosylated somatostatin analogues. Feihu Guo, PhD[1], Ting Liu, MD[2], Jin Du, PhD[3]; [1]HTA Company LTD., Beijing, China, [2]Nuclear and Radiation Safety Centre, Ministry of Environmental Protection, Beijing, China, [3]China Isotope & Radiation Corporation, Beijing, China. (1972)

Objectives: The aims of this study were doing the synthesis of Al/Fe^{18}F labeled glycosylated somatostatin analogues, the investigation of the SSTR positive tumor-targeting, the PET imaging in tumor bearing nude mice.
Methods: The glycosylated somatostatin analogue Glu-Lys(NOTA)-Octreotate was synthesized, and labelled using the chelation reaction with Al/Fe^{18}F complex. The octanol-water partition coefficient and the stability in saline and calf serum were investigated as well. The studies were focused on the biodistribution and the Micro-PET imaging in nude mice bearing AR42J tumor.
Results: The chemical purity of Glu-Lys(NOTA)-Octreotate was more than 95%, and synthetic yield was 11%. Glu-Lys([Al^{18}F]NOTA)-Octreotate (***1***) and Glu-Lys([Fe^{18}F]NOTA)-Octreotate (***2***) were prepared in 72% and 40% labeling rates, >95% RP after purification, and 25~30 min preparation time. (***1***) and (***2***) showed excellent water-solubility with logP value of -4.23 ± 0.19 and -4.18 ± 0.15, respectively. (***1***) was stable, but RP of (***2***) decreased significantly after incubation in the saline and the fetal bovine serum at 37℃ for 120min, this indicated that (***2***) was unstable in vitro. The biodistribution experiments in normal mice showed: both (***1***) and (***2***) were fast clear from blood, liver uptake was very low, all excluded by kidney. The uptake in pancreas which showed SSTR express was high. The high bone uptake of (***2***) was showed gradually with in 120min post injection. The biodistribution experiments and Micro-PET scans of (***1***) in nude mice bearing AR42J tumor showed: The high uptake was found in tumor, and tumor delineation of Micro-PET was clear. Receptor blocking experiments showed that the uptake of (***1***) in tumor was receptor-mediated.
Conclusions: A glycosylated somatostatin analogues was radio-synthesized fast and efficiently with Al^{18}F, Fe^{18}F labelled conjugate of (***2***) was unstable in vitro and in vivo and not suitable for PET imaging. The targeting of the probe (***1***) to the SSTR positive tumors was excellent. (***1***) is expected for PET imaging of SSTR positive tumors, and this study provides experimental basis for further research and development PET probes which could be used for the SSTR positive tumors diagnosis clinically.

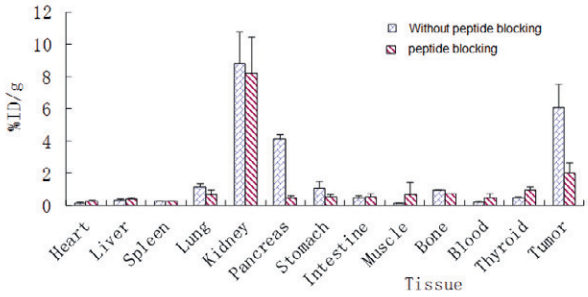

Fig. 1 The biodistribution of Glu-Lys([Al18F]NOTA)-Octreotate in mice bearing AR42J tumor

Authors listed for this abstract reported no relevant financial disclosures.

1812

Influence of anti-anxiety medication on gastric emptying studies. Fritzgerald C. Leveque, CNMT, Jeanine P. Drury, CNMT, Xiyao Zhao, Maria-Bernadette S. Tomas, MD, Christopher J. Palestro, MD, Kenneth J. Nichols, PhD; Northwell Health, New Hyde Park, NY, USA. (1841)

Objectives: Among contraindications for gastric emptying studies are medications that can complicate the interpretation of results. Anti-anxiety medications are not among these, yet there is evidence that pts may have some abnormal microbial biota that produce both abnormal gastric symptoms & anxiety or depression (J Affect Disord. 2017;208:22-32). Therefore, the objective of our investigation was to determine if there were relationships between anti-anxiety medication & gastric emptying.
Methods: Data were examined for 164 pts (age = 47±18 years; 116 female; 48 male) referred for evaluation of gastric symptoms who underwent gastric motility studies. No patient had diabetes. Pt charts were reviewed to determine whether they were on anti-anxiety medication at the time of the test. The imaging protocol for liquid emptying involved dynamic imaging of the stomach region for 30 min following ingestion of 7.4 MBq ^{111}In-DTPA in 10 mL water immediately followed by 300 cc water, & computing the $T_{1/2}$ of liquid gastric emptying. To evaluate solid gastric emptying, pts ingested a standardized meal consisting of 4 ounces of egg whites labeled with 37 MBq ^{99m}Tc-sulfur colloid, along with 2 pieces of bread & 4 grams of jam. Simultaneous 1-min anterior & posterior static images were collected with pts erect. Attenuation-corrected conjugate view counts were determined within manually drawn regions over the stomach, & per cent retention values recorded at 1-hr intervals for 4 hrs. The criteria for an abnormal liquid emptying study was $T_{1/2}$ > 20 min, & for a solid emptying study > 10% gastric retention at 4 hrs.
Results: 37/164 pts (23%) were on anti-anxiety medication at the time of the test. 92 (56%) pts had normal liquid & solid gastric emptying studies. 29 (18%) pts had abnormal liquid & solid gastric emptying studies, 58 (35%) pts had abnormal liquid gastric emptying studies, & 44 (26%) had abnormal solid gastric emptying studies. 29 (18%) pts had abnormal liquid & normal solid, while 15 (9%) pts had abnormal solid & normal liquid. There was a significant tendency of pts with abnormal liquid emptying to also have abnormal solid emptying (χ^2 = 22.7, p < 0.0001). Significantly fewer pts had abnormal liquid emptying who were on medication than those who were not (14% versus 42%, p = 0.001), with more rapid emptying time (18±18 versus 25±25 min, p = 0.04). There was a significant tendency of pts on medication to have both liquid & solid normal emptying results (χ^2 = 9.0, p = 0.003), & significantly more pts on medication had both liquid & solid normal emptying results than pts not on these medications (78% versus 48%, p = 0.001).

Conclusions: Our results suggest that anti-anxiety medications may accelerate gastric emptying in some pts who are referred for motility studies. If confirmed in a larger series of pts, then it could be advisable to take these medications into account in the interpretation of study results.

Authors listed for this abstract reported no relevant financial disclosures.

1813

Correlation between SBR and SUV for each correction in the dopamine transporter SPECT. Akihiro Shiokawa[1], Masahisa Onoguchi, PhD[1], Takayuki Shibutani[1], Takahiro Konishi[2], Hiroto Yoneyama, PhD[2], Yuta Maeda[1]; [1]Department of Quantum, Graduate School of Medical, Kanazawa University, Kanazawa, Japan, [2]Department of Radiological Technology, Kanazawa University Hospital, Kanazawa, Japan. (2751)

Objectives: Recently, the standardize uptake value (SUV) is validated as the quantitative index in many SPECT examinations. Although the dopamine transporter SPECT is mainly used a specific binding ratio (SBR) as a quantitatively index, the SUV has not fully evaluated. Thus, we have to reveal the correlation of SBR and SUV by each correction method to confirm the utility of SUV. The goal of this study is to reveal correlation between SBR and SUV for each correction in the dopamine transporter SPECT.
Method: The ^{123}I solution was filled in two types of striatal phantom such as separated or integrated caudate and putamen. The radioactive concentrations of ^{123}I solution created 36.0, 26.6, 18.0, 13.2 and 4.7 kBq/mL corresponding radioactive ratio of approximately 8:6:4:3:1. We created different phantom of 6 patterns as separating type and 4 patterns as integrating type. SPECT scans used a dual head SPECT/CT system (Discovery NM/CT 670 Q.suit Pro, GE Healthcare Japan, Co., Ltd.) equipped with extended-low-energy general-purpose (ELEGP) collimator. SPECT acquisition was performed using a 128×128 matrix 1.0 zooming, with 120 projections a circular orbit of 15 cm radius, and pixel size of 4.42 mm and total acquisition time was 28-min. The SPECT images were reconstructed using ordered subset expectation maximization (OSEM) incorporating attenuation correction (AC), scatter correction (SC) and resolution recovery (RR). The subset and iteration of OSEM parameter were 10 and 6. Butterworth filter was used as smoothing filter, and a power and cut-off frequency were 16 and 0.45 cycles/cm. We created transverse images of four correction patterns with AC, AC and SC (ACSC), AC and RR (ACRR), and AC,SC and RR (ACSCRR). The SBR and SUV_{mean} were calculated using DaT view (AZE Co., Ltd.) and Q.Metrix (GE Healthcare Co., Ltd.) software programs. True value defined as the radioactive concentration ratio of the well-type scintillation counter, and we compared the true and measured values to reveal the correlation of SBR and SUV_{mean} by each correction.
Results: The correlation coefficient of true and measured values for SBR and SUV_{mean} was 0.954 and 0.951 with AC, 0.975 and 0.954 with ACSC, 0.964 and 0.958 with ACRR and 0.971 and 0.960 with ACSCRR, respectively, thereby all correction methods significantly showed excellent positive correlation both SBR and SUV_{mean} ($p<0.001$). Furthermore, the SBR and SUV_{mean} with ACSC were 12% lower value than those with AC. In addition, the SBR with ACRR was 5% lower value than that with AC, whereas SUV_{mean} with ACRR was 36% higher value than that with AC.
Conclusions: The SUV_{mean} could evaluate as quantitative index as well as SBR for dopamine transporter SPECT. Furthermore, the correlation of SBR and SUV_{mean} by each correction method has revealed.

Authors listed for this abstract reported no relevant financial disclosures.

1814

The effect of different regions of interest on the quantitative evaluation in amyloid PET images. Natsumi Shimokawa[1], Go Akamatsu, PhD[2], Miyako Kadosaki[1], Ayano Shoji[1], Naoki Hashimoto[1], Saki Kimoto[1], Masayuki Sasaki, MD, PhD[3]; [1]Kyushu University, Fukuoka, Japan, [2]Molecular Imaging, National Institute of Radiological Sciences, Chiba, Japan, [3]Dept Rad Sci Sch of Health Sci Kyushu Univ, Fukuoka, Japan. (1761)

Purpose: The quantitative analysis of amyloid positron emission tomography (PET) images can be used to determine the amyloid β (Aβ) deposition in the cerebral cortex, which is used for the diagnosis of Alzheimer's disease (AD). However, the appropriate regions of interest (ROIs) and reference area on the images must be assessed in order to calculate the quantitative values. These values depend on the setting methods of the ROIs. The purpose of this study was to examine the effect of different ROIs on the quantitative evaluation in amyloid PET images.
Methods: One hundred and sixty-six patients including 58 normal controls (NCs), 62 cases of mild cognitive impairment (MCI), and 46 cases of early AD were retrospectively investigated. They underwent amyloid PET at Japanese Alzheimer's disease neuroimaging initiative (J-ADNI). Clinical data were obtained by the National Bioscience Database Center (NBDC). ROIs were placed using an Automatic-anatomic-labeling region of interest (AAL-ROI) based on the anatomical brain region and an Empirically PiB-prone ROI (EPP-ROI) specialized for Aβ deposition. We evaluated the mean cortical standardized uptake value ratio (mcSUVR), which was calculated by averaging the five ROIs (posterior cingulate gyrus and precuneus, frontal lobe, temporal lobe lateral side, parietal lobe lateral side, occipital lobe). The reference region was the cerebellar cortex.
Results: The mcSUVR of NCs, MCI and AD were 1.39±0.34, 1.82±0.50, and 2.11±0.47 for EPP-ROI and 1.24±0.27, 1.56±0.38, and 1.78±0.37 for AAL-ROI, respectively. Significant differences were observed among these groups ($P<0.05$). The mcSUVR of EPP-ROI was significantly higher than that of AAL-ROI by 11.6%±3.47%, 15.5%±4.51%, and 18.2±3.09% for NCs, MCI and AD, respectively. In addition, the mcSUVR of EPP-ROI was higher than that of AAL-ROI by 10.3%±2.53%, 13.2%±2.55%, and 18.7±1.92% for negative, equivocal and positive, respectively.
Conclusions: This study suggested that the ROI influenced the quantitative values. The EPP-ROI result in higher SUVR values than the AAL-ROI between negative and positive. These results implied that the EPP-ROI can distinguish disease rather than AAL-ROI.

Authors listed for this abstract reported no relevant financial disclosures.

1815

A novel method to assist visual inspection of striatal uptake in DaT SPECT study: simulation of SBR maps based on MR anatomical images. Kaoru Satou[1], Keisuke Matsubara, PhD[2], Mamoru Kominami[1], Fumiko Kinoshita[1], Masanobu Ibaraki[3], Hajime Osaka[4], Hideto Toyoshima[1], Toshibumi Kinoshita, MD, PhD[5]; [1]Research Institute for Brain and Blood Vessels-Aki, Akita, Japan, [2]Research Institute for Brain and Blood Vessels Aki, Akita, Japan, [3]Akita Research Institute of Brain and Blood Vessel, Akita, Japan, [4]Research Institute for Brain and Blood Vessels-Akita, Akita, Japan, [5]Research Intitute for Brain and Blood Vessels - Ak, Akita, Japan. (2702)

Objectives: Dopamine transporter imaging with 123I-ioflupane SPECT (DaT SPECT) is a powerful tool to diagnose Parkinson's disease and other neurodegenerative disorders with parkinsonism. Primarily, uptake patterns in striatum (comma-shaped, period-shaped, etc.) on DaT SPECT images are visually evaluated. However, variability of shapes in striatum and scan angles can confound the apparent DaT uptake patterns and prevent accurate visual inspection. We aimed to develop a novel method to assist the accurate visual inspection of striatal uptake patterns in DaT SPECT. To solve the issue of variability in striatal shapes and scan angles, we simulated striatum-background ratio (SBR) maps based on magnetic resonance (MR) anatomical images acquired from individuals. The simulated map virtually mimics uptakes with healthy condition for each individual, and thus enables to compare the uptake patterns between virtually-generated healthy and measured SBR maps.
Methods: Procedures of the novel method are the followings: 1) striatal segmentation of individual MR images; 2) simulation of SBR maps with assigning virtual uptake values to segmented regions; 3) smoothing for simulated SBR maps with point spread function (PSF) to spatial resolution of SPECT scanner; 4) comparison between measured and simulated SBR maps. T1-weighted MR and DaT SPECT images were acquired from seven individuals including one healthy volunteer and six patients with suspected Parkinson's disease. The striatal segmentation of the individual MR T1 images were performed with FreeSurfer software package. The segmented striatal regions were manually revised with supervising by a neuroradiologist. The virtual uptake values (striatum:background=10:1) were assigned to generate the simulated SBR maps. Gaussian kernels with 14 x 14 x 20 mm full width half-maximum, corresponding with SPECT

scanner resolution, were applied in smoothing for the simulated SBR maps. Image registration between MR T1 and SPECT images were performed with normalized mutual information criteria by SPM12 software package. We compared between measured and simulated SBR maps both visually and quantitatively. For the quantitative comparison, number of voxels with SBR higher than 20% of maximum values on SBR maps (n_{max20}) and %ratio of n_{max20} between measured and simulated SBR maps (n_{max20}[measured] / n_{max20}[simulated] * 100) were calculated.
Results: Simulated SBR maps for a healthy volunteer and three patients diagnosed with essential tremor, cases with comma-shaped uptakes on measured SBR maps, visually corresponded with measured SBR maps for the same individuals. The %ratio of n_{max20} in these subjects were higher than 50% (52.6 - 82.3%). Low %ratio of n_{max20} (0.0 - 32.6%) were observed in three patients diagnosed with Parkinson's disease, cases with period-shaped uptakes on measured SBR maps. In visual inspection for these subjects, obvious differences in uptake patterns between simulated and measured SBR maps were observed.
Conclusion: The novel method to simulate SBR maps can precisely mimic uptakes in healthy condition for individuals, and assist accurate visual inspection in DaT SPECT studies.

Authors listed for this abstract reported no relevant financial disclosures.

1816

Uniformity phantom test of PET/MR. Byung Jin Kim, BS[1], Yong-Seok Lee[1], Yong-Hyun Cho[1], Moonsun Kim, MS[2], Moon Illsang[1], Hong Jae Lee[1], Gyeong Woon Noh[1], Jin Chul Paeng, MD, PhD[1], Jae Sung Lee, PhD[3], Keon Wook Kang, MD, PhD[1], Dong Soo Lee, MD, PhD[1], June-Key Chung, MD, PhD[1]; [1]Nuclear Medicine, Seoul National University Hospital, Seoul, Korea, Republic of, [2]Radiology, Seoul National University Hospital, Seoul, Korea, Republic of, [3]Seoul National University, Seoul, Korea, Republic of. (3175)

Purpose: Image uniformity of PET using pure water phantom is hard to visualize with PET/MR 3T unlike PET/CT. The water phantom for the PET/MR needs appropriate additives to control susceptibility and conductivity in the water. The purpose of this study was to investigate the optimal concentration of gadolinium diethylenetriamine pentaacetic acid (Gd-DTPA) and sodium chloride (NaCl) solution for acquiring good image uniformity with a water phantom on PET/MR.
Materials and Methods: A cylindrical phantom of 9.52L was filled with demineralized water, 21 kBq/ml F-18 solution, Gd-DTPA as a T1 relaxation modifier and NaCl as a conductivity modifier. Various concentrations of Gd-DTPA (0-0.2 mM) and NaCl (0-200 mM) mixtures were prepared for the phantoms. DIXON MR sequences were simultaneously performed with PET acquisitions. PET/MR image of each phantom was acquired for 10 minutes per bed position. PET data were reconstructed using OSEM with 2 iterations, 21 subsets and a 6 mm FWHM of Gaussian filter. The MR Image uniformity was estimated with a percent integral uniformity (PIU) and the nonuniformity of PET image was evaluated by a coefficient of variation (CV).
Results: MR-based attenuation correction (MRAC) maps that acquired from the water phantom without Gd-DTPA or NaCl solution caused image artifacts along to a phase direction in MR. When Gd-DTPA was only added in the water phantom, artifacts of the MRAC showed a tendency to decrease but did not disappear completely. A mixture of 0.2 mM Gd-DTPA and 150 mM NaCl was the most suitable concentration for water filled uniformity phantom at the PET/MR image without artifacts. The PIU corresponding to the MRAC map and the DIXON image was 100%, 83.1% respectively. The CV of PET was 6.3%.
Conclusion: We suggest that Gd-DTPA and NaCl are useful additives which are easily accessible and handle safely in clinical practice when performing a uniformity phantom test with water on PET/MR.

Authors listed for this abstract reported no relevant financial disclosures.

1817

Relationships between age and liquid gastric emptying studies. Fritzgerald C. Leveque, CNMT, Jenna N. Mirabile, Xiyao Zhao, Maria-Bernadette S. Tomas, MD, Christopher J. Palestro, MD, Kenneth J. Nichols, PhD; Northwell Health, New Hyde Park, NY, USA. (1845)

Objectives: Pts presenting with gastric symptoms may have abnormally delayed liquid &/or solid phase gastric emptying. While evaluation of solid phase gastric emptying is a widely practiced scintigraphic procedure, liquid phase studies are not as well documented. We wished to determine whether either form of abnormal gastric emptying is associated with pt demographics, as a potential indication that normal limits may need to account for age, gender, or diabetes effects.
Methods: Data were examined retrospectively for 412 pts (age = 49±19 years; 289 female; 123 male), including 29 with diabetes, who underwent gastric motility studies. Liquid emptying was assessed first using LAO planar 30-min dynamic imaging of the stomach following ingestion of 7.4 MBq ^{111}In-DTPA in 10 mL water immediately followed by 300 cc water. The $T_{1/2}$ of liquid gastric emptying was computed from the resulting activity-time curves derived from manually drawn gastric region of interest counts. Solid phase gastric emptying was evaluated by simultaneous 1-min anterior & posterior images collected over 4 hrs, following ingestion of a standardized meal labeled with 37 MBq ^{99m}Tc-sulfur colloid. Attenuation-corrected conjugate view counts were determined within manually drawn regions over the stomach, & per cent retention values recorded at 1-hr intervals for 4 hrs.
Results: Using conventional criteria for solid phase gastric abnormality of >10% retention at 4 hrs, 28% (117/412) of pts had abnormal solid phase gastric emptying. By this criterion, ROC analysis indicated that the threshold of abnormality for abnormal liquid emptying was $T_{1/2} \geq$ 20 minutes, in agreement with publications suggesting this threshold of abnormality based on 30 normal volunteers (J Nucl Med 2009;50:726-31). Abnormal solid emptying was influenced by diabetes ($\chi^2 = 6.0$, $p = 0.02$), but was not associated with sex ($\chi^2 = 0.0003$, $p = 0.99$) or age ($\chi^2 = 1.3$, $p = 0.25$). In contrast, abnormal liquid emptying was significantly associated with age ($\chi^2 = 14.5$, $p = 0.0001$), & presence of diabetes ($\chi^2 = 4.8$, $p = 0.03$), but not sex ($\chi^2 = 0.05$, $p = 0.82$). Liquid emptying $T_{1/2}$ was significantly correlated with age for all pts ($r = -0.26$, $p < 0.0001$, $N = 412$), & for pts with reported normal liquid & normal solid emptying ($r = -0.27$, $p = 0.0001$, $N = 227$), but not for pts with reported abnormal liquid emptying ($r = -0.13$, $p = 0.15$, $N = 138$).
Conclusions: The fact that abnormal liquid emptying was significantly associated with age suggests the potential need for prospective studies that measure rates of gastric emptying of liquids in normal subjects, to enable applying age-adjusted normal limits to pts undergoing gastric emptying studies.

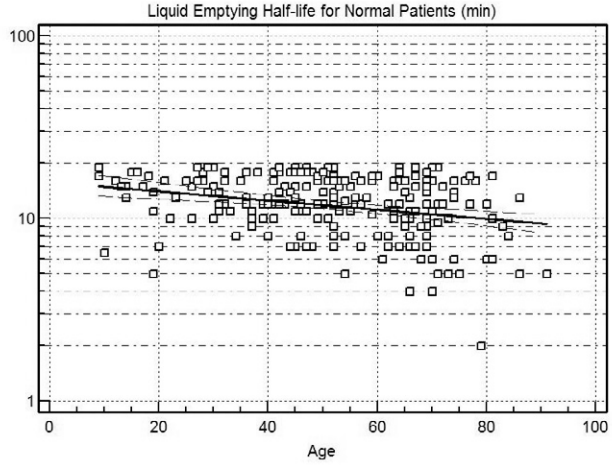

Authors listed for this abstract reported no relevant financial disclosures.

1818

The impact of respiratory motion and image noise on the accuracy and variability of PET-derived volumetric parameters. Tetsu Nakaichi, MS[1,2], Wataru Kawakami, PhD[1], Shozo Yamashita, PhD[1], Haruki Yamamoto[1], Masayuki Sasaki, MD, PhD[3]; [1]Public Central Hospital of Matto Ishikawa, Hakusan, Japan, [2]Kyushu University, Fukuoka, Japan, [3]Dept Rad Sci Sch of Health Sci Kyushu Univ, Fukuoka, Japan. (1177)

Objectives: The accuracy and variability of metabolic volume (MV) and total glycolysis (TG) were essential to establish them as biomarkers, and depend on which delineation algorithms were selected. The usefulness of the contrast-oriented algorithm (COA) has been validated in radiotherapy planning for lung cancer, which accurately corresponds to pathological specimens. However, it is assumed that only tumors have slight respiratory motion or image noise is not considered sufficiently. The present study aimed to examine the impact of respiratory motion and image noise on the accuracy and variability of MV and TG by COA, using a lung tumor simulated phantom.
Methods: A NEMA IEC body phantom filled with ^{18}F solution simulated several target-to-background ratios (TBRs) ranging from 4 to 20 (4, 8, 12, 16, 20) for creating site-specific regression equations using COA. The regression equations were calculated for spheres with diameters equal to or larger than 28mm and not affected by the partial volume effect (nPVE), and spheres no more than 22mm and affected by PVE. To simulate a lung tumor, spheres were filled with ^{18}F solution, which has almost the same radioactivity concentration as a sphere with TBR of 4. It moved towards the cranio-caudal direction at amplitudes of 0 (static), 1 cm, and 2 cm using a respiratory gating platform. PET data from each amplitude was acquired in the three-dimensional list mode for 10 min. Seven PET images at different scan start times were reconstructed using ordered-subset expectation maximization algorithm, each with durations of 1, 1.5, 2, and 2.5 min for each amplitude's data. COA was compared with 41% and 50% of maximum standardized uptake value (SUV) which is general delineation algorithms. The relative error (RE) from the ideal value based on *a priori* knowledge of internal tumor volume (ITV), and mean of coefficient of variation (CV) for each duration and amplitude were measured for MV and TG.
Results: TG had comparatively better accuracy and variability than MV. In particular, its properties were more prominent as the amplitude increased. MV and TG by COA have the best accuracy and variability than other delineation algorithms; however, RE and CV deteriorated in decreasing the durations and increasing the amplitude. For MV by COA, the maximum RE were -7.4, -39.1, and -58.9%, and CV were 4.4, 5.4, and 7.5% for the amplitude of 0, 1 cm, and 2 cm, respectively. On the other hand, for TG by COA, the maximum RE were 4.8, -21.8, and -32.7%, and CV were 4.4, 3.8, and 4.7% for the amplitude of 0, 1 cm and 2cm, respectively. The maximum differences with decreasing durations by COA were RE of -2.3% and CV of 2.2% for MV, and RE of -2.7% and CV of 2.1%
for TG, respectively.
Conclusions: In conclusion, TG by COA was found to be the most reliable metric for physical aspects; however, the impact of respiratory motion on the accuracy and variability of PET-derived volumetric parameters were considerably greater than that of decreasing the duration.

Authors listed for this abstract reported no relevant financial disclosures.

1819

Effect of the difference in tube voltage on attenuation coefficients and quantitative assessment of bone SPECT/CT: a phantom study. Kengo Hashizume[1], Yoya Tomita[1], Yasutaka Ichikawa, MD[2], Akira Kamigiri[1], Tsuyoshi Yamada[1], Naoya Kubooka[1], Hiroaki Maki[3], Hajime Sakuma, MD, PhD[1]; [1]Mie University Hospital, Tsu, Japan, [2]Mie University Hospital, Tsu, Mie, Japan, [3]Mie University Hospital, Central Division of Radio, Tsu, Japan. (1338)

Objectives: Quantitative assessment of bone SPECT/CT has obtained increasing interest in recent years. CT-based attenuation correction (CTAC) is necessary for accurate quantification of tracer uptake in SPECT/CT imaging. The attenuation coefficients on CTAC map might be influenced by the difference in tube voltage of CT. However, the impact of tube voltage on the attenuation coefficients has not been evaluated. The aim of this phantom study was to evaluate the effect of various tube voltages on attenuation coefficients and quantitative assessment of tracer uptake in bone SPECT/CT imaging.
Materials and Methods: SPECT/CT imaging was performed with a uniform cylindrical water phantom on GE Discovery 670. The phantom contained six 30-mm-diameter cylinders. One of the six cylinders was filled with water and the rest with 5 different concentrations of K_2HPO_4 solution corresponding to CT numbers of 200, 400, 600, 800, and 1000 Hounsfield units (HU) to simulate bone with different densities. In addition, the six cylinders contained the same radioactivity concentration (207 kBq/ml) of ^{99m}Tc-pertechnetate solution. The background part contained 17 kBq/ml of ^{99m}Tc-pertechnetate solution. SPECT data were acquired using low-energy high resolution collimation, a 128 x 128 matrix, and 120 views for 30 s/view. CT scanning was performed with 4 different tube voltages of 80, 100, 120, and 140 kVp and with fixed tube current of 200 mA (Figure 1). Accordingly, 4 different CTAC maps were generated from those CT images (Figure 2). Then, attenuation correction of SPECT images was obtained with 4 different CTAC maps and ordered subset expectation maximization (10 subsets and 2 iterations). The attenuation coefficients in the cylinders on the 4 different CTAC maps were measured. In addition, the radioactivity concentration in the cylinders on the 4 different SPECT images were measured.
Results: The attenuation coefficients measured on the 4 different CTAC maps were shown in Figure 3. The attenuation coefficients at high tube voltage were slightly greater than those at low tube voltage, especially in the high CT density cylinders (e.g. attenuation coefficients in the cylinders with 1000 HU: 0.239 cm^{-1} at 140 kVp vs 0.229 cm^{-1} at 80 kVp). The radioactivity concentration measured on the 4 different SPECT images were shown in Figure 4. Overestimation of the radioactivity concentration in the higher CT density cylinders was observed at any tube voltage. The overestimation was smaller when the lower tube voltage was used. For instance, the radioactivity concentration in the cylinder with 1000 HU was overestimated by 5.4% at 140 kVp and by 3.0% at 80 kVp, when compared with those in the cylinder with 0 HU.
Conclusions: Higher tube voltage in CT leads to increase in attenuation coefficients on CTAC maps, especially in the regions of high CT density. The radioactivity concentration in the regions with > 600 HU is overestimated at any tube voltage. The overestimation is smaller when using the lower tube voltage, such as 80 or 100 kVp. The current results will serve as a basis for the optimization of CT parameters for attenuation correction in quantitative bone SPECT/CT imaging.

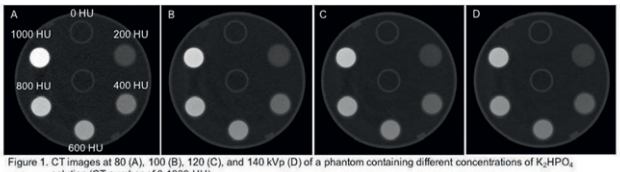

Figure 1. CT images at 80 (A), 100 (B), 120 (C), and 140 kVp (D) of a phantom containing different concentrations of K_2HPO_4 solution (CT number of 0-1000 HU).

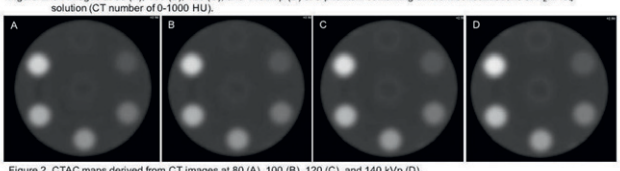

Figure 2. CTAC maps derived from CT images at 80 (A), 100 (B), 120 (C), and 140 kVp (D).

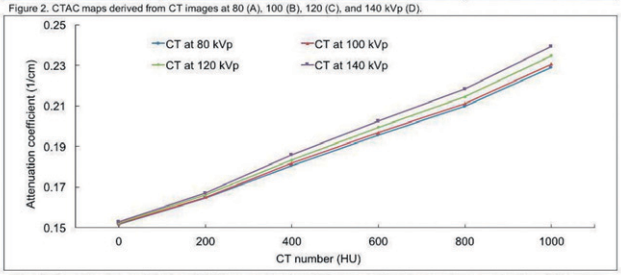

Figure 3. The attenuation coefficients on CTAC maps derived from CT images at different tube voltages as a function of CT numbers.

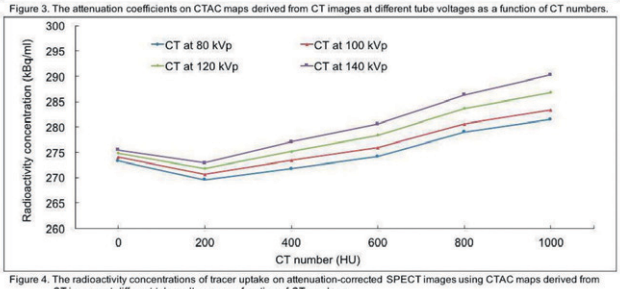

Figure 4. The radioactivity concentrations of tracer uptake on attenuation-corrected SPECT images using CTAC maps derived from CT images at different tube voltages as a function of CT numbers.

Authors listed for this abstract reported no relevant financial disclosures.

1820

Estimation of Cut-off Value for diagnosing Breast Cancer by 18F-FDG PET/MRI< and : for > Comparison of SUV and ADC. Tatsuya Horita[1], Toshimitsu Utsuno[2], Hiroaki Kurihara[3]; [1]Natinal Cancer Center Hospital, Tokyo, Japan, [2]National Cancer Center Japan, Tokyo, Japan, [3]Tokyo, Japan. (2229)

Background and Objectives: 18F-fluorodeoxyglucose (FDG) PET/MRI uses the glycolysis system to functionally evaluate tumors by measuring tumor uptake of radioactive FDG. In contrast, the apparent diffusion coefficient (ADC) measures cellular densities. ADC measures feature a large overlap between benign and malignant tumors, which changes greatly depending on the type of equipment and region of interest (ROI). This study aimed to estimate the cut-off values of standardized uptake value (SUV) and ADC of normal breast and primary tumor breast tissues using PET/MRI images.
Methods: Twenty consecutive female patients with breast cancer were enrolled in this retrospective study between January and November 2017. Whole-body PET/MRI studies of 18F-FDG were performed with a scan protocol of 2 min/bed acquisition at 1 h post injection. Breast PET/MRI studies were performed with a scan protocol of 10 min/bed acquisition at 90 min post injection. ROIs for tumorous and normal breast tissues were the axis planes on which SUVmax existed. SUVearly was each SUVmax of the primary tumor and normal breast during whole-body acquisition. SUVdelay was each SUVmax in breast acquisition. ΔSUV was calculated by subtracting SUVearly from SUVdelay. We measured SUVearly, SUVdelay, ΔSUV, ADC, and the time intensity curve(TIC). Cut-off values were calculated from the ROC curve generated from the primary tumor and normal breast tissues.
Results: SUVearly, SUVdelay, ΔSUV, and ADC were significantly different between primary tumor and normal breast tissues, and the cut-off values were 2.3, 4.1, 1.38, and 0.000972, respectively. The sensitivity of SUVdelay was 0.95 and the specificity was 1.0. The sensitivity and specificity of ADC were 0.85 and 0.9, respectively. SUVdelay showed a tendency of small overlap when comparing SUVdelay and ADC. Comparing SUV of the primary tumor with ADC generated a correlation coefficient of 0.11, indicating that no correlation was observed.
Conclusions: The cut-off values for primary breast cancer tumorous tissue were 2.3 (SUVearly), 4.1 (SUVdelay), and 0.000972 (ADC). There was no correlation between SUVdelay and ADC. It is difficult to diagnose primary tumor with ADC alone. Calculating the cut-off value from each measured value is essential for diagnosis. Each cut-off value serves as a reference for diagnosis.

Authors listed for this abstract reported no relevant financial disclosures.

1821

The Japanese harmonization technology study for multicenter analysis of PET SUV using vendor-neutral software: J-Hart study. Yuji Tsutsui, BS[1], Go Akamatsu, PhD[2], Hiromitsu Daisaki, PhD[3], Takuro Umeda[4], Matsuyoshi Ogawa[5], Hironori Kajiwara[6], Shigeto Kawase[7], Minoru Sakurai[8], Hiroyuki Nishida[2], Keiichi Magota, PhD[9], Kazuaki Mori[10], Masayuki Sasaki, MD, PhD[11]; [1]Kyushu University Hospital, Fukuoka, Japan, [2]Molecular Imaging, Institute of Biomedical Research and Innovation, Kobe, Japan, [3]Department of Radiological Technology, Gunma Prefectural College of Health Sciences, Gunma, Japan, [4]Cancer Institute Hospital of Japanese Foundation F, Tokyo, Japan, [5]Yokohama City Univ., Yokohama, Japan, [6]Center Hospital of National Center for Global Health and Medicine, Tokyo, Japan, [7]Kyoto University Hospital, Kyoto, Japan, [8]Clinical Imaging Center for Healthcare, Nippon Medical School, Tokyo, Japan, [9]Hokkaido University Graduate School of Medicine, Sapporo, Japan, [10]Toranomon Hospital, Tokyo, Japan, [11]Dept Rad Sci Sch of Health Sci Kyushu Univ, Fukuoka, Japan. (1957)

Purpose: The Japanese Harmonization Technology (J-Hart) study aimed to determine the usefulness of vendor-neutral software on the SUV derived from positron emission tomography (PET). The effects of SUV harmonization were evaluated based on the reproducibility across several scanners and the repeatability of each scanner.
Materials and Methods: Twelve PET scanners at 9 institutions were included in this study. A National Electrical Manufacturers Association (NEMA) International Electrotechnical Commission (IEC) body phantom was filled with ^{18}F solution with a background activity of 2.65 kBq/mL and a sphere-to-background ratio of 4. A PET image with 30-minutes acquisition was reconstructed to determine the parameters for harmonization using vendor-neutral software. The SUV_{max} of the spheres was compared with the reference range proposed by the Japanese Society of Nuclear Medicine (JSNM) and the digital reference object (DRO). The coefficient of variation (CV) of the SUV_{max} across 12 PET scanners (CV_{repro}) was measured by the PET images with 30-minutes acquisition. The CV of the SUV_{max} across 15 frames (CV_{repeat}) in each scanner was measured by the PET images with 2-minutes acquisition × contiguous 15 frames.
Results: Three PET scanners did not require an additional Gaussian filter (GF) for harmonization, whereas the other nine required additional FWHM values of GF ranging from 5 to 9 mm. The SUV_{max} of these nine scanners fell within the JSNM reference range after harmonization. The pre- and post-harmonization CV_{repro} of six spheres ranged from 3.83% to 15.3% (9.45 ± 4.69%) and from 2.30% to 10.7% (6.05 ± 3.61%), respectively ($P < 0.05$). The pre- and post-harmonization CV_{repeat} of nine scanners ranged from 5.00% to 8.98% (6.59 ± 1.29%) and from 2.65% to 6.72% (4.88 ± 1.64%), respectively ($P < 0.05$).
Conclusions: Harmonizing SUV using vendor-neutral software produced SUV_{max} for 12 scanners that fell within the JSNM reference range of a NEMA IEC body phantom. SUV harmonization improved the reproducibility and the repeatability of SUV_{max}.

Recovery coefficients of 12 PET scanners obtained from 30-min PET image. Comparison among pre- (a) and post- (b) harmonization RC.

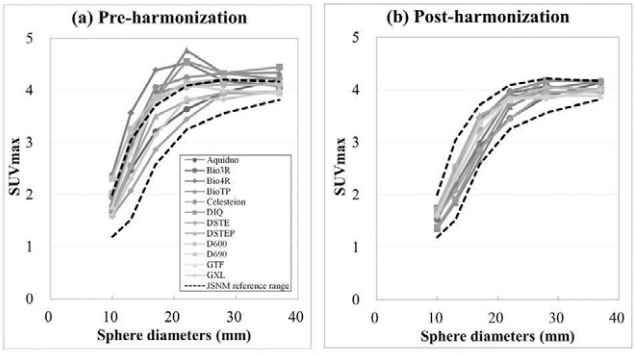

Effects of harmonization on repeatability. Pre- and post-harmonization comparisons of coefficients of variation of the SUV_{max} for 15 frames (CV_{repeat}).

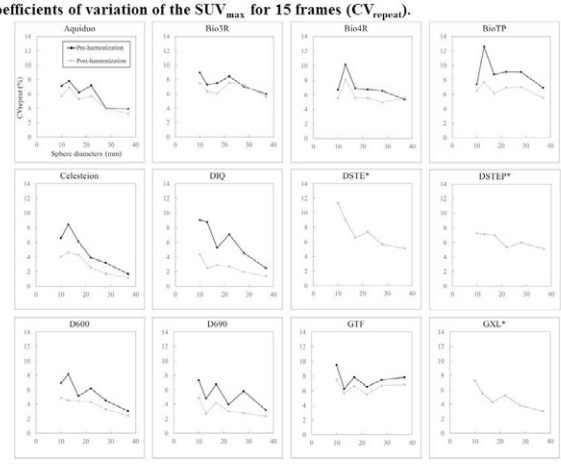

Authors listed for this abstract reported no relevant financial disclosures.

1822

Quality control testing for dedicated molecular breast imaging systems. Sara M. Nardinger, CNMT, Thuy T. Tran, Tiffinee Swanson, Lacey R. Ellingson, Courtney M. Solberg, CNMT, Michael K. O'Connor, PhD, Carrie B. Hruska, PhD; Mayo Clinic, Rochester, MN, USA. (2958)

Aim: Molecular breast imaging (MBI) is a nuclear medicine test that uses small dedicated gamma cameras designed for imaging of the breast. Despite growing adoption of MBI, there is currently a lack of guidance on appropriate quality control procedures for MBI detectors. Routine testing is important for monitoring changes in system performance and may be needed for obtaining and maintaining accreditation from regulatory bodies. Modern MBI units differ from conventional gamma cameras in many ways. Our study objective is to provide practical guidance for physics testing of MBI systems with recommendations for changes to existing quality control procedures that enable them to be applied to MBI systems.
Methods: Some physics tests designed for conventional gamma cameras, such as intrinsic uniformity, count rate parameters, and overall system performance for SPECT, do not apply to dedicated MBI systems. Other tests warrant special considerations. For example, the pixelated nature of the MBI system can cause aliasing artifacts in resolution measurements using bar phantoms or line sources. The limited space between detector heads (dual-head systems) prevents the use of ACR-type phantoms. Because of the short bore collimators, there is a heightened sensitivity to contaminants in Co-57 sheet sources. When evaluating sensitivity, a modified imaging setup will be needed for a dual-headed MBI unit that cannot fully rotate. Lastly, it would be beneficial to measure the contrast of lesions detected by the system, as the primary function of these systems is hot-spot detection.
Results: For dedicated molecular breast imaging systems, we recommend using Table 1 as a guide for evaluating system performance.
Conclusions: Routine physics testing of dedicated molecular breast imaging equipment is important for monitoring changes in system performance. Modern MBI units differ from conventional gamma cameras in many ways. Therefore, some existing quality control procedures need to be modified to be applicable for evaluating MBI units.

Table 1. Recommended quality control testing program for MBI systems.

Test	Equipment	Frequency	Acquisition Details	Passing Criteria
Uniformity	Co-57 sheet source or fillable phantom	Daily	7.5 Mcts	≤5% integral uniformity
Spatial Resolution	4-quadrant bar phantom	Semi-annually	7.5 Mcts; phantom angled across FOV	Meets manufacturer's specifications
Sensitivity	Flask	Annually	120 second images	≤10% difference between 2 detectors
Energy Resolution	Point source or fillable phantom	Annually	2 keV energy windows; 1 minute images	FWHM ≤ 10%
Lesion Contrast Test	Contrast detail phantom	Quarterly	1 Mcts; Images at 3 depths	CNR >3; Count number of visible lesions at each depth

* All tests should be performed at acceptance testing and following major service work.

Authors listed for this abstract reported no relevant financial disclosures.

1823

Classification of AD/MCI/NC from Amyloid PET Images using Deep Learning CNN Algorithm. Hyun Jin Yoon, PhD[1], Young Jin Jeong, MD[2], Jieun Jeong, MD[1], Do-Young Kang, MD,Ph.D[3]; [1]Dong-A University Medical Center, Busan, Korea, Republic of, [2]Dong-A University, Busan, Korea, Republic of, [3]Dong-A University Hosp., Busan, Korea. (2300)

Objectives: Early diagnosis of dementia helps in finding suitable treatments that reduce or even prevent future cognitive dysfunction in patients. In this paper, we use a Convolutional Neural Network (CNN) to classify the brain PET images of Alzheimer's disease (AD) patients and for mild cognitive impairment (MCI) in a normal control (NC).
Methods: All subjects had an intravenous injection of 300 MBq of F-18 florbetaben (FBB), and PET/CT acquisition was started 90 min after the radio-tracer injection. The image data were labeled into NC, MCI and AD by the findings of the neurologist. We performed data augmentation using various methods such as flip, rotation, and GAN, in addition to preprocessing and data augmentation for AlexNet, in order to supplement a number of deficient data. Artificial intelligence (AI) learning was simulated using the Mini-batch Stochastic Gradient Descent (MSGD) algorithm, and the learning rate was 5e-5 and the epoch was 100.
Results: Using the CNN and the algorithm AlexNet, we successfully classified F18-FBB PET images of AD from NC where the accuracy of test data on trained data reached 98.14%. In this work, the CNN, which is one of the deep learning neural network architectures, was used in order to distinguish the AD, MCI from the NC. Accuracy was 98.33%, NC recall was 99.16%, MCI recall was 95.83% and AD recall was 98.16% after enhancing the data by increasing the number of data using rotation and LR flip. Accuracy increased by 4.96%, NC recall increased by 10.68%, MCI recall decreased by 0.23%, and AD recall increased by 9.65% after enhancing the data by increasing the number of data to 4020 using DCGAN.
Conclusion: The AlexNet implemented CNN is considered to be a good algorithm for classifying NC, MCI, and AD in 18F-FBB amyloid PET

brain images. Accuracy and recall were improved when data were enhanced through data augmentation through rotation and left and right reversal.

Authors listed for this abstract reported no relevant financial disclosures.

1824

Relationship between radioactivity concentration ratio and cross-talk correction effect for simultaneous ^{99m}Tc and ^{18}F acquisition using small-animal SPECT-PET/CT system. Takayuki Shibutani, RT, MS[1,2], Masahisa Onoguchi, RT, Ph.D[1,2], Takayuki Kanno, RT[2], Takafumi Mochizuki, MD, Ph.D[3], Kazuhiro Shiba, Ph.D[4], Seigo Kinuya, MD, Ph.D[5]; [1]Department of Quantum Medical Technology, Institute of Medical, Pharmaceutical and Health Sciences, Kanazawa University, Kanazawa, Japan, [2]Department of Quantum Medical Technology, Guraduate School of Medical Sciences, Kanazawa University, Kanazawa, Japan, [3]Kanazawa Advanced Medical Center, Kanazawa, Japan, [4]Division of Tracer Kinetics, Advanced Science Research Center, Kanazawa University, Kanazawa, Japan, [5]Department of Nuclear Medicine, Institute of Medical, Pharmaceutical and Health Sciences, Kanazawa University, Ishikawa, Japan. (1924)

Objectives: The ^{18}F energy spectrum for a small-animal SPECT-PET/CT system with a clustered multi-pinhole collimator is composed 511 keV annihilation radiation photo-peaks, and additional 170 keV backscatter photo-peak. If ^{99m}Tc and ^{18}F scans are simultaneously performed, the ^{99m}Tc image has the influence of cross-talk occurred by overlapping the 170 keV backscatter photo-peak of ^{18}F and 141 keV photo-peak of ^{99m}Tc. Although the influence of cross-talk has to accurately correct, the effect of correction has not been fully evaluated. The objective of this study was to reveal the influence and the correction effect of cross-talk and different radioactivity concentration ratio.
Methods: Small-animal SPECT-PET/CT scanner used a triple-detectors gamma camera (VECTor^{+}/CT, MILabs B.V., Netherlands) with high-energy ultrahigh-resolution rat and mouse type clustered multi-pinhole collimator (HE-UHR-RM). A fillable cylindric chamber 30 mm (body part) of NEMA-NU4 phantom filled in ^{99m}Tc or both of ^{99m}Tc and ^{18}F solution. Furthermore, two small-region chambers were filled with non-radioactive water and ^{99m}Tc attenuated half radioactive concentration of body part. The radioactive concentration of ^{99m}Tc and ^{18}F were approximately 6.0 and 78.0 MBq/mL, and ^{18}F/^{99m}Tc ratio set 0.4-13 using radioactive decay. All data were acquired using list-mode of 30 min/frame, and total acquisition time was 14 hours. Main energy windows of ^{99m}Tc and ^{18}F were 141 keV ± 10% and 511 keV ± 10%, in addition, the sub energy window of 7% window width set on the upper and lower sides of main energy window both ^{99m}Tc and ^{18}F using triple energy window (TEW) technique. Transverse image was reconstructed using pixel-based ordered subset expectation maximization (POSEM) algorithm, and the number of subset and iteration was 32 and 8. The reconstructed transverse image was added all slices including two small-region chambers to perform the image analysis, thereby used integral value in circular-shape region of interest (ROI) drawing on the body part and two small-region chambers of added transverse image. The scatter content ratio by cross-talk calculated from ^{99m}Tc integral values of simultaneous ^{99m}Tc and ^{18}F scan and independent ^{99m}Tc scan. Furthermore, the effect of cross-talk correction defined by ^{99m}Tc integral values of simultaneous ^{99m}Tc and ^{18}F scan with and without TEW correction. We compared the ^{99m}Tc image of simultaneous ^{99m}Tc and ^{18}F scan reference to the ^{99m}Tc image of the independent ^{99m}Tc scan.
Results: The scatter content ratio for the body part and small-region chamber with ^{99m}Tc solution was gradually increased 10-50% as higher ^{18}F/^{99m}Tc ratio, whereas the scatter content ratio small-region chamber with non-radioactive water was exponentially increased as higher ^{18}F/^{99m}Tc ratio. However, all scatter content ratio conversely decreased at ^{18}F/^{99m}Tc ratio of more than 8. Although the integral value of body part and small-region chamber with ^{99m}Tc solution became similar value at the independent ^{99m}Tc scan, the small-region chamber with non-radioactive water could not correct scatter by cross-talk at the ^{18}F/^{99m}Tc ratio of more than 2.
Conclusion: We revealed the influence and correction effect of cross-talk and different radioactivity concentration ratio. The ^{99m}Tc image simultaneously acquired ^{18}F/^{99m}Tc ratio of less than 2 could exactly correct scatter by cross-talk from ^{18}F.

Authors listed for this abstract reported no relevant financial disclosures.

1825

A comparison and examination of visual and quantitative evaluations in amyloid positron emission tomography. Natsumi Shimokawa[1], Go Akamatsu, PhD[2], Miyako Kadosaki[1], Ayano Shoji[1], Naoki Hashimoto[1], Saki Kimoto[1], Masayuki Sasaki, MD, PhD[3]; [1]Kyushu University, Fukuoka, Japan, [2]Molecular Imaging, National Institute of Radiological Sciences, Chiba, Japan, [3]Dept Rad Sci Sch of Health Sci Kyushu Univ, Fukuoka, Japan. (1772)

Purpose: Amyloid β (Aβ) deposition in the cerebral cortex is useful for the early and/or differential diagnosis of Alzheimer's disease (AD), and amyloid positron emission tomography (PET) is the only examination that can directly visualize cerebral Aβdeposition. Although visual evaluation is the standard for amyloid PET examinations, depends on physicians reviewing the images. Therefore, an objective quantitative evaluation is considered to be useful for image interpretation. In this study, we compared and examined the visual and quantitative evaluations of amyloid PET findings.
Method: A total of 166 patients, including 58 normal controls (NCs), 62 cases of mild cognitive impairment (MCI), and 46 cases of early AD, were retrospectively investigated. They underwent amyloid PET examination at Japanese Alzheimer's disease neuroimaging initiative (J-ADNI). The amyloid accumulation of four cerebral cortex areas (posterior cingulate gyrus-precuneus, frontal lobe, temporal lobe lateral side, parietal lobe lateral side) were evaluated by visual and quantitative evaluations. We compared the results of visual evaluation (positive, equivocal, negative) by three nuclear medicine physicians and quantitative evaluation with the standardized uptake value ratio (SUVR) on each area and examined the relationship with the clinical diagnosis.
Results: The visual evaluation and SUVR were significantly correlated with $\rho>0.80$ in each of the 4 regions ($P<0.05$). The sensitivity and specificity of the quantitative evaluation compared with the visual evaluation by a receiver-operating characteristic analysis were 93% and 99%, respectively. In the four regions which were recognized to be accumulated by visual evaluation, the SUVR was the highest (2.20±0.33) at the posterior cingulate gyrus-precuneus, followed by the values of 2.04±0.31 at the frontal lobe, 1.99±0.23 at the temporal lobe lateral side and 1.97±0.26 at the parietal lobe lateral side. For each clinical diagnosis, the SUVR was 1.39±0.34 for NC, 1.82±0.50 for MCI and 2.11±0.47 for AD.
Conclusions: The visual evaluation on amyloid PET and the quantitative evaluation by SUVR showed high correlation. In addition, the sensitivity and specificity of quantitative evaluation were high. Based on these results, it is suggested that the quantitative evaluation was useful as an adjunct to visual assessment in Amyloid PET.

Authors listed for this abstract reported no relevant financial disclosures.

1826

Determination of optimal position around two devices for automated ^{18}F-FDG infusion. Noriaki Miyaji[1], Kazuki Motegi[1], Shohei Fukai[1], Kenta Miwa, PhD[2], Takuro Umeda[1], Takashi Terauchi, MD[1], Mitsuru Koizumi, MD, PhD[1]; [1]The Cancer Institute Hospital, Japanese Foundation For Cancer Research, Tokyo, Japan, [2]Department of Radiological Sciences, International University of Health and Welfare, Ohtawara, Japan. (1843)

Objectives: Radiation protection is a concern for staff who administer radionuclide tracers to patients via automated infusion devices. Variations in radiation dose around devices should be confirmed to reduce staff exposure to radiation. The present study aimed to determine the optimal position around two devices for automated ^{18}F-FDG infusion.
Methods: We measured radiation doses at the anterior, posterior and lateral sides of the AI-300 (Sumitomo Heavy Industries, Ltd.) and UG-05 (Universal Giken Co. Ltd.) devices using an ICS-321 (Hitachi Aloka Medical Ltd.) survey meter. The amounts of staff exposure to radiation

while injecting approximately 28 - 30 patients per day with ^{18}F-FDG were compared between the two devices from January 2014 to December 2015. All medical staff working with radionuclides wore individual PDM-112 or PDM-122 dosimeters (Hitachi Aloka) on the abdomen.
Results: The dose equivalent rates of both devices were the lowest on the anterior side when loading vials with ^{18}F-FDG and the lateral side when administering ^{18}F-FDG to patients. The cumulative doses of both devices were reduced at the lateral side by a maximum of 83% for the UG-05 compared with the AI-300. Staff were exposed to 12.9 and 14.1 μSv/day of radiation when using the AI-300 and UG-05, respectively.
Conclusions: Although the radiation doses measured at the three sites were significantly higher for the AI-300 than the UG-05, staff exposure to radiation did not significantly differ between the two devices. The difference in radiation doses between AI-300 and UG-05 might be attributable to the geometry of the shielding materials. Our findings indicated that staff exposure to radiation could be minimized by approaching automated infusion devices from the lateral aspect when administering radionuclide tracers to patients.

Authors listed for this abstract reported no relevant financial disclosures.

1827

Impact of reconstruction algorithm with PSF and TOF and reconstruction parameter in fractal analysis: Evaluation by changed the number of updates. Yukito Maeda[1], Nobuyuki Kudomi, PhD[2], Yuka Yamamoto[3], Tetsuhiro Hatakeyama, MD[3], Yoshihiro Nishiyama[3]; [1]Dept. of Radiology, Kagawa University Hospital, Kagawa, Japan, [2]Kagawa Univ, Kagawa, Japan, [3]Kagawa University, Kagawa, Japan. (1755)

Objectives: Fractal analysis has been attracting attention for image analysis as one of the texture analysis, and would be of use in characterization of tumor grade. However, the impacts of corrections in reconstruction algorithms and its parameters have not been demonstrated in fractal analysis. The purpose of this study was to test influence of its corrections of point spread function (PSF) and time of flight (TOF), and the number of updates to fractal dimension.
Methods: We used a brain tumor phantom with sphere part filled with ^{18}F-FDG. We scanned twice with the background with ^{18}F-FDG and water, respectively. The reconstruction algorithms applied were ordered-subsets expectation maximization (OSEM), OSEM + PSF, OSEM + TOF and OSEM+PSF+TOF. We changed the number from 21 to 120. We measured fractal dimension for 37-mm hot region using pixel counting
Results: Change in fractal dimension was small independent of the number of update for the background with water. The dimension of OSEM+PSF and OSEM+PSF+TOF decreased as the number of update increased. When the number of update were 84, the fractal dimension of OSEM, OSEM+PSF, OSEM+TOF and OSEM+PSF+TOF were 1.99×10^{-5}, 2.54×10^{-5}, 2.05×10^{-5} and 2.54×10^{-5}, respectively. In the case of background with radioactive solution, the fractal dimension of all reconstruction algorithm increased as the number of updates increased. When the number of updates was 84, the fractal dimension of OSEM, OSEM+PSF, OSEM+TOF and OSEM+PSF+TOF were 11.2×10^{-5}, 12.4×10^{-5}, 4.27×10^{-5} and 5.65×10^{-5}, respectively.
Conclusion: The fractal dimension changed according to the reconstruction algorithm and the number of updates. These results should be noted in fractal analysis.

Authors listed for this abstract reported no relevant financial disclosures.

1828

Simultaneous PET/MRI in Brain Tumor Recurrence and Radiation Necrosis: Assessing the Efficacy of 11C-methionine PET and Apparent Diffusion Coefficient. Toshimitsu Utsuno[1], Tatsuya Horita[2], Hiroaki Kurihara[3]; [1]National Cancer Center Japan, Tokyo, Japan, [2]National Cancer Center Hospital, Tokyo, Japan, [3]Tokyo, Japan. (2221)

Objectives: 11C-methionine (Met) PET imaging is a sensitive tool to visualize brain tumor recurrence and radiation necrosis. In this study, we aimed to investigate the difference between PET standardized uptake value (SUV) and MR apparent diffusion coefficient (ADC) using simultaneous Met-PET/MRI in patients with brain tumor recurrence and radiation necrosis.
Methods: 10 patients of glioblastoma (n=9) and metastatic brain tumors (n=1) who had been previously treated with radiotherapy were studied by Met-PET/MRI scan. Whole-brain Met-PET/MRI scan was performed 10min after the tracer injection. And the acquisition was 10min per bed position in 3D TOF mode. A simultaneous MRI Echo planar diffusion imaging was carried out with the following parameters: axial acquisition with slice thickness = 5mm, b values = 0 and 1000. A diagnosis of recurrent tumor or radiation necrosis was made based on MRI followed by the observations. Region of interest (ROI) were placed within tumor and normal white matter of the same patient for the retrospective analysis. Maximum SUV, tumor versus normal tissue uptake ratio (TNR), and minimum ADC were calculated and compared between brain tumor recurrence and radiation necrosis. Voxel-based-correlations between those parameters were evaluated in tumor recurrence.
Results: SUV and TNR were significantly higher in tumor recurrence than in radiation necrosis. The mean SUV and TNR in tumor recurrence was 5.7 ±2.3 and 3.3 ±1.2 respectively, while in radiation necrosis it was SUVmean = 2.78±0.5 ($P<0.05$) and TNR = 1.84±0.35 ($P<0.05$). ADC were not significantly different between tumor recurrence and radiation necrosis. The mean ADC in tumor recurrence was 0.69 ±0.15 $\times10^{-3}$ mm^2/s, while in radiation necrosis it was $0.60\pm0.22\times10^{-3}$ mm^2/s ($P>0.05$). There was not voxel-based-correlation between TNR and ADC(r =0.02, 0.14, -0.11, -0.2) in tumor recurrence.
Conclusions: While Met-PET can provide valuable information to differentiate the tumor recurrence among radiation necrosis, there was a poor correlation of ADC between the recurrence and the necrosis. We proved results of position accuracy higher than previous research by using simultaneous PET/MRI.

Authors listed for this abstract reported no relevant financial disclosures.

1829

Effect of Gaussian smoothing filter for CT-based attenuation correction mapon quantitative assessment in bone SPECT/CT: a phantom study. Yoya Tomita, PhD, Yasutaka Ichikawa, MD, Kengo Hashizume, Akira Kamigiri, Tsuyoshi Yamada, Hiroaki Maki, Hajime Sakuma, MD, PhD; Mie University Hospital, Tsu, Japan. (1451)

Objectives: Quantitative assessment of bone SPECT/CT has obtained increasing interest recently. CT-based attenuation correction (CTAC) is necessary for accurate quantification of tracer uptake in SPECT/CT imaging. For attenuation correction, CTAC maps are smoothed by a 3-dimensional (3D) Gaussian filter in order to match the spatial resolution of SPECT images. The size of Gaussian filter is usually optimized based on the full-width at half-maximum (FWHM) on SPECT system. Approximately 10 mm of Gaussian filter is usually employed for CTAC in SPECT/CT imaging. However, to date, the impact of Gaussian filter size on quantification of tracer uptake in SPECT/CT imaging has not been evaluated. The aim of this phantom study was to assess the effect of Gaussian filter size on quantitative assessment in bone SPECT/CT imaging.
Materials and Methods: SPECT/CT imaging was performed with a uniform cylindrical water phantom on GE Discovery 670. The phantom contained six 30-mm-diameter cylinders. One of the six cylinders was filled with water as a reference and the rest with 5 different concentrations of K_2HPO_4 solution corresponding to CT numbers of 200, 400, 600, 800, and 1000 Hounsfield units (HU) to simulate bone with different densities (Figure 1). Also, six cylinders contained the same radioactivity concentration (207 kBq/ml) of ^{99m}Tc-pertechnetate solution. The background contained 17 kBq/ml of ^{99m}Tc-pertechnetate solution. The SPECT data were acquired using low-energy high resolution collimation, a 128 x 128 matrix, and 120 views for 30 s/view, and CT data were acquired with 120 kVp and 100 mA. The CTAC maps were smoothed with Gaussian filter ranging from 0 to 30 mm FWHM in 2 mm increments. Therefore, 16 different CTAC maps were generated. Then, attenuation correction of SPECT images was performed with those CTAC maps. 3D ordered subset expectation maximization (10 subsets; 2 iterations) was employed for the SPECT image reconstruction. The attenuation coefficients in the cylinders were measured on the 16 different CTAC maps. In addition, the radioactivity concentration in the

cylinders were measured on the 16 different attenuation-corrected SPECT images.
Results: CTAC maps smoothed the different size of Gaussian filter are depicted in Figure 2. The attenuation coefficients in the higher CT density is declining with increasing the size of Gaussian filter (Figure 3). In contrast, there was no substantial effect of Gaussian filter size on attenuation coefficients in the cylinder with 0 HU. The attenuation coefficients on the CTAC maps smoothed with 0, 10, 20, and 30 mm of Gaussian filter were 0.240 cm^{-1}, 0.230 cm^{-1}, 0.212 cm^{-1}, and 0.194 cm^{-1} in the cylinders with 1000 HU, and 0.153 cm^{-1}, 0.152 cm^{-1}, 0.152 cm^{-1}, and 0.150 cm^{-1} in the cylinders with 0 HU, respectively. The results of radioactivity concentration measurements are shown in Figure 4. Overestimation of the radioactivity concentration in the higher CT density cylinders was observed in the setting of Gaussian filter < 20 mm, when using the radioactivity concentration in the cylinders with 0 HU as a reference. With a Gaussian filter of 10 mm, 5.4% overestimation of radioactivity concentration was observed in the cylinders with 1000 HU. The overestimation was smaller with larger Gaussian filter (20-26 mm).
Conclusions: Higher CT numbers cause increase in attenuation coefficients on CTAC maps, leading to erroneous increase in radioactivity concentration measurements. The larger FWHM of a Gaussian filter for CTAC maps can reduce the erroneous increase in tracer uptake in high density region. The current results will serve as a basis for the optimization of CT parameters for attenuation correction in quantitative bone SPECT/CT imaging.

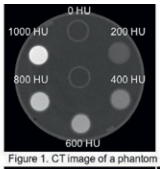

Figure 1. CT image of a phantom containing different concentrations of K_2HPO_4 solution (CT number of 0-1000 HU).

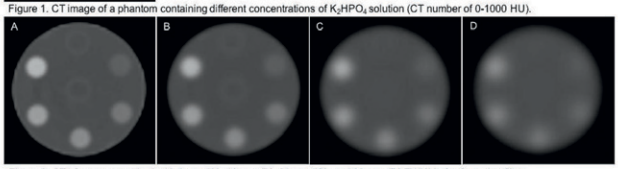

Figure 2. CTAC maps smoothed with 0 mm (A), 10 mm (B), 20 mm (C), and 30 mm (D) FWHM of a Gaussian filter.

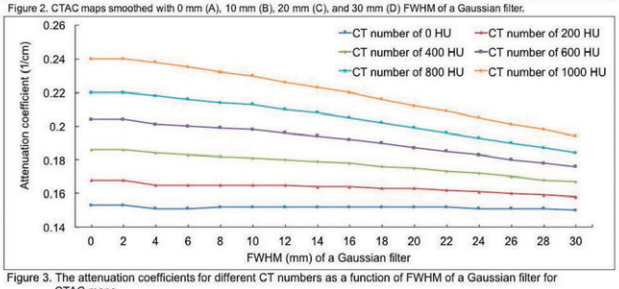

Figure 3. The attenuation coefficients for different CT numbers as a function of FWHM of a Gaussian filter for CTAC maps.

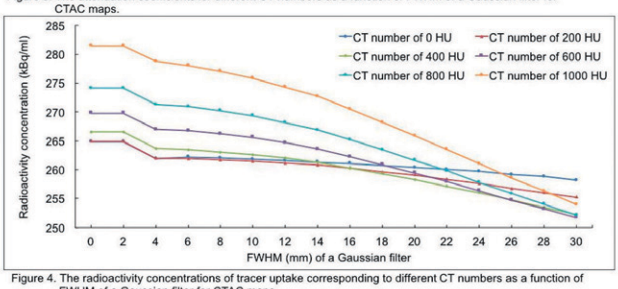

Figure 4. The radioactivity concentrations of tracer uptake corresponding to different CT numbers as a function of FWHM of a Gaussian filter for CTAC maps.

Authors listed for this abstract reported no relevant financial disclosures.

1830

Studies on variation of the standardized uptake value and metabolic tumor volume in analysis software for PET/CT using digital phantoms. Shinichiro Matsuzawa[1], Shinji Abe[2], Ryuto Mukumoto[1], Chinatsu Hasegawa[1], Tetsuro Odagawa[1], Katsuhiko Kato, MD, PhD[1]; [1]Nagoya University Graduate School of Medicine, Nagoya, Japan, [2]Department of Radiological Technology, Nagoya University Hospital, Nagoya, Japan. (43)

Background and Purpose: For PET/CT, indices such as the standardized uptake value (SUV) and the metabolic tumor volume (MTV) are used to evaluate tracer accumulation. Differences in these indices may occur even with the use of the same PET scanner due to different algorithms in the analysis software programs. In this study, we examined the causes for differences among 5 analysis software programs using digital phantoms.
Materials and Methods: 5 software programs were used in this study, syngo.via (VB10, Siemens), GI-PET (AZE Virtual Place Hayabusa ver 6.0, AZE, Japan), Metavol (v.1, Hokkaido University + University of California, Los Angeles), VOX-BASE II (REV2.65.0411, J-MAC SYSTEM, Japan), and Advantage Workstation (Volume Share 5, GE). We made 2 kinds of digital phantoms. The first phantom was aimed to examine the influence of changing slice thickness. Rectangular phantom was made by piling up 9 slices. 8 rectangular phantoms were made by changing slice thickness from 1mm to 8mm. The second phantom was aimed to examine measurement accuracy of SUVpeak. We set a SUVmax voxel and cubic accumulation with has high SUV value in low values area in the phantom. Region of interest was drawn on PET images and SUV and MTV were obtained with 5 software programs.
Results: When slice thickness was 2mm or 3mm, SUVmax obtained with GI-PET was lower than the true value. A thick slice was made by piling slices to make cubic voxels for GI-PET. Therefore, SUVmax was lower than the true value because voxel values were averaged. Only MTV obtained with syngo.via and Advantage Workstation were consistent with the true value. SUVpeak obtained with GI-PET was lower than the true value. GI-PET defines the peak as the "average value in $1cm^3$ sphere centered on the pixel showing the maximum value". Differences in SUVpeak seemed due to the differences in the definition of SUVpeak.
Conclusion: Results suggested that the differences in the indices obtained with four software programs are attributable to varied handling of PET slice thicknesses. It is necessary to understand the characteristics of the software program prior to examination. The same software program has to be used for the follow-up examinations of the same patients.

Authors listed for this abstract reported no relevant financial disclosures.

1831

Volume estimation of radio-activated material in inner concrete walls of a cyclotron room at a PET research facility. Kei Wagatsuma[1], Masayuki Kunugi[2], Kenta Miwa, PhD[3], Keiichi Oda, PhD[4,1], Jun Toyohara, PhD[5], Kenji Ishii, MD[5]; [1]Research Team for Neuroimaging, Tokyo Metropolitan Institute of Gerontology, Tokyo, Japan, [2]Radio Isotope Center, Tokyo Metropolitan Institute of Gerontology, Tokyo, Japan, [3]Department of Radiological Sciences, International University of Health and Welfare, Ohtawara, Japan, [4]Hokkaido University of Science, Sapporo, Japan, [5]Tokyo Metropolitan Institute of Gerontology, Tokyo, Japan. (1751)

Purpose: Neutrons generated by the nuclear reaction that produces positron emitters bombard and radio-activate the concrete walls of rooms housing non-self-shielded compact medical cyclotrons. The assessment of residual radioactivity concentrations in the concrete is necessary to estimate the amounts of radio-activated waste involved during the decommission of positron emission tomography (PET) facilities. The present study aimed to identify the amounts of radio-activated concrete in a cyclotron room at a clinical and pre-clinical PET research facility.
Methods: The compact medical cyclotron Cypris 370 (Sumitomo Heavy Industries, Ltd.) had been operated from June 1990 to March 2013. The accelerated particles comprised protons (maximum energy, 18 MeV) and deuterons (maximum energy, 10 MeV) and the cooling period was 40 months. The cyclotron is housed in a concrete vault that was not using

low-activation concrete with a floor area of 500.0 × 397.5 cm^2 and a height of 285.0 cm. The concrete walls and floor of the vault are 150 cm thick, and the ceiling is 160 cm thick. Cylindrical cores (diameter, 5 cm; length, 65 cm) were bored into the north, south east and west walls, the ceiling and the floor, to analyze radioactive concentrations, components and moisture content of the concrete. The gamma-ray spectrum of the cores was measured using a high-purity germanium semiconductor detector. Neutron transport in the cyclotron room was calculated using PHITS version 2.88 to evaluate the spectrum of neutron fluxes. The radioactive concentrations in the concrete of the vault were calculated using DCHAIN-SP ver. 2014. Radio-activated material was identified by the measured or calculated total radioactive concentration (ΣD, Bq/g) < 0.1.
Results: The measured and calculated radionuclides in the concrete comprised ^{46}Sc, ^{54}Mn, ^{60}Co, ^{134}Cs, ^{152}Eu and ^{154}Eu, and 90% of the ΣD comprised ^{60}Co and ^{152}Eu. The radioactive concentration was maximal at 6 -12 cm from the surface of the concrete, which was radio-activated to a depth of 2.0 to 38.0 cm. **Conclusions:** The dominant radionuclides in the radio-activated concrete of a cyclotron room in a PET research facility were ^{60}Co and ^{152}Eu. The concrete was radio-activated to a depth of < 40 cm.

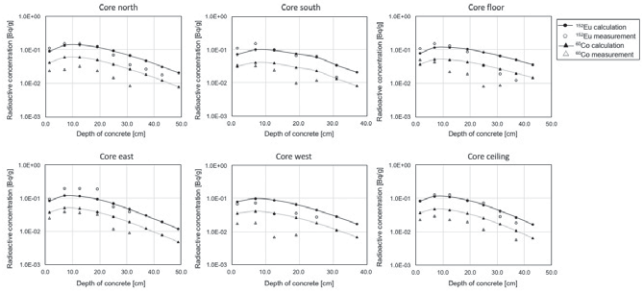

Authors listed for this abstract reported no relevant financial disclosures.

1832

Evaluation of left ventricular mechanical dyssynchrony in patients with left ventricle hypertrophy and normal gated SPECT-MPI.
Madan Parmar, Dharmender Malik, DNB, Gurwinder Kaur, Ashwani Sood, Harpreet Singh, Komalpreet Kaur, Bhagwant R. Mittal, MD, DNB; Department of Nuclear Medicine, Postgraduate Institute of Medical Education & Research, Chandigarh, India. (2688)

Objectives: Assessment of left ventricular mechanical dyssynchrony (LVMD) using gated SPECT-MPI is well established. Multiple factors like end-stage renal disease, diabetes mellitus, increased left ventricle (LV) mass/hypertrophy and hypertension could potentially affect the phase parameters. However there is little information about the effect of left ventricular hypertrophy (LVH, detected on ECG) on the phase parameters. Aim of the present study was to evaluate the prevalence of LVMD in patients with LVH and normal gated SPECT-MPI study.
Methods: Data of sixty-seven patients (31 female) with LVH and sixty age & sex matched controls (30 female) both with normal gated SPECT-MPI (SSS<3 and LVEF >55%) were retrieved. The variables including phase standard deviation (PSD), phase bandwidth (PBW), gated LV mass and LVEF were calculated retrospectively. LVMD was calculated based on cut-off value (>mean+2SD) obtained from controls. Multivariate logistic regression analysis was applied to assess the correlation between various confounding factors.
Results: Gated LV mass (gm) (134.88 ± 31.3 vs 91.35 ± 16.5; p-value <0.001) and phase parameters (PSD & PBW in degree) were significantly greater in patients with LVH (13.8±7.6 vs 7.3±2.3 and 38.5±19.6 vs 25.7±7.1; p-value 0.004, respectively) compared to the controls. The LV volumes (ml) (EDV: 43.16 ± 12.9 vs 51.9 ± 16.8; ESV: 11.3 ± 9.6 vs 16.5 ± 13.3; p-value >0.05, respectively) and LVEF (%) was found to be lower in patients with LVH than the control group (74.2 ± 12.7 vs 78.5 ± 10.4; p-value >0.05), however difference was not statistically significant. LVMD was detected in sixteen (24%) patients with the pre-defined cut-off values for PSD (>11.9) and PBW (>39.9) derived from the controls. Multivariate logistic regression analysis revealed gated LV mass being single most important independently associated confounding factor with LVMD in LVH patients (OR: 5.31; 95% CI 2.74-8.13; p 0.006).
Conclusions: Patients with LVH had significantly more LVMD than the control group, even in absence of abnormal perfusion/scar, electrical dyssynchrony and preserved LVEF and increased gated LV mass was associated with increased incidence of LVMD. The patients with LVH showing LVMD may require aggressive management in spite of normal perfusion and adequate LVEF.

Authors listed for this abstract reported no relevant financial disclosures.

1833

Optimization Methods for radiolabelling of DOTA-EB-cRGDfK with ^{111}In.
Shih-Ying Lee, Sheng-Nan Lo, Yuan-Ruei Huang, Ming-Wei Chen, Ming-Hsin Li, Chih-Hsien Chang; Institute of Nuclear Energy Research, Taoyuan City 32546, Taiwan. (2797)

Objectives: The tripeptide Sequence RGD (Arg-Gly-Asp) has specific binding affinity of integrin $\alpha_v\beta_3$ receptor. Integrin $\alpha_v\beta_3$ plays an important role in the regulation of tumor growth, angiogenesis, local invasiveness, and metastatic potential. Recent reports show that integrin $\alpha_v\beta_3$ expressed in many breast cancer specimens of breast cancer patients. To target integrin $\alpha_v\beta_3$ receptor, EB-cRGDfK were link with DOTA and then labeled with ^{111}In. The aim of this study was to find an optimization Methods of ^{111}In labelling, and demonstrate ^{111}In-DOTA-EB-cRGDfK has potential for diagnosis of breast cancer.
Methods: Quality control of DOTA-EB-cRGDfK precursor were >90% by High-performance liquid chromatography (HPLC). DOTA-EB-cRGDfK precursors were dissolved in DMSO. $^{111}InCl_3$ was from Institute of Nuclear Energy Research, and were delivered in 0.01N HCl. The experiments were performed in 300μL volumes. We use 20~60μg of DOTA-EB-cRGDfK precursor in this labeling experiment. The reaction mixtures in different pH (1M Sodium acetate) were test. Heating were performed in a temperature-controlled heating system (Eppendorf, ThermoMixer C). The labeling yields of ^{111}In-DOTA- EB-cRGDfK product were analyzed by radio-instant thin-layer chromatography (ITLC), and the radiochemical purities were analyzed by radio-HPLC.
Results: Kinetics of labelling of DOTA-EB-cRGDfK with ^{111}In was optimal at pH6. When we use 30μg DOTA-EB-cRGDfK precursor, the labelling with ^{111}In was completed after 10, min at 95℃.The labeling yields of ^{111}In-DOTA- EB-cRGDfK were 97.1% in pH6.0 reaction buffer and 90.4% in pH4.5 reaction buffer. In the same condition, we use 20μg DOTA-EB-cRGDfK precursor, the labelling with ^{111}In needs more time about 20 min at 95℃to achieve >90%.The labeling yields of ^{111}In-DOTA-EB-cRGDfK were 96.1% in pH6.0 and 58.9% in pH4.5. At the same heating time about 15min at 95℃, we compare with different DOTA-EB-cRGDfK precursor usage amounts. The DOTA-EB-cRGDfK precursor we use in this experiment were 20, 25, 30, 40, 60μg, the labeling yields of ^{111}In-DOTA-EB-cRGDfK were follow 81.3%,97.7%, 98.2% and 98.7%, 95.6%.
Conclusions: We demonstrate that ^{111}In-DOTA-EB-cRGDfK has better labeling yields in pH6 than in pH4.5 (1M Sodium acetate). Optimization Methods of ^{111}In-DOTA-EB-cRGDfK labelling, is use 30~40μg DOTA-EB-cRGDfK precursor, dissolved in pH6 (1M Sodium acetate) reaction mixture, heating at 95℃. Only need 15min, we can get the ^{111}In-DOTA-EB-cRGDfK products with labeling yields and radiochemical purities >90%. ^{111}In-DOTA-EB-cRGDfK has high specific activities and potential, can become a new radiopharmaceutical for breast cancer imaging.

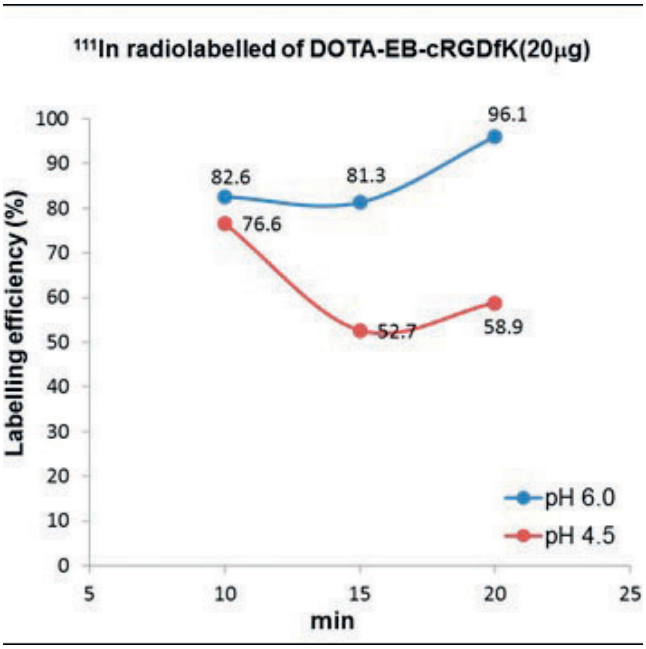

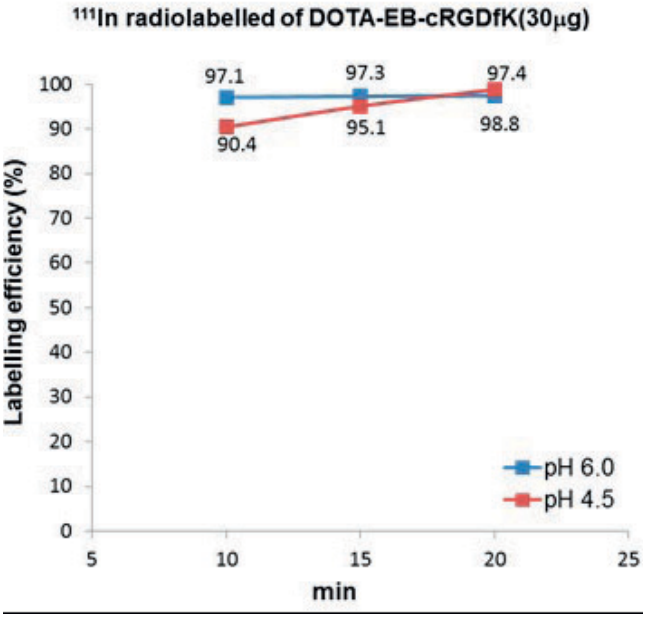

Authors listed for this abstract reported no relevant financial disclosures.

1834

Preliminary pharmacokinetic study of a bispecific peptide for pretargeting immunotherapy of amyloidosis using PreClinical SPECT/CT. Alan Stuckey, CNMT[1], Angela D. Williams, MS[2], Tina A. Richey[3], Sallie D. Macy, technologist[4], Craig Wooliver[5], Steve Kennel, PhD[6], Jonathan S. Wall[7]; [1]Radiology, University of Tennessee Graduate School of Medicine, Knoxville, TN, USA, [2]University of Tennessee Graduate School of Medicine, Knoxville, TN, USA, [3]University of Tennessee, Knoxville, TN, USA, [4]UT Graduate School of Medicine, Knoxville, TN, USA, [5]Medicine, University of Tennessee Graduate School of Medicine, Knoxville, TN, USA, [6]University of Tennessee Graduate School of Medicine, Knoxville, TN, USA, [7]University of Tennessee, Graduate School of Medicine, Knoxville, TN, USA. (1599)

Objectives: Preliminary pharmacokinetic study of a bispecific peptide for pretargeting immunotherapy of amyloidosis using PreClinical SPECT/CT
Amyloid deposition in abdominothoracic organs and peripheral nerves results in cytotoxicity and disruption of tissue architecture leading to organ dysfunction. Removal of amyloid would improve organ function, prolong patient survival, and enhance quality of life. Passive immunotherapy, using amyloid-reactive monoclonal antibodies (mAbs) has been shown to improve organ function and reduce amyloid load, but only in a subset of patients evaluated.
To enhance the utility of one therapeutic mAb, 11-1F4 (Blood. 2010;116(13):2241-4), which has shown efficacy in ~ 60% of patients with light chain-associated (AL) amyloidosis, but is anticipated to be ineffective in other forms of the disease, we have developed a bifunctional, synthetic "peptope" comprising a pan-amyloid-reactive peptide, p5 (Sci Rep. 2016;6:22695), and a high-affinity, linear epitope for 11-1F4, known as A12. This bispecific synthetic peptide, designated p93, may serve a dual purpose as diagnostic imaging agent, when radiolabeled, and as a therapeutic agent for enhancing 11-1F4-based immunotherapy in many forms of systemic amyloid-associated disorders. Herein we describe data related to two critical factors in the use of the amyloid-bound half-life, which will influence the mAb targeting efficiency and the amyloid-binding specificity, which will affect off-target immunological effects.
Peptope p93 was synthetized as an all L-amino acid peptide with a single D-tyrosine residue at position 2 to allow radioiodination that was resistant to dehalogenation in vivo. Female mice (n = 3) with severe, systemic serum amyloid protein A (AA) amyloidosis received 125I-p93 IV in the lateral tail vein and SPECT/CT images acquired under anesthesia at 4 h, 24 h, 72 h and 168 h post injection. Region of interest analyses were performed using SPECT data to quantify the activity associated with the liver and spleen - major sites of amyloid deposition in these mice. The muscle was used a negative control tissue. Following necropsy the liver and spleen at 168 h pi contained 2.2 %ID/g and 2.1 %ID/g, respectively. Specific binding to amyloid at this time point was demonstrated autoradiographically.
These data indicate that the bound amyloid bound half-life, estimated using a two-phase exponential was ~8 h and ~37 h for tfast and tslow. Furthermore, given the excellent safety profile a similar amyloid reactive peptide (NOAEL >17 mg/Kg in preclinical studies) this would allow delivery of significant amounts of peptope to amyloid deposits in patients, serving as a pre-targeting agent, prior to delivery of therapeutic mAb 11-1F4. We anticipate that this strategy will enhance and expand the utility of this mAb, or similar reagents, for the treatment of amyloidosis.

Authors listed for this abstract reported no relevant financial disclosures.

1835

Performance Evaluation of the Discovery NM/CT 670 CZT. Masafumi Takahashi[1], Yuuki Miyazaki[1], Atsushi Kondo[1], Toshihiko Ehara[1], Kenji Koga[1], Ichiro Matsunari, MD[2]; [1]Saitama Medical University Hospital, Iruma-gun, Japan, [2]Division of Nuclear Medicine, Department of Radiol, Saitama Medical University Hospital, Iruma-gun, Japan. (2711)

Objectives: The Discovery NM/CT 670 CZT is the first commercially available cadmium-zinc-telluride (CZT)-based whole-body SPECT/CT. The aim of this study was to evaluate the performance of this SPECT system using phantoms and 99mTc-sources.

Methods: Energy resolution, system sensitivity, uniformity, spatial resolution, count rate characteristics, and count linearity were evaluated using wide-energy high-resolution (WEHR) collimators, which were exclusively designed for this CZT camera. A 99mTc flood source was used for measurements of energy resolution, system sensitivity, uniformity of planar images, and count rate characteristics. Spatial resolution was evaluated using a 99mTc line source. A JS-10 SPECT phantom was used for assessment of count linearity.
Results: The system achieved the energy resolution of 6.18 % in full-width at half maximum (FWHM) at 140 keV. System sensitivity was 78 cps/MBq at 5 cm distance from the source. The integral uniformity of planar image was 2-3%. Planar spatial resolution was 5 mm in FWHM at 2 cm distance from the source, whereas SPECT spatial resolution was 3-4 mm with iterative reconstruction and resolution recovery function at 10 cm of rotation radius. Count rate characteristics were excellent up to 50,000 cps. Finally, there was excellent linearity between 99mTc concentration and measured counts.
Conclusion: The results showed that the Discovery NM/CT 670 CZT has good overall performance with high energy resolution, spatial resolution, and excellent count rate characteristics, and should be suitable for clinical use.

Authors listed for this abstract reported no relevant financial disclosures.

1836

New automated methods for integrated quality control of 18F-FDG. Nuria Gonzalez-Montalban, Arkadij Elizarov, PhD, Artem Lebedev, PhD; Trace-Ability, Inc, Culver City, CA, USA. (1915)

Objectives: Quality Control is the most labor-intensive part of the radiopharmaceutical production. Highly skilled operators perform multiple tests for every batch of radiopharmaceutical produced, some of these tests are highly subjective. Production facilities allocate considerable resources to remain compliant with cGMP guidelines. Here we present a set of tests that can be automatically performed on a standard laboratory hardware, with no operator intervention. Specifically, we focus on the incorporation of the bacterial endotoxin assay into the QC protocol.
Methods: A multimode plate reader integrated with a pipetting robot was used as a hardware platform. The analysis was performed using modified 384 well plate and the reactions were performed in 96 well plates located on the deck of the pipetting robot. Bacterial endotoxin was analyzed using a stabilized LAL extract co-lyophilized with chromogenic reagents.
Results: Endotoxin assay needed to be incorporated into the suite of test comprised of visual assessment, analysis of residual kryptofix, ethanol and acetonitrile as well as TLC analysis, half-life measurement and radioactivity concentration measurements. Since these assays are performed on the same platform they compete for both sensing and pipetting hardware, and cannot be performed at the optimal timing. For that reason, a compromise in individual tests performances had to be reached to unify all of them into one procedure. Specifically, Endotoxin assay had to be performed at suboptimal time and temperature, that led to loss of linearity. To circumvent these limitations, we have developed a statistical algorithm that allows for robust quantification of Endotoxin in the presence of these confounding factors.
Conclusions: We successfully integrated the Bacterial Endotoxin assay into the comprehensive suite of QC test that are required for release of clinical doses of 18F-FDG. A mathematical algorithm, robust in presence of random light scattering events, temperature variability and pipetting imprecision, was developed to convert the experimental data into endotoxin concentrations. This allowed for Endotoxin assay performance to improve under suboptimal conditions established by the requirements of other assays in the suite.

Authors listed for this abstract reported no relevant financial disclosures.

1837

A comparison of efficiency, workflow, and safety of dispensing hot cells in a PET radiochemistry laboratory. Morgan R. Yeske, Kristin Graf, Ph.D.; Mayo Clinic-Arizona, Phoenix, AZ, USA. (2520)

Aim: A comparison of efficiency, workflow, and safety of dispensing hot cells in a PET radiochemistry laboratory.
Objectives: There exists a wide selection of lead lined dispensing hot cells for the handling of PET drug products within an ISO 5 environment. With the plethora of manufacturers and differing designs, it is often difficult to select the right piece of equipment for a particular operation. Moreover, the high cost and large size of dispensing hot cells often limits a facility's ability to select more than one or make changes in the future.
The PET Radiochemistry Facility at the Mayo Clinic in Arizona is a brand new facility that opened in September 2016. The current layout includes two distinctly different types of dispensing hot cells. One is an Amercare A^2 PET Dispensing Isolator, with a rudimentary remote manipulator, glove port access and an Automated Dose Dispenser (ADD). The other is a Von Gahlen modular hot cell with airlock, laminar flow insert, and two fully articulating mechanical arms. We are in a unique position to offer a direct comparison between two significantly different designs used in the same practice.
Methods: One major distinction between the two dispensing units is the way in which drug product is drawn out of the bulk vial. The Amercare unit utilizes a semi-automated robot, while the Von Gahlen relies on manual manipulations of the individual operator. A study of the accuracy and precision of each technique was performed by withdrawing fixed amounts of liquid from bulk vials and calculating the actual volume withdrawn via weight measurements. Other important factors of a dispensing unit such as the ease of use, functionality and workflow efficiency were also evaluated.
Results: The accuracy and precision study demonstrated that the Amercare unit exhibited 96.0% recovery (n=192) with an average relative standard deviation of 3.7% across a range of 0.1 to 6.0 mL. Manual drawing using the Von Gahlen unit yielded 102.9% recovery (n=192) with an average relative standard deviation of 3.5% across a range of 0.1 to 6.0 mL. The Amercare unit is limited in its use of the remote manipulator, forcing the user to do many manipulations via the glove ports. The gloves tend to be cumbersome and degrade quickly in the presence of strong cleaning agents. The Von Gahlen unit, on the other hand, offers much more sophisticated movements with the use of the articulating mechanical arms, but requires a relatively experienced user to maximize efficiency. It seems obvious that using the Amercare unit would result in more radiation exposure to the extremities though we are still currently in the process of collecting data to support this assertion.
Conclusions: Overall, the accuracy and precision measurements between the two units were comparable. Though each unit has some unique advantages, we have found the ease of use and potential radiation safety aspects of the Von Gahlen unit to be superior to that of the Amercare unit.

Authors listed for this abstract reported no relevant financial disclosures.

1838

The experimental research of the effect of pioglitazone on ^{18}F-FDG uptake in A549 lung cancer cells and RAW264.7 macrophages. Qin Lu-ping, master; The Third Affiliated Hospital of Sun Yat-Sen University, Guangzhou, China. (82)

Introduction: To investigate the effects of pioglitazone on ^{18}F-FDG uptake of A549 lung cancer cells and RAW264.7 macrophages.
Method: A549 lung cancer cells and RAW264.7 macrophages were treated with different concentrations of pioglitazone (10μg/ml, 20μg/ml, 50μg/ml, 100μg/ml and 200μg/ml) respectively for 1 hour, after that incubated with ^{18}F-FDG for another 1 hour, then the change of ^{18}F-FDG uptake in these cells was measured separately by a γ counter. Both types of cells were treated with 100μg/ml pioglitazone for 1 hour, next incubated with ^{18}F-FDG for 1 hour, 2 hour, 3 hour, 4 hour, 5 hour and 6 hour,finally the variation of ^{18}F-FDG uptake in these cells was measured separately by the γ counter at six different time points.
Result: ^{18}F-FDG uptake of lung cancer cells in five different concentrations groups of pioglitazone were both higher than that in the blank control

group(both P<0.05,figure 1). However, in macrophages, no significant difference was discovered in ^{18}F-FDG uptake between the drug concentration 10μg/ml group, 20μg/ml group, 50μg/ml group and the blank control group respectively (both P>0.05), and ^{18}F-FDG uptake in the dug concentration 100μg/ml group and 200μg/ml group were both lower than that in the blank control group (both P<0.05,figure 2). AT Six different time points, ^{18}F-FDG uptake in the drug groups were both higher than that in the blank control group in lung cancer cells (both P<0.05,figure 3), whereas, compared with the control group, ^{18}F-FDG uptake in the drug groups had no obvious changes in macrophages(both P>0.05,figure 4).

Conclusion: Pioglitazone can increase the ^{18}F-FDG uptake of A549 lung cancer cells in short term, but make the ^{18}F-FDG uptake of RAW264.7 macrophages unchanged or reduced.

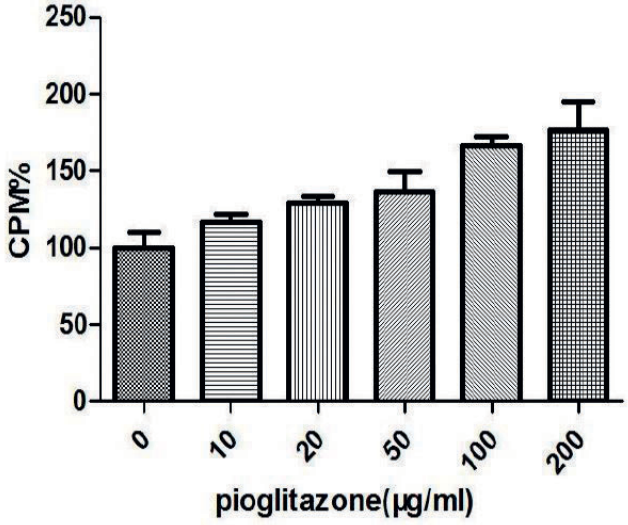

Figure 1. The effect of pioglitazone on 18F-FDG uptake in A549 lung cancer cells.

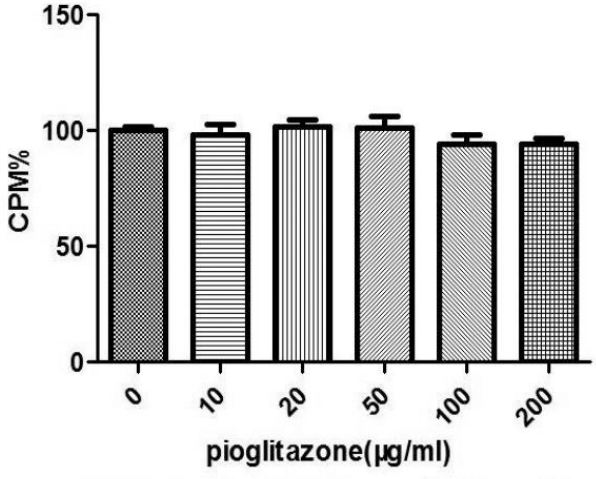

Figure 2. The effect of pioglitazone on 18F-FDG uptake in macrophages.

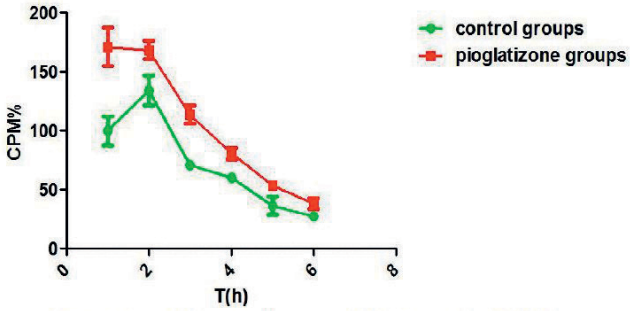

Figure 3. The effect of 100 μ g pioglitazone on 18F-FDG uptake in A549 lung cancer cells at six different time points.

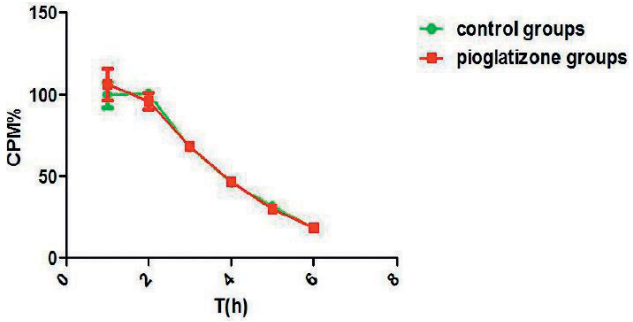

Figure 4. The effect of 100 μ g pioglitazone on 18F-FDG uptake in macrophages at six different time points.

Authors listed for this abstract reported no relevant financial disclosures.

1839

Clinical validation of cardiac risk stratification on myocardial SPECT using different reconstruction algorithm and normal database in a semiconductor camera system. Yuji Kawakami[1], Akio Nagaki[1,2], Kunihito Tsuboi[1], Masahisa Onoguchi, PhD[2], Takayuki Shibutani[2]; [1]Kurashiki Central Hospital, Okayama, Japan, [2]Department of Quantum Medical Technology, Graduate School of Medical Sciences, Kanazawa University, Kanazawa, Japan. (1368)

Objectives: A spectrum dynamics (SD) algorithm is cardiac dedicated software program using an iterative reconstruction algorithm. The SD algorithm improves a spatial resolution compared with the conventional ordered subset expectation maximization (OSEM) algorithm. However, it is not clear whether this algorithm affects the evaluation of risk stratification. The purpose of this study was to validate the reconstruction algorithm and the normal database for cardiac risk stratification using the summed stress score (SSS) of myocardial perfusion imaging (MPI).

Methods: The total of 101 patients summed 51 patients with Technetium-99m tetrofosmin (27 males and 24 females) and 50 patients with thallium-201 (28 males and 22 females) underwent adenosine stress-rest MPI. This study enrolled from normal to severely abnormal patients stratified by SSS (normal n=14, mild abnormal n=8, moderate abnormal n=10 and severely abnormal n=19 for ^{99m}Tc, normal n=12, mild abnormal n=7, moderate abnormal n=11and severely abnormal n=20 for ^{201}Tl). MPI was performed using the semiconductor camera (D-SPECT; Spectrum Dynamics Medical, Inc.). Myocardial SPECT images were reconstructed using both the OSEM and SD algorithm, which analyzed with quantitative perfusion SPECT (QPS) software. The SSS calculated by the Japanese and the US normal database was used to compare two reconstruction algorithms.

Result: SSS of OSEM and SD with the Japanese normal database were 8.88±5.68 and 7.24±5.22 for ^{99m}Tc ($p<0.001$), 9.54±5.89 and 6.64±5.70 for ^{201}Tl ($p<0.001$). Meanwhile, SSS of OSEM and SD referenced with the US normal database were 7.35±5.61 and 5.80±5.28 for ^{99m}Tc ($p<0.001$), 6.44±4.79 and 5.06±4.76 for ^{201}Tl ($p<0.001$), respectively. The SD algorithm significantly decreased average SSS compared with the OSEM algorithm. SSS with US normal database were lower than SSS with the

Japanese normal database. The difference of SSS in two reconstruction algorithms was not affected by severity of SSS. The difference of SSS in two normal database increased with increasing SSS score in ^{201}Tl.
Conclusion: The SD algorithm was underestimated SSS in comparison with the OSEM algorithm, in addition, the US normal database was underestimated SSS in comparison with the Japanese normal database. Difference of reconstruction algorithm and the normal database may affect cardiac risk stratification.

Authors listed for this abstract reported no relevant financial disclosures.

1840

Confirmation of independence of stomach, small bowel and large bowel motility. Fritzgerald C. Leveque, CNMT, William Wamp, CNMT, Xiyao Zhao, Maria-Bernadette S. Tomas, MD, Christopher J. Palestro, MD, Kenneth J. Nichols, PhD; Northwell Health, New Hyde Park, NY, USA. (1833)

Objectives: Whole gut transit studies can be helpful for determining if a pt has a motility disorder of the stomach, small bowel or colon. Because assessing all 3 components is a time consuming process, requiring repeated data acquisitions over 3 days, we wished to ascertain whether abnormal motility of one portion of the GI tract reliably predicts abnormality of another, & whether colonic transit abnormality is more reliably indicated by abnormalities seen earlier or later in the study, in the interest of shortening &/or simplifying these evaluations.
Methods: Data were reviewed retrospectively for 29 pts (age = 47±21 years; 21 female; 8 male) who were referred for evaluation of possible gastrointestinal motility disorders. Following consensus guidelines (J Nucl Med 2013;54:2004-13), pts consumed a standardized meal labeled with 37 MBq ^{99m}Tc-sulfur colloid & 7.4 MBq ^{111}In-DTPA in 300 cc water, after which dual-energy anterior & posterior 1-min static images were collected each hr for 4 hrs for pts imaged upright between 2 opposing rectangular large-field-of-view detectors. Algorithms written in Visual Basic combined counts corrected for radioactive decay of conjugate views for manually drawn stomach regions for all time points, from which were computed percentage of gastric retention @ 4 hr. For small bowel transit, additional ^{111}In-DTPA posterior & anterior images were acquired at 5 & 6 hrs post-ingestion. For colonic transit, additional ^{111}In-DTPA posterior & anterior images were acquired at 24, 48 & 72 hrs post-ingestion & counts in regions of interest determined for the 7 segments of the large bowel, from which center-of-counts were computed for each of the 3 days. Pt reports were reviewed as to whether the physicians' overall visual impressions entered for the study were normal or abnormal for the stomach, small bowel & large bowel.
Results: Physicians' visual impressions were that 34% (10/29) of gastric, 0% of small bowel, & 83% (24/29) of large bowel studies were abnormal. The impression of abnormal gastric emptying did not predict the impression of abnormal large bowel motility (χ^2 = 0.05, p = 0.82). The % stomach activity @ 4 hr did not predict small bowel transit @ 6 hrs (r = -0.12, p = 53), nor colonic transit (p > 0.05). ROC analysis indicated visually abnormal gastric emptying corresponded to % activity retained @ 4 hrs > 10% (accuracy 94±6%, sensitivity = 90%, specificity = 100%), & that visually abnormal large bowel emptying corresponded to large bowel center-of-counts @ 24 hr <=2.8 (accuracy 77±13%, sensitivity = 71%, specificity = 80%).
Conclusions: Our results in this initial small sample of pts confirm that stomach, small bowel & large bowel motility are independent of one another, & suggest that neither visual nor semi-quantitative analysis of one level of the GI tract reliably predicts an abnormality of another, so that acquiring the full set of data over 72 hrs is necessary for a complete, reliable assessment of pts being evaluated for GI tract problems.

Authors listed for this abstract reported no relevant financial disclosures.

1841

Influence of scatter correction on measurement of the heart-to-mediastinum ratio by SPECT-CT. Ryuto Mukumoto[1], Tetsuro Odagawa[1], Shinichiro Matsuzawa[1], Chinatsu Hasegawa[1], Shinji Abe[2], Katsuhiko Kato, MD, PhD[1]; [1]Nagoya University Graduate School of Medicine, Nagoya, Japan, [2]Nagoya University Hospital, Nagoya, Japan. (45)

Purpose: In myocardial sympathetic nerve scintigraphy, the heart-to-mediastinum ratio (HMR) is widely used as an indicator of myocardial I-123 MIBG uptake. It is difficult to accurately quantify HMR because of the presence of 529 keV scatter component from I-123 MIBG. I-123 Dual Window (IDW) is used as a method of correction for 529 keV scatter component and the quantitativity of HMR is improved. In this study, we obtained the synthetic planar image (Sy planar image) by using the count density map and attenuation map from the SPECT-CT images. We compared HMR calculated from the planar image with scatter correction by using IDW method and the Sy planar images with or without scatter correction. We also examined the effect of scatter correction on HMR calculated from the Sy planar images.
Methods: We defined the radioactivity concentration ratio of the myocardium, mediastinum, and liver as 15:1:10, and enclosed these concentrations of I-123 MIBG solutions into the respective areas of the torso phantom. The planar image was acquired using the low-medium energy general purpose collimator. HMR calculated from the planar image with scatter correction using IDW method was defined as the reference value in this experiment. SPECT acquisition was performed for by using 360 degrees rotation. Images were reconstructed by using 360 degrees data and 180 degrees data from each projection angle with or without scatter correction. We obtained the Sy planar images by using the all reconstructed data and the attenuation map obtained from the CT images. HMRs calculated from the Sy planar images were compared with the reference value.
Results: HMRs calculated from the planar images with scatter correction using IDW method was 2.51. In the 360 degrees reconstruction of Sy planar image with scatter correction, HMR was 2.58, which was 3% higher than the reference value. In the 180 degrees reconstruction of Sy planar images with scatter correction, HMRs were 2,47 to 2.62, which corresponded to -1.5 to +4% of reference value.
Conclusion: We found that the Sy planar images with scatter correction gave higher HMRs than the reference value. In reconstruction of SPECT-CT images, scatter correction was performed by setting multiple energy windows. Therefore, many scatter components were removed and higher HMRs were obtained.

Authors listed for this abstract reported no relevant financial disclosures.

1842

The influence of radioactivity ratio on harmonization of PET image. Akira Maebatake, MS[1], Shota Takemoto[2], Hideo Yamamoto, MPAS[2], Yuki Yamashiro[3], Atsushi Nakanishi, MD,PhD[4], Koji Murakami, MD, PhD[5]; [1]Radiology, Juntendo University Hospital, Tokyo, Japan, [2]Juntendo University Hospital, Tokyo, Japan, [3]Juntendo Radiology, Tokyo, Japan, [4]Juntendo University, Tokyo, Japan, [5]School of Medicine, Keio University, Tokyo, Japan. (2597)

Purpose: The standardized uptake value (SUV) is primarily used for analysis of fluorodeoxyglucose (FDG) PET. The SUV is varied with PET scanner characteristics, acquisition protocols, and reconstruction algorithms. Harmonization is used to adjust the recovery coefficient of each PET scanner into the reference range and minimize the variation in SUV measurements. However, few studies, which have evaluated the influence of different radioactivities on harmonization using a phantom. The purpose of this study is to evaluate the influence of radioactivity ratio on the harmonization of a PET image using a phantom.
Materials and Methods: A National Electrical Manufacturers Association (NEMA) body phantom was filled with different concentrations of ^{18}F solution. The radioactivity ratios of hot spheres in comparison to the background were 4:1 and 2:1. The value 2.65 kBq/mL was chosen to represent the background activity. PET data were acquired from a 30 min

scan using a Biograph mCT flow scanner (S1) and a Celesteion scanner (S2). The S1 PET images were reconstructed by using the ordered-subsets expectation maximization (OSEM) algorithm, OSEM with time-of-flight (TOF), OSEM with point spread function (PSF), and OSEM with PSF+TOF algorithms. On the other hand, S2 images were reconstructed by using the OSEM, OSEM with TOF, and OSEM with PSF+ TOF algorithms. The full-width at half-maximum of the Gaussian filter (GF-FWHM) varied from 1 mm to 10 mm. The harmonization of the PET image was evaluated by SUVmax. The SUVmax was plotted as a function of the sphere diameter and compared to the reference range proposed by the European Association of Nuclear Medicine (EANM).

Results: At the radioactivity ratio of 4:1, GF-FWHM was that is included in the EANM reference range was changed by the reconstruction algorithms and scanners. For S1, the FWHM ranges of the OSEM, OSEM+PSF, OSEM+TOF, and OSEM+PSF+TOF were 5-8 mm, 6-9 mm, 6-8 mm, and 7-9 mm, respectively. For S2, the value of OSEM, OSEM+TOF, and OSEM+PSF+TOF were 3-5 mm, 7-9 mm, and 8-9 mm, respectively. At the radioactivity ratio of 2:1, the FWHM range of the OSEM, OSEM+PSF, OSEM+TOF, and OSEM+PSF+TOF for S1 were 3-4 mm, 4-6 mm, 3-4 mm, and 4-5 mm, respectively. For S2, the value of OSEM, OSEM+TOF, and OSEM+PSF+TOF were 4-5 mm, 5-6 mm, and 5-6 mm, respectively. When the radioactivity was low, the GF-FWHM that is to adjust in the reference range were small.

Conclusions: The results of this study suggested that the harmonization of SUVmax was influenced by the radioactivity ratio, regardless of reconstruction algorithms.

Authors listed for this abstract reported no relevant financial disclosures.

1843

Removing Leniency Error in Student Clinical Evaluations. Tiffinee Swanson, MHA, CNMT, RT(R), Michelle Bartel, CNMT, James Long, CNMT, Nicole Fischer, MSTD, CNMT; Mayo Clinic, Rochester, MN, USA. (1432)

Background: Evaluating clinical performance is an essential component of nuclear medicine technology programs. Previously, our program evaluated clinical performance using a Likert scale of 1-4, four being favorable. Over the past 2 years, the overall student evaluation scores ranged from 3.79 to 4.0 making it difficult to differentiate student performance. Further, scores did not illustrate substantial growth over time, with an average score of 3.90 in semester 1 and 3.95 in semester 2. Leniency error, in which students' abilities are rated higher than performance metrics(*1*), removed the ability to draw meaningful conclusions from student scores. Our objective was to create a clinical assessment that would allow for differentiation of clinical performance among students and demonstrate student growth over the program duration.

Methods: Students were evaluated weekly at the end of each clinical rotation. Students selected a clinical instructor to complete the evaluation based on which technologist they worked most with during the clinical rotation. Electronic evaluation forms were completed using an online clinical management system. Students were assessed on five categories of clinical skill including collaboration and teamwork, preparedness and initiative, communication, clinical accuracy, and clinical confidence. A new scale was developed to indicate the student's clinical skill in the previously mentioned categories and included the following classifications: entry level student (score of 0), advanced entry level student (25), intermediate student (50), advanced intermediate student (75), and entry level CNMT (100). Additional yes (score of 100) or no (0) questions were implemented to reflect whether the student upheld the following mandatory skills throughout the entire clinical rotation: punctuality, integrity, patient and procedural verification, dose verification, patient-focused care, and safety guidelines. Individual student evaluation scores were calculated using a weighted scale. Clinical skill scores were averaged for each week and weighted at 70% of the overall score, while the mandatory skill scores were averaged and weighted at 30%. Overall evaluation scores were available for students to view on the online clinical management system and were reviewed with the student at the completion of each semester (quarters 2 and 4).

Results: Between November 2017 and August 2018, a total of 258 evaluations were completed for 7 students in the Mayo Clinic Nuclear Medicine Technology Program. Evaluations that were completed more than 14 days following rotation completion were excluded from analysis (n=12). The average overall student score for quarter one was 40.52$\pm$ 6.19(range 34.04-50.63). Average student score for quarter two was 53.22$\pm$11.31 (range 33.25-67.33). Average student score for quarter three was 75.9$\pm$ 9.94(range 65.0-87.07). The average score for quarter four was 89.92$\pm$7.14 (range 78.13-96.03). The relationship between the average student evaluation scores and corresponding quarter showed a strong linear correlation (R=0.99), demonstrating a student's progression of skill over time (Figure 1).

Conclusions: Improving both the criteria and scale used for clinical evaluation of nuclear medicine technology students allowed for differentiation of clinical performance among students. The ability to assess student growth highlighted the opportunity to provide coaching as a way to improve student performance and thus improve evaluation scores. As a result, quarterly and as-needed student coaching has been implemented. One limitation to be addressed is that students self-select the clinical instructor to complete the evaluation, and may only select technologists that provide positive feedback. Future work includes the development of a rubric for clinical instructors to more consistently define entry level student, advanced entry level student, intermediate student, advanced intermediate student, and entry level CNMT.

Authors listed for this abstract reported no relevant financial disclosures.

1844

Utility of Somatostatin receptor-targeted imaging with Ga-68 DOTATATE PET/MRI in the management of progressive meningiomas. Kathleen E. Mertel, BS, CNMT, RT(CT)[1], Seyed M. Mohammadi, CNMT,RT(N)(CT), PET[2], Nghi C. Nguyen, MD, PhD[3], James M. Mountz, MD, PhD[4], Ashok Muthukrishnan, MD[2]; [1]Nuclear Medicine, UPMC Presbyterian, Pittsburgh, PA, USA, [2]UPMC, Pittsburgh, PA, USA, [3]Department of Radiology, University of Pittsburgh/UPMC, Pittsburgh, PA, USA, [4]Radiology - Nuclear Medicine, University of Pittsburgh, Pittsburgh, PA, USA. (1854)

Aim: Utility of Somatostatin receptor-targeted imaging with Ga-68 DOTATATE PET/MRI in the management of progressive meningiomas

Meningiomas are the most common type of intracranial tumors. Although these brain tumors are generally benign, some of these could be very aggressive which require extensive surgery followed by radiotherapy. Treating such refractory meningiomas could be extremely challenging. Various treatment protocols are in vogue such as cytotoxic chemotherapy and targeted therapies. One such relatively newer targeted therapy option employs sandostatin, a somatostatin analog that specifically targets somatostatin receptors (SSR) that are overly expressed in these tumors. Furthermore, a radioactive version of such a treatment called Peptide receptor radiotherapy with Lu-177 DOTATATE is becoming increasingly popular for such meningiomas outside the United states. As an imaging biomarker to his therapy, Octreoscan imaging has been used in the past to document the avidity of these SSR in such tumors. But with Ga-68 DOTATATE currently replacing Octreoscan nationwide in the NET imaging arena secondary to its excellent imaging characteristics, it would probably be the best to evaluate these recurrent aggressive meningiomas using Ga-68 DOTATATE PET/MRI. We have employed this imaging technique in such brain tumors to document their SSR avidity which in turn greatly helps the neurosurgeons and neurooncologists guide the appropriate treatment in such challenging and aggressive tumors.

Learning objectives of this educational exhibit:

1. To review the PET/MRI Ga-68 DOTATATE workflow in meningiomas.
2. To discuss expected PET/MRI image findings in a typical SSR positive meningioma with and without Gadolinium MRI contrast
3. To compare the Ga-68 DOTATATE with F-18 FDG PET/MRI findings
4. To discuss various therapy options in such GA-68 DOTATATE positive refractory meningiomas.

Authors listed for this abstract reported no relevant financial disclosures.

1845

Individualized Planning in Radionuclide Therapy with Lu-177: How and Why to Do? Tadeu TA Kubo, MSc, MBA[1], Ana Luiza Silva Lima Kubo, DSc[2], Gustavo Tukamoto, MSc[2], Fernando Fernandes, MSc[3,4], Danielle Wiecek, BSc[5], Renato Dimenstein, Tecnologist[6], Marcelo Henrique Mamede Lewer, MD, PhD[7]; [1]CDTN - Centro de Desenvolvimento da Tecnologia Nuclear, Rio De Janeiro, Brazil, [2]PhysRAD, Rio De Janeiro, Brazil, [3]Hospital Universitario Antonio Pedro, Niteroi, Brazil, [4]PhysRAD, Rio de Janeiro, Brazil, [5]Nuclear medicine Sector, RAD DIMENSTEIN, São Paulo, Brazil, [6]Sao Paulo, Brazil, [7]Universidade Federal Minas Gerais, Belo Horizonte, Brazil. (1400)

Objectives: To review imaging acquisition protocols, quantification methods (2D and 3D), softwares that can be useful and expected results for radionuclide therapy with Lu-177.
Methods: The Lu-177 radionuclide has two main energy photopeak (113 keV and 208 keV). The first photopeak will be overlapped by several scattered photons from the most energetic one. So its important to use the best available collimator and protocol. For instance data can be acquired using an energy window of 20% centered over the 208 keV photopeak and adjacent windows with 10% for scatter correction (considering a medium energy general purpose collimator - MEGP). Others design are possible for parallel hole collimator low energy high resolution (LEHR) and high energy general purpose (HEGP). **Acquisition method:** whole-body with conjugate views. Speed: 10 cm/min, flood phantom fillable with Lu-177 if SPECT/CT is not available. Acquisition times: before therapeutic dose (flood phantom), before urination after therapeutic dose: 0h 24 h, 48h, 96 h and 168 h after administration.
Results: Individualized planning in radionuclide therapy is necessary due to the wide variability between patients biokinetic behavior. This presentation propose an overview of the required steps for the accomplishment of the internal dosimetry in the treatment of neuroendocrine tumors:a. the types of neuroendocrine tumorb. the radionuclide available for treatment (tumor size)c. the planar, SPECT and PET methods useful for imaging acquisitiond. the protocol suggested by MIRD 16, MIRD 23, MIRD 26 and how to use the softwarese. the types outcomes of image quantification to be used in worksheet or paid software.
Conclusions: We review expected topics to become able to decide which collimator choose in the nuclear medicine department, to understand the application of triple-energy-window correction for scattering, to do image quantification using free and paid softwares that can automatically calculate residence time and provide dose using whole body images (2D). Also to realize that from SPECT images (3D) we could understand the overlap of organ quantification or apply directly for voxel-based dosimetry, where the regions of interest are delimited and the results appear as a function of the dose based on residence time.

Authors listed for this abstract reported no relevant financial disclosures.

1846

Investigation of Collimator Broad Correction for Dopamine Transporter SPECT Imaging using Monte-Carlo Simulation. Keita Funada[1], Akihiko Takahashi[2], Kazuhiko Himuro[2], Shingo Baba, MD, PhD[3], Masayuki Sasaki, MD, PhD[4]; [1]Health Sciences, Kyushu University, Fukuoka-shi, fukuoka-ken, Japan, [2]Kyushu University, Fukuoka, Japan, [3]Kyushu University Hospital, Fukuoka, Japan, [4]Dept Rad Sci Sch of Health Sci Kyushu Univ, Fukuoka, Japan. (1794)

Purpose: Dopamine transporter (DaT) single-photon emission computed tomography (SPECT) is used in the diagnosis of Parkinson's syndrome and dementia with Lewy bodies. The accumulation of ^{123}I-ioflupane in a striatum decreases in these diseases. The collimator removes scattered rays and improves image quality in SPECT. However, the spatial resolution of images is decreased by the collimator septa. The striatum is a small tissue and deeply located; hence, it can be easily affected by spatial resolution deterioration in the SPECT device. Thus, correcting the spatial resolution in imaging the accumulation of ^{123}I-ioflupane is essential. The widely used spatial resolution correction methods are collimator broad correction (CBC) and three-dimensional frequency distance relationship (3D-FDR). CBC is used for the ordered subset expectation maximization (OSEM) method, and 3D-FDR is used for the filtered back projection (FBP)
Methods: The purpose of this study is to quantitatively assess the influence of spatial resolution correction on DaT SPECT images using Monte Carlo simulation. [Method]The simulation is an in-house code called Monte Carlo simulation of electron and photon (MCEP). The Computed Tomography (CT) image of the striatum phantom data was installed in the simulation code as a voxel data. The number of voxels was 512 × 512 × 76, and the dimension of voxel was 0.6 × 0.6 × 1 mm. The radioactivity concentration of the background is 5.56 kBq/mL or 7.44 kBq/mL. The ratio of the activity concentrations in the striata to that in the background was (right striatum, left striatum) = (6.03, 3.01) and (8.04, 4.03). The collimator of the gamma camera was an LEHR collimator. The image reconstruction software used was the Prominence Processor™ (version 3.1). The Butterworth filter (cutoff frequencies: 0.5 cycles/cm, order: 8) was applied to the projection data. Image reconstruction was carried out using the OSEM (iteration = 6, subset = 10) with or without the CBC and the FBP with or without the 3D-FDR. The projection images were reconstructed with attenuation correction (Chang method) and scatter correction of a triple energy window. The reconstructed images were evaluated using contrast recovery coefficient (CRC). The CRC value was calculated using the region-of-interest of the right and left striata and the background.
Result: The CRC value of the images reconstructed using FBP with 3D-FDR was 73.3%, and the CRC of the images without 3D-FDR was 62.4 %. On the contrary, the CRC of the images constructed using OSEM was 73.3%, and the CRC of the images without the CBC was 63.7%.
Conclusion: The CRC values were improved more than 10% using the spatial resolution correction. There was little difference between the OSEM and the FBP method.

Authors listed for this abstract reported no relevant financial disclosures.

1847

Comparison of calculation accuracy of gross tumor volume between respiratory gated and non-gated PET/CT at the diaphragm boundary. Shuto Nakazawa[1], Takuro Umeda[2], Noriaki Miyaji[3], Shohei Fukai[4], Takashi Terauchi, MD[5], Mitsuru Koizumi, MD, PhD[6]; [1]The Cancer Institute Hospital of Japanese Foundati, Tokyo, Japan, [2]Cancer Institute Hospital of Japanese Foundation F, Tokyo, Japan, [3]Japanese Foundation For Cancer Research, TOKYO, Japan, [4]Japanese Foundation For Cancer Research, Tokyo Koto, Japan, [5]Cancer Institute Hospital, Japanese Foundation for, Tokyo, Japan, [6]Cancer Institute Hospital, Department of Nuclear M, Tokyo, Japan. (2179)

Objectives: In radiation therapy, assessment of the metabolic tumor volume (MTV) is useful to delineate the area of the gross tumor volume (GTV). However, a tumor at the diaphragm boundary is affected by respiratory motion. Therefore, an attenuation correction error may provide inaccurate quantitative values for the MTV. Here, we compare clarify GTV delineation accuracy between respiratory gated and non-gated PET/CT at the diaphragm boundary.
Method: The ling/diaphragm boundary was simulated using a phantom containing F solution (10.6 kBq/ml). Tumors were simulated using spheres (diameter, 11-38 mm) containing F and located at the positions of the lungs and liver. The tumor background ratios (TBR) were 2, 4, and 8. The phantom was moved from the superior to inferior direction with a 20-mm motion displacement at 3.6 s intervals. The recovery coefficient (RC), volume RC (VRC), and standardized uptake value (SUV) threshold were calculated using stationary, non-gated (3D), and gated (4D) PET/CT. For comparison, we calculated the true value of the RC and VRC from stationary image.
Result: In lung cancer simulation, RC and VRC in 3D PET images were, respectively, underestimated and overestimated in smaller tumors, and whereas both improved in 4D PET images regardless of tumor size and TBR. The most suitable SUV threshold was about 30% in 4D PET images. In liver cancer simulation, RC and VRC were, respectively, underestimated and overestimated in smaller tumors, and when the TBR was lower, but both improved in 4D PET images when tumors were > 17 mm and the TBR was > 4. The most suitable SUV threshold tended to depend on the TBR.
Conclusions: The delineation accuracy of GTV was improved by considering tumor size, TBR and using the most suitable SUV threshold

acquired from 4D PET images. However, it is neccessary to set the most suitable SUV threshold because it tends to depend on the TBR.

Authors listed for this abstract reported no relevant financial disclosures.

1848

Targeted Peptide Conjugated ^{131}I-PAMAM (G5.0) inhibits MTC Cells Proliferation. Li J. Xie; First Affiliated Hospital of Kunming Medical University, Kunming, China. (1172)

Objectives: We aimed to load ^{131}I into the conjugation of targeting peptide SRESPHP to 5th generation dendrimer (PAMAM(G5.0) and evaluated it as targeting probe to medullary thyroid carcinoma (MTC) cells and cell proliferation in vitro.
Methods: PAMAM (G5.0)-SR and PAMAM (G5.0) were radiolabeled with ^{131}I by the chloramine T. The labeling rate and stability were determined by radio-thin layer chromatography(TLC); their lipid-water partition coefficients were evaluated. The targeting of two ^{131}I-radiotracers (^{131}I-PAMAM(G5.0)-SR, ^{131}I-PAMAM(G5.0)) to MTC were determined in blocking uptake test using TT tumor cells. The median lethal dose of two probes against the MTC were also determined by CKK-8 kit. The secretion of calcitonin was detected by calcitonin kits.
Results: The labeling yields of the 2 ^{131}I radiotracers (^{131}I-PAMAM(G5.0)-SR, ^{131}I-PAMAM(G5.0)) were all above 70%, and the radiochemistry purity were all greater than 90% after purification. The 2 probes in PBS system were stable over 24 hours, and showed excellent water solubility. Blocking uptake test in TT cells showed that ^{131}I-PAMAM (G5.0)-SR had significant higher uptake than the blocking groups. (t=7.315, 22.590 and 22.570; all P<0.01). The median lethal dose of ^{131}I-PAMAM (G5.0)-SR was just 513.6kBq/mL. The secretion of calcitonin in vitro showed that after ^{131}I-PAMAM (G5.0)-SR treatment, the levels of calcitonin secretion decreased gradually over time, but there was no statistical significant compared with ^{131}I- PAMAM (G5.0) ($P>0.05$).
Conclusions: ^{131}I-PAMAM (G5.0)-SR could target medullary thyroid carcinoma cells and is
potential for diagnosis and for therapy by inhibiting cell proliferation.
Keywords: SRESPHP, PAMAM (G5.0), radioactive iodine-131, targeting, medullary thyroid carcinoma cells

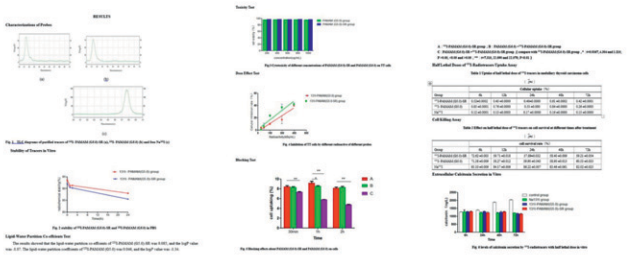

Authors listed for this abstract reported no relevant financial disclosures.

1849

An alternative clue to set axial angle parallel to the AC-PC on brain perfusion SPECT imaging: Usefulness of frontal lobe bottom and cerebellum tuber vermis line. Yasuhiro Inokuchi, RT; Radiology, Edogawa Hospital, Edogawaku, Tokyo, Japan. (41)

Objectives: In 1988, Tarairach et al were reported that anterior commissure and posterior commissure (AC-PC) line can be used as a standard imaging reference line for the stereotaxis in the human brain using MR imaging. The AC-PC line is able to be created by visualizing AC and PC using a high resolution MR imaging. If axial images using the AC-PC line was able to create at other modality, between the images of different modalities can be compare anatomical structure using the same slice. However, the nuclear medicine (NM) images of low resolution are not able to visualize AC and PC. Therefore, axial images by the AC-PC line are not able to create at NM images. This present study proposes that Frontal lobe bottom and Cerebellum tuber vermis (FLB-CTV) line on brain perfusion scintigraphy images is useful to determine axial angle parallel to the AC-PC line.
Materials and Methods: This study was approved by the Review Board, and the need to obtain informed consent was waived for this retrospective study. Firstly, angular differences between the AC-PC line and the FLB-CTV line on midsagittal brain MR images of 100 patients were measured. The FLB-CTV line was defined as a connecting line the frontal lobe bottom and the cerebellum tuber vermis (Fig 1). Secondly, we used the FLB-CTV line of the brain computed tomography attenuation correction (BCTAC) images as a reference line and calculated with angler differences of the FLB-CTV line between the NM images and the BCTAC images on the brain perfusion scintigraphy (BPS) imaging of 100 patients. The inter-reader reproducibility of the FLB-CTV line measurements on NM images in BPS imaging of 50 patients were evaluated using the intra-class correlation coefficient (ICC) and 95% confidence interval (CI), for two readers (reader 1: radiological technician with 13 years of experience; reader 2: radiological technician with 4 years of experience). The AC-PC line and the FLB-CTV line were measured using an angle measurement tool in PACS monitor by midsagittal image at each modality.
Results: Angular differences between those two lines on midsagittal brain MR images for 100 patients were measured, and the mean and standard deviation were -1.24 degrees and 1.14 degrees respectively. Angler differences of the FLB-CTV line between the NM images and the BCTAC images were measured, and the mean and standard deviation were 0.87 degrees and 0.48 degrees respectively. The ICC of the FLB-CTV line measurements on NM images in BPS imaging was 0.99 (95%CI: 0.98-0.99).
Conclusion: The FLB-CTV line were demonstrated that it is approximately parallel to the AC-PC line and can be created by the NM images in the BPS imaging. The FLB-CTV line is useful as an alternative clue to set axial angle parallel to the AC-PC line.

Authors listed for this abstract reported no relevant financial disclosures.

1850

Feasibility study of SPECT/CT Standard uptake value in differentiating benign and malignant Bone lesions. Meng Qingyuan[1], Shou Yi, MD[2], Zhiwen You[1], Jianjun Jiang[1], Jieping Song, MS[1], Zhao Jun, MD[1]; [1]Shanghai East Hospital, Shanghai, China, [2]East Hospital Affiliated to Tongji University, Shanghai, China. (2798)

Objectives: To investigate the quantitative tomography of thoracic vertebrae and lumbar vertebrae by using SPECT imaging (SPECT / CT) of Technetium 99m methylene phosphate (99m) methylene phosphate (99m) methylene phosphate (99mTc-99m) single photon emission computed tomography (SPECT) to investigate the feasibility of SUVmax for differential diagnosis of benign and malignant bone lesions.
Methods: 201 patients received systemic bone imaging and quantitative tomography were collected from our hospital. The dosage of injection was 25 mCi. The machine was Siemens SymbiaIntevoSPECT / CT. The sampling parameters were as follows: 20 seconds per frame, 30 frames were obtained. Single probe rotated 180 °, single rotation 6 °; After reconstructing images using ordered subset conjugate gradient (OSCG) algorithm ROI mapping technique was used to measure SUV (standard uptake value) values of thoracic vertebrae and lumbar vertebrae. As the patient's thoracic vertebra lumbar standard uptake value. 2 senior physicians diagnosed with nuclear medicine were diagnosed and followed up by other imaging and clinical procedures. The number of normal vertebral bodies and lesions measured by SUVmax quantitative analysis were: 1 thoracic vertebrae: 300 normal males, 37 benign lesions and 43 malignant tumors bone metastases foci; There were 348 normal females, 14 benign lesions and 13 lesions with bone metastatic foci in malignant tumors; 2 lumbar vertebrae: 140 normal males, 20 benign lesions and 41 bone metastatic lesions in malignant tumors; 185 females were normal, 86 benign lesions and 21 lesions were bone metastatic foci in malignant tumors. Statistical analysis was performed on three groups of data corresponding to same site and sex.
Results: Thoracic SUVmax was 8.1978 ±1.67770 in male, normal group and 10.2395 ±1.50301 in benign lesion group. Malignant tumor bone metastasis foci group was 20.3726 ±12.17745; Female normal group 7.8410 ±1.8138, benign lesion group 10.6743 ±1.60675, malignant tumor bone metastasis lesion group 15.3925 ±6.96563. lumbar SUVmax: 8.3825

±1.83047 in male normal group and 14.0980 ±4.57783 in benign lesion group,Bone metastatic foci were 27.0380 ±13.91251 in malignant tumor group, 7.8104 ±1.78647 in normal female group and 13.7201 ±4.27948 in benign lesion group. Tumor bone metastasis foci were 18.1186 ±6.40714 in malignant tumors. SPSS 20 statistical analysis showed statistical differences between three groups ($P < 0.041$, $P < 0.001$).
Conclusion: Preliminary results show that SUVmax can differentiate benign and malignant lesions from bone lesions. SUVmax has certain cross between three groups. It is worth noting that SUVmax range is wider in malignant tumor bone metastasis foci. Clinical application should distinguish different genders and different vertebral bodies, and combine them with morphological signs of CT bone window to comprehensive judgment.

Authors listed for this abstract reported no relevant financial disclosures.

1851

^{99m}Tc-sestamibi washout reflects the salvaged myocardium after percutaneous coronary intervention in patients with acute myocardial infarction. Mieko Ota[1], Shinro Matsuo, MD, PhD[2], Takashi Kato, MD[1]; [1]Gifu Prefectural General Medical Center, Gifu, Japan, [2]Kanazawa University Hospital, Kanazawa, Ishikawa, Japan. (1682)

Background: The accelerated clearance of ^{99m}Tc-sestamibi (MIBI) had been observed in most of acute myocardial infarction (AMI) patients after successful percutaneous coronary intervention (PCI). Previous report suggests that the myocardial washout rate of MIBI is thought to be a novel marker for the diagnosis of myocardial damage or dysfunction. This observation was associated with mitochondrial dysfunctional and regional left ventricular dysfunction of the myocardium. The ^{99m}Tc-MIBI washout may be an indicator of tissue salvage and a predictor of late functional recovery in patients with AMI after PCI. However, the relationship between the washout size with ^{99m}Tc-MIBI the defect area size of simultaneous ^{99m}Tc-sestamibi myocardial SPECT adenosine-stress images is remained to be elucidated.
Purpose: The purpose of this study is to investigate the mean of defect area size using ^{99m}Tc-MIBI myocardial perfusion single photon emission computed tomography (MPS) rest imaging, of early phase and delayed phase for patients with AMI after the successful PCI, compared with the defect area size of simultaneous ^{99m}Tc-MIBI MPS adenosine-stress imaging.
Methods: 29 consecutive AMI patients (23 men and 6 women; mean age 71±8.4 years old.) who underwent successful PCI on admission were enrolled in this study. Rest ^{99m}Tc-MIBI MPS images were obtained at the early phase of 1 hour after the injection of^{99m}Tc-MIBI at a dose of 740 MBq and at the delayed phase of 4 hours after the injection. Stress ^{99m}Tc-MIBI MPS images were obtained at 1 hour after adenosine-stress (120μg/kg/min, infusion). The three kinds of images that show defect size were obtained using ^{99m}Tc-MIBI MPS imaging; a rest early phase image, a rest delayed phase image, and adenosine stress image. The three kind factors of defect size, including total perfusion defect (TPD), EXTENT (TPD, EXTENT by QPS: Cedars-Sinai Medical Center, USA), and visual perfusion defect summed score (DSS) were compared with MIBI washout.
Result: Rest ^{99m}Tc-MIBI MPS imaging was performed within 10 days (average 6.5 days) after the PCI. After within 9 days (average 2.3 days) from rest ^{99m}Tc-MIBI MPS imaging, ^{99m}Tc-MIBI MPS adenosine-stress imaging was performed. In the TPD and the EXTENT, the stress score was significantly smaller than the rest delayed phase score (TPD: 22.2±14.3% vs. 27.8±14.0%, $p<0.001$; EXTENT: 27.3±17.4% vs. 35.0±17.6%, $p<0.001$), and the rest early phase score was significantly smaller than the rest delayed phase score (TPD: 21.5±14.9% vs. 27.8±14.0%, $p<0.001$; EXTENT: 27.3±18.1% vs. 35.0±17.6%, $p<0.001$), but between the stress score and the rest early phase score was not significantly. In the DSS, the stress score was significantly smaller than the rest delayed phase score (12.4±9.1% vs. 14.6±8.9%, $p<0.001$), and the rest early phase score was significantly smaller than the rest delayed phase score (10.7±9.5% vs. 14.6±8.9%, $p<0.001$), and the stress score was significantly smaller than the rest early phase score ($p<0.01$). The defect area with increased washout included the residual ischemic area. At the follow-up, patients with accelerated washout of MIBI had a functional recovery of left ventricle. The stress defect area size was significantly smaller than the delayed phase defect area size. The defect area size at the delayed phase indicated was related to tissue salvage and a predictor of late functional recovery. But the stress defect area size was related to the patency of the infarct-related artery. This finding indicated that it may be valuable to employ the resting MIBI washout to differentiate between viable and non-viable in AMI patients after PCI.
Conclusions: The global rest ^{99m}Tc-MIBI washout could be a sensitive indicator to evaluate the potential utility for the evaluation of AMI patients. Washout rate determined from ^{99m}Tc-MIBI reflects the extent of myocardial damage in AMI.

Authors listed for this abstract reported no relevant financial disclosures.

1852

Non-uniformity images - effect of NaI(Tl) Crystal Hydration. Milena Dimcheva, Sonya Sergieva, MD, PhD, Aleksandra Jovanovska; Sofia Cancer Center, Sofia, Bulgaria. (3062)

Introduction: NaI(Tl) - Thallium-doped sodium iodide scintillation crystals can suffer from hydration, which changes the optical properties of the crystal and consequently produces areas of non-uniformity in gamma camera images. The aim of this study is to confirm the crystal hydration using an asymmetric energy window of a dual-head SPECT/CT system, Siemens.
Methods: Intrinsic calibration study was performed by placing a point source of Tc-99m positioned in front of the uncollimated detectors. Image analysis was done with symmetric energy window of the Tc-99m on-peak (140 keV), asymmetric low energy window off-peak - 10%(126 keV) and asymmetric high energy window off-peak + 10%(154 keV).
Results: The results, received from the detector #1 gave the following uncorrected uniformity parameter values: The integral uniformity for the CFOV was found to be between 4.04% and 4.07% while the integral uniformity for the UFOV was between 6.51% and 6.54%. The differential uniformity for the CFOV was between 2.34% and 2.38% while the differential uniformity for the UFOV was between 3.53% and 3.57%. Both asymmetric energy window images show clearly multiple focal spots due to crystal hydration: discrete hot spots in the asymmetric low energy window image and discrete cold spots in the asymmetric high energy window image.
Conclusions: For confirmation of crystal hydration, additional images should be made with an asymmetrically positioned energy window. When hydration can be seen in images obtained with the asymmetric energy window, the gamma camera must be used with care until the crystal was replaced.

Authors listed for this abstract reported no relevant financial disclosures.

1853

Evaluate the distribution of radiolabeled-pHCT74 peptide drug in colon cancer model. Wei-Lin Lo[1], Chen-Hsien Liang[1], Liang-Cheng Chen[2], Ming-Hsin Li[3]; [1]Institute of Nuclear Energy Research, Taoyuan, Taiwan, [2]Taoyuan city, Taiwan, [3]Institute of Nuclear Energy Research, Tauyuan City, Taiwan. (98)

Introduction: The pHCT74 peptide, identified by phage display, is a 12-amino-acid small peptide specifically binds to α-enolase. The aims of this study were to explore the distribution of ^{68}Ga-DOTA-pHCT74 peptide drug in HCT116 human colon cancer cell line, and demonstrated radiolabeled-peptide drug may offer imaging evaluation platform for tumor.
Methods: DOTA-pHCT74 peptide were synthesized and labelled with ^{68}Ga in Institute of Nuclear Energy Research (INER). Tumor xenografts were produced in 6-wk-old female NOD/SCID mice by subcutaneous injection of 5 x 10^6 HCT116 cells. These animals were used for nanoPET/CT imaging of ^{68}Ga-DOTA-pHCT74 peptide. Each mouse was scanned for 40 min by nanoPET/CT system.
Results: The labeling efficiencies of ^{68}Ga-DOTA-pHCT74 peptides were more than 90%. NanoPET/CT imaging indicated that liver, kidney, bladder and tumor were the major distribution area. The obvious uptakes in nanoPET/CT images of tumor sites were observed at 0.5 h after injection of ^{68}Ga-DOTA-pHCT74. The tumor uptakes was 0.74 %ID/g. The tumor/muscle ratio of ^{68}Ga-DOTA-pHCT74 was 3.74.

Conclusions: NanoPET/CT imaging showed that ^{68}Ga-DOTA-pHCT74 could accumulate in tumor area of human colon cancer. This study could provide the potential capability as diagnostic drug for colon cancer in the future.

Authors listed for this abstract reported no relevant financial disclosures.

1854

Radioactivity concentration dependence of BCF used in quantitative analysis of bone scintigraphy. Chinatsu Hasegawa[1], Ryuto Mukumoto[2], Shinichiro Matsuzawa[2], Shinji Abe[3], Katsuhiko Kato, MD, PhD[1]; [1]Nagoya University Graduate School of Medicine, Nagoya, Japan, [2]Nagoya University, Nagoya, Japan, [3]Nagoya University Hospital, Nagoya, Japan. (2344)

Objectives: In order to perform quantitative evaluation using quantitative analysis software of bone scintigraphy, GI-BONE (AZE, Japan), it is necessary to calculate becquerel calibration factor (BCF). BCF was calculated as the ratio of radioactivity concentration (Bq/ml) in the phantom at the time of scanning to the measured SPECT count density per scan duration (count/ml/sec). BCF should be a constant value regardless of the radioactivity concentration filled with the cylindrical phantom at the time of scanning. Generally, when calculating BCF, it is recommended to enclose the radioactivity concentration of about 15 to 20 kBq/ml into the cylindrical phantom. In this study, we determined the change in BCF when we changed the radioactivity concentration of Tc-99m enclosed into the cylindrical phantom.
Methods: A cylindrical phantom was filled with 7 kinds of Tc-99m solution; 0.9, 2.1, 4.0, 4.9, 8.2, 17.6, and 40.5 kBq/ml. SPECT-CT acquisition was performed for 360°rotation with low-energy high-resolution (LEHR), and SPECT data were reconstructed under the same conditions as used in bone scintigraphy at our hospital. Circular region of interest were drawn on 11 images around the center of the cylindrical phantom, the mean BCF and the standard deviation of BCF were calculated in each Tc-99m concentration, respectively.
Results: When the radioactivity concentration of Tc-99m were 8.2 kBq/ml or more, the mean BCF showed almost constant value. However, when the Tc-99m concentration were 0.9, 2.1, 4.0, and 4.9 kBq/ml, the mean BCF varied. The standard deviation of BCF were large at any Tc-99m concentrations.
Conclusion: When the radioactivity concentration of Tc-99m were higher than the recommendation radioactivity concentration, the mean BCF showed almost constant value. When the radioactivity concentration of Tc-99m were lower, the mean BCF varied. The standard deviation of BCF were large at any Tc-99m concentrations.

Authors listed for this abstract reported no relevant financial disclosures.

1855

Development of new database software seamlessly integrating information concerning PET/CT tests. Kaori Yanagisawa[1], Rikuta Ishigaki, PhD[2], Keiichi Nomura[1], Yoshihisa Muramatsu, PhD[1], Hirofumi Fujii, MD, PhD[3]; [1]Department of Radiologic Technology, National Cancer Center Hospital East, Chiba, Japan, [2]Kyoto College of Medical Science, Kyoto, Japan, [3]Division of Functional Imaging, EPOC, National Cancer Center, Yokohama, Japan. (55)

Objectives: The comprehensive management of information about injected radioactivity and image quality is important for the optimization of PET/CT tests. The injected radioactivity can be reported by using new automatic injectors equipped with sophisticated functions such as MWM (modality worklist management), REM-NM (radiation exposure monitoring for nuclear medicine), and radiopharmaceutical radiation dose structure report (R-RDSR). Image quality in PET/CT tests is commonly controlled by noise equivalent count (NEC). The purpose of this research is to develop "onti", a piece of application software that automatically builds a set of database by integrating injected radioactivity and images quality index in PET/CT tests.
Methods: We designed "onti"that it could extract information about injected radioactivity and R-RDSR from an injector and information about image quality factors from DICOM private tags of PET images in PACS servers. This software automatically calculated $NEC_{patient}$ using factors obtained from DICOM image data. It integrated injected radioactivity with image quality indices. We demonstrated the usefulness of this system using 5 sets of test data whose $NEC_{patient}$ values were already known. The scanner and automatic injector used in this evaluation were Discovery iQ (GE Healthcare, Milwaukee, WI) and AI300 (Sumitomo Heavy Industries, Ltd, Tokyo,Japan), respectively.
Results: "onti" successfully extracted information about injected radioactivity and image quality factors from the injector and PACS server, respectively. $NEC_{patient}$ was automatically calculated using extracted factors and obtained results corresponded well with previously calculated values. Finally, "onti" uccessfully integrated the information about injected radioactivity with that about image quality index.
Conclusions: We have successfully developed new database software "onti"that provides an environment that can seamlessly handle the information about both injected radioactivity and image quality index.

Authors listed for this abstract reported no relevant financial disclosures.

1856

NEMA NU2-2012 Performance Measurements of the United-Imaging uPMR790: A HD TOF Simultaneous PET/MR System. Tuoyu Cao, PhD[1], Shuguang Chen[2], Lifang Pang[3]; [1]United Imaging Healthcare, Shanghai, China, [2]Zhongshan Hospital, Fudan University, Shanghai, China, [3]Department of Nuclear Medicine, Zhongshan Hospital, Shanghai, China. (2454)

Objectives: The United-Imaging uPMR790 is a clinical integrated whole body Time-of-Flight (TOF) PET/MR scanner from Shanghai United Imaging Healthcare Co. The system is capable of simultaneous PET and MRI acquisition with 450ps time resolution, world's highest 2.8 mm spatial resolution (at the center of FOV with NEMA standard) and world's longest 32cm axial field of view. The high definition digital PET detector enhances small lesions detectability and improves quantification accuracy by reducing partial volume effect. The long axial coverage provides streamlined whole-body workflow by reducing the total number of bed stations. Only two other whole body simultaneous PET/MR systems had been reported so far due to unique technical challenges such as electromagnetic interference between MRI and PET subsystems. In this work, the United-Imaging uPMR790 was fully evaluated for the first time and the effects of interference from MR operation.
Materials and Methods: NEMA performance measurement was performed on the newly installed United-Imaging uPMR790 PET/MR scanner at Shanghai Zhongshan hospital. The uPMR790 system comprises a 3T super conducting magnet, a gradient system with a set of second order active shimming coil (50mT/s, 200T/m/s), and a 48 channel radio frequency (RF) receiving system. The PET detector system is installed between the gradient coil and body coil. The entire PET ring comprises 20 modules with a transverse field of view of 60cm and an axial field of view of 32cm. Each module contains 5×14 blocks with 14 blocks along the axial direction. And each block has 4 SiPM detector channels coupled with a 7×8 array of 15.5×2.76×2.76 mm^3 LYSO crystals through proprietary design of internal light guide. The entire system comprises 112 rings and each ring contains 700 crystal channels, making 78400 crystal channels in total. The PET system performance was evaluated following the NEMA NU2-2012 standards. Data acquisition was performed in the absence and presence of continuous MR pulsing during the entire data acquisition. A two point DIXON sequence, which is the sequence for PET attenuation correction was used. The RF power level was set to 400V, similar to the situation of a normal whole body MR scan. In addition, to evaluate the performance under extreme situations, image quality was tested under an extra set of MR sequences, including Echo Planar Imaging (EPI) and Single Shot Fast Spin Echo (SSFSE). All measurements was conducted at Shanghai Zhongshan Hospital. The system was fully calibrated and a quality assurance test was done before each NEMA measurement.

Results:
Image quality:
MR idle
MR pulsing -DIXON
MR pulsing -EPI

□
Contrast
10 mm - hot
0.509510
0.489634
0.494000
Recovery
13 mm - hot
0.631080
0.713210
0.754806
17 mm - hot
0.728150
0.702970
0.717516
22 mm - hot
0.715243
0.716481
0.745663
28 mm - cold
0.714990
0.714394
0.751092
37 mm - cold
0.792371
0.777951
0.830279
Lung
0.089560
0.091851
0.086992
Background
10 mm - hot
0.074785
0.089544
0.092866
variability
13 mm - hot
0.061033
0.076512
0.078524
17 mm - hot
0.048786
0.061869
0.062054
22 mm - hot
0.041081
0.049583
0.050185
28 mm - cold
0.036418
0.040667
0.042619
37 mm - cold
0.029880
0.033839
0.034782
Lung
0.034864
0.038687
0.040430
Spatial Resolution (FWHM/mm):
1cm-X 1cm-Y
1cm-Z
10cm-X
10cm-Y
10cm-Z
20cm-X
20cm-Y
20cm-Z
MR idle
2.85
2.90
2.48
3.15
3.33
2.85
4.84
5.01
3.78
MR pulsing
2.80
2.97
2.42
3.08
3.33
2.84
4.57
4.64
3.73
Clinical Images:
32 케cm 케
(a)
(b)
(c)

Conclusions: NEMA measurement demonstrates consistent ideal image contrast recovery and spatial resolution.
Results with MRI pulsing reveal no PET image quality degradation during MR pulsing. The system achieves superior PET/MR imaging quality, fusion accuracy and accelerated workflow in clinical settings.

Authors listed for this abstract reported no relevant financial disclosures.

1857

Comparison between SiPM-based and PMT-based TOF-PET/CT to detect sub-centimeter spheres. Reo Nemoto, BS[1], Kenta Miwa, PhD[2], Kei Wagatsuma[3], Tensho Yamao[2], Yuto Kamitaka[2]; [1]Radiology, International University of Health and Welfare Hospital, Nasushiobara, Japan, [2]Department of Radiological Sciences, International University of Health and Welfare, Ohtawara, Japan, [3]Research Team for Neuroimaging, Tokyo Metropolitan Institute of Gerontology, Tokyo, Japan. (1320)

Objectives: The new-generation Discovery MI (DMI) has silicon photomultipliers (SiPM) instead of PMT, and thus offers good intrinsic timing resolution. The DMI has been for penalized likelihood reconstruction (PL). Combining the DMI with SiPM and PL might be enable the accurate detection of small lesions. The present study aimed to compare the abilities of SiPM- and PMT-based TOF-PET/CT to detect sub-centimeter spheres representing small lesions.
Methods: We used a DMI and Discovery 710 (D710) PET/CT (GE healthcare) to image a NEMA body phantom comprising six spheres (diameter: 4, 5, 6, 8, 10, 13 mm) containing ^{18}F solutions with target-to-background ratios (TBRs) of 8. The PET data were reconstructed using a baseline OSEM algorithm +PSF, +TOF, +PSF and TOF, and penalized likelihood (PL). The reconstructions included OSEM applied iteration numbers of 2 - 6 and Gaussian filters of 0, 2 and 4 mm. We investigated β-values of 50 - 300 using the PL. The duration of acquisition varied from 2 to 100 minutes. The dimensions of the reconstructed image matrices were 192 × 192, 256 × 256 and 384 × 384. Recovery coefficients (RC) and lesion detectability were calculated as the physical evaluation.
Results: The RC values were higher in spheres ≤ 10 mm with the PL, than with the other reconstruction models. The trends of D710 and DMI were almost identical. The D710 overestimated the RC, whereas DMI became closer to the true value. Both OSEM+PSF and PL identified RC overestimation at 13 and 8 mm, respectively, due to the overshoot of edge artifacts. The ability to detect lesions was better for the D710 than the DMI.

In contrast, the ability of DMI+PL to detect spheres of ≤ 5 mm was best among the reconstruction methods. Longer acquisition periods improved the ability of DMI to detect lesions. The RC and lesion detectability of the DMI and D710 did not vary according to matrix size, although DMI was visually more prominent as a function of increasing matrix size.
Conclusions: The quantitation and detectability of sub-centimeter spheres is better than those of conventional PMT-based PET/CT when SiPM-based PET is combined with PL.

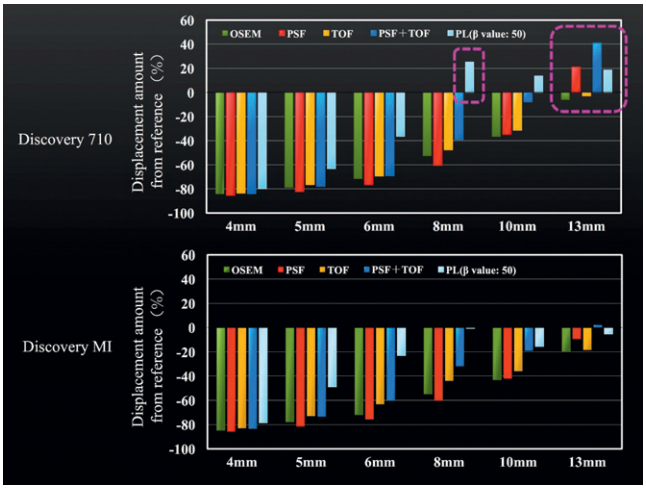

Authors listed for this abstract reported no relevant financial disclosures.

1858

Impact of reconstruction algorithm with PSF and TOF and reconstruction parameter in fractal analysis: Evaluation by changed the Gaussian filter size. Yukito Maeda[1], Nobuyuki Kudomi, PhD[2], Yuka Yamamoto[3], Tetsuhiro Hatakeyama, MD[3], Yoshihiro Nishiyama[3], [1]Dept. of Radiology, Kagawa University Hospital, Kagawa, Japan, [2]Kagawa Univ, Kagawa, Japan, [3]Kagawa University, Kagawa, Japan. (1806)

Objectives: Fractal analysis has been attracting attention for image analysis as one of texture analysis, and would be of use in characterization of tumor grade. However, the impacts of reconstruction algorithm and reconstruction parameter have not been demonstrated in fractal analysis. The purpose of this study was to test influence of PSF and TOF in reconstruction and the Gaussian filter size to fractal dimension.
Methods: We used a brain tumor phantom with sphere part filled with ^{18}F-FDG. We scanned twice with the background with ^{18}F-FDG and water, respectively. The reconstruction algorithms applied OSEM, OSEM + point spread function (PSF), OSEM + time of flight (TOF) and OSEM + PSF + TOF. The FWHM in filter was changed from 0 to 10 mm. We measured fractal dimension for 37mm hot region using pixel counting.
Results: In the case of background with water, the fractal dimension of OSEM and OSEM+TOF increased as FWHM increased. The fractal dimension of OSEM + PSF and OSEM + PSF + TOF increased at FWHM>4mm. When FWHM was 6mm, the fractal dimension of OSEM, OSEM + PSF, OSEM + TOF and OSEM + PSF + TOF were 3.20×10^{-5}, 2.47×10^{-5}, 3.17×10^{-5} and 2.50×10^{-5}, respectively. The difference of fractal dimensions of OSEM and OSEM + TOF was small. The difference of fractal dimensions of OSEM + PSF and OSEM + PSF + TOF was small. In the case of background with radioactive solution, the fractal dimension of all reconstruction algorithm decreased as the FWHM increased. When the FWHM was 6mm, the fractal dimension of OSEM, OSEM+PSF, OSEM+TOF and OSEM+PSF+TOF were 6.89×10^{-5}, 5.30×10^{-5}, 6.26×10^{-5} and 5.02×10^{-5}, respectively. The difference of fractal dimension was small so that FWHM were large.
Conclusion: The fractal dimension changed according to the reconstruction algorithm and the gaussian filter size. These results should be noted in fractal analysis.

Authors listed for this abstract reported no relevant financial disclosures.

Technologist Student Presentations

A Note on 2018 Technologist Student Abstracts

For the Technologist Student Abstract track, **30 scientific papers** have been accepted for presentation at the 65th SNMMI Annual Meeting at the Philadelphia Convention Center, Philadelphia, PA. The Program Committee for the SNMMI Technologist Section (SNMMI-TS) will be hosting 3 oral sessions to present these scientific papers, to be held on Monday, June 25; refer to the 2018 Annual Meeting Program Book for specific times and locations. Each oral session is 90 minutes in duration and includes up to fifteen 6-minute presentations per session.

For the Technologist Students Abstract track, **4 scientific posters** have been accepted for presentation. The SNMMI-TS Program Committee will be hosting a Technologist "Meet the Author" poster session, scheduled for Monday, June 25, from 3:00PM-4:30PM. The posters will be on display and available for viewing by attendees in the Poster Hall (Exhibit Hall C).

SNMMI Abstracts Online: Accepted abstracts for the 65th SNMMI Annual Meeting are citable and searchable by visiting the JNM website at: http://jnm.snmjournals.org/

TS17: Student Tech Papers I

Moderator: Jay Smith, BSRS, CNMT, ARRT, RT(R)(N)
Co-Moderator: Angela Macci-Byers, Ed.D., MPM, RT(N), CNMT, FSNMMI-TS

2122

Situs Inversus with Dextrocardia MPI Protocol using SPECT/CT. Tristian B. Maki, Carlyn M. Johnson, MSEd, CNMT, Amy Bell, BS, CNMT, Abigail S. Grancorvitz, BS, CNMT; Nuclear Medicine, Marshfield Medical Center, Marshfield, WI, USA. (4029)

Purpose: Dextrocardia with situs inversus is a condition where a patient's heart along with their chest and abdominal organs are oriented in a mirror image from the anatomical norm. Therefore, the patient's heart lies to the right of the midline with the apex of the heart pointing toward the right side of the body. SPECT/CT systems work well when performing myocardial perfusion imaging (MPI) procedures on patients with standard anatomy, but oftentimes the camera protocols fail to easily acquire dextrocardia with situs inversus patients due to their condition. The purpose of this research is to establish a MPI protocol for imaging patients who have dextrocardia with sinus inversus to be utilized by our department.
Methods: A SPECT phantom with a cardiac insert (Data Spectrum Corporation) containing a mid-anterior defect was acquired using a Siemen's Symbia T-series SPECT/CT system equipped with low energy high resolution (LEHR) collimators. The cardiac insert and the phantom were filled with 0.35 mCi and 4.52 mCi of Tc-sestimibi, respectively. The camera manufacturer's acquisition protocol for situs inversus used the same parameters as a standard MPI study with the exceptions that the starting angle was at 135 and the camera heads were positioned so that Head 1 was at the right lateral and Head 2 at the anterior. Acquired images were then processed using the camera manufacturer's situs inversus processing protocol, which flipped the images to appear in standard anatomic position for easier reading by the physicians.
Results: The camera manufacturer's protocols successfully acquired and processed the cardiac phantom placed in a dextrocardia with situs inversus position on the imaging table. During the reconstruction process, masking the background was difficult because the short axis images did not appear on the computer screen. The protocol states that "images might not appear," however, since this step is required to center the images properly, the user must blindly manipulate the images until they appear in standardized position for reading. The defect in the mid anterior wall of the cardiac phantom was visualized, but the lack of labels made locating the defect extremely difficult. Since this protocol was acquired with a phantom, other issues, such as gating, patient motion, electrocardiogram (EKG) lead placement, etc., may further complicate the protocol when acquiring a patient.
Conclusions: Images acquired using a cardiac phantom placed in the dextrocardia with situs inversus position were successfully acquired and reconstructed, albeit with many difficulties. The camera manufacturer's protocol, which has not been validated, offered a starting point for our department to successfully develop a protocol for this type of patient.

Authors listed for this abstract reported no relevant financial disclosures.

2123

Physician dictation times before and after implementation of Syngo Workflow and Nuance. Hali E. Priest, Abigail S. Grancorvitz, BS, CNMT, Carlyn M. Johnson, MSEd, CNMT; Nuclear Medicine, Marshfield Medical Center, Marshfield, WI, USA. (4030)

Objectives: The Joint Commission (TJC) utilizes physician dictation times as a quality metric for comparing healthcare organizations. To better facilitate this metric, the Marshfield Clinic implemented Nuance, a voice recognition system along with syngo Workflow (sWF), a program used to manage workflow in a radiology department, to track procedures, enable physician dictation of patient reports, and eventually uploads finalized reports to Combined Medical Records (CMR); without this process the patient reports would not be visible to referring physicians. This study analyzes the time it takes from the completion of a nuclear medicine procedure to physician report upload to CMR before and after the implementation of syngo WorkFlow and Nuance.
Methods: Two hundred -three patient request end times and physician dictated times were gathered 13 weeks before and 13 weeks after the go live date for sWF and Nuance. The difference between the end times and dictated times was documented and averaged for each time period. Minimum, maximum, and average standard deviation values were also calculated and documented. It is important to note that data was not analyzed four days before and twelve days after the go live date of sWF due to the WannaCry Crisis that occurred during that time period at the Marshfield Medical Center.
Results: Before sWF and Nuance were implemented, the average patient turnaround time was 72 minutes with a minimum time of 2 minutes, a maximum time of 600 minutes, and an average standard deviation of ±103 minutes. After implementation, the average time is 101 minutes with a minimum time of 7 minutes, a maximum time of 534 minutes, and an average standard deviation of ±95 minutes.
Conclusion: Theoretically, sWF and Nuance should decrease the patient report turnover rate, however, this is not currently being witnessed at our facility. It is presumed that overtime, once the physicians get more comfortable with the program, sWF and Nuance should indeed minimize the patient report turnaround times.

Authors listed for this abstract reported no relevant financial disclosures.

2124

Assessment of I-123radioiodine percent uptake measurements based on thyroid phantom insert positions for goiter and non-goiter patients in nuclear medicine. Ryann M. Hall, B.S.; Nuclear Medicine Technology, Indiana University Purdue University-Indianapolis, Indianapolis, IN, USA. (4036)

Objectives: The purpose of this research is to assess whether or not patients' 24-hour radioiodine uptake (RAIU) is affected when ^{123}I capsules are measured in the non-goiter insert position of the thyroid phantom for goiter patients, and in the goiter insert position of the thyroid phantom for non-goiter patients.
Materials and Methods: Data was collected prospectively with a sample size of 12 patients. Patients were classified as goiter (>25g) or non-goiter <25g) based off their dictated thyroid gland weight. Each ^{123}I dose and background were measured using a thyroid uptake probe centered 25 cm above a Lucite thyroid neck phantom in both the goiter and non-goiter insert positions. ^{123}I capsules were administered orally. Patients returned 24 hours later for uptake calculations. Goiter and non-goiter 24-hour RAIU calculations, as well as goiter and non-goiter therapy doses were statistically compared using a paired, two-sample for means t-test with an alpha of 0.05.
Results: Placing the thyroid phantom insert in the non-goiter position and obtaining measurements for goiter patients resulted in a p-value < 0.05. With the thyroid phantom in the goiter position for non-goiter patients, p-value >0.05. Two-sample for means t-test for the therapy doses produced a p-value less than 0.05 for goiter therapy doses, p > 0.05 for non-goiter therapy doses.
Conclusion: There was a significant increase for goiter patients' 24-hour RAIU when ^{123}I doses were measured in the non-goiter insert position during the uptake portion of the exam, but not for non-goiter patients' 24-hour RAIU when their uptake was measured in the goiter position. Using the non-goiter 24-hour RAIU percentage to calculate therapy doses for goiter patients leads to the administration of a higher ^{131}I dose.

Authors listed for this abstract reported no relevant financial disclosures.

2125

Ra-223-dichloride therapy in metastatic castration-resistant prostate cancer. How often is the therapy regimen discontinued early and why? Ashley A. Surran; Lifespan/ Rhode Island Hosptial School of Medical, Providence, RI, USA. (4042)

Objectives: The purpose of this retrospective review is to evaluate the frequency with which patients being treated with Ra-223-dichloride therapy for castration-resistant prostate cancer (mCRCP) with bone metastases at our institution do not complete the full 6-dose course of therapy and the reasons for the discontinuation. The data obtained will be helpful in identifying patients who are the best candidates for this therapy and will help suggest ways to increase completion rates of Ra-223 therapy in the future.
Methods: Pertinent clinical information was reviewed on all 62 patients who began Ra-223 dichloride therapy at our institution between 01/2013 and the present time, including all patients who had either completed therapy or permanently discontinued therapy by the end of 2017. For patients who had discontinued therapy prior to receiving all 6 doses, we reviewed information in the electronic medical record or sent a survey to the referring physician to ascertain why the therapy was discontinued.
Results: Only 30/62 patients (48.4%) completed the full 6 dose therapy regimen. The 32 patients who did not complete the full regimen were grouped into the following reasons for discontinuation based on the review of the medical record: A) disease progression; B) non-prostate related illness; C) side effects of treatment (other than marrow suppression); D) decreasing blood counts; E) perceived absence of benefit of Ra-223 therapy; and F) Other. Adequate information regarding reasons for discontinuing Ra-223 therapy could not be obtained in five patients. Of the 27 patients who did not complete their treatment regimen and had adequate clinical information to evaluate reasons for discontinuation, 14 (52%) discontinued due to disease progression; 3 (11%) due to non-related illness; 2 (7%) because of non-hematologic side effects of the treatment; 5 (19%) due to dropping blood counts; and 3 (11%) due to lack of perceived benefit of the treatment.
Conclusions: Only 48.4% of patients who began Ra-223 completed the full 6 dose regimen and of the 51.6% that did not, 52% stopped early due to disease progression. Hematologic and non-hematologic side effects accounted for only 26% of early discontinuations. We hypothesize that starting Ra-223 Dichloride earlier in the treatment plan for patients with mCRPC may increase the number of patients completing and benefitting from the treatment.

Authors listed for this abstract reported no relevant financial disclosures.

2126

Initial Experience: An In-House Look at the Comparison Between a Digital Whiteboard to the Traditional Patient Tracking System. Nicholas A. Dunn; Saint Louis University, Saint Louis, MO, USA. (4045)

Objectives: Patient tracking and throughput are important for quality patient care. The current system tracks patients within the hospital and ancillary departments. Nuclear medicine technologists and physicians in the St. Louis area have reported dissatisfaction with the current patient tracking systems being used in the hospital(s) in which they work. The tracking system that was used shows when the patient is registering, being transported or in an imaging department, using a manual whiteboard located in the department. Physicians at our institution interpret exams for multiple hospitals and better patient tracking may assist in efficiency and cost savings. The purpose of this study is to design a more user-friendly and more detailed patient tracking system. The new system was built, with assistance from our facility PACs staff. PACs is the acronym for Picture Archiving and Communication System, which functions to acquire, store, transmit, and display digital images and their associated text. to convey the same information staff would find on a manual whiteboard in a Nuclear Medicine Department, displaying the current status of all patients including common items such as exam, time point within exam, uptake times, imaging, study completion and resident report draft completion.
Methods: A digital whiteboard was designed and created for the Nuclear Medicine department at Saint Louis University Hospital. Both the digital whiteboard as well as the manual whiteboard tracking systems were used and logs were kept comparing physician and technologist phone calls, time spent determining patient status and lost time from extra travel of physicians. Surveys were also distributed to the 5 physicians and 5 technologists. These surveys included 9 questions about the user-friendliness of the new tracking system and its benefits to the department compared to the manual whiteboard tracking system.
Results: The preliminary survey results showed there was an increase in overall satisfaction of the user-friendly digital whiteboard compared to the manual whiteboard patient tracking system. Physicians have reported that they are traveling less between hospitals to review patient studies. Technologists responded with decreased time answering patient exam status questions. Preliminary results also show that since the digital whiteboard was designed and created in-house, it can be customized to fit in any department with specific needs, without incurring additional cost.
Conclusions: Although the preliminary survey results show the digital whiteboard was beneficial to the physicians and technologists at Saint Louis University Hospital, more research needs to be done on a digital whiteboard to see how it works for other hospitals or departments.

Authors listed for this abstract reported no relevant financial disclosures.

2127

Fasting and Warming Prior to Molecular Breast Imaging in Clinical Practice Environment. Alyssa P. Drake, 55094[1], Tiffinee Swanson[2], Lacey R. Ellingson[3], Thuy T. Tran[4], Jennifer Geske[5], Matt Johnson[5], Michael K. O'Connor, PhD[6], Carrie B. Hruska, PhD[3]; [1]Mayo Clinic School of Health Sciences, Eau Claire, WI, USA, [2]Rochester, MN, USA, [3]Mayo Clinic, Rochester, MN, USA, [4]Mayo Clinic, Rosemount, MN, USA, [5]Mayo Clinic School of Health Sciences, Rochester, MN, USA, [6]Radiology, Mayo Clinic, Rochester, MN, USA. (4052)

Objectives: Molecular Breast Imaging (MBI), performed with 300 MBq Tc-99m sestamibi and a dedicated gamma camera, has shown utility in detecting breast cancer occult on mammography due to dense breast tissue (Rhodes et al., AJR 2015; Shermis et al., AJR 2016). Strategies to improve uptake of sestamibi in breast tissue and allow for further reduction in the administered activity have been explored. Patient preparation including fasting prior to the exam and warming of the breasts were shown to increase breast uptake of Tc-99m sestamibi in a controlled research setting (O'Connor et al., JNMT 2015). Pre-examination instructions including a 3- hour fast and warming of the upper torso via a warm blanket prior to injection have been implemented at our institution, but validation in the clinical setting is lacking. Our objective was to assess patient compliance with pre-examination instructions and to evaluate whether image count density, a surrogate measure of breast uptake, was improved with fasting and warming in the clinical environment.

Methods: Under an IRB-approved and HIPAA compliant protocol, we performed a retrospective review of patients who had an MBI examination at Mayo Clinic Rochester between July 2016 and October 2017 (N=1428). Patients were excluded from analysis if dose infiltration was suspected (N=13), if residual activity was not recorded (N=7), if fasting or warming status was not known (N=10), or if the prescribed activity was higher than 300 MBq (N=1), leaving 1397 available for analysis. A subset of 100 subjects was randomly selected for count density analysis, including four groups of 25 subjects with the following preparation statuses: fasting and warmed, fasting and not warmed, not fasting and warmed, not fasting and not warmed. Count density of the breast tissue was measured by drawing regions of interest within an area of normal (non-lesion) breast parenchyma on the right mediolateral oblique view of the lower detector, avoiding the pectoral muscle and edges of the breast. Patients with breast implants were excluded from count density analysis (N=2). Count density was expressed as cts/cm^2/MBq of administered activity. Characteristics between groups were compared by either chi-squared test or Fisher's exact test and by one-way ANOVA or Kruskal-Wallis test.

Results: Of 1397 patients, the number and proportion of patients with each status was 1133 (81%) fasting and warmed, 54 (3.9%) fasting and not warmed, 185 (13%) not fasting and warmed, 25 (1.8%) not fasting and not warmed. Overall, 1187 of 1397 (85%) subjects reported compliance with fasting instructions and 1318 of 1397 (94%) used a warm blanket prior to injection. No significant differences were observed between groups in regard to age, menopausal status, and exogenous hormone use (all p>0.36). There was no significant difference (p=0.75) in count density between patients who fasted (average = 7.5 counts/cm2/MBq) vs. those who did not fast (average = 7.3 counts/cm2/MBq). There was also no difference in count density between the non-warmed (7.1 counts/cm2/MBq) and warmed (7.7 counts/cm2/MBq) patients (p=0.26).

Conclusions: Our results showed a high compliance rate with fasting and warming instructions, however, findings suggest that a 3-hour fast and warming of the upper torso, does not result in significant improvements in image count density in the clinical environment. These findings are in contrast to count density improvements observed in a controlled research study as a function of fasting or warming, where serial examinations were assessed within the same patient. A limitation of the current analysis conducted in clinical practice is that fasting status is patient-reported and time spent warming is patient-directed, which may result in higher variability in fasting and warming protocol. Additional research using a larger sample size is needed to confirm these findings and determine if count density from fasting and warming can be replicated in the clinical setting.

Authors listed for this abstract reported no relevant financial disclosures.

2128

Radiolocalization of Unusual Soft Tissue and Bone Lesions for Intraoperative Localization: Technical factors, localization quality, patient safety, success rates and spectrum of applications. Andi Wallig[1], Nicole Fischer[2], James Long, CNMT[3], Tiffinee Swanson[2], Brendan McMenomy[1], Jason R. Young[4]; [1]Mayo Clinic School of Health Sciences, Rochester, MN, USA, [2]Rochester, MN, USA, [3]Mayo Clinic, Rochester, MN, USA, [4]Maricopa Medical Center, Phoenix, AZ, USA. (4053)

Objectives: The goal of this study was to retrospectively analyze the use of Tc-99m microaggregated albumin (MAA) for intraoperative localization of non-standard soft-tissue and bone lesions (not pulmonary or breast). We sought to describe the types of lesions localized, technique, patient safety, scintigraphic image quality and localization success based on experience of a single tertiary referral center.

Methods: An IRB compliant, retrospective review of patients that underwent non-standard soft-tissue and bone radiotracer localization using ^{99m}Tc-MAA prior to surgical excision between September 2010 and September 2017 was performed. The following data was recorded: patient demographics, lesion location, lesion size, radiotracer injection technique, radiotracer injection complications, scintigraphy technique, quality of localization by radiologist consensus, intraoperative time, lesion identification in surgery, and pathological diagnosis.

Results: A total of 22 non-standard radiolocalization exams were identified. Anatomic sites of lesions included rib (7), lymph node (4), abdominal wall (3), mesenteric (3), retroperitoneal (2), chest wall (1), anterior mediastinum (1) and iliac bone (1). The average lesion size was 14mm (range 5-23mm). Eighteen (82%) radiotracer injections used CT guidance and 4 (18%) used ultrasound guidance. The mean activity of ^{99m}Tc MAA administered was 11.8MBq (range 11.1-18.5 MBq). The needle gauge used most often for injection was 22 (range 17-25 gauge). Injections were made within soft tissue lesions, and immediately overlying bone lesions. No injection complications were reported. The average length of surgery was 140 minutes (range 23- 517 minutes). Surgical excision of the localized lesion was combined with other surgical procedures at times. All images were acquired on a 128x128 matrix immediately after radiotracer injection; 18 (82%) cases used LEHR collimation, 3 (13.5%) cases used MEGP collimation, and 1 (4.5%) case used LEGP collimation. The mean number of counts acquired during anterior imaging was 81,232 (range 22,068-210,508) with an average acquisition time of 1.43 minutes (range 0.57-3.44 min). The mean number of counts acquired during lateral imaging was 120,300 (range 50,928-222,593) with an average acquisition time of 1.34 minutes (range 0.34-4.11 min). By scintigraphy, all the cases demonstrated focal tracer activity at the lesion site; nineteen cases (86%) had no surrounding activity while two cases (9%) had mild and one case (5%) had moderate surrounding activity. Three cases had mild to moderate tracer activity in solitary draining lymph nodes but these did not seem to interfere with surgical localization. The lesion was identified with a gamma probe during surgery in 100% of cases. All but two cases (20/22) had samples sent to pathology. Of those samples sent to pathology, 100% were identified and given a diagnosis. Of all the localized lesions, 41% (9/22) received the diagnosis of metastatic disease.

Conclusions: Radiolocalization of non-standard lesions is a safe and effective technique that can guide surgical removal of lesions located in sites that are difficult to identify intraoperatively such as rib (figure 1a), mesentery (figure 1b) and abdominal wall (figure 1c). Differences in injection and imaging parameters had little effect on the efficacy of radio-localization. Therefore, imaging can be tailored to accommodate patient needs, physician preference, or clinical workflow.

Figure 1

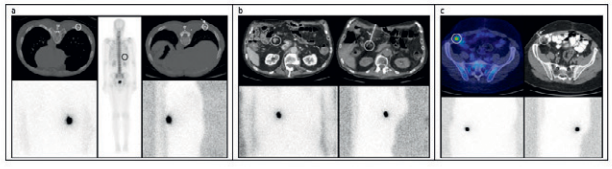

Authors listed for this abstract reported no relevant financial disclosures.

2129

Review of myocardial perfusion confidence scores in supine and prone imaging to ameliorate protocol standards. Haley Biros, Thomas Holly, Scott Leonard, MS, CNMT, Preeti Kansal, Lisa Riehle, Gary L. Dillehay, MD, FACNM, FACR, FSNMMI; Northwestern Memorial Hospital, Chicago, IL, USA. (4065)

Objectives: Standard patient positioning for SPECT myocardial perfusion imaging (MPI) studies is supine. The total scan time if there is limited movement is ~20 minutes. When the patient is able, an additional set of images in the prone position (~8 minutes) is routinely performed, which can help with soft tissue attenuation and subdiaphragmatic tracer activity. Anecdotally, some of our physicians think the image quality or the ability to interpret a study as normal or abnormal is better with the prone images, despite the shorter imaging time. However, this has not been systematically studied. We hypothesized that readers would have greater confidence (more likely to read a study as definitely normal or definitely abnormal) reading prone studies than supine studies.
Methods: A total of 148 patients clinically referred for MPI who had undergone both supine and prone acquisitions were studied. Two nuclear cardiologists reviewed only the stress images (both supine and prone) for each patient. A confidence score was given to each supine and prone processed study: 5=Definitely Normal, 4=Probably Normal, 3=Equivocal, 2=Probably Abnormal, 1=Definitely Abnormal. The studies were then checked for their actual clinical interpretation to see if they were categorized as normal or abnormal. Differences in the score were analyzed using a paired t-test with a p-value of <0.05 being significant.
Results: Of the 148 studies, 119 were identified as normal and 29 abnormal. The average supine and prone confidence scores are given below. Abnormal Study Averages: Normal Study Averages: Prone Supine Prone Supine 2.04 1.96 4.39 3.95 p = 0.7 p = 0.0001.
Conclusions: Reading physicians were more confident in interpreting normal studies acquired in the prone position as normal, than in the supine position. Patient position did not affect the confidence in reading abnormal studies. Further research may identify patients who should be preferentially imaged in the prone position to minimize scan time and improve clinical interpretive confidence.

Authors listed for this abstract reported no relevant financial disclosures.

2130

Residual activity analysis of Tc-99m MAA administered interarterially in patients preparing for radioembolization. Breanne Hemann[1], Vanessa L. Gates, MS[2], Lisa Riehle[1], Gary L. Dillehay, MD, FACNM, FACR, FSNMMI[1]; [1]Northwestern Memorial Hospital, Chicago, IL, USA, [2]Department of Radiology, Northwestern Memorial Hospital, Chicago, IL, USA. (4068)

Objectives: Future radioembolization dosimetry using Yttrium-90 may require knowing the amount of activity of Tc-99m macro aggregated albumin (MAA) used for the diagnostic SPECT/CT image. The objective of this study is to determine the administered activity of MAA by analyzing the initial assays and final residual assays of the syringe used to infuse the MAA.
Methods: Kits of MAA were transferred to a 3-mL syringe with a leur-lock attached. Prior to administration to the patient, the syringe was assayed in a dose calibrator. Once the initial activity and assay time were documented, the dose was transported to the interventional suite and administered to the patient via a micro catheter placed in a tumor supplying hepatic artery. Following administration, the syringe was assayed for residual activity. All activities were decayed to the time of administration. The percent residual was defined as the decayed residual divided by the decayed administered activity, multiplied by 100. Analysis included linear regression between the percent residual and the time range between labeling and administration. The effect of catheter type or length and the physician administering the MAA was also analyzed.
Results: Twenty-seven MAA administrations were evaluated. The mean administered activity of MAA was 66 ± 10 MBq (43-85 MBq) with the mean percent residual being 17 ± 11% (2-39%). Linear regression analysis did not show any statistically significant relationship between the time between kit preparation and administration. Analysis of catheter type was limited due to lack of variance in type used. When analyzing variance in administration technique used by different physicians, a bias was noted.
Conclusion: These results show that there is residual present, however there is no relationship between the time of labeling to time of administration and the residual amount. Occasionally, the residual was greater than 20% indicating a need for future research to determine the minimal amount of MAA needed for quantitative SPECT/CT imaging.

Authors listed for this abstract reported no relevant financial disclosures.

2131

An evaluation of qualities of nuclear medicine technology program graduates and employability. Sarah S. Brosmer; Health Professions Programs, Indiana University School of Medicine, Indianapolis, IN, USA. (4058)

Objectives: The purpose of this research was to evaluate the association between qualities of nuclear medicine technology graduates and programs and employability.
Methods: Using the REDCap online software, a questionnaire was created with questions regarding initial employment, graduate qualities and program qualities. An employability scale was created from the initial employment questions. The REDCap system used the email list of NMTCB certificants who passed the exam in the last five years to generate the invitations wit individualized embedded links to the survey. All surveys completely filled out by the respondents were used for this research. Using the quantified qualities answers and the employability scores, the individual qualities were broken into four subgroups: optimally employable, less than optimally employable, averagely employable, and unemployable. An ANOVA test was performed to test the statistical significance of the individual quality. The mean, standard deviation, and counts were calculated for the qualities with a p-value less than 0.05, which is considered significant.
Results: 3,930 surveys were distributed. 885(22.5%) respondents returned completed surveys. Of the 10 qualities evaluated in the survey, six of them had statistically significant findings. The following qualities had p-values below 0.05: number of board attempts (0.0002), number of clinical sites (0.03), GPA (0.03), number of clinical clock hours (0.006), nuclear medicine programs in a 100-mile radius (0.001), and highest level of education (0.03).
Conclusions: Nuclear medicine technology programs and students in the program should focus on the qualities of GPA, clinical sites, and clinical clock hours to ensure student success in obtaining employment. Students should make an extra effort to limit the number of board attempts and increase their level of education.

Authors listed for this abstract reported no relevant financial disclosures.

TS22: Student Tech Papers II

Moderator: Jay Smith, BSRS, CNMT, ARRT, RT(R)(N)
Co-Moderator: Angela Macci-Byers, Ed.D., MPM, RT(N), CNMT, FSNMMI-TS

2139

Gallium-68 Dotatate. Garrick L. Morgan, B.S. NMT[1,2], Ann M. Voslar, MHA/Ed, BS-Nuclear M[3], Beth A. Bates, CNMT[4]; [1]Nuclear Medicine, Froedtert Memorial Lutheran Hospital, Milwaukee, WI, USA, [2]University of Wisconsin - La Crosse, La Crosse, WI, USA, [3]NM/PET, Froedtert Memorial Lutheran Hospital, Milwaukee, WI, USA, [4]Hartford, WI, USA. (4025)

Objectives: Neuroendocrine tumors (NETs) can hide within the body due to their minimal side effects and ability to mirror the side effects of other common diseases. Patients battling with NETs often undergo multiple diagnostic procedures before a true diagnosis can be found. Gallium-68 Dotatate is a positron emission tomography (PET) agent used in the detection of somatostatin receptor 2 (SSTR-2) positive neuroendocrine

tumors (NET). The purpose of this study is to introduce the positive clinical outcomes we have seen with Gallium-68 Dotatate.
Methods: In collaboration with our Nuclear Medicine physicians, several Ga-68 Dotatate studies were reviewed. 4 clinical case studies will be presented which include comparisons to I-123 MIBG, In-111 pentetreotide, and F-18 FDG.
Results: Patient 1 presented with 2 meningiomas on the right hemisphere found on FDG PET, the Ga-68 Dotatate study revealed a small en plaque meningioma on the left hemisphere which was missed on a prior MR. Patient 2 presented with a primary endobronchial carcinoid tumor with known metastatic disease. The Ga-68 Dotatate revealed axial and appendicular bone disease along with increased metastatic disease compared to F-18 FDG. Patient 3 presented with neuroendocrine pathology found in the lymphatic system during an exploratory laparotomy. Dedicated CT and In-111 Penteteotide study discovered a large mesenteric mass but no metastatic disease. The patient underwent chemo and followed up with a Ga-68 Dotatate study which was positive for metastatic disease. Patient 3 underwent surgery to remove the metastatic disease. Post resection, the Ga-68 Dotatate study found continued SSTR-2 neuroendocrine avidity. Patient 4 presented with metastatic paraganglioma and underwent an I-123 MIBG study which found 2 masses in the chest wall. Two days later a Ga-68 Dotatate study found innumerable focal uptake within the lymphatic system, liver, axial and appendicular skeleton which were not reported on the MIBG or recent CT.
Conclusion: Ga-68 Dotatate has given hope to doctors and patients who have encountered the battles of neuroendocrine tumors. Patients with somatostatin receptor 2 positive neuroendocrine tumors who receive a PET scan with Ga-68 Dotatate display an increased sensitivity and specificity of metastatic uptake when compared to F18-FDG, In-111 pentetreotide, and I-123 MIBG. With the aid of the Ga-68 Dotatate PET studies, physicians have greater confidence in evaluating patients with NETs when comparing to CT or MRI. Increased imaging sensitivity and specificity for a previously difficult disease to asses has led to faster and better outcomes for patients. Ga-68 Dotatate has been an effective tool for assessing tumor progression in response to therapies/surgeries.

Authors listed for this abstract reported no relevant financial disclosures.

2140

Comparing Standardized Uptake Values of Q.CLEAR. Kara Selk, Stacy Hampton, Ann Voslar; Nuclear Medicine Technology, Froedtert, Milwaukee, WI, USA. (4026)

Objectives: Compare and contrast standardized uptake values (SUV) of reconstructed Positron Emission Tomography/Computed Tomography (PET/CT) scans with the filter Q.CLEAR on a PET/CT system. Q.CLEAR is a full-convergence PET/CT filter with 25 iterations to increase the resolution and control low levels of noise on PET/CT scans. Q.CLEAR was produced to detect and provide more accurate SUVs for cancers with small lesions.[1] Cancers rely on SUV values to determine treatment and evaluate if the treatments are working. Lymphoma is a cancer of the lymphatic system which includes lymphatic capillaries, vessels, ducts, and lymph nodes. An average lymph node has the diameter size of 0.5-2.0 centimeters, which can be hard to detect if cancerous.[2] The purpose of this study is to compare the SUV values of a lymphoma patient's PET/CT scan and the reprocessed Q.CLEAR scan SUV.
Methods: The data collected was from 54 PET/CT scans of patients who were diagnosed with lymphoma. Each of the 54 scans was reprocessed using Q.CLEAR. Using an AW server, a region of interest (ROI) was drawn on the original PET/CT scan in an area of increased uptake. If the patient did not have any cancerous lesions, a ROI was placed in the liver to determine a sample SUV to use for this study. Each ROI was copied and pasted, in the same location, onto the scan that had been reprocessed with Q.CLEAR. The SUV_{max} from each ROI was recorded. The data was entered into excel to calculate the average between the two values and to perform a T-test to find the significance of the data.
Results: The data was divided into two groups. Group A includes all 54 patients, while group B includes the 31 patients who had small lesions, discarding the data used from the liver ROIs. Group A showed that the Q.CLEAR scans had an average SUV 0.247 higher than the original PET/CT scan. The T-test calculated was 2.253 with a p-value of 0.01. Group B had an average SUV of 0.590 higher on the Q.CLEAR scans. The T-test calculated was 1.697 with a p-value of 0.10.
Conclusion: The data that was collected from Group A showed that there was no significant difference between SUV values whether the scan was processed with Q.CLEAR or under normal PET/CT reconstruction. When discarding the data using the liver ROIs, and focusing on Group B, small cancerous lesions, the statistical significance increased by a factor of 10, making it 10 times more likely for Q.CLEAR to increase the SUV_{max} of a given lesion. The data leads to understand that Q.CLEAR has a greater probability of collecting a higher SUV in patients with smaller lesions.
References: 1. Q.CLEAR Quantitative SUV you and your Patient can Trust. (2014). GE Healthcare. http://www3.gehealthcare.com 2. Mayo Clinic Staff. (1998-2018). Lymphoma. Mayo Clinic. https://www.mayoclinic.org

Authors listed for this abstract reported no relevant financial disclosures.

2141

Discrepancy between physical and effective diameter in the Seimens Biograph mCT PET/CT. Valerie M. Carrizales[1], Ryan Warhoover, CNMT[2], Crystal Botkin, MPH, CNMT, PET[1], Sarah Frye, MBA, CNMT, PET, NCT[1], Medhat M. Osman, MD, PhD, MS[3]; [1]Department of Clinical Health Sciences, Doisy College of Health Sciences, Saint Louis University, St. Louis, MO, USA, [2]Department of Veterans Affairs St. Louis Health Care System, John Cochran Division, St. Louis, MO, USA, [3]Division of Nuclear Medicine, Saint Louis University Hospital, St Louis, MO, USA. (4034)

Objectives: In modern nuclear medicine, there is an increasing need for equipment that can accommodate larger patients. This has resulted in Positron Emission Tomography/Computed Tomography (PET/CT) scanners, which are marketed extensively for their solution to this trend. Specifically, vendors of the Siemens Biograph mCT have increased their table weight limit to 500lbs (227kg) and increased bore diameter to 780mm. However, despite the fact that larger patients can now be inserted in the PET/CT scanner, a large portion of them is often excluded in the imaged FOV due to the discrepancy between the physical (780mm) and the effective diameter of the bore (500mm). The purpose of this study is to draw attention to this discrepancy that exists between the PET/CT physical diameter acquired verses the effective diameter used in the processed PET/CT images of a single institution's Siemens Biograph mCT scanner.
Methods: The acquisition and processing parameters were reviewed for the Siemens Biograph mCT PET/CT scanner. The scanner defaults to acquire PET scans in 700mm of the 780mm physical gantry size, while the CT defaults to acquire the full 780mm. However, only the inner 500mm of the CT scan are used to reconstruct the final PET/CT processed images. The CT area between the 500mm dimensions used for processing and the 780mm gantry outer edge is excluded. Consequently, the PET area between 500mm and 700mm is also excluded in the processed images to match the smaller 500mm CT diameter. Images were then reviewed to appreciate the discrepancy.
Results: The evaluated PET/CT parameters revealed the capacity of the excluded area between 500-700mm to create a problem for larger patients who fit within the physical gantry, but whose body habitus exceeds the effective 500mm diameter. This would result in the exclusion of any body and/or limb area which lies outside of the inner 500mm. Thus, despite its acquisition, the excluded body anatomy would not be used in the processed images read by the physician.
Conclusion: After reviewing the acquisition and reconstruction parameters of the Biograph mCT, as well as PET/CT images, there is current exclusion of a considerable portion of patient anatomy, the extent and clinical impact of which has not been fully evaluated. Thus, future research should be done with the Siemens Biograph mCT, to assess any potential effects of this exclusion, and, if so, how they may be remedied. Additionally, increased awareness should be disseminated to institutions with other PET/CT scanners to determine if similar discrepancies are occurring so as to ensure that the best possible quality of care is being received by the patient.

Authors listed for this abstract reported no relevant financial disclosures.

2142

Prostate Cancer Patients and PET/CT: Comparing and Contrasting ^{18}F-FDG and^{18}F-Fluciclovine. Hailey Broska; Saint Louis University, Saint Louis, MO, USA. (4037)

Objectives: ^{18}F-Fluciclovine is a medical imaging synthetic amino acid used in detecting recurrent prostate cancer which was approved by the Food and Drug Administration (FDA) in May 2016. ^{18}F-Fluciclovine was developed to widen the use of Positron Emission Tomography (PET) imaging in the ways that ^{18}F-FDG is limited. The purpose of the study is to compare and contrast^{18}F-Fluciclovine to ^{18}F-FDG in regards to the imaging and scheduling of prostate cancer.
Methods: This retrospective study reviewed the imaging protocols for both ^{18}F-Fluciclovine and ^{18}F-FDG from a single institution. The imaging protocols were reviewed to educate technologists about the differences and how the flow of patients may differ between the two radiopharmaceuticals.
Results: The protocols for imaging and scheduling at this single institution are significantly different between ^{18}F-FDG and ^{18}F-Fluciclovine for patients with prostate cancer. ^{18}F-FDG is used for staging and restaging all cancers for both genders and all ages because it is a radioactive glucose. ^{18}F-FDG has an intense uptake in the brain, kidneys, and bladder. ^{18}F-Fluciclovine has normal uptake in the liver, pancreas, with minimal kidney clearance. ^{18}F-Fluciclovine is used for staging male prostate cancer patients with biochemical recurrence. The dose for ^{18}F-Fluciclovine is 10 mCi for all patients rather than weight based (0.14 mCi/kg) like ^{18}F-FDG. ^{18}F-FDG has an uptake time of an hour and a half before imaging, whereas ^{18}F-Fluciclovine has an uptake time of four minutes before imaging. Imaging time for both radiopharmaceuticals is about 30-45 minutes. At our institution, the schedule allows for 1-2 ^{18}F-Fluciclovine patients two days a week because they are several hours away from the radiopharmacy. The department can schedule ^{18}F-FDG patients every 45 minutes, performing 10-12 studies per day.
Conclusion: Our study showed that for this single institution, scheduling is more difficult for ^{18}F-Fluciclovine since their radiopharmacy is several hours away. This department can perform more studies per day with ^{18}F-FDG. If another institution is closer to a radiopharmacy that provides ^{18}F-Fluciclovine, they may be able to accommodate more patients per day. ^{18}F-Fluciclovine patients can be scheduled every 40-45 minutes without the hour and a half uptake time.

Authors listed for this abstract reported no relevant financial disclosures.

2143

MR based attenuation correction and μ map production in PET/MR breast imaging. Amy R. Sulikowski, Scott Leonard, MS, CNMT, Michelle Gruchot, Lisa Riehle, Gary L. Dillehay, MD, FACNM, FACR, FSNMMI; Northwestern Memorial Hospital, Chicago, IL, USA. (4039)

Objectives: Attenuation correction (AC) is necessary for data quantification in PET imaging. PET reconstructions without AC appear to show areas of low attenuation (patient surface and lungs) as having increased uptake. A transmission-based AC map (μ-map), obtained from rotating rod sources or through CT, is created and utilized during the PET emission data reconstruction. Traditional methods for μ-map creation are unavailable in PET/MR imaging, therefore, MR imaging sequences (DIXON) are utilized to generate the required μ-map. Voxel intensities in an MR image decrease as their distance from the radio frequency coil increases. This can lead to the creation of incomplete μ-maps. Initial investigation of breast PET/MR imaging with a Siemens Biograph mMR has inspired this discussion.
Methods: Diagnostic MR imaging of the breasts is generally performed with only a dedicated breast coil. A volunteer was initially imaged utilizing a DIXON sequence with only a breast coil. A second scan was then completed utilizing both the breast coil and a surface coil on the subject's back. To simulate lesions in a patient, conical 1.5 mL vials containing a clinically relevant concentration of F-18 FDG were placed in the axillary and mediastinal regions of the volunteer. Standardized uptake values (SUVs) were obtained from regions of interest drawn around the axillary and mediastinal sources to compare the effects on PET AC images derived from an incomplete μ-map (breast coil only) versus a complete μ-map (breast and surface coils).
Results: The DIXON sequence with the breast coil alone generated an incomplete μ-map, as anticipated. SUVs of the axillary source increased from 2.08 to 10.48 when a complete μ-map was generated with the addition of a surface coil. SUVs of the mediastinal source increased from 1.30 to 3.30.
Conclusions: In PET/MR imaging, care must be taken to ensure that the DIXON sequence has adequate MR signal to generate complete μ-maps. Incomplete μ-maps result in PET reconstructions having uncompensated PET counting losses, inaccurate quantification, and underestimated SUVs.

Authors listed for this abstract reported no relevant financial disclosures.

2144

A Retrospective Study Comparing Computed Tomography (CT) and ^{68}Ga - DOTATATE PET/CT in Small Bowel Carcinoid Tumors. Breanna M. Guttmacher, Ann Packard, Hannah R. Monahan, M.D., Nicole Fischer, CNMT, James Long, CNMT, PET, Ayse T. Kendi, M.D., Stephen Broski, MD; Mayo Clinic, Rochester, MN, USA. (4051)

Background: Neuroendocrine tumors (NETs) are a rare type of neoplasm which arise from the nervous and endocrine system and are characterized by an overexpression of somatostatin receptors (SSTRs). Carcinoid tumors are a subset of NETs that are often found in the gastrointestinal tract, most commonly the small bowel. When found early, these tumors are usually asymptomatic and detected incidentally on an exam or procedure performed for a different reason. However, if the tumor metastasizes to the liver, the patient may experience carcinoid syndrome. Carcinoid syndrome is caused by the release of serotonin and other hormones by the tumor that can result in difficulty breathing, abdominal pain, a fast heart rate, and redness in the face and neck. Imaging carcinoid tumors has historically relied upon a combination of CT and ^{111}In-pentetreotide scintigraphy, the latter of which exploits the tendency of carcinoid tumors to overexpress SSTRs. Recently, the FDA has approved the use of ^{68}Ga - DOTATATE PET/CT in the evaluation of NETs, which also functions by binding to SSTRs, namely the SSTR2 subtype. Therefore, the purpose of this study was to evaluate the clinical impact of ^{68}Ga - DOTATATE PET/CT compared to conventional imaging with CT in patients with small bowel carcinoid tumors.
Methods: This IRB, HIPPA compliant, retrospective study included patients who underwent ^{68}Ga - DOTATATE PET/CT and contrast enhanced CT for imaging of small bowel carcinoid tumors from November 2016 to July 2017. Any patient who had not had a CT within 3 months of the ^{68}Ga - DOTATATE PET/CT and/or any under the age of 18 years old were excluded from this study. Imaging reports were searched for the presence or absence of metastatic disease in mesenteric, retroperitoneal, iliac chain and upper abdominal lymph nodes, peritoneum, liver, bone, and sites outside of the abdomen and pelvis. Metastatic patterns between ^{68}Ga - DOTATATE PET/CT and CT were then compared.
Results: Twenty-nine patients with a primary small bowel carcinoid tumor (mean age 59 ±8 years, range 35-76; 15 M and 14 F) who had both a CT and ^{68}Ga - DOTATATE PET/CT imaging within 3 months were included in this study. Twenty of 29 (70%) patients had metastatic mesenteric adenopathy on ^{68}Ga - DOTATATE versus 13/29 (44%) on CT. Eight of 29 (28%) patients had metastatic retroperitoneal lymph node adenopathy on ^{68}Ga - DOTATATE versus 4/29 (14%) on CT. ^{68}Ga - DOTATATE PET/CT demonstrated iliac chain lymph node metastases in 5/29 (17%) patients versus 2/29 (7%) on CT. Two of 29 (7%) patients had upper abdominal lymph nodes metastases on CT compared to 8/29 (28%) on ^{68}Ga - DOTATATE PET/CT. Ten of 29 (35%) patients had peritoneal metastatic disease on ^{68}Ga - DOTATATE versus 2/29 (7%) on CT. ^{68}Ga - DOTATATE PET/CT demonstrated liver metastases in 18/29 (62%) patients versus 13/29 (45%) on CT. Six of 29 (21%) patients had bone metastasis on ^{68}Ga - DOTATATE versus 2/29 (7%) on CT. ^{68}Ga - DOTATATE PET/CT showed evidence of distant metastatic disease in 20/29 (70%) patients including distant lymph nodes, cardiac, and pleural lesions. Overall, metastatic disease was identified in 27/29 (93%) patients with ^{68}Ga - DOTATATE PET/CT, compared with only 14/29 (48%) with CT.
Conclusions: In patients with small bowel carcinoid tumors, ^{68}Ga-DOTATATE PET/CT detected more metastases than contrast enhanced CT, resulting in a considerable clinical impact. The incidence of peritoneal

metastatic disease is also higher than previously reported, and better diagnosed by ^{68}Ga- DOTATATE PET/CT than conventional CT.

Authors listed for this abstract reported no relevant financial disclosures.

2145

Molecular Imaging Evaluation of Phosphaturic Mesenchymal Tumor-Induced Osteomalacia. Claire L. Paul[1], Stephen Broski, MD[2], Nicole Fischer[3], James Long, CNMT[2]; [1]Mayo Clinic School of Health Sciences, Rochester, MN, USA, [2]Mayo Clinic, Rochester, MN, USA, [3]Rochester, MN, USA. (4054)

Background: Tumor-induced osteomalacia (TIO), also called oncogenic osteomalacia, is a rare condition characterized by renal phosphate wasting and osteomalacia due to the production of fibroblast growth factor-23 (FGF-23) by phosphaturic mesenchymal tumors (PMTs). These tumors can occur in bone or soft tissue anywhere in the body and are often small and slow growing. Because of this, they are notoriously difficult to detect, but localizing them is critical, as surgical resection is curative. A variety of nuclear medicine techniques have been employed in PMT evaluation over the years, evolving from planar scintigraphy to PET/CT. The primary aim of this study was to evaluate the role of molecular imaging in PMT localization. Secondary aims include semiquantitative analysis of PET/CT examinations and laboratory value correlation.
Methods: This IRB-compliant, retrospective study included patients who underwent molecular imaging evaluation for pathologically-confirmed PMTs at our institution between April 2001 to July 2017. Images were evaluated for the presence of increased radiotracer uptake in PMTs. Planar and SPECT ^{99m}Tcsestamibi and ^{67}Ga-Citrate examinations were considered positive if there was uptake above adjacent background bone or soft tissue activity. ^{18}F-FDG PET was considered positive if lesion activity exceeded mediastinal blood pool, while ^{111}In-Octreoscan and ^{68}Ga-DOTATATE PET were considered positive for a Krenning score of ≥ 2. A chart review was performed for clinical and laboratory correlation.
Results: 23 patients (mean age 59.7 years (range 34-78), 15 M, 8 F) were included and a combined 29 nuclear medicine exams were evaluated (nine ^{99m}Tc-Sestamibi scans, four ^{111}In-Octreoscan scans, 13 ^{18}F-FDG PET/CT scans, two ^{68}Ga-DOTATATE PET/CT scans, and one ^{67}Ga-Citrate scan). There were eight bone lesions, 7/8 of which were entirely intraosseous, and one that demonstrated an extraosseous component. There were 15 soft tissue lesions. Lesion locations included 11 (47.8%) in the lower extremity, three (13%) in the pelvis, three (13%) in the spine, three (13%) in the upper extremity, two (8.7%) in the thoracic trunk soft tissues, and one (4.35%) in the head and neck region. The mean maximal lesion diameter was 3.1 ± 1.9 cm (range 1.1 - 9.8 cm). Exam results were recorded as follows: ^{18}F-FDG PET/CT (11/13 positive), ^{99m}Tc-Sestamibi (8/9 positive), ^{111}In-Octreoscan (2/4 positive), ^{68}Ga-DOTATATE PET/CT (2/2 positive), and ^{67}Ga-Citrate (1/1 negative). The average SUV_{max} of ^{18}F-FDG PET and ^{68}Ga-DOTATATE PET was 4.1 ±2.5 (range 1.5 - 10.8) and 14.1 ± 6.7 (range 9.3 - 18.8), respectively. Fourteen of 20 patients had abnormal phosphorus levels, with a mean phosphorus of 2.1 ± 0.99 (range 1.1-5.5). Thirteen of 14 patients had elevated total alkaline phosphatase (AP) levels, with average total AP of 210.93 ± 85.81 (range 63-348). In patients with a bone-specific AP fraction, 7/9 were elevated, with an average level of 53.11 ± 34.13 (range 11-104). 8/13 patients had elevated parathyroid hormone levels 120.69 ± 123.25 (range 27-462), while 8/10 patients had increased serum FGF23 levels (2396.5 ± 6368.71, range undetectable- 20,500).
Conclusions: Given their variable location and small size, whole body imaging is necessary for PMT localization. PMTs demonstrate variable uptake of several radioisotopes, and thus functional molecular techniques have an important role in the diagnostic algorithm. Based on our results and available data in the literature, PET/CT, and in particular ^{68}Ga-DOTATATE PET/CT, may become the preferred examination for PMT localization.

Authors listed for this abstract reported no relevant financial disclosures.

2146

Evaluation of PET/CT acquisition parameters in Ga-68 Dotatate imaging. Tehreem Hussain, B.A Psychology[1], Katie Tucker[2], Scott Leonard, MS, CNMT[3], Lisa Riehle[3], Gary L. Dillehay, MD, FACNM, FACR, FSNMMI[3]; [1]Nuclear Medicine, Northwestern Memorial Hospital, Villa Park, IL, USA, [2]Northwestern Memorial Hospital, Naperville, IL, USA, [3]Northwestern Memorial Hospital, Chicago, IL, USA. (4057)

Objectives: Neuroendocrine tumors (NETs) are slow growing tumors that are difficult to diagnose due to their nonspecific symptoms. Ga-68 Dotatate is a radiolabeled DOTA-conjugated somatostatin analogue that binds to somatostatin receptors and is overexpressed in NETs. Ga-68 Dotatate PET/CT scans are valuable in the detection and staging of neuroendocrine tumors. The objective of this study is to evaluate the impact of reduced acquisition time on image quality and lesion detection for Ga-68 Dotatate scans.
Methods: Currently, a standard 5min/bed image is acquired for all patients. For this study, an additional 5 minute list-mode (single bed) acquisition was performed on each patient. The list-mode data for each patient was then reconstructed into 3, 4 and 5 min/bed static images. Overall image quality, lesion detectability and interpretation confidence for each time point was scored on a 1-5 scale. The SUVs of at least two lesions per patient were analyzed for all three reconstructions.
Results: With the limited data available, 3 min/bed reconstructions appear to contain more noise, as anticipated. Visual analysis suggested all relevant lesions could be identified in the 3, 4 and 5 min/bed reconstructed data.
Conclusions: Despite the limited data available reduction of acquisition time per bed appears to not adversely affect lesion detectability (despite increased image noise). Inclusion of up to 15 additional data sets may allow stratification of acquisition parameters based on patient BMI.

Authors listed for this abstract reported no relevant financial disclosures.

2147

^{11}C-Choline PET for Evaluation of Renal Tubular Function. Alyssa L. Splan[1], MaKenna Borofka[1], Kevin Casper, M.D.[2], Nicole Fischer, C.N.M.T.[2], Tina Gunderson, M.S.[2], Andrew Rule, M.D.[2], John Lieske, M.D.[2], Michael Romero, Ph.D.[2], Christopher Harker Hunt, MD[2], Timothy R. DeGrado, PhD[2]; [1]Mayo Clinic School of Health Sciences, Rochester, MN, USA, [2]Mayo Clinic, Rochester, MN, USA. (4063)

Purpose: The aim of this study is to evaluate renal cortical choline activity on ^{11}C-Choline PET/CT as a potential noninvasive biomarker for renal tubular function.
Method and Materials: An IRB approved retrospective chart review was performed of 1602 consecutive male patients that had ^{11}C-Choline PET/CT according to standard protocol for prostate cancer between 1/3/2017 and 10/30/2017. Standard protocol includes imaging from mid thighs to orbits beginning 5 minutes after injection of the radiotracer. All scans were reconstructed with standard 3D OSEM. Patients with renal function data in their medical record within 6 months of the PET/CT testing that included serum creatinine and eGFR (Modification of Diet in Renal Disease equation) and a urinalysis with predicted 24 hour protein were screened. Those with serum creatinine of 0.8-1.3 mg/dL, eGFR >60 mL/min/1.73m^2, and a predicted 24-hour protein <200 mg/24 hr were defined as "normal renal function" group while those with serum creatinine >1.3 mg/dL, eGFR ≤45 mL/min/1.73m^2, and a predicted 24-hour protein >1000 mg/24hr were defined as an "abnormal renal function" group. Standard uptake values (SUV) were determined from volumetric regions of interest (5-10 mL in volume) in the renal cortex of each kidney. Data was collected and analyzed using GE Advantage Workstations, GE Picture Archiving Communication System (PACS), and MIM Version 6.6.7 DICOM Viewing and Storage software. Statistical analyses were completed using commercial software (JMP) and a student's t-test for continuous variables and the chi-square test for categorical variables. RESULTS. In this pilot study, 7 men with abnormal renal function were compared to 20 age and sex matched men with normal renal function (average age 75.1±7.8 vs 72.3±6.2 yrs). Abnormal renal function patients had a SUVmean in the right and left renal cortex of 9.6±2.6 and 9.9±1.8, respectively. In the normal renal function group SUVmean was 15.7±5.0 and 15.0±4.2 in the right and left renal

cortex, respectively. Thus, renal cortical uptake of ^{11}C-Choline was 39% ($p<0.0005$) and 34% ($p<0.0002$) lower in the abnormal renal function group for right renal cortex and left renal cortex, respectively. CONCLUSION. Patients with reduced GFR and proteinuria showed significantly reduced renal cortical ^{11}C-Choline uptake.
Clinical Relevance/Application: This pilot demonstrates that renal cortical ^{11}C-Choline uptake can be quantified in clinical PET/CT scans, and is markedly reduced in men with reduced GFR and proteinuria. It has previously been reported that patients with chronic kidney disease have reduced renal tubular handing of drugs including (but not limited to) those transported by the organic cation transporters OCT1 and OCT2. The current study confirms this observation using ^{11}C-Choline that is also transported by at least OCT1 and OCT2. This decreased accumulation of choline could reflect decreased proximal tubular mass, decreased proximal tubular function, or both. It will be of interest to determine whether functional measurement of choline uptake adds diagnostic or prognostic information beyond measured GFR and proteinuria.

Authors listed for this abstract reported no relevant financial disclosures.

2148

Initial Findings with 18-F-Fluciclovine. Shane R. Hammerseng, Kadie Fahl; Nuclear Medicine, Froedtert, Milwaukee, WI, USA. (4064)

Objectives: Provide an overview and findings for the PET/CT (Positron Emission Tomography/Computed Tomography) scan using the radiopharmaceutical 18-F- Fluciclovine (Axumin). 18-F-Fluciclovine is used in patients with a history of previously treated prostate cancer which now have a rising Prostate Specific Antigen (PSA) level.
Methods: Two to three technologists have been used for the 18-F-Fluciclovine studies. Upon arrival to the department an IV is placed in the patient's right arm to avoid bifurcation on the left side. The patient is then positioned on the imaging table, a landmark set at the base of the skull is used for a CT scout. Immediately before injecting the patient, assay the dose of 18-F-Fluciclovine. The patient is then injected while on the imaging table, followed by a 20cc saline flush. The patient's arms are raised above their head for scanning. The 18-F-Fluciclovine syringe is measured following injection. A scout image and CT images are obtained immediately following the injection. A low dose CT scan is used for attenuation correction on the PET/CT scanner for better image resolution and anatomical overlay. PET imaging is begun 3-5min post injection (a timer has been used to keep track of time). The first two bed positions of the PET/CT scan should cover the prostate bed before the bladder fills. Dose availability is limited due to production, quality control, and delivery limitations from an outside pharmacy. Currently 18-F-Fluciclovine doses are available Tuesday-Thursday after 1pm. Due to the immediate imaging following the injections of 18-F-Fluciclovine, an appointment prior to the patients scheduled time needs to be reserved.
Results: The PET/CT images and reports of 50 patients between the ages of 56-82 were analyzed. Of the 50 patients 80% of the scans were positive for disease and 20% were negative. 54% of the patients were found to be positive for metastatic disease, 10% had boney metastasis and the remaining had nodal disease. 56% of the patients were also found to have recurrence of disease in the prostate bed. Initial scan times were seen to be around the 4 minute plus point however with repetition and the use of a third technologist, the average time dropped to 3min and 20s.
Conclusions: 18-F-Fluciclovine is showing very promising results for diagnosing recurrent disease and determining metastatic disease. With these findings orders for this scan should continue to increase. Initial findings show that the availability of a third technologist greatly improves the timing of the procedure, allowing for improved patient care and comfort with great imaging quality.

Authors listed for this abstract reported no relevant financial disclosures.

2149

ADNI-3: F18-AV-1451 as an imaging biomarker for Alzheimer's disease. Janet Cardenas, CNMT[1], Katie Tucker[2], Lisa Riehle[1], Gary L. Dillehay, MD, FACNM, FACR, FSNMMI[1]; [1]Northwestern Memorial Hospital, Chicago, IL, USA, [2]Northwestern Memorial Hospital, Naperville, IL, USA. (4071)

Objectives: Alzheimer's Disease (AD) is one of the most prevalent forms of dementia. Early diagnosis of AD is particularly challenging, as symptoms do not become apparent until cognitive function is lost. Therefore, identifying and validating early onset AD biomarkers is essential for the development of effective treatment. The formation of amyloid plaques and neurofibrillary tangles are two major physiological contributions to the degradation of the nerve cells in the brain that result in AD. [1] The neurofibrillary tangles consist of tau proteins that build up in the spaces between nerve cells, blocking axonal transport. AV-1451 is a new PET radiopharmaceutical under investigation for imaging tau pathologies in AD. ADNI3 is a continuation of the AD Neuroimaging Initiative (ADNI), a public collaboration between academia and industry to study biomarkers of AD.
Methods: Two female and five male subjects were studied. Eligible subjects had no history of risk factors for specific cardiac dysrhythmias associated with sudden death, and were not on any medication(s) known to prolong QT intervals. Subjects were cognitively normal (normal control), had mild cognitive impairment, or had mild AD. Prior to the study, cognitive function of subjects was unknown. Based on the likelihood that amyloid-negative participants show slower rates of tau deposition, all subjects underwent 18F-AV-45 (florbetapir) imaging to indicate amyloid status prior to the AV-1451 study. Subjects were administered 8mCi of 18F-AV-45 for florbetapir imaging and 10mCi of AV-1451 for tau imaging. Seventy-five minutes post-injection, patients were imaged on a Siemens Biograph TruePoint PET/CT for a 30 minute acquisition in list mode. Reconstructions were performed per ADNI-3 protocol, as defined by the Laboratory of Neuro Imaging (LONI).
Results: In accordance with literature defined positive studies, brain images of abnormal subjects showed diffuse increased accumulation of AV-1451. Images that did not show increased accumulation of AV-1451 were considered normal.
Conclusion: Abnormal subjects showed high selectivity for binding to tau proteins. In the ADNI3 study, patients will be followed 2-5 years to optimize, standardize and validate clinical trial measures and biomarkers used in ongoing AD research. Accurately diagnosing the cause of AD aids in directing therapy, improving patient safety and minimizing the risk of preventable complications.
[1] "Amyloid Plaques and Neurofibrillary Tangles," *BrightFocus Foundation,*

Authors listed for this abstract reported no relevant financial disclosures.

TS27: Student Tech Papers III

Moderator: Jay Smith, BSRS, CNMT, ARRT, RT(R)(N)
Co-Moderator: Angela Macci-Byers, Ed.D., MPM, RT(N), CNMT, FSNMMI-TS

2157

Radiation Exposure to Visitors to Nuclear Medicine Department Waiting Areas. Kinsey Smith; Indiana University Purdue University Indianapolis, Indianapolis, IN, USA. (1775)

Objectives: The Nuclear Regulatory Commission (NRC) limits the amount of radiation exposure that members of the general public receive from non-patient radioactive sources, and this limit is 20 microsievert (μSv) in any one hour. Visitors to nuclear medicine department waiting areas receive radiation exposure from radioactive patients. The purpose of this research was to prospectively determine if visitors receive radiation exposure greater than 20 μSv from patient sources, which are currently unregulated by the NRC.

Methods: Luxel optically stimulated luminescence (OSL) dosimeters (n=18) were placed on the walls of nuclear medicine department waiting areas in three hospitals, two per waiting area, over the course of three months. At the end of each month the area monitors were sent to Landauer to have their radiation exposure determined, and were replaced with the next set of area monitors. The exposure rate was calculated by dividing the radiation exposure readings received from Landauer by the number of hours the departments were open each month. The average amount of time visitors spent in the waiting areas was observed over one day. The total visitor exposure was calculated by multiplying the average visitor waiting time by the exposure rate. The total visitor exposures for all three hospitals were averaged and compared to the 20 μSv limit for the general public.
Results: The average visitor exposure for all three hospitals was 0.783 μSv and the highest exposure was 2.793 μSv. The average visitor exposure and the maximum exposure were less than the limit for the general public of 20 μSv in any one hour.
Conclusions: Visitors to nuclear medicine department waiting areas do not receive radiation exposure greater than the limit for the general public of 20 μSv for non-patient sources.

Authors listed for this abstract reported no relevant financial disclosures.

2158

Radiation Exposure Concerns: F18 Fluciclovine radiation exposure from the patient to the public. Autumn Erwin[1], Anna McMunn, PET[2], Crystal Botkin, MPH, CNMT, PET[1], Sarah Frye, MBA, CNMT, PET, NCT[1], Medhat M. Osman, MD, PhD, MS[3]; [1]Department of Clinical Health Sciences, Doisy College of Health Sciences, St. Louis University, Saint Louis, MO, USA, [2]SSM Health Saint Louis University Hospital, St. Louis, MO, USA, [3]Division of Nuclear Medicine, St. Louis University Hospital, St Louis, MO, USA. (4035)

Objectives: Positron Emission Tomography (PET) radionuclides have a higher radiation burden than general nuclear medicine radionuclides; therefore, a patient receiving PET radiopharmaceuticals may be giving off more radiation than allowed by the Nuclear Regulatory Commission (NRC) guidelines for an unrestricted area which is 2 mR/hr. These patients are released to the public or to other departments in the hospital after the completion of their imaging study. A previous study involving F18 FDG indicated that patients were being released while emitting radiation higher than 2 mR/hr. The study also showed that after a thirty-minute wait, the patient voiding after the PET scan helped lower the amount of radiation emitted to under 2 mr/hr. However, there is a one-hour uptake period after injection for the FDG scans while F18 Fluciclovine patients are imaged immediately after injection. This difference could lead to F18 Fluciclovine patients being released with higher radiation levels as their bodies have less time to filter the radiopharmaceutical. The purpose of this study is to evaluate the radiation being emitted from a F18 Fluciclovine PET patient before releasing the patient to the public.
Methods: This study was performed at a single institution on standard of care F18 Fluciclovine PET patients. The protocol for these patients with prostate cancer includes no uptake time after injection and patients are free to leave after the scan. After receiving the standardized dose of 10 mCi of F18 Fluciclovine, patients underwent a scan that lasted approximately thirty minutes. Following the scan, the patient was surveyed with a cutie pie ionization survey meter. The initial survey was taken immediately after the scan, one meter away from the patient at bladder level. After a half an hour wait, the patient was surveyed again using the same method as the immediate survey. Then the patient was surveyed a third-time post void. These readings were used to evaluate whether the patients were emitting more than 2 mR/hr as this is the action level not to be exceeded in an unrestricted area per NRC guidelines.
Results: Six F18 Fluciclovine patients were included in this study. The initial survey found all six patients to be above 2 mR/hr (range: 2.2-3.5). After the thirty-minute wait, only one patient was measured under 2 mR/hr (1.85mR/hr) while the five other patients were measured at 2.1 mR/hr or greater (range: 2.1-2.6). After urination, one patient was measured at 1.68 mR/hr while two other patients measured at 2.0 mR/hr. The other three patients were still greater than 2.0 mR/hr (range: 2.1-2.4). The difference between the initial survey and the thirty-minute wait was divided by the initial survey. This product was then averaged leading to a 14% decrease in mR/hr during the thirty-minute wait. The difference of the thirty-minute wait survey and the survey post urination was divided by the original number taken from the thirty-minute wait. This number was then averaged. The result was a 6% decrease in mR/hr found after urination.
Conclusion: F18 Fluciclovine patients are being released after their PET scans into unrestricted areas despite emitting radiation that is exceeding NRC level guidelines. Based on this initial study, there needs to be an average decrease of 35% in the amount of radiation the patients are emitting before they are released into an unrestricted area. Since Fluciclovine is imaged immediately after injection, as opposed to having an extended uptake time, a waiting period along with voiding after the scan should be recommended. The radiation exposure from patients undergoing Fluciclovine is higher than that from patients undergoing FDG, therefore, discharge instructions should be adjusted accordingly. This recommendation is for the safety of other hospital workers and the public.

Authors listed for this abstract reported no relevant financial disclosures.

2159

Radiation exposure assessment of tungsten vial shields vs. lead glass vial shields. Lilibeth Ugarte[1], Bernard McKay, BS, CNMT[2], Tim Houston[1], Lisa Riehle[1], Gary L. Dillehay, MD, FACNM, FACR, FSNMMI[1]; [1]Northwestern Memorial Hospital, Chicago, IL, USA, [2]Nuclear Medicine - Radiopharmacy, Northwestern Memorial Hospital, Chicago, IL, USA. (4040)

Objectives: Vial shields are an essential component of the radiation safety program in any nuclear pharmacy or nuclear medicine hot lab. Northwestern Memorial Hospital's standard practice is to use commercially available lead glass vial shields when reconstituting technetium 99m (Tc-99m). As high activity Tc-99m sestamibi kits are prepared on a daily basis, the objective of this study is to evaluate the radiation shielding properties of two commercially available vial shields from Biodex Medical Systems.
Methods: The Biodex High Density Lead Glass Vial Shield (001-075) was evaluated by adding 1,421 mCi of Tc-99m into a 10 mL sterile vial. The Biodex Tungsten Vial Shield (053-805) was evaluated by adding 1,428 mCi of Tc-99m into a 10 mL sterile vial. Measurements were recorded using a Fluke 451B ion chamber to determine the radiation exposure on the surface of both shielding configurations. Following the exposure readings, a thermoluminescent dosimeter (TLD) was placed on each vial shield for 30 minutes. The tungsten shield and the lead glass shield contained 1,404 mCi and 1,405 mCi of Tc-99m, respectively, at the time the TLDs were placed. Following a 30 minute exposure time, TLDs were removed and sent to Landauer for processing and analysis.
Results: Ion chamber readings taken at the surface of both the tungsten and lead glass shields were 0.360 mR/h and 13.7 mR/h, respectively. Based on these measurements, the tungsten shield resulted in a 97.4% reduction in surface exposure compared to the lead glass shield. The TLD analysis from Landaur reported "M" (dose equivalents below the minimum measurable quantity of 10 mrem) for the tungsten shield, and 60 mrem exposure for the lead glass shield.
Conclusions: The results demonstrate that tungsten shielding significantly reduces radiation exposure when compared to lead shielding. Based on these findings, Northwestern Memorial Hospital has implemented the use of tungsten vial shields for high activity Tc-99m preparations to minimize radiation exposure and adhere to the ALARA principle.

Authors listed for this abstract reported no relevant financial disclosures.

2160

The Effect of Temperature on Particle Clumping in ^{99m}Technetium-MAA. Arielle G. Knafel, B.S.[1], Cybil J. Nielsen, MBA, CNMT, FSNMMI-TS[2], Kara Weatherman, PharmD[3]; [1]Nuclear Medicine Technology, Indiana University School of Medicine, Indianapolis, IN, USA, [2]Indiana University NMT Program, Indianapolis, IN, USA, [3]Purdue University, West Lafayette, IN, USA. (4041)

Objectives: The purpose of this research is to evaluate the effect of temperature on particle clumping in 99mTechnetium-MAA.

Methods: A Draximage™ 99mTechnetium-MAA kit was reconstituted with 3330 MBq to produce 16 doses containing ~200 MBq and ~300,000 particles each. Eight total environments were tested. The conservative environments, based on realistic temperatures doses may be exposed to during transit or storage, ranged from -6.7 to 42.5 degrees Celsius. A room temperature 21.6°C dose served as the control. The extreme environments had a temperature range of 65.3-82.1 degrees Celsius. Two doses were tested in each respective environment, an indirect exposure (shielded by a lead pig) and a direct exposure (unshielded). All dose particles were measured and counted every 30 minutes for a total of 5.5 hours and compared to that of the control. A single sample t-test was used to compare both the shielded and unshielded particle clumping data to that of the control. Additional statistical tests were done to determine the relevance of exposure time to particle clumping.
Results: The conservative environments demonstrated a collective p-value of 0.5 and showed no statistically significant difference in the occurrence of particle clumping following environmental exposure. The extreme environments demonstrated statistically significant increases in the occurrence of particle clumping as temperature increased.
Conclusions: Reconstituted 99mTechnetium-MAA kits demonstrate no change in particle clumping when exposed to hot and cold temperatures typically encountered during storage and/or transit. Based on this research, evidence does not support the Draximage™ package insert recommendation for a specific storage temperature following kit reconstitution for the prevention of particle clumps.

Authors listed for this abstract reported no relevant financial disclosures.

2161

Development of Tc99m DMSA Complex 2 Quality Control Test.
Erika Olson[1], Andrew Paulsen, PharmD[2]; [1]Mayo Clinic School of Health Sciences, Litchfield, MN, USA, [2]Mayo Clinic, Rochester, MN, USA. (4050)

Objectives: Background Technetium 99m Dimercaptosuccinic acid (Tc99m DMSA) is a diagnostic radiopharmaceutical used for the assessment of renal parenchymal disorders, renal structure, and morphology. Currently no United States drug manufacture is producing the DMSA kit in order to make Tc99m DMSA. Compounding the DMSA kit may be a solution to this shortage. When Technetium99m sodium pertechnetate (Na TcO4-) is added to a DMSA kit, two complexes are formed. Tc99m DMSA Complex 1 is quickly formed and within 10-15 minutes converts to Tc99m DMSA complex[1]. Complex 2 is the desired form which localizes in the kidney, whereas complex 1 is readily excreted by the kidneys[1]. Oxygen contamination in the kit and an improper ratio of stannous ion (Sn2+) to ligand may favor complex 1 over complex 2 in the chemical reaction[2]. Current radiochemical purity testing does not differentiate between Tc99m DMSA complex 1 and complex 2. The aim of this study was to evaluate the effectiveness of a new radiochemical purity testing method for compounded DMSA which can identify and differentiate Tc99m DMSA complex 1 and complex 2.
Materials and Methods: A compounded DMSA kit was used with the following formulation: 1.0 mg dimercaptosuccinic acid, 0.42 mg stannous chloride dehydrate, 0.70 mg ascorbic acid, and 50.0 mg inositol dissolved in 2ml of N2 purged 0.9% NaCl. Tc99m DMSA was prepared by adding up to 40mCi of Na TcO4- in 0.1-0.5 ml to the compounded DMSA kit and up to 15 minutes was allowed for the reaction to occur. Three DMSA kits were prepared in this manner and radiochemical purity testing was conducted using ITLC with SA paper (90mm) as a solid phase and methanol for mobile phase[1]. Then, an additional ITLC test was performed on each kit to identify Tc99m DMSA complex 2 using 51A paper (90mm x 10mm) as the solid phase and 0.9% NaCl as the mobile phase. The sample origin was placed 15 mm from the bottom of the strip and the strip was developed until solvent front was 85 mm. The developed 51A strip was then scanned using an ITLC scanner. To revert complex 2 back to complex 1 the kits were heated at 100 degrees for 2 hours[3]. After heating, the Tc99m DMSA solution was filtered through a 0.2 micron filter and passed through a Bio-Gel P-10 column (1cm x 1cm) in order to purify complex 1 from any remaining complex 2[2]. ITLC testing was repeated using the 51A paper and 0.9% NaCl method as described previously on the purified Tc99m DMSA complex 1.
Results: Radiochemical purity testing for all three kits was ≥ 98% Tc99m DMSA using the SA paper and methanol. The findings of this study are displayed in Table 1. When testing for Tc99m DMSA complex 2 with 51A paper and 0.9% NaCl we found on average that, 87.8% of the radioactive counts were located at the origin and up to 20 mm past origin (15-35 mm from bottom of strip). When testing for Tc99m DMSA complex 1 with 51A paper and 0.9% NaCl we found on average that 80% of the radioactive counts were past 20 mm above the origin (35mm-85mm from the bottom of the strip).
Conclusion: Using the 51A ITLC paper with 0.9% NaCl is an effective quality control method to identify and differentiate between Tc99m DMSA complex 1 and complex 2. The preferred Tc99m DMSA complex 2 remains mostly at origin with slow migration up the strip, whereas the Tc99m DMSA complex 1 migrates readily up the strip. Performing this quick and simple test on a preparation of Tc99m DMSA can help to ensure the correct complex is present for effective localization and imaging. This test may be more necessary when using compounded formulations of DMSA kits, as opposed to manufactured kits.

Authors listed for this abstract reported no relevant financial disclosures.

2162

Comparison of delivered and residual Technetium labeled Diethylenetriamine-pentaacetic acid when ventilating: corrugated vs. non-corrugated tubing.
Connor M. McIntosh[1], Ann M. Voslar, MHA/Ed, BS-Nuclear Medicine[2], Carrie Wolter, BS-Nuclear Medicine[1]; [1]Froedtert Memorial Lutheran Hospital, Milwaukee, WI, USA, [2]NM/PET, Froedtert Memorial Lutheran Hospital, Milwaukee, WI, USA. (4061)

Objectives: The use of corrugated tubing during a lung aerosol exam results in the deposit of Technetium Diethylenetriamine-pentaacetic acid (Tc-DTPA) in the grooves of the tubing, reducing the amount of Tc-DTPA deposited in the lungs. This study examined whether non-corrugated tubing would allow more Tc-DTPA to be deposited into the lungs in comparison to the standard, corrugated tubing. An increase of Tc-DTPA delivered to the lungs could allow for a decrease in the prescribed dose, reducing the radiation exposure to patients and technologists**.**
Methods: Utilizing the same ventilation kit, two non-clinical experiments were performed using corrugated and non-corrugated tubing. Three trials were conducted for each type of tubing. The length (68cm) and bore (2.3cm) of the tubing were held constant in each trial along with the activity (24.0 ±0.5mCi) and volume (4.0±0.1mL) of Tc-DTPA. An ambu bag was attached to the tubing during ventilation to simulate a lung reservoir and ensure a closed system. For each trial, the ventilation time was eight minutes with an oxygen flow of ten liters. Immediately following ventilation, the tubing and ambu bag were imaged on a gamma camera for two minutes, utilizing a Low Energy All Purpose collimator. The position of the tubing was held constant during ventilation utilizing a hand drawn outline of the tubing and ambu bag. Two regions were drawn for each trial, one around the tubing and the other around the ambu bag. During imaging, the boundaries of these regions were marked with cobalt markers. The regions were drawn six times and averaged to ensure accuracy. The counts of each region were recorded, and the corrugated and non-corrugated trials were compared.
Results: The average counts yielded from the corrugated tubing and associated ambu bag regions were 112,655 and 320,228, respectively. The average counts yielded from the non-corrugated tubing and associated ambu bag regions were 45,119 and 701,835, respectively.
Conclusions: This study proved that after ventilation, the non-corrugated tubing retained 149.7% less counts when compared to the corrugated tubing. In addition, the ambu bag attached to the non-corrugated tubing retained 119.2% more counts than the ambu bag attached to the corrugated tubing. A higher amount of Tc-DTPA delivered to the lungs would allow for a lower prescribed dose, while keeping the same image sensitivity. Further research should be conducted to see how much the prescribed dose of Tc-DTPA may be reduced to keep patient radiation exposure as low as reasonably achievable.

Authors listed for this abstract reported no relevant financial disclosures.

2163

Breakdown Significance of MAA in a Syringe and Vial Post Compounding. Megan Nagel; Froedtert & MCW, Milwaukee, WI, USA. (4066)

Objectives: The prices of Macroaggregated Albumin (MAA) vials have become more expensive, making it more affordable to order unit doses from commercial pharmacies. The objective of this study is to determine if there is a difference in quality control (QC) results when comparing commercially drawn unit doses that have the potential to sit for 6 hours versus radiopharmacy prepared doses drawn directly from vials at the time of injection. When doing QC, a minimal amount of free TcO_4^- and hydrolyzed reduced (HR) TcO_4^- is preferred to ensure that there is a higher amount of technetium bound to the MAA particles.
Methods: QC is done on every compounded kit to make sure that the diagnostic radiopharmaceutical is suitable to administer to the patient. QC consists of a radiochemical quality test, a radionuclide quality test, a chemical impurity test, as well as a pH test. After the 15 minutes' incubation time for the compounded MAA kit, seven syringes are initially drawn up. To mimic commercially drawn unit doses, six syringes were drawn up for each hour until expiration (time 0-6 hours). A seventh syringe is drawn up to indicate time zero for the immediate QC results of the kit. Every hour, radiochemical QC is done on one of the six syringes and a new sample is drawn up from the MAA vial. Radiochemical quality of the radiopharmaceutical is how much radioactivity in the right chemical form is present in the radiopharmaceutical. Radiochemical quality is evaluated by using chromatography strips designated for Tc99m-MAA. The chromatography test shows what percent of free TcO_4^- and hydrolyzed reduced TcO_4^- there is in the compounded kit; ultimately giving you the labeling efficiency. Radionuclide quality test is how much of the radionuclide activity desired there is compared to the total amount of radioactivity of the source. The source being Mo-99 from the Molybdenum generator and the desired radionuclide is Tc-99m. This is only done once for this research right away at time zero when the 15 minute incubation period is over. The ratio should be less than 0.15 microcuries of Mo-99 per millicuries of Tc-99m. Chemical impurity test is testing to see how much aluminum residual in the Tc-99m eluate from the generator, if there is too much aluminum in the eluate it causes a decrease in binding efficiency. Another test is done to evaluate the pH of the radiopharmaceutical that is administered to the patient. Testing the pH is done simply by using pH paper. A pH out of the range of 4.75-7.5 is not acceptable to administer to the patient. Both of these tests are done once initially at time zero and only need to be done once for this research.
Results: Multiple trials were done on five different compounded MAA kits. The lowest QC result was 98.7% from the syringes and the lowest QC result for the vial is 98.8%. There was no correlation of more breakdown of MAA with time, meaning that QC results did not differ as the time of expiration of the kit progressed.
Conclusions: Looking at the results, there is no significant difference in QC data that would lead to the assumption that the breakdown of MAA is greater in a syringe compared to a vial. Ordering unit doses could save the hospital money and therefore this institution will continue to order unit doses from commercial pharmacies without the concern of HR TcO_4^- or free TcO_4^- being a problem. **FIGURES/IMAGES:**

TRIAL 1		
time (hour)	% bound vial	% bound syringe
0	0.994	0.994
1	0.992	0.993
2	0.989	0.992
3	0.988	0.991
4	0.991	0.987
5	0.992	0.997
6	0.989	0.996

TRIAL 2		
time (hour)	% bound vial	% bound syringe
0	0.990	0.990
1	0.998	0.998
2	0.98	0.997
3	0.997	0.989
4	0.993	0.997
5	0.997	0.999
6	0.995	0.997

TRIAL 3		
time (hour)	% bound vial	% bound syringe
0	0.997	0.997
1	0.998	0.999
2	0.995	0.993
3	0.998	0.998
4	0.994	0.996
5	0.996	0.998
6	0.994	0.994

REFERENCES: Loveless VS. Quality Control of Radiopharmaceuticals. Fundamentals of Nuclear Pharmacy. 2009; XV:151-174. doi:10.1007/0-387-21702-9_8.

Authors listed for this abstract reported no relevant financial disclosures.

2164

Evaluation of Tc-99m Sestamibi residual in Becton Dickinson syringes and optimizing the configuration for dispensing. Carly Schaaf[1], Tim S. Houston, PharmD[2], Bernard McKay, BS, CNMT[3], Lisa Riehle[1], Gary L. Dillehay, MD, FACNM, FACR, FSNMMI[1]; [1]Northwestern Memorial Hospital, Chicago, IL, USA, [2]Northwestern Memorial Hospital, Orland Park, IL, USA, [3]Nuclear Medicine - Radiopharmacy, Northwestern Memorial Hospital, Chicago, IL, USA. (4073)

Objectives: Tc-99m sestamibi is one of the most commonly used SPECT radiopharmaceuticals for myocardial perfusion imaging. Northwestern Medicine's standard practice was to draw rest Tc-99m sestamibi doses in 1cc syringes QS'd to 0.5mL and stress Tc-99m sestamibi doses in 3cc syringes QS'd to 1.5mL. The purpose of this study is to evaluate the extent of adhesion of Tc-99m sestamibi in the syringe post injection and to identify the best configuration for dispensing Tc-99m sestamibi unit doses to decrease residual activity.
Methods: Northwestern Medicine's standard rest and stress Tc-99m sestamibi doses are 9mCi and 32mCi, respectively. To evaluate the extent of Tc-99m sestamibi adhesion to the syringe, 10 rest doses were drawn up in 1cc Becton Dickinson (BD) syringes and QS'd to 0.5mL. Three more sets of 10 rest doses were drawn up in 3cc BD syringes and QS'd to the following volumes: 0.5mL, 1.0mL, and 1.5mL (10 doses per volume). Each dose was then assayed in an AtomLab 500 dose calibrator and both time and activity were recorded. Post assay, each dose was immediately dispensed into a sterile evacuated vial and the empty syringe was re-assayed to measure residual activity. This procedure was repeated to evaluate stress doses. Three sets of 10 stress doses were drawn up in 3cc BD syringes and QS'd to the following volumes: 0.5mL, 1.0mL, and 1.5mL (10 doses per volume). Data was recorded and the average residual and average percent loss for each syringe size and configuration was calculated.
Results: The configuration that resulted in the lowest residual activity for rest doses is the 3cc syringe QS'd to 1.0mL. This configuration resulted in an average residual activity of 1.46mCi with an average loss of 15.4% of the original dose. This average residual is 46.7% lower than the configuration that was originally used to dispense rest doses. The configuration that resulted in the lowest residual activity for stress doses is the 3cc syringe QS'd to a final volume of 1.5mL. This configuration resulted in an average residual activity of 3.68mCi with an average loss of 12% of the original

dose. This average residual is 17.6% lower as compared to the average residual when QS'd to 1.0mL (4.47mCi) and 22.7% less than the average residual when QS'd to 0.5mL (4.77mCi).
Conclusions: As a result of this study, Northwestern Medicine has changed its standard practice. Rest Tc-99m sestamibi doses are now drawn up in 3cc syringes QS'd to 1.0mL. Stress Tc-99m sestamibi doses will continue to be drawn up in 3cc syringes QS'd to 1.5mL since this configuration resulted in the least amount of residual activity.

Authors listed for this abstract reported no relevant financial disclosures.

2165

Alternative Administration Methods for Lutathera Therapy.
Abdullatif K. Dire, Nuclear Medicine Technology, Denise Gansen, Andrew Paulsen; Nuclear Medicine Technology, Mayo Clinic School of Health Sciences, Rochester, MN, USA. (4078)

Objectives: Lutathera (Lutetium Lu-177 Dotatate) is a Lu-177-labeled somatostatin analogue to treat somatostatin receptor-positive neuroendocrine tumors. The Lutathera is supplied in a glass vial, and the entire contents of the vial are administered to the patient in order to deliver a 200 mCi therapeutic dose. Treatment with Lutathera also consists of an infusion of Amino Acids for renal protection purpose that is started 30 minutes prior to start Lutathera infusion. The Amino Acids are infused for a total of four hours. Also, antiemetic drugs can be administered 30 minutes before the start of Lutathera infusion. A reliable and safe method for delivering the Lutathera dose directly from the manufacturer's glass vial is needed, which allows for concomitant drug administration and patient mobility.
Materials and Methods: Two administration techniques were compared for administration of Lutathera. Residual activities of the drug vial and tubing were measured after administration. Administration Method I The Lutathera dose vial was placed in a Lantheus generator elution shield. The vial was spiked with a vented IV spike, inverted, and hung on the IV pole. The Lutathera line was piggy-backed to an IV bag containing sterile normal saline solution. An infusion pump was used to deliver the Lutathera at a rate of 50 mL/hr until the vial was empty. The vial was then rinsed with a back-flush of 20-25 mL of the saline. The rinse was then administered at 50 mL/hr until gone. A second IV pump was used to administer the Amino Acid solution. All pumps, IV bags, and the shielded Lutathera vial were hung from an IV pole on wheels which allowed for patient mobility. Five patients were treated using Method I. Administration Method II The Lutathera dose vial was placed into a 30 mL vial shield from Mallinckrodt. The vial shield was attached to the IV pole in the upright position. A 3.5 inch spinal needle was inserted through the Lutathera vial septum and advanced to the bottom of the vial. This was connected to a primed micorbore extension set, which was piggy-backed into a sterile normal saline line. A secondary medication set with DUO-VENT spike was introduced into the Lutathera vial with a 21 gauge one inch needle, which was connected to50 ml bag of sterile normal saline. An IV pump was used to administer the Lutathera and saline. The drug was infused at 50 mL/hr for 15 minutes. At the end of the 15 minutes, the rate was increased to 100 ml/hr for 5 minutes. The rate was increased to 200 ml/hr and allowed to rununtil gone. The Amino Acids were administered using a second pump. All pumps, IV bags, and the shielded Lutathera vial were attached to an IV pole on wheels which allowed for patient mobility. Six patients were treated with Method 2.
Results: Both methods allowed for the following: the Luathera drug vial was shielded, the patient was able to move during therapy, the Luathera was administered directly from manufacturer's glass vial, and concomitant medications could administered appropriately. Average residual measurements in the IV lines and drug vial for Method 1 and Method 2 were 2.49 mCi (1.2% of 200 mCi dose) and 2.18 mCi (1.09% of 200 mCi dose) respectively.
Conclusion: Both methods tested proved to be acceptable for administration of Lutathera. However, we observed that Method II does have some advantages over Method I. Method I requires a large bore IV spike to be inserted in the vial septum. There is greater potential to displace the septum on the Lutathera vial using an IV spike compared to a spinal needle. Also, inverting the spiked Lutathera vial in method I has an increased risk of leaks. Back-flushing the Lutathera vial using Method I requires staff to spend more time next to the patient compared to Method II, which increases radiation exposure to the staff. Relatively, both methods performed very well in delivering the entire dose to the patients had low residual measurements. After this comparison, we suggest Method II is the optimal method for administering Lutathera.

Authors listed for this abstract reported no relevant financial disclosures.

Technologist Student Posters

1859

Radiation Safety: A Students' Perspective.
Christina Rivas, Student, Maui Cervantes; University of the Incarnate Word, San Antonio, TX, USA. (81)

Objectives: When first entering this program, although the field of study is very interesting, one of the main concerns was the increased exposure of radiation we would receive. With incidents such as the Radium Girls, it's evident that overexposure to radiation can cause detrimental effects. Furthermore, with preconceived notions such as developmental effects on offspring from radiation exposure and an increased risk in cancer due to overexposure to radiation, friends and family even began to question whether this career was a safe one. Therefore, proper education on principles such as ALARA and understanding the basic behavior of radiation is essential to efficiently working with radioactive materials to reduce exposure to ourselves and others around us. As nuclear medicine students in the south Texas region of the United States we have taken this opportunity and address this issue within our cohort. The primary focus of this perspective paper is to establish the importance of providing our fellow classmates with the literature about un-necessary radiation exposure.
Methods: In the planning of our student perspective paper, we defined the objective of the paper and identified the data sources. Our data consisted of database research and peer reviewed articles. The database's search consisted of key terms such as; radiation safety, harmful radiation effects, nuclear medicine, radiation hormesis, low-level radiation effects, ALARA, and employee radiation exposure.
Results: Radiation exposure generates reactive chemical mutations, which cause cell damage. Currently, discussion about radiation protection is parallel with the application of the linear-no-threshold (LNT) model which assumes that even low amounts of radiation may increase cancer risk. However, the opposite may also be beneficial. Radiation Hormesis, a theory developed by Hermann Muller, explains that the body deals with damage through an adaptive response, which includes double-strand break repair, antioxidant production and immune-system removal of surviving damaged cells. This biological process leads to a reduced cancer rate within the body. Nonetheless, there is sufficient evidence to validate the claims of negative effects of unnecessary exposure. The discussion of both the risk as well as the benefits need will provide students with a broader perspective of radiation exposure to both the technologist and the patient.
Conclusion: Based on database research, active campaigns such as Image Gently and Image Wisely were launched to raise awareness about the reduction in radiation dose during pediatric and adult medical imaging studies, respectively, in a healthcare setting. As a student and future occupational worker, it is our duty to not only learn what is known but also stay informed as much as possible on our scope of practice. Although there are contradicting ideas to the linear-no-threshold such as the radiation hormesis theory, more research will be needed to further emphasize its strength and application to patient care and occupational exposure. While the idea behind radiation hormesis is reasonable: small amounts of radiation are beneficial, and the opposite is true; too much of anything is never good. We believe that the radiation hormesis theory should be implemented in the curriculum of nuclear medicine students to better inform us and help us make an informed decision on occupational practices. We think that it is important that patients and occupational workers alike be informed on as much as possible about the effects of radiation exposure to reduce the fear of radiation. Although overexposure is harmful, exposure during diagnostic imaging is conclusively beneficial to the patient, and can even be the tool to help save a patient's life. Writing this paper provided us the opportunity to raise awareness about radiation exposure among our peers, instructors,

and preceptors. We wish to continue to advocate in the awareness of unnecessary radiation exposure throughout our careers related to radiology.

Authors listed for this abstract reported no relevant financial disclosures.

1860

Optically stimulated luminescence dosimeters versus thermoluminescence dosimeters accuracy in a PET facility. Lauren M. Rampolla[1], Chelsee Gavel[1], Donna L. Mason, MS, CNMT, RT(N)[2]; [1]Nuclear Medicine, Robert Morris University, Pittsburgh, PA, USA, [2]Robert Morris University, Moon Township, PA, USA. (1724)

Objectives: Dosimetry is the measurement of radiation doses and is important to monitor personnel exposure levels to maintain the as low as reasonably achievable (ALARA) philosophy. Radiation dosimeters used to measure absorbed radiation are thermoluminescence dosimeters (TLD's) or optically stimulated luminescence dosimeters (OSLD's). Accuracy refers to how close data comes to the accepted value. Dosimeter readings must be accurate so radiation workers have a definitive assessment of exposure. The aim of this study is to compare the accuracy of TLD's and OSLD's under identical conditions.
Methods: One OSLD and one TLD were attached to the top of the Discovery VCT PET/CT scanner at UPMC Hillman Cancer Center and Washington Hospital (dosimeter set 1: four dosimeters comprising two of each type at each facility). After thirty patients, the dosimeters were removed and another pair (set 2) was placed for an additional thirty patients at each facility. Both facilities use [Fluorine-18]fludeoxyglucose FDG, and Hillman also uses [Gallium-68] dotatate. Key information from each scan included radiopharmaceutical and dose, bed number, and whether the CT was for attenuation or diagnostic purposes. The eight exposed dosimeters and control dosimeters were sent to Laundauer to be read.
Results: Although eight dosimeters were analyzed, only a report for set 2 was received. For comparison to the reported results, predicted baseline exposure values were calculated for each patient using the PET dosage, bed number, and exposure rate formula, and the results were summed for each set of thirty patients to produce total baseline values. The predicted baseline and reported values are detailed in Table 1 showing lower predicted values and higher OSLD vs. TLD results.

	Predicted Baseline (mrem)	Landauer (mrem)
Washington	263	OSLD - 630 TLD - 503
Hillman	212	OSLD - 580 TLD - 512

Table 1.

Conclusions: The difference between predicted and actual values was unexpected. It was realized that the predicted values based only on PET dosages did not include the CT contribution or decay effects from injection time to scan time, both of which would have been difficult to calculate. Therefore, it is not possible from this study to make a definitive assessment of relative dosimeter accuracy. The higher OSLD values, however, are consistent with literature that OSLD's are more sensitive than TLD's. These results show that great care must be taken in the design of experiments to understand as much as possible the effect of input variables on predicted results, in this case the combined contribution CT dosages and radioisotope decay on the baseline PET predictions. Such understanding is important to ensure all critical experimental factors are accounted for.

Authors listed for this abstract reported no relevant financial disclosures.

1861

Lu-177 DOTATATE therapy for progressive metastatic neuroendocrine tumors: Multidisciplinary team work and role of technologists, nurses, physicists and physicians. Autumn Copeland[1], Kathleen E. Mertel, BS, CNMT, RT(CT)[2], Seyed M. Mohammadi, CNMT, RT(N)(CT), PET,[3] Cindy Steiner, MS[4], Kelly Mannella, MS, DABSNM[5], Michael Sheetz, MS, CHP, DABMP[5], Ashok Muthukrishnan, MD[3]; [1]Nuclear Medicine, UPMC Presbyterian Shadyside, Pittsburgh, PA, USA, [2]Irwin, PA, USA, [3]UPMC, Pittsburgh, PA, USA, [4]Radiation Safety, UPMC Presbyterian Shadyside, Pittsburgh, PA, USA, [5]Radiation Safety, University of Pittsburgh, Pittsburgh, PA, USA. (4046)

Objectives: Treatment of metastatic neuroendocrine tumors is multidisciplinary and generally involves surgery, radiation, chemotherapy, and somatostatin analog therapy. A relatively newer form of treatment known as Peptide Receptor Radiotherapy (PRRT) has become increasing popular in various parts of the world for treating these tumors. One such therapy using Lutetium-177 DOTATATE (Lutathera®) has been recently approved by the FDA for its use in advanced Gastroentero-pancreatic neuroendocrine tumors (GEP-NETs). Our institution was one of the major sites to be involved in the Expanded access /compassionate access protocol before its FDA approval. The experience of treating over 17 GEP-NET patients during the past year has helped us develop a successful working knowledge in therapy administration and post-therapy imaging protocols. Learning objectives of this educational exhibit: 1. To review the Lu177 DOTATATE workflow logistics from scheduling to therapy and post therapy imaging. 2. To review the eligibility criteria for the treatment and the bloodwork and test required for follow up of the patients. 3. To discuss in depth the multi-disciplinary team work required during the therapy administration including the nursing needs, medication requirements, monitoring during treatment, administration technique, radiation safety concerns. 4. To discuss in detail about the amino acid requirements during the therapy: comparison between the off-the-shelf amino acid solution vs the custom-made compounded amino acid solution in terms of composition, osmolality, volume, tolerability and side effects. 5. To review the future directions of PRRT therapy in terms of other disease pathologies.

Authors listed for this abstract reported no relevant financial disclosures.

1862

Re-evaluating the value of CT-based attenuation correction in Myocardial Perfusion Imaging. HyeIn Lee, BSc; Medical Radiation Sciences, The Michener Institute, Toronto, ON, Canada. (4077)

Purpose: The purpose of this literature review paper was to critically re-evaluate and summarize controversy regarding the diagnostic value of CTAC for MPI SPECT/CT studies from the most recently published research papers.
Methods: PubMed and OVID Database was used to search for relevant articles, published in 2007 to 2017, with 20 articles selected for review. The following keywords were utilized: SPECT/CT, MPI and CTAC. The articles were rated for quality using QUADAS-2 for primary research, and AMSTAR-2 for systematic reviews. Summary of sensitivity, specificity and diagnostic odds ratio from each of the articles was summarized, along with QUADAS-2 or AMSTAR-2 scores of each article. One article was structured as a systematic review, 18 articles were categorized as primary research, and the last article was eliminated from rating as it was identified as a review paper.
Results: Of the 20 articles selected for review, 9 articles supported the use of CTAC as a means of increasing diagnostic quality of MPI studies (average QUADAS-2 score 11.1/18, range 9 to 16). Two articles were ambiguous, making statements that both support and oppose the utilization of CTAC (average QUADAS-2 score 11.25/18). Five articles opposed the use of CTAC, providing alternatives such as gated SPECT without AC (average QUADAS-2 score 11.2/18, range 4 to 18). The final article was identified to be irrelevant to CTAC, as it discussed RAC in its methodology with no mention of CTAC. Methodology of each article varied significantly in terms of individual MPI protocols, radiopharmaceuticals used, as well as choice of stressing agents.
Conclusion: Considering the additional radiation dose delivered to the patient with the use of CTAC, efforts have been made to correctly identify and reduce the radiation dose. However, the diagnostic value of CTAC continues to be a controversial topic and systematic reviews on a larger scale must be conducted to settle the controversy. Through comparison of various MPI protocols, radiopharmaceuticals of choice, stressing agents of choice, and changes in specificity, sensitivity, and diagnostic odds ratio of the procedure, more comprehensive conclusion on diagnostic value of CTAC for MPI SPECT/CT can be made.

Authors listed for this abstract reported no relevant financial disclosures.

ABSTRACT AUTHOR INDEX

ABSTRACT AUTHOR INDEX

ABSTRACT AUTHOR INDEX